WA School of Mines: Minerals, Energy and Chemical Engineering

Department of Petroleum Engineering

Effect of Organics and Nanoparticles on CO_2-Wettability of Reservoir Rock; Implications for CO_2 Geo-Storage

Muhammad Ali

ORCID: 0000-0002-2446-3072

Scopus ID: 57203080456

https://scholar.google.com.au/citations?user=3QOBwXUAAAAJ&hl=en

https://www.researchgate.net/profile/Muhammad-Ali-10

This thesis is presented for the Degree of

Doctor of Philosophy (Petroleum Engineering)

of

Curtin University

May 2021

DECLARATION OF ACADEMIC INTEGRITY

To the best of my knowledge and belief, this thesis contains no material previously published by any other person except where due acknowledgement has been made.

This thesis contains no material which has been accepted for the award of any other degree or diploma in any university.

Name: Muhammad Ali

Signature: 

Date: May 18, 2021

COPYRIGHT

I warrant that I have obtained, where necessary, permission from the copyright owners to use any third-party copyright materials reproduced in the thesis (e.g. questionnaires, artwork, unpublished letters), or to use any of my own published work (e.g. journal articles) in which the copyright is held by another party (e.g. publisher, co-author).

Name: Muhammad Ali

Signature: 

Date: May 18, 2021

DEDICATION

I would like to dedicate my thesis to my father, Muhammad Anwar Sahito, who has been my biggest motivation throughout my education; to my mother, Gulnar Sahito, for her prayers; to my wife, Roohina Alisha Almas Ali, for her support; to my lovely daughter Aafreen Noor Sahito, and my beloved son Affan Ali Sahito.

ACKNOWLEDGMENT

In The Name of Allah, The Most Gracious, The Most Merciful

Firstly, I would like to express my utmost sincere appreciation to my supervisor Dr. Mohammad Sarmadivaleh. I am grateful for his continual guidance and knowledge, which have provided the energy for me to push through the difficulties during my PhD research.

Besides my advisor, I would like to thank the rest of my thesis committee, Dr. Reza Rezaee (Chairperson), Dr. Ali Saeedi (Associate Supervisor), and Dr. Stefan Iglauer (Associate Supervisor), for their insightful comments and encouragement, but also for the hard questions, which incentivised me to widen my research from various perspectives.

I thank my colleagues and friends for the stimulating discussions, the sleepless nights we spent working together before deadlines, and all the fun that we have had in the last three years.

I also acknowledge the support provided by the Australian Government (Research Training Program formerly Research Training Scheme) as well as Curtin University for providing supervision and resources for this research studies.

Last but not the least, I would like to thank my family—my parents, my brothers and sisters—for supporting me spiritually throughout the writing of this thesis and my life in general.

ABSTRACT

Hypothesis: Globally, a vast amount (millions of tons) of CO_2 is stored underground into geological storage reservoirs every year, however, these aquifers have minute concentrations of organic acids such as lignoceric acid C_{24} (LiA), stearic acid C_{18} (SA), lauric acid C_{12} (LuA), and hexanoic acid C_6 (HA). The literature is well documented with the existence of organic acids in geo-storage formations (i.e. deep saline aquifers) but their influence on residual and structural trapping capacities and hence contamination security is still required to be understood. Additionally, the role of nanoparticles is very pivotal in various nano-energy applications. The small concentrations of nanomaterial (in deionized water or brine) can drastically shift hydrophobic surfaces to hydrophilic in anoxic conditions (contains organic acids) for CO_2/brine/mineral systems. However, applications of nanomaterials and their associated concentrations are rarely tested at realistic reservoir conditions.

Experimental: In the present work, we have analyzed that how various alkyl chain organic acids influence the CO_2-wettability of the geological storage formations for various ageing times (7 days and 12 months). Thereafter, these organic-aged surfaces were aged with different nano-fluid concentrations for 5 hours to reverse the organic effect. To do that, we have aged different proxy samples (calcite for carbonate, quartz for sandstone and mica for cap-rock) with various alkyl chain length organic acids at monotonically reduced concentrations (10^{-2} to 10^{-10} mol/L). In addition to this, we have used different nanoparticles (silica for quartz and alumina for mica) and their associated concentrations (0.05, 0.1 0.25, and 0.75 wt%) dispersed in deionized water for comprehending their effect on CO_2-wettability reversal.

Findings: When proxy samples of different geological storage formations were aged in various organic acid concentrations for a one-year ageing time, the hydrophilic surfaces turned into super-hydrophobic at realistic geo-storage conditions. However, in cap-rock geo-storage rocks, this effect was optimally minimized by 0.25 wt% of alumina nano-formulation and in sandstone geo-storage rocks, this effect was optimally minimized by 0.1 wt% of silica nano-formulation. Further, mechanically permanent adsorption of alumina and silica nanoparticles were observed on the surface of proxy geological storage samples. This reversal of wettability due to nano-suspensions may provide safe structural and residual trapping thresholds and as well as increased containment security.

PUBLICATIONS DURING PHD CANDIDATURE

JOURNAL PUBLICATIONS AS PART OF THE THESIS

CHAPTER 3:

1. **Ali, M**., Al-Anssari, S., Arif, M., Barifcani, A., Sarmadivaleh, M., Stalker, L., ... & Iglauer, S. (2019). Organic acid concentration thresholds for ageing of carbonate minerals: Implications for CO_2 trapping/storage. Journal of colloid and interface science, 534, 88-94.
2. **Ali, M**., Arif, M., Sahito, M. F., Al-Anssari, S., Keshavarz, A., Barifcani, A., ... & Iglauer, S. (2019). CO_2-wettability of sandstones exposed to traces of organic acids: Implications for CO_2 geo-storage. International Journal of Greenhouse Gas Control, 83, 61-68.
3. **Ali, M**., Aftab, A., Arain, Z. U. A., Al-Yaseri, A., Roshan, H., Saeedi, A., ... & Sarmadivaleh, M. (2020). Influence of Organic Acid Concentration on Wettability Alteration of Cap-Rock: Implications for CO_2 Trapping/Storage. ACS Applied Materials & Interfaces, 12(35), 39850-39858.

CHAPTER 4:

4. **Ali, M**., Sahito, M. F., Jha, N. K., Arain, Z. U. A., Memon, S., Keshavarz, A., Iglauer, S., ... & Sarmadivaleh, M. (2020). Effect of nanofluid on CO_2-wettability reversal of sandstone formation; implications for CO_2 geo-storage. Journal of colloid and interface science, 559, 304-312.
5. **Ali, M**., Aftab, A., Awan, F. U. R., Akhondzadeh, H., Keshavarz, A., Saeedi, A., ... & Sarmadivaleh, M. (2021). CO_2-wettability reversal of cap-rock by alumina nanofluid: Implications for CO_2 geo-storage. Fuel Processing Technology, 214, 106722.

RELATED JOURNAL PUBLICATIONS AS NOT PART OF THE THESIS

1. Iglauer, S., **Ali, M**., & Keshavarz, A. (2021). Hydrogen Wettability of Sandstone Reservoirs: Implications for Hydrogen Geo-Storage. Geophysical Research Letters, 48(3), e2020GL090814.

2. Al-Anssari, S., **Ali, M**., Alajmi, M., Akhondzadeh, H., Khaksar Manshad, A., Kalantariasl, A., ... & Keshavarz, A. (2021). Synergistic Effect of Nanoparticles and Polymers on the Rheological Properties of Injection Fluids: Implications for Enhanced Oil Recovery. Energy & Fuels, 35 (7), 6125–6135.
3. Jha, N. K., **Ali, M**., Iglauer, S., Lebedev, M., Roshan, H., Barifcani, A., ... & Sarmadivaleh, M. (2019). Wettability alteration of quartz surface by low-salinity surfactant nanofluids at high-pressure and high-temperature conditions. Energy & Fuels, 33(8), 7062-7068.
4. Nazarahari, M. J., Manshad, A. K., **Ali, M**., Ali, J. A., Shafiei, A., Sajadi, S. M., ... & Keshavarz, A. (2021). Impact of a novel biosynthesized nanocomposite (SiO_2@ Montmorilant@ Xanthan) on wettability shift and interfacial tension: Applications for enhanced oil recovery. Fuel, 298, 120773.
5. Ali, M., Awan, F. U. R., **Ali, M**., Al-Yaseri, A., Arif, M., Sánchez-Román, M., ... & Iglauer, S. (2021). Effect of Humic Acid on CO_2-Wettability of Sandstone Formations. Journal of Colloid and Interface Science, 588, 315-325.
6. Abdulelah, H., Al-Yaseri, A., **Ali, M**., Giwelli, A., Negash, B. M., & Sarmadivaleh, M. (2021). CO_2/Basalt's Interfacial Tension and Wettability Directly from Gas Density: Implications for Carbon Geo-Sequestration. Journal of Petroleum Science and Engineering, 108683.
7. Arain, Z. U. A., Al-Anssari, S., **Ali, M**., Memon, S., Bhatti, M. A., Lagat, C., & Sarmadivaleh, M. (2020). Reversible and irreversible adsorption of bare and hybrid silica nanoparticles onto carbonate surface at reservoir condition. Petroleum, 6(3), 277-285.
8. Al-Khdheeawi, E. A., Mahdi, D. S., **Ali, M.**, Iglauer, S., & Barifcani, A. (2021). Reservoir Scale Porosity-Permeability Evolution in Sandstone due to CO_2 Geological Storage. Available at SSRN 3818887.
9. Jha, N. K., Lebedev, M., Iglauer, S., **Ali, M**., Roshan, H., Barifcani, A., ... & Sarmadivaleh, M. (2020). Pore scale investigation of low salinity surfactant nanofluid injection into oil saturated sandstone via X-ray micro-tomography. Journal of colloid and interface science, 562, 370-380.
10. Haghighi, O. M., Zargar, G., Khaksar Manshad, A., **Ali, M**., Takassi, M. A., Ali, J. A., & Keshavarz, A. (2020). Effect of environment-friendly non-ionic surfactant on interfacial tension reduction and wettability alteration; Implications for enhanced oil recovery. Energies, 13(15), 3988.

11. Awan, F. U. R., Keshavarz, A., Azhar, M. R., Akhondzadeh, H., **Ali, M**., Al-Yaseri, A., ... & Iglauer, S. (2021). Adsorption of nanoparticles on glass bead surface for enhancing proppant performance: A systematic experimental study. Journal of Molecular Liquids, 115398.

NON-RELATED JOURNAL PUBLICATIONS AS NOT PART OF THE THESIS

1. **Ali, M**., Jarni, H. H., Aftab, A., Ismail, A. R., Saady, N. M. C., Sahito, M. F., ... & Sarmadivaleh, M. (2020). Nanomaterial-Based Drilling Fluids for Exploitation of Unconventional Reservoirs: A Review. Energies, 13 (13), 3417.
2. **Ali, M**., and Aftab, A. (2020). Unconventional Reservoirs. Scholarly Community Encyclopedia, DOI: 10.32545/encyclopedia202007.0023.v3.
3. Aftab, A., **Ali, M**., Sahito, M. F., Mohanty, U. S., Jha, N. K., Akhondzadeh, H., ... & Iglauer, S. (2020). Environmental friendliness and high performance of multifunctional tween 80/ZnO-nanoparticles-added water-based drilling fluid: an experimental approach. ACS Sustainable Chemistry & Engineering, 8 (30), 11224-11243.
4. Aftab, A., **Ali, M**., Arif, M., Panhwar, S., Saady, N. M. C., Al-Khdheeawi, E. A., ... & Iglauer, S. (2020). Influence of tailor-made TiO_2/API bentonite nanocomposite on drilling mud performance: Towards enhanced drilling operations. Applied Clay Science, 199, 105862.
5. Mahesar, A. A., **Ali, M**., Shar, A. M., Memon, K. R., Mohanty, U. S., Akhondzadeh, H., ... & Keshavarz, A. (2020). Effect of Cryogenic Liquid Nitrogen on the Morphological and Petrophysical Characteristics of Tight Gas Sandstone Rocks from Kirthar Fold Belt, Indus Basin, Pakistan. Energy & Fuels, 34(11), 14548-14559.
6. Al-Rubaye, A., Al-Yaseri, A., **Ali, M**., & Mahmud, H. B. (2021). Characterization and analysis of naturally fractured gas reservoirs based on stimulated reservoir volume and petro-physical parameters. Journal of Petroleum Exploration and Production Technology, 11(2), 639-649.
7. Mahesar, A. A., Shar, A. M., **Ali, M**., Tunio, A. H., Uqailli, M. A., Mohanty, U. S., ... & Keshavarz, A. (2020). Morphological and petro physical estimation

of eocene tight carbonate formation cracking by cryogenic liquid nitrogen; a case study of Lower Indus basin, Pakistan. Journal of Petroleum Science and Engineering, 107318.

8. Memon, K. R., Mahesar, A. A., **Ali, M**., Tunio, A. H., Mohanty, U. S., Akhondzadeh, H., ... & Keshavarz, A. (2020). Influence of Cryogenic Liquid Nitrogen on Petro-Physical Characteristics of Mancos Shale: An Experimental Investigation. Energy & Fuels, 34 (2), 2160-2168.
9. Akhondzadeh, H., Keshavarz, A., Al-Yaseri, A. Z., **Ali, M**., Awan, F. U. R., Wang, X., ... & Lebedev, M. (2020). Pore-scale analysis of coal cleat network evolution through liquid nitrogen treatment: A Micro-Computed Tomography investigation. International Journal of Coal Geology, 219, 103370.
10. Awan, F. U. R., Keshavarz, A., Akhondzadeh, H., Al-Anssari, S., Al-Yaseri, A., ... **Ali, M**., & Iglauer, S. (2020). Stable Dispersion of Coal Fines during Hydraulic Fracturing Flowback in Coal Seam Gas Reservoirs—An Experimental Study. Energy & Fuels, 34 (5), 5566-5577.

RELATED CONFERENCE PUBLICATIONS AS NOT PART OF THE THESIS

1. Jha, N. K., **Ali, M**., Sarmadivaleh, M., Iglauer, S., Barifcani, A., Lebedev, M., & Sangwai, J. (2018, November). Low Salinity Surfactant Nanofluids for Enhanced CO_2 Storage Application at High Pressure and Temperature. In Fifth CO_2 Geological Storage Workshop.
2. Al-Khdheeawi, E. A., Mahdi, D. S., **Ali, M**., Fauziah, C. A., & Barifcani, A. (2020, October). Impact of Caprock Type on Geochemical Reactivity and Mineral Trapping Efficiency of CO_2. In Offshore Technology Conference Asia. Offshore Technology Conference.
3. Al-Anssari, S., Arain, Z. U. A., Shanshool, H. A., **Ali, M**., Keshavarz, A., Iglauer, S., & Sarmadivaleh, M. (2020, November). Effect of Nanoparticles on the Interfacial Tension of CO_2-Oil System at High Pressure and Temperature: An Experimental Approach. In SPE Asia Pacific Oil & Gas Conference and Exhibition. Society of Petroleum Engineers.
4. Al-Anssari, S., Arain, Z. U. A., Barifcani, A., Keshavarz, A., **Ali, M**., & Iglauer, S. (2018, November). Influence of Pressure and Temperature on CO_2-

Nanofluid Interfacial Tension: Implication for Enhanced Oil Recovery and Carbon Geo-sequestration. In Abu Dhabi International Petroleum Exhibition & Conference. Society of Petroleum Engineers.

RELATED AND NON-RELATED JOURNAL PUBLICATIONS UNDER REVIEW

1. **Ali, M**., Jha, N. K., … & Sarmadivaleh, M. (2021). An Overview of Recent Advances in CO_2 Geological Storage, Experimental Procedures and Influencing Parameters. Advances in Colloid and Interface Science, Under Review.
2. **Ali, M**., Jha, N. K., Iglauer, S., Sarmadivaleh, M. (2021). Hydrogen Wettability of Quartz Substrates Exposed to Organic Acids; Implications for Hydrogen Trapping/Storage in Sandstone Reservoirs. Journal of Petroleum Science & Engineering, Under Review.
3. **Ali, M**., Shar, A. M., Mahesar, A. A., & Al-Yaseri, A. (2021). Evaluation of Cryogenic Liquid Nitrogen Fracturing on the Development of Tight Gas Carbonate Rocks in the Lower Indus Basin, Pakistan. Fuel, Under Review.
4. Mohanty, U. S., **Ali, M**., Azhar, M. R., Al-Yaseri, A., Keshavarz, A., Iglauer, S. (2021). Recent advances in the production of syngas ($CO + H_2$) through bi-reforming of CH_4 in the presence of various catalysts: A Review. International Journal of Hydrogen Energy, Under Review.
5. Memon, S., Feng, R., **Ali, M**., … & Sarmadivaleh, M. (2021). Supercritical CO_2-Shale interaction induced natural fracture Closure: Implications for $scCO_2$ hydraulic fracturing in Shales. Fuel, Under Review.
6. Mohanty, U. S., Awan, F. U. R., **Ali, M**., Aftab, A., Keshavarz, A., Iglauer, S. (2021). Rheology of Low Salinity Zirconia Nanoparticles based Sodium Alginate Polymer Suspension for Enhanced Oil Recovery. The Canadian Journal of Chemical Engineering, Under Review.
7. Akhondzadeh, H., Keshavarz, A., Awan, F. U., **Ali, M**., … & Lebedev, M., (2021). Liquid Nitrogen Fracturing Efficiency in Different Coal Ranks Through Medical and Micro Computed Tomography. Journal of Natural Gas Science & Engineering, Under Review.

8. Al-Yaseri, A., Abdulelah, H., Yekeen, N., **Ali, M**., Zhang, Y. (2021). CO_2/Shale Interfacial Tension Directly from Fluid Density. Colloids and Surfaces A: Physicochemical and Engineering Aspects, Under Review.
9. Al-Yaseri, A., Ali, M., **Ali, M**., Taheri, R., Wolff-Boenisch, D. (2021). Western Australia Basalt-CO2-Brine Wettability at Geo-Storage Conditions; Implications for CO_2 Trapping Capacities. Journal of Colloid and Interface Science, Under Review.

CONTENTS

LIST OF FIGURES

LIST OF TABLES

LIST OF SCHEMES

Chapter 1 Overview and Thesis Objectives

1.1 Background

CO_2 storage in the geological porous media is a promising technique to mitigate the anthropogenic CO_2 greenhouse gas emissions which are proven cause of global warming (Blunt, Fayers, & Orr Jr, 1993; III, 2013), resulting in a considerable increase in the temperature of the planet earth (S. J. Davis, Caldeira, & Matthews, 2010; Karl, Melillo, Peterson, & Hassol, 2009; Solomon, Plattner, Knutti, & Friedlingstein, 2009). Based on a combined report of the National Oceanic and Atmospheric Administration and National Aeronautics and Space Administration, the average earth's temperature in the middle of the 20th century have risen by 0.99 °C (1.78 °F) in 2016 (NASA & NOAA, 2016). The rise in the earth's temperature at these elevated levels hold a direct risk to the planet species including humans. CO_2 emissions around the globe have risen dramatically from 280 ppm in 1750 to 401.5 ppm in 2017 over the timescale of two centuries (S. Davis, Williams, & Boundy, 2016; Grim, 2017; Nordhaus, 2014). There are many methods applied to diminish CO_2 emissions, including carbon-free solar panels, carbon-free wind power and CO_2 geological storage (Chu & Majumdar, 2012; Gerber, Henderson, & Makkar, 2013; Herrero et al., 2016; Lackner, 2003; Schiermeier, Tollefson, Scully, Witze, & Morton, 2008). However, from all the above methods, CO_2 geological storage has proven to be an efficient method for reducing anthropogenic greenhouse gas emissions (Lackner, 2003; Matter & Kelemen, 2009; Matter et al., 2016). Through this method, millions of tonnes of CO_2 emissions are stored globally into geological storage formations (i.e. deep saline aquifers, basaltic rocks, coal bed methane formations, tight shale formations and depleted hydrocarbon reservoirs) (Ali, Aftab, et al., 2020). The estimated CO_2 emissions throughout the world in 2020 was 36.8 billion tons, which was reduced by 2.94 billion tons (8% reduction). This reduction was the result of the forced shutdown of the global industry caused by the COVID-19 pandemic, hence resulting in the sharpest reduction of CO_2 emissions since World War II (IEA, 2020). Whereas, future estimated values for CO_2 emissions by 2050 will increase to 43.08 billion tons (Newell, Raimi, & Aldana, 2019), which depicts an alarming condition. Therefore, it is pertinent to store the vast amount of CO_2 emissions into geological formations for mitigating the damage to

climate and enhanced rise in earth's temperature (Metz, Davidson, & De Coninck, 2005; Orr, 2009).

Carbon sequestration and storage (CSS) is mainly based on capturing CO_2 from fossil burning sources (such as CO_2 emitters like fossil burning power plants) and further transporting it to the location where it can be injected into the geological storage media (destined sinks, such as deep saline aquifers and depleted hydrocarbon reservoirs) (Ali, 2018; Holloway, 2007; Stephen A Rackley, 2017). Globally, there is an abundance of these formations that can provide a long term safe storage for the permanent CO_2 immobilisation (Ali, Aftab, et al., 2020; Ali, Al-Anssari, et al., 2019; Ali, Arif, et al., 2019; Ali, Sahito, et al., 2020; Metz et al., 2005), thus mitigating enhanced rise in earth's temperature. Once CO_2 is injected into geological storage formations, it is rendered into the porous medium following various trapping mechanisms. These trapping mechanisms include structural or hydrodynamic trapping which is dominant trapping mechanism in cap-rocks and sedimentary formations (Al-Khdheeawi, Mahdi, Ali, Fauziah, & Barifcani, 2020; Ali, Aftab, et al., 2020; Arif, Al-Yaseri, Barifcani, Lebedev, & Iglauer, 2016; Arif, Barifcani, Lebedev, & Iglauer, 2016; Iglauer, Al-Yaseri, Rezaee, & Lebedev, 2015; Iglauer, Pentland, & Busch, 2015), residual or capillary trapping which is dominant trapping mechanism in sedimentary formations (Iglauer, Wülling, Pentland, Al-Mansoori, & Blunt, 2011; C. Pentland, El-Maghraby, Georgiadis, Iglauer, & Blunt, 2011), diffusion and adsorption trapping which is dominant trapping mechanism in organic shale and coal seams (Arif, Lebedev, Barifcani, & Iglauer, 2017b; Busch et al., 2008; Golding et al., 2011; Kaveh, Wolf, Ashrafizadeh, & Rudolph, 2012) and dissolution and mineral trapping which is dominant trapping mechanism in basaltic and sedimentary formations (Agartan et al., 2015; Al-Khdheeawi, Vialle, Barifcani, Sarmadivaleh, & Iglauer, 2017b; Golding et al., 2011; Iglauer, 2011; Matter et al., 2016).

Structural or hydrodynamic and residual trapping mechanisms are significantly important during the starting period (first two decades) of the CO_2 geological storage (Stefan Bachu, 2008). In the structural trapping process, injected CO_2 enters in overlying strata of low permeability (Z. Li, Dong, Li, & Huang, 2006) due to buoyancy factor and exerts force on the formation fluid and cap-rock. The behaviour of the buoyancy force is not paralleled with gravity force and displaces all volume of low

density when compared to formation fluid below the cap-rock (Mackay, 2013). Because of this, the discontinuity (due to pressure) occurs across the porous media resulting in two-phase separation causing capillary pressure. However, the difference in the density of two phases through a distance of different molecules has corresponded with the nano-pore size of reservoir rock. To understand this, Dake developed an approach and accounted for the measurement of capillary pressure using cylindrical capillary radius model (Dake, 1983), and observed that the capillary pressure which raised from the interface curvature in the cap-rock is highly uncertain because of complicated pore network morphology (Iglauer, Pentland, et al., 2015). Capillary pressure maximises when the interface between two fluids may reside in a smaller radius size of pores, indicating that structural trapping depends upon the entry of interface into small pores over capillary pressure. This phenomenon is essential in porous shale rock with very small pores resulting prevention of non-wetting fluid migration, thus mitigating CO_2 leakage (S. Krevor et al., 2015). However, the morphology of cap-rock is quite complicated when compared to the model (Dake, 1983) or capillary tubes with multiple sizes of diameter (Dullien, 1991). Therefore, different pore geometry was referred to understand the complexity of the pore system, such as the pore network model (Ebrahimi, Jamshidi, Iglauer, & Boozarjomehry, 2013), and imaging of pore space via micro CT-scan (Abdulla et al., 2020; Ramandi, Pirzada, Saydam, Arns, & Roshan, 2019). In the residual trapping mechanism, during the active injection when supercritical CO_2 plume travelled upward below the impermeable layer, it leaves the clusters of CO_2 captured in the restrained pore matrix (Garcia, Kaminska, & Mercedes Maroto-Valer, 2010). This happens mainly when capillary pressure is decreasing during the imbibition process, for instance, at the lower edge of the CO_2 plume, where the column of formation water reinvades the pore matrix formerly occupied by CO_2 (Garcia et al., 2010). This process plays an integral part in the durable security of underground CO_2 projects, as it ensures supplementary form of the trapping in conjunction with primary trapping support (structural trapping), which normally depends on the integrity of cap-rock (stratigraphic seal) to prevent CO_2 leakage. Residual entrapment is mainly controlled by two factors, wetting and capillary forces which controls the process of displacement and equilibrium state in the pore matrix. This phenomenon is mostly analyzed using capillary pressure curve relating pressure difference in wetting and non-wetting fluid and their saturation profile.

In this context, the geo-storage rock's property which measures its adhering behaviour in the surrounding of CO_2 with other aqueous fluids (such as brine in the porous media), is widely known as wettability (Arif, Abu-Khamsin, Zhang, & Iglauer, 2020; Fauziah, Al-Khdheeawi, Barifcani, & Iglauer, 2019; Iglauer, 2017; Iglauer, Al-Yaseri, et al., 2015; Iglauer, Pentland, et al., 2015). It is one of the pivotal parameter which is directly or indirectly related to determining structural and residual trapping potential. It is depicted in previous studies that less water-wet geo-storage formations are prone to reduced CO_2 storage capacities (Al-Khdheeawi, Vialle, Barifcani, Sarmadivaleh, & Iglauer, 2017a; Arif, Lebedev, Barifcani, & Iglauer, 2017a; Chaudhary et al., 2013; Iglauer, Al-Yaseri, et al., 2015; Rahman, Lebedev, Barifcani, & Iglauer, 2016). It is found in the literature that CO_2 geo-storage formations (i.e. deep saline aquifers and depleted hydrocarbon reservoirs) are typically weakly water-wet, hence, micro pores of porous media are filled with the formation water (Al-Khdheeawi, Mahdi, Ali, Iglauer, & Barifcani, 2021; A. Z. Al-Yaseri, Lebedev, Barifcani, & Iglauer, 2016; Arif, Al-Yaseri, et al., 2016; Sarmadivaleh, Al-Yaseri, & Iglauer, 2015). Hypothetically, wettability governs the ability of injected CO_2 to displace the formation water and induce below the impermeable layer (cap-rock) due to buoyancy factor causing structural trapping (Iglauer, 2017; Iglauer, Al-Yaseri, et al., 2015; Iglauer, Pentland, et al., 2015). Once CO_2 injection is stopped, the column of formation water will exert pressure back on injected CO_2 causing capillary trapping (Al-Menhali & Krevor, 2016; Iglauer, Wülling, et al., 2011; S. Krevor et al., 2015; Tokunaga & Wan, 2013). This phenomenon takes decades for its completion. However, a thorough review of CO_2 wettability of geological storage media depicts that, there are a lot of complexities to understand the wettability mechanism and its associated CO_2 trapping relative to brine/rock systems (M. Arif, S. Abu-Khamsin, & S. Iglauer, 2019a; Arif et al., 2020; Iglauer, 2017; Iglauer, Al-Yaseri, et al., 2015; Iglauer, Pentland, et al., 2015; C. Pentland et al., 2011; Rahman et al., 2016).

To understand the supercritical CO_2 behaviour in the brine/rock systems many approaches have been taken into account including relative permeability curve, capillary pressure curve, Amott Harvey Index, US Bureau of Mines (USBM) core flood method, molecular dynamic simulation, micromodel experiments and imaging techniques such as X-micro tomography or nuclear magnetic resonance to examine behaviour of wettability alteration. However, all these approaches provides indirect

wettability assessment, whereas, the best way to characterize the wettability of CO_2/brine/mineral systems is by conducting contact angle (advancing and receding contact angles on a tilted plate) experiments which provides direct quantitative wettability assessment (Al-Anssari, Barifcani, Wang, Maxim, & Iglauer, 2016; Ali, Sahito, et al., 2020; Arif, Barifcani, Lebedev, et al., 2016; Iglauer, Al-Yaseri, et al., 2015; Iglauer, Pentland, et al., 2015). Previously, many studies have depicted a comprehensive overview of CO_2-wettability dependant on various factors like pressure, temperature, salinity, formation type, surfactants and chemicals (Abbaszadeh, Shariatipour, & Ifelebuegu, 2020; Abramov, Keshavarz, & Iglauer, 2019; Al-Yaseri, Roshan, Lebedev, Barifcani, & Iglauer, 2016; Arif et al., 2019a; Chiquet, Broseta, & Thibeau, 2007; Fauziah et al., 2019; Haghighi et al., 2020; Hansen, Hamouda, & Denoyel, 2000; Iglauer, Al-Yaseri, et al., 2015; N. K. Jha, Iglauer, Barifcani, Sarmadivaleh, & Sangwai, 2019). However, mineral surfaces used in these wettability studies are chemically cleaned which can only be obtained in strongly oxidizing conditions, such as, UV-ozone or oxygen plasma atmosphere (Iglauer, Salamah, Sarmadivaleh, Liu, & Phan, 2014; Love, Estroff, Kriebel, Nuzzo, & Whitesides, 2005). Such an overview of the wettability information comprehends the quantitative analysis of the residual and structural trapping capacities in ideal situations. Whereas, real geological storage conditions are anoxic where reductive conditions succeed (Froelich et al., 1979; Townsend, Prince, & Suflita, 2003). These geo-storage formations contains dissolved organic material (Akob, Cozzarelli, Dunlap, Rowan, & Lorah, 2015; Louk et al., 2017; Lundegard & Kharaka, 1994; Stalker, Varma, Van Gent, Haworth, & Sharma, 2013), which is substantial enough to significantly alter the wettability of the CO_2/brine/rock system (Ali, 2018; M. Ali et al., 2021; Gomari & Hamouda, 2006; Iglauer, Ali, & Keshavarz, 2020). Indeed the adsorption of organic (partial mono molecular) layer on the mineral surface is competent enough to influence the wettability of the reservoir rocks (sandstone, carbonate, and cap-rock) (Adamson & Gast, 1967; Gaines, 1966; Kuhn & Möbius, 1971; Ankit Kumar et al., 2020; Maboudian & Howe, 1997; Shafrin & Zisman, 1962; Zasadzinski, Viswanathan, Madsen, Garnaes, & Schwartz, 1994). Nevertheless, these organic acid contaminations can diminish the CO_2 containment security and geo-storage capacity. Thus it is pertinent to augment threshold concentrations of organic acids and their influence on CO_2-wettability of reservoir rock to ensure optimized

conditions for CO_2 geo-storage (Al-Anssari, Arif, et al., 2018; Tosun, 2020). Additionally, many approaches have been taken to improve the wetting characteristics of oil-wet (due to the presence of organic acids) geo-storage formations, including surfactants and nanoparticles (Al-Anssari, Arif, Wang, et al., 2017a, 2017b; Al-Anssari, Arif, et al., 2018; Al-Anssari et al., 2016; N. Jha et al., 2018; N. K. Jha, Ali, et al., 2019; N. K. Jha, Iglauer, et al., 2019; N. K. Jha, Iglauer, & Sangwai, 2017; N. K. Jha et al., 2020; Nwidee, Al-Anssari, Barifcani, Sarmadivaleh, & Iglauer, 2016). However, nano-formulations have shown great potential for reversing the wettability to more water-wet conditions resulting in positive progress towards CO_2 geo-storage trapping potential (note: various nanoparticles are used depending on the type of formation) (Muhammad Ali et al., 2021; Ali, Sahito, et al., 2020). In a nutshell, viability of CO_2-underground storage process can be better improved with both concerns such as optimization of wettability of reservoir rock through nano-fluid interaction and augmenting the effects of organic acids on the geological storage potential. Thus, in present work, influence of various organic acids and their threshold concentrations (which are commonly dissolved in hydrocarbon traces) and nanoparticles are discussed on various types of geo-storage formations (like, sandstone, carbonate and cap-rock) for determining the CO_2 geo-storage potential. This information will be useful for the reservoir models which calculates the CO_2 geo-storage capacities to account for the thresholds of organic acids and nano-fluids. So that an accurate decision can be made for the reduced uncertainty and CO_2 geo-storage project's feasibility.

1.2 Motivation

Since the last past decade, several studies have been documented to encounter the diversified behaviour of wettability alteration such as transformation of wettability from highly oil-wet system to water-wet system in underground CO_2 storage conditions (Al-Anssari, Arif, et al., 2018; N. Jha et al., 2018). However, significant uncertainties and complexities in the measurement of the contact angle indicated that taking one contact angle from the published literature can be proven to high error. Researchers observed a high deviation in the prediction of capillary scaling during hydrophilic interactions which was described by variation in wettability from water-

wet to mixed-wet systems of supercritical CO_2 (Al-Menhali & Krevor, 2017; Singh, Bijeljic, & Blunt, 2016). Moreover, the silica surface occurred partially de-wetting while measuring the wettability of CO_2/brine (Fauziah et al., 2019). Experimental studies have examined the effect of pressure, temperature, salinity and formation type on the wettability alteration, however, the effect of organic traces (which are the major component of realistic geo-storage formations) along with the influence of nanomaterials in the presence of organic acids on the CO_2-wettability have not been reported yet (Abbaszadeh et al., 2020; Jing, Yang, & Tang, 2021). Thus, there is a need to investigate the effect of organic traces on the wettability of reservoir rocks containing mineral (such as calcite, mica, and quartz) at which CO_2 geo-storage capacities are considerably affected. As well as, the process of CO_2 storage enhancement via nano-fluid interactions.

1.3 Objectives

This work is aimed to achieve comprehensive information on the CO_2-wettability variation of sedimentary rocks due to the effect of organic acids and nanomaterials. Based on the above background and motivation, the objectives given below are set for this research:

1. To examine the influence of various organic acids (hexanoic acid, lauric acid, stearic acid, and lignoceric acid) on the wettability of various rock/CO_2/brine systems as a function of acid concentration at ambient and carbon sequestration conditions.
2. To determine the influence of various nano-fluid (Silica and Alumina nanoparticles) concentrations on reversal of wettability to more water-wet for various nano-fluid/CO_2/brine systems as a function of nano concentration at ambient and carbon sequestration conditions.
3. To analyze the above information for determining the thresholds of organic acids and nano-concentrations responsible for wettability shift, which in return will help to better understand their effects on the ability of CO_2 to distribute across the geo-storage formation.

1.4 Thesis Organization

This thesis contains five chapters and is divided as below:

Chapter 1 provides the introduction and relative summary of background to the CO_2 geo-storage potential and relative influencing factors.

Chapter 2 provides in detail background for the CO_2 storage behaviour, trapping mechanisms, their governing factors, previous studies and a summary of current work.

Chapter 3 comprises three published articles that have documented systematic examination of various organic acids (hexanoic acid C_6, lauric acid $C_{12,}$ stearic acid C_{18} and lignoceric acid C_{24}) and their associated concentrations (10^{-2} to 10^{-10} mol/L) on the wettability alteration of geo-storage formations (carbonate, sandstone and cap-rock) at variable geo-storage temperature and pressure conditions.

Chapter 4 comprises two published articles that provides the information on the analysis of wettability reversal (at variable geo-storage pressure and temperature conditions) from hydrophobic to hydrophilic conditions due to the various nano-fluid interactions (silica and alumina nanoparticles) at various concentrations (0.05 wt%, 0.1 wt%, 0.25 wt% and 0.75 wt%) in the presence of various organic acids (hexanoic acid C_6, lauric acid $C_{12,}$ stearic acid C_{18} and lignoceric acid C_{24}) for various geo-storage formations (sandstone and cap-rock).

Chapter 5 provides the conclusion and recommendations for future research work. Figure 1-1 illustrates the pictorial view of the thesis layout in detail.

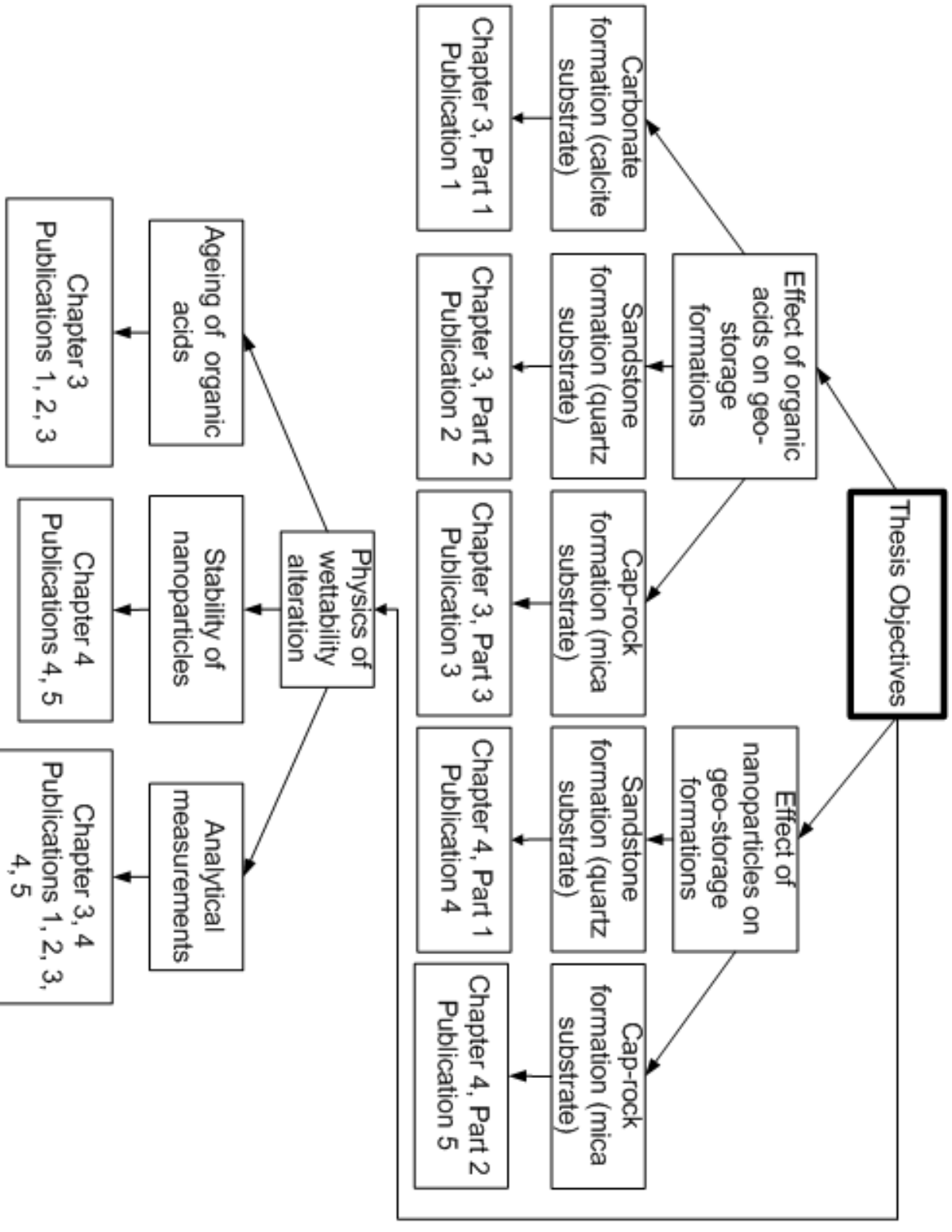

Figure 1-1 Thesis Layout

Chapter 2 Literature Review

2.1 Introduction

This chapter provides a review on the importance of CO_2 storage and environmental problems caused by CO_2 emissions (a greenhouse gas). The possible options for underground CO_2 storage are discussed using carbon sequestration and storage (CSS) in deep saline aquifers and depleted hydrocarbon reservoirs. Underground CO_2 storage has been highly influenced by the wetting characteristics of the rock-forming minerals which governs the capability of CO_2 to dispense through the geo-storage formation, and it also governs CO_2 injection flow rates, properties and dynamics of the fluid flow across the formation, containment security and underground CO_2 project's certainty (Akhondzadeh et al., 2020; Iglauer, 2017; Iglauer, Al-Yaseri, et al., 2015; Iglauer, Pentland, et al., 2015). The wetting characteristics of the geo-storage formations are directly responsible for determining the structural and residual trapping capacities of CO_2 (Al-Khdheeawi et al., 2017a; Al-Menhali & Krevor, 2016; Iglauer, Al-Yaseri, et al., 2015; Iglauer, Pentland, et al., 2015; Rahman et al., 2016) and it has been found that wettability has indirect effect on dissolution and minerals trapping capacities (Agartan et al., 2015; Al-Khdheeawi et al., 2017a, 2017b; Al-Khdheeawi, Vialle, Barifcani, Sarmadivaleh, & Iglauer, 2017; Iglauer, 2011). Wettability is a pertinent parameter that is very intricate and to augment this influence one should ruminate all characteristics at realistic underground conditions. Therefore we have critically analysed the most fundamental factors and gaps to the current knowledge in the context of underground CO_2 storage. This chapter initially focuses on supercritical CO_2 behaviour and its operational principles and storage options with global statics of CO_2 geological storage projects. Thereafter, trapping mechanisms are evaluated which are responsible for the long term immobilization of CO_2 in underground formations. Afterwards, experimental techniques to determine the wettability of the rock/fluid system are discussed to emphasize the importance of advancing and receding contact angles about structural and residual trapping capacities. Further, effects of realistic geo-storage conditions such as temperature, pressure, variable salinity, and formation type on the wettability alteration of the reservoir rock is provided forming a basis for technical evaluation. Next, the focus has been shifted to examine the effects of organic

acids which are normally found in the depleted hydrocarbon reservoirs or deep saline aquifers and have a significant impact on the wettability shift. Finally, the effects of nanomaterial on the optimization and alteration of the wettability of the CO_2/brine/mineral system have been discussed.

2.2 Climate Protection and CO_2 Storage

The oxidation of fossil fuels (i.e. crude oil, natural gas and coal) are the main cause of anthropogenic CO_2 emissions, with an estimated value of 30 billion tons per year (Administration, 2011). The change in climate temperature due to CO_2 emissions is defined by the term (the carbon-climate response), which is the ratio between cumulative CO_2 emissions to increase in temperature. It is estimated that climate temperature rise by 1.0 – 2.1 °C per 3600 billion tons of CO_2 emissions (Matthews, Gillett, Stott, & Zickfeld, 2009). However, the natural carbon cycle consumes a portion of CO_2 emissions from climate which includes terrestrial vegetation and oceans beds. Whereas, a large portion of CO_2 emissions remain untouched. CO_2 is recognized as the largest contributor to greenhouse gas emissions which is 65% (Hussain et al., 2019)**.** CO_2 storage is considered environmentally friendly and operationally feasible practice to cut high-cost pathway for the protection of the environment; controlling the global warming below 2 °C by the end of the 21st century (W. Huang, Chen, & Anandarajah, 2017; Klutse et al., 2018; Meinshausen et al., 2009). Scholars believed that deforestation and the release of toxic chemicals in flora and fauna ended 2020 with unprecedented challenges (medical, economic, social and environmental) that has caused global warming (Chahal, 2020; Toquero, 2020). However, it was found that two important factors such as an increase in temperature due to CO_2 emissions may have promoted the viral problems (Aguilar et al., 2015). Additionally, researchers found that this has caused the infection in the living organisms resulting in growth in pathogens. Thus, investigators are working together to minimize the effect of CO_2 by storing it in underground formations for mitigating climate change via CSS (Kalam et al., 2020). Nevertheless, this technique is not implemented at the adequate scale where it is needed, owing to its commercial, economic, and technical challenges. Thus, scholars are focusing to balance commercial, policies, environmental and scientific priorities via CO_2 sequestration in

underground reservoirs, or its utilization for enhanced oil recovery (EOR) (Ampomah et al., 2016).

2.3 Underground CO_2 Behaviour

CO_2 is a very important component of our atmosphere and its environmental concentration usually ranges up to 350 ppm (Rosenberg, 1981). CO_2 is a non-toxic, colourless, odourless, and non-flammable gas (X. Zhang, Xiao, Zhou, & Tang, 2014). Figure 2-1 illustrated the typical phase behaviour of CO_2 relative to change in temperature and pressure in the underground system. CO_2 can change its phases into solid, liquid, gas, and supercritical conditions at a prevailing temperature and pressure conditions. Typically, CO_2 keep gases state (below 0.5MPa) and further change into liquid state above this pressure. CO_2 can coexist in three different states at 56.56 °C and 0.5 MPa (Ali, 2018), which is called the triple point. However, at 31.10 °C and 7.38 MPa, a critical point occurs in CO_2 phase behaviour (H. Zheng, Zhong, Mao, & Zheng, 2018). Above these pressure and temperature conditions, CO_2 changes in a dense liquid state which is commonly referred to as a supercritical fluid state (Ingrosso & Ruiz-López, 2017; Rao, Bao, Liu, Taylor, & Liao, 2020). Thus, supercritical CO_2 establishes the behaviour of both gases and liquid phases (Budisa & Schulze-Makuch, 2014). Therefore, it is used in supercritical form for the oil and gas industry applications (i.e. CO_2 storage and enhanced oil recovery) (Al-Bayati, Saeedi, Myers, White, & Xie, 2019; Blunt et al., 1993; Godec, Kuuskraa, & Dipietro, 2013; Qin et al., 2020).

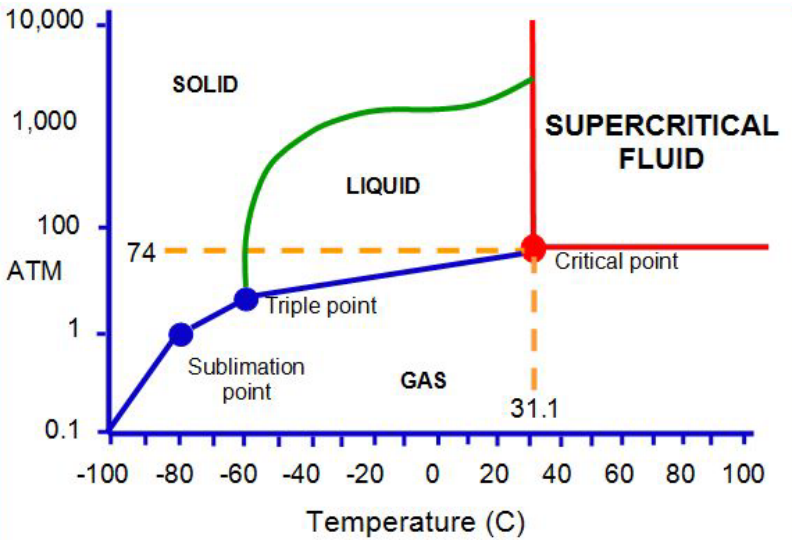

Figure 2-1 Phase diagram of CO_2, adapted from (King & Bott, 2012).

2.4 Carbon Sequestration and Geo-Storage

CSS is considered the most attractive technique to capture CO_2 emissions (greenhouse gas) from both stationary (power plants) and non-stationary (automobiles) sources and introduce it in the geological rock for sustainable environmental growth and CO_2 storage durability (Nunes, Meireles, Pinto Gomes, & Almeida Ribeiro, 2020; Reddy, Gopakumar, & Chetri, 2019; Tang et al., 2020). The CO_2 emissions from stationary sources are estimated at approximately 13 billion tons per years and non-stationary sources are estimated at approximately 2.5 billion tons per year (Administration, 2011). The other CO_2 emissions are sourced from chemical processes for the formation of cement and steel, but their portion to cumulative values are minor (Boden, Marland, & Andres, 1995).

The main aim of this process is to protect the environment from anthropogenic CO_2 release which is responsible for climate change (Hinkle, Hargett, & Bailon, 2017; Nunes et al., 2020), and global warming (Hinkle et al., 2017; Hussain et al., 2019). Figure 2-2 IEA presents future forecast to mitigate the CO_2 emission into the environment (dell'energia, 2010).

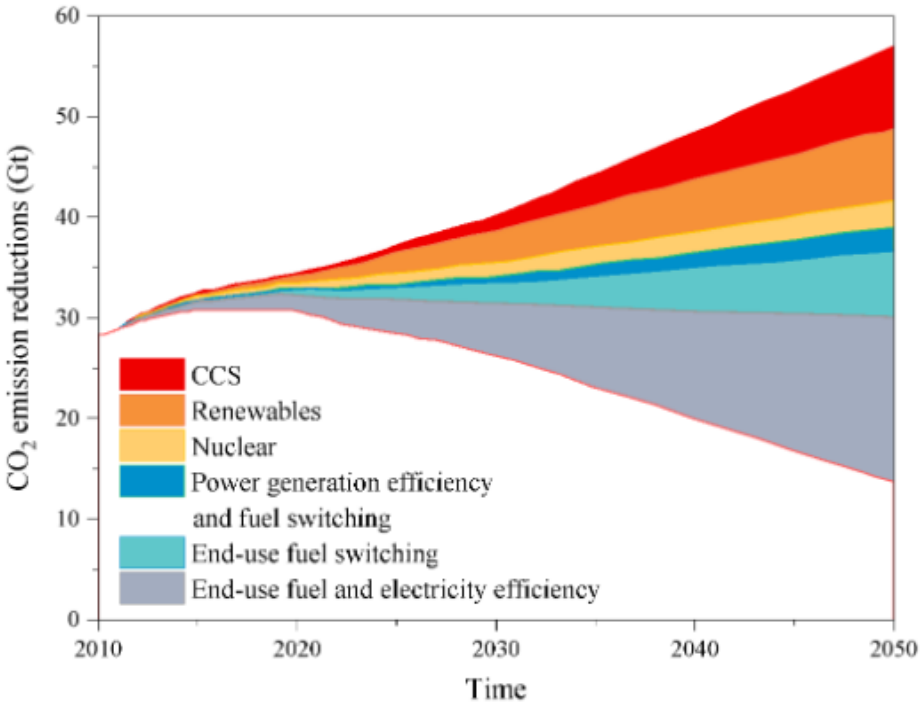

Figure 2-2 IEA unveils the technologies that will be used for mitigation of CO_2, adapted from (dell'energia, 2010).

2.4.1 CSS Operational Principle

CO_2 capture and storage process are mainly divided into four different types such as i) capturing of CO_2 ii) compressing of CO_2 iii) transporting of CO_2 and iv) Injecting of CO_2 (Porrostami, Zahedi Amiri, & Etemad, 2020; Sahle, Saito, Fürst, & Yeshitela, 2018). Initially, CO_2 is captured from big CO_2 stationary sources, for example, power generation plants, chemical processing plants, coal-fired based plants, and several other carbon emitters (like automobiles). These all sources are responsible for producing 30 billion tons of CO_2 into our environment and thereafter natural carbon cycles and other mechanisms remove about half of produced CO_2 and the remaining half, which is 15 billion tons remain in our environment, which is the main cause of global warming (the annual growth in CO_2 release is around 2 ppm) (Lemonnier & Ainsworth, 2018). CO_2 Capturing technique is typically based on the pre-combustion, oxyfuel combustion and post-combustion capture (Porrostami et al., 2020; Sahle et al., 2018). Then, CO_2 (captured) is compressed using high-pressure compressors (with an operational capacity of more than 10 MPa). Thereafter, compressed CO_2 is transported to storage location via pipelines and cargo ships. The transportation of CO_2 is considered safe due to its non-flammable nature when compared to natural gas (Xu et al., 2018). Finally, compressed CO_2 is injected into underground formations at adequate injection parameters (for example rate of injection and injection pressure) for permanent immobilization. The overall flow process of CSS is illustrated in Figure 2-3. These parameters depend on the petro-physical properties, and physiochemical properties of the geological rock which are determined through careful screening (via pilot and simulated experimental trials) (Berger, Yoksoulian, Freiburg, Butler, & Roy, 2019; Plaisant, Maiu, Maggio, & Pettinau, 2017).

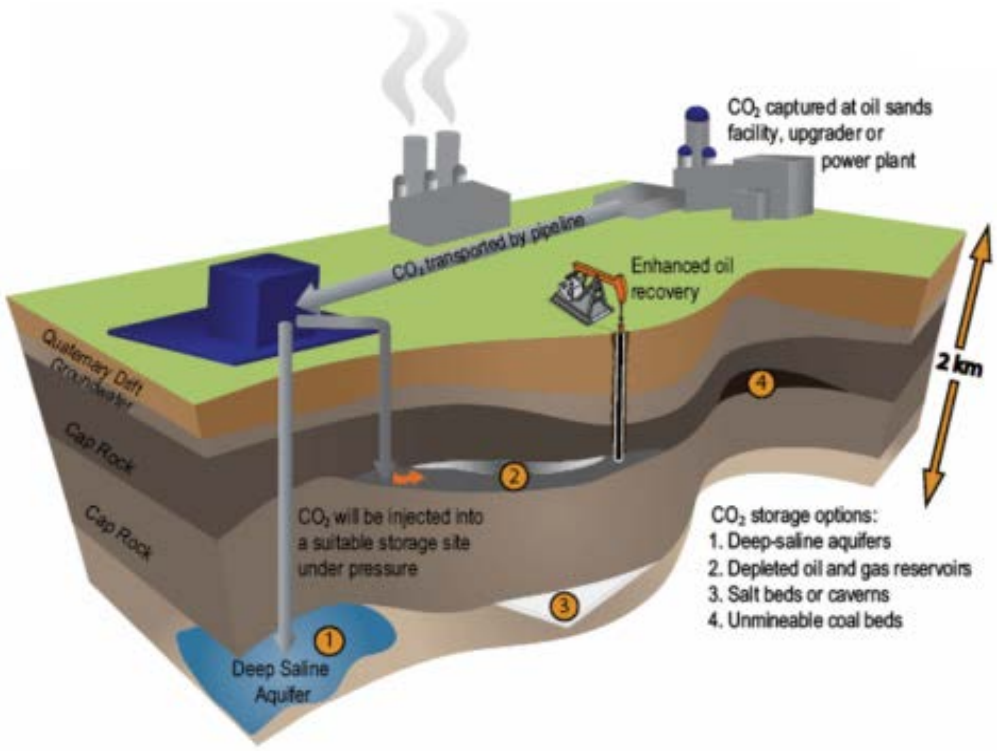

Figure 2-3 Carbon sequestration and storage mechanism, adapted from (Zhou, He, Romankiewicz, & Fridley, 2015).

2.4.2 Global CCS Project Developments

Globally, CO_2 injection is primarily used in the EOR process. It was first started from Permian Basin (in West Texas) and adjacent premises (south New Mexico) which comprises an area of 190,000 km^2 (Wilcox, 2012). Presently, there are more than 51 CSS projects are scheduled to be operational throughout the world Table 2-1. However, merely 19 CO_2 underground storage projects are currently operational. As per data published in a report, it is estimated that CSS has the potential to mitigate 19% of total CO_2 emissions by 2050 (dell'energia, 2010). Nevertheless, serious efforts are needed in CSS projects for improving their safety and economic liability. Further, public willingness is essential for the implementation of the field scale CSS projects, which can be obtained by continuous government support. Table 2-1 provides 48 years of large scale data for the CO_2 projects. CO_2 has been majorly stored in the saline aquifers compared to other geological storage formations (Mac Dowell, Fennell, Shah, & Maitland, 2017). Around half of CO_2 geo-storage projects have been scheduled for EOR projects (Mac Dowell et al., 2017). However, CO_2 is not adequately mixed with hydrocarbons and traces of organic acids present in the geo-storage formation may

result in a complex behaviour of rock wettability preventing permanent immobilization of CO_2 in the depleted hydrocarbon reservoirs and deep saline aquifers (Ali, Arif, et al., 2019; Ali, Sahito, et al., 2020).

Table 2-1 CCS projects data from 1972 to 2020's end, adapted from (C. Cao et al., 2020).

Strategy	Saline Aquifer	Under Evaluation	Depleted Gas Reservoirs	EOR	Total
Project quantity	21	24	3	3	51
Average capture capacity (Mtpa)	1.92–4.05	1.75–1.81	2.5–2.83	2.7–2.87	1.92–2.86
Capture capacity (Mtpa)	40.35–85.1	42.11–43.41	7.5–8.5	8.1–8.6	98.06–145.61

Importantly, there are five commercial CO_2 sequestration projects (In Salah CO_2 project, Gorgon CO_2 project, Sleipner CO_2 project, Snøhvit CO_2 project, and Weyburn CO_2 project) which are currently operational and are considered the world's largest projects. Table 2-2 explains in detail the project location, storage capacity, formation type, and phase development.

Table 2-2 Largest CO_2 storage projects worldwide, adapted from (Metz et al., 2005).

Project	Storage formation	CO_2 stored (M tons/year)	Project phase
In Salah (Algeria)	Sandstone formation (onshore)	1	Risk assessment stage and Monitoring
Gorgon (Australia)	Sandstone saline aquifer (onshore)	4	Not available
Sleipner (Norway)	Sandstone saline aquifer (offshore)	1	Modelling and monitoring stage
Snøhvit (Norway)	Sandstone saline aquifer (offshore)	0.7	Not available
Weyburn (Canada)	Carbonate formation (onshore)	1.7	Risk assessment, performance assessment, and monitoring,

2.4.3 Geological CO_2 Storage Media

Carbon capture and storage provide an appropriate option for the removal of CO_2 from the atmosphere via permanent immobilization in underground geological storage formations (Ajayi, Awolayo, Gomes, Parra, & Hu, 2019). The major CO_2 sinks are categorized in various types of geological formations such as; depleted and existing hydrocarbon reservoirs (for EOR process) (Blunt et al., 1993; Metz et al., 2005), deep saline aquifers (Ali, Aftab, et al., 2020; Ali, Al-Anssari, et al., 2019; Ali, Arif, et al., 2019; Ji & Zhu, 2015), basaltic rocks (Ahmed Al-Yaseri & Jha, 2021; Matter, Takahashi, & Goldberg, 2007), coal seams (Su, Liang, Zou, Niu, & Li, 2019; Viete & Ranjith, 2006) and organic-rich shales (Arif, Lebedev, et al., 2017b; Kang, Fathi, Ambrose, Akkutlu, & Sigal, 2011).

Deep saline aquifers, depleted and existing hydrocarbon reservoir rocks (oil and gas) are considered as major potential CO_2 storage media. Both storage media have the vast capacity of storing CO_2 and are abundantly present throughout the world (Ali, Aftab, et al., 2020; Blunt et al., 1993). The amount of CO_2 that can be stored in both formations may comprise more than 50% of the total accumulated underground CO_2 storage capacity. These geological formations are typically either sandstone or carbonate rocks (M. Arif, S. A. Abu-Khamsin, & S. Iglauer, 2019b). Carbonate rocks are considered as highly permeable and provide ease for large amount of CO_2 injection when compared to sandstone rocks which have low permeability (Durand, 2005). Whereas, the cap-rock which provides a seal to trap buoyant CO_2 for preventing capillary leakage is typically shale (Arif, Al-Yaseri, et al., 2016; Arif, Barifcani, Lebedev, et al., 2016). Globally, the Intergovernmental Panel on climate change (IPCC) information shows that hydrocarbon reservoirs can store between 675 (lower estimate) to 900 billion tons of CO_2 (upper estimate). Whereas, saline aquifers has between 1,000 to 100,000 billion tons of estimated CO_2 storage capacity (Durand, 2005; Metz et al., 2005). In addition to these, basaltic rocks have recently shown great potential for storing CO_2 in mineralized form by a process called CarbFix. In this process, CO_2 and water are injected together in basalt formations, which causes a rapid chemical reaction for storing CO_2 in carbonized form (Gislason & Oelkers, 2014). An advantage of this process is that it does not require concentrated CO_2 while injection which can store up to 100 kg of CO_2 in a cubic meter area of basalt (Gíslason,

Sigurdardóttir, Aradóttir, & Oelkers, 2018). Further, organic-rich shales is another adequate candidate for permanent immobilization of CO_2. These geological formations are widely known as low porous impermeable sedimentary rocks with the ability to store a substantial amount of CO_2 (Kang et al., 2011). In these formations, CO_2 is permanently trapped in an adsorbed state within exceptionally distributed organic matter, such as kerogen. Finally, coal seam reservoirs have also depicted them as promising candidate for storing CO_2 in deep and un-minable coal seams for the application of enhanced coal bed methane recovery (Su et al., 2019; Viete & Ranjith, 2006). In coal seam reservoirs CO_2 can exist in three different scenarios, 1) pore matrix filled with free CO_2, 2) CO_2 dissolution in pore matrix's liquid, 3) gas trapped as adsorbate on a coal surface. However, not all porous mediums can be suited for permanent storage of CO_2, some may lack the proper storage environment, cap-rock seal or trapping mechanism. In that context, physical trapping of gas may prevail or may create a free gas-cap which may not provide long-term storage potential.

2.5 CO_2 Trapping Mechanisms in Geological Storage Media

In carbon geo-storage locations, the pertinent hazard is the leakage of CO_2 through artificial (e.g. wells) or natural (e.g. fractures, faults) ways to the environment (Al-Rubaye, Al-Yaseri, Ali, & Mahmud, 2021; Dahraj, Ali, & Khan, 2016). This is due to the buoyant nature of CO_2 which flows in the upward direction in any given storage conditions (Iglauer, Pentland, et al., 2015). However, keeping the nano to micropore size specifications in the geological formations, CO_2 is preferred to be injected in a supercritical phase. The supercritical state of CO_2 may have the ability to vary its phase relative to physiochemical conditions. To restrict upward migration and leakage of CO_2, various physiochemical trapping mechanisms have been investigated. These trapping mechanisms include structural or hydrodynamic trapping (in sandstone, carbonate, and cap-rock formations) (Ali, Aftab, et al., 2020; Arif, Al-Yaseri, et al., 2016; Arif, Barifcani, Lebedev, et al., 2016; Iglauer, Al-Yaseri, et al., 2015; Iglauer, Pentland, et al., 2015), capillary or residual trapping (in carbonate, and sandstone formations) (M. Ali et al., 2021; Iglauer, Wülling, et al., 2011; C. Pentland et al., 2011), mineral and dissolution trapping (in carbonate, sandstone, and basaltic formations) (Agartan et al., 2015; Al-Khdheeawi et al., 2020; Al-Khdheeawi et al.,

2017b; Gislason & Oelkers, 2014; Iglauer, 2011), adsorption and diffusion trapping (in organic-rich shales, clay interlayers, and coal seams) (Busch et al., 2008; Golding et al., 2011; Kang et al., 2011; Kaveh et al., 2012; Su et al., 2019). It requires a thorough investigation of different physiochemical interactions and complexities to select feasible storage formation for ensuring the containment security of the above trapping mechanisms for mitigating the upward CO_2 movement.

2.5.1 Structural (Hydrodynamic) Trapping of CO_2

Structural (hydrodynamic) trapping can be referred to as the trapping of CO_2 either in the form of supercritical fluid or gas beneath the cap-rock (impermeable rock), which has larger capillary entry pressure than buoyancy force of CO_2 (Iglauer, Pentland, et al., 2015). When CO_2 gas is injected into the geological storage formation it exerts pressure on the aqueous phase (brine) and free CO_2 moves upward due to the density differences between the formation fluids in the reservoir. This upward movement of CO_2 is credited to the difference between capillary forces (the force which retains CO_2 in the pore matrix) and buoyancy forces (the force which supports upward movement) (D. Zhang & Song, 2014). This upward movement of CO_2 is not paralleled with gravity forces and displaces all volume of lower density when compared to formation fluid below the cap-rock (Mackay, 2013), trapping itself structurally. This physical trapping may have both lateral and vertical seals (Iglauer, Al-Yaseri, et al., 2015) and also known as structural/stratigraphic or hydrodynamic trapping. This process is very pivotal for any storage location to mitigate CO_2 leakage via cap-rock during the first decade while other trapping mechanisms come into effect (Stefan Bachu, Gunter, & Perkins, 1994).

For the structural trapping process, the efficiency of the trapping mechanism is measured using structural information of the sedimentary basin. This provides detailed information regarding the location of high and low permeability strata that has a complicated plumbing system, which influence the fluid flow control throughout the basin. There are several types of stratigraphic and structural traps or a combination of both which are used for the physical trapping of CO_2. Traditional structural traps have anticline folds or sealed fault blocks as illustrated in Figure 2-4 (a and b).

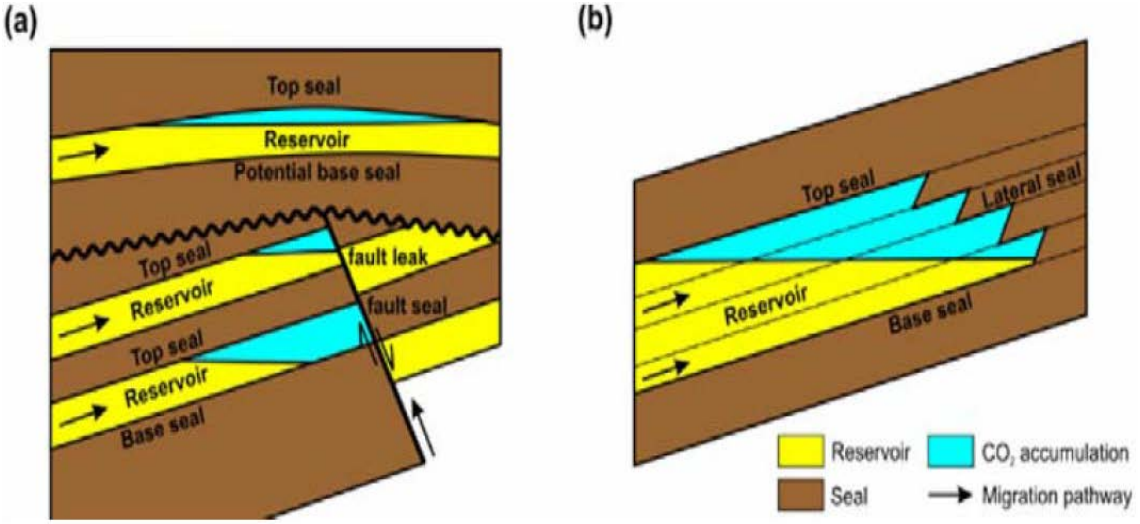

Figure 2-4 (a) structural trapping (b) stratigraphic trapping for the storage of CO_2, adapted from (D. Zhang & Song, 2014).

Stratigraphic or structural traps are commonly found in geological formations which contained oil and gas for millions of years. In such geological formations, the storing capacity is certainly based on pore space volume. Hydrodynamic trapping systems are mostly found in sedimentary basins (saline aquifers) that have significantly poor flow rates. CO_2 injected in these deep structural traps can take millions of years to flow back to the surface (due to buoyancy forces) and discharge back into the atmosphere. For this trapping mechanism, the storing capacity of the rock is affected by the formation permeability and absolute porosity (Gunter, Bachu, & Benson, 2004). Nevertheless, the CO_2 storage by structural mechanism is mainly based on the sealing potential of the cap-rock, posing a great challenge to select the appropriate location (Song & Zhang, 2013).

2.5.2 Residual Trapping of CO_2

During CO_2 injection in the geological formation, it exerts the pressure and relocates the formation water (brine) in a co-current way. Once injection of CO_2 is paused, due to differences in the density of brine and CO_2, the brine column exerts the back pressure and fluids start to flow in a counter-current way resulting in upward flow of CO_2 and downward flow of brine (Y. Zhang, Kogure, Nishizawa, & Xue, 2017). Consequently, the wetting fluid (such as brine) reinvades in the pore matrix formerly

occupied by CO_2 (Garcia et al., 2010). In such a mechanism, the brine pushes CO_2, thus a considerable volume of CO_2 becomes trapped in small clusters of porous media, Figure 2-5. Hence, separated CO_2 becomes trapped for permanent immobilization, known as residual trapping (Iglauer et al., 2019). Fundamentally, once the non-wetting phase is isolated in the narrow and small pore spaces, it remains captured by capillarity for permanent immobilization. The residual trapping mechanism thwarts a huge journey of the CO_2 in the subsurface, diminishing the chance of upward CO_2 movement and coincidental delivery to groundwater or the atmosphere. This mechanism separates the moderately enormous continuous CO_2 (subcritical) plume into numerous little ganglia with bigger surface region to volume proportions, encouraging long-term disintegration and precipitation response, which further improves trapping security (Sun et al., 2020).

Various trial contemplates have been directed to explore immiscible CO_2 (subcritical) flow and residual catching conduct at the pore-to-core (for example µm to cm) scale inside porous geological storage media. For example, 2D micromodels (Gunning, Ennis-King, LaForce, Jenkins, & Paterson, 2020; Kazemifar, Blois, Kyritsis, & Christensen, 2016), sandstones (Ali, Sahito, et al., 2020; Rushton, Wagner, Pearce, Rochelle, & Purser, 2020), sand packs (Chaturvedi & Sharma, 2020; Gauteplass et al., 2020), shales (Goodman et al., 2020; W. Li, Zhang, Nan, Pang, & Jin, 2020), and carbonates (Snippe, Berg, Ganga, Brussee, & Gdanski, 2020; Walspurger, Cobden, Safonova, Wu, & Anthony, 2010). In addition to this, simulation work has been conducted to determine the capillary trapping capacities in geological storage formations (Al-Khdheeawi et al., 2017a; Al-Khdheeawi et al., 2017). For this, two major approaches have been utilized for investigating the residual trapping capacities (S. C. Krevor, Pini, Zuo, & Benson, 2012).

1. Measurement of relative permeability data.
2. Measurement of capillary pressure curve and gas saturation profile.

Through these observations, it was observed that residual trapping can significantly prevent the movement of CO_2 resulting in a high volume of CO_2 being trapped in geological formations (Iglauer, Pentland, et al., 2015; Ruprecht, Pini, Falta, Benson, & Murdoch, 2014). It was also observed that heterogeneity, injection rate, and the ratio

of viscous forces to the gravity forces, have a significant effect on the immobilized fraction of CO_2. Thus, increasing the ratio of viscous to gravity forces and injection rate will improve the sweeping behaviour, consequently, providing a significant enhancement in CO_2 residual trapping capacities (Rezk, Foroozesh, Zivar, & Mumtaz, 2019).

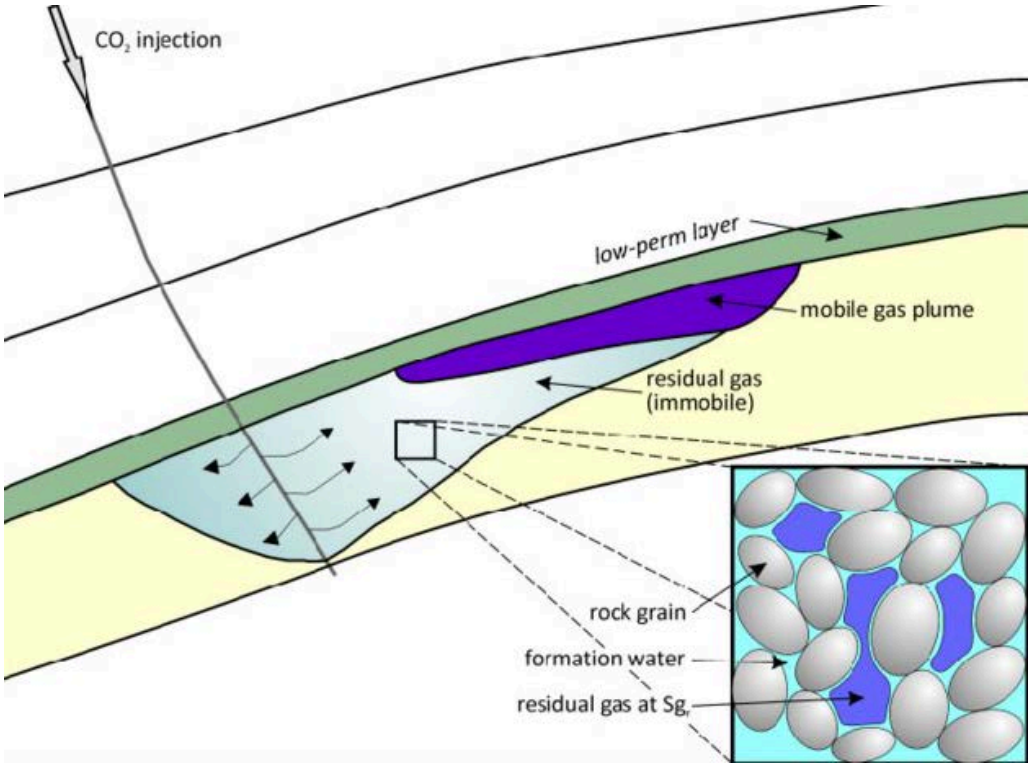

Figure 2-5 Schematic of the entrapped CO_2 in the small clusters of porous media, adapted from (Juanes, Spiteri, Orr Jr, & Blunt, 2006).

2.5.3 Solubility (Dissolution) Trapping of CO_2

Dissolution of CO_2 in the formation fluid is commonly referred to as solubility trapping (W. Li, Nan, Zhang, You, & Jin, 2020). Importantly, after CO_2 injection, it travels upward to interface between cap-rock and reservoir and thereafter laterally distribute under the cape rock (such as shale) as a distinct phase (Figure 2-6). Afterwards, CO_2 will come in contact with the hydrocarbons (in depleted oil reservoirs) and formation brine (in deep saline aquifers) resulting in the mass transfer due to CO_2 dissolution in the formation fluids. This process will continue until the equilibrium state is achieved, thereby improving the residual and structural trapping capacities (Ali, 2018; Gutiérrez & Lizaga, 2016). CO_2 solubility in formation fluid is

based on temperature, pressure, and salinity of the formation brine (Chang, Coats, & Nolen, 1996). The dissolution of CO_2 in formation water is caused by molecular diffusion at the interface of formation water and the free gas phase. However, the CO_2 dissolution process is very lengthy due to the smaller molecular diffusion coefficient. It is believed that it may take thousands of years for CO_2 to be dissolved in the formation water completely (Lindeberg & Wessel-Berg, 1997).

When CO_2 dissolve in the formation brine due to the molecular diffusion, it will slightly increase the density of the formation water. It is shown from previous studies that CO_2 dissolution will bring up the density of formation brine by 1% compared to the normal formation water (S Bachu & Adams, 2003; Ajitabh Kumar et al., 2004). Thereby making it heavier, which will trigger the downward flow of formation brine due to the gravity forces. Such a process will further improve the mixing of formation brine and CO_2, causing diffusion mechanism at a rapid scale, resulting in high dissolution of CO_2. This process provides two main benefits such as minimizing the upward movement of CO_2 and improving the storing capacity of the geological formation. (Ajayi et al., 2019; W. Zhang et al., 2009; J. Zheng, Chong, Qureshi, & Linga, 2020).

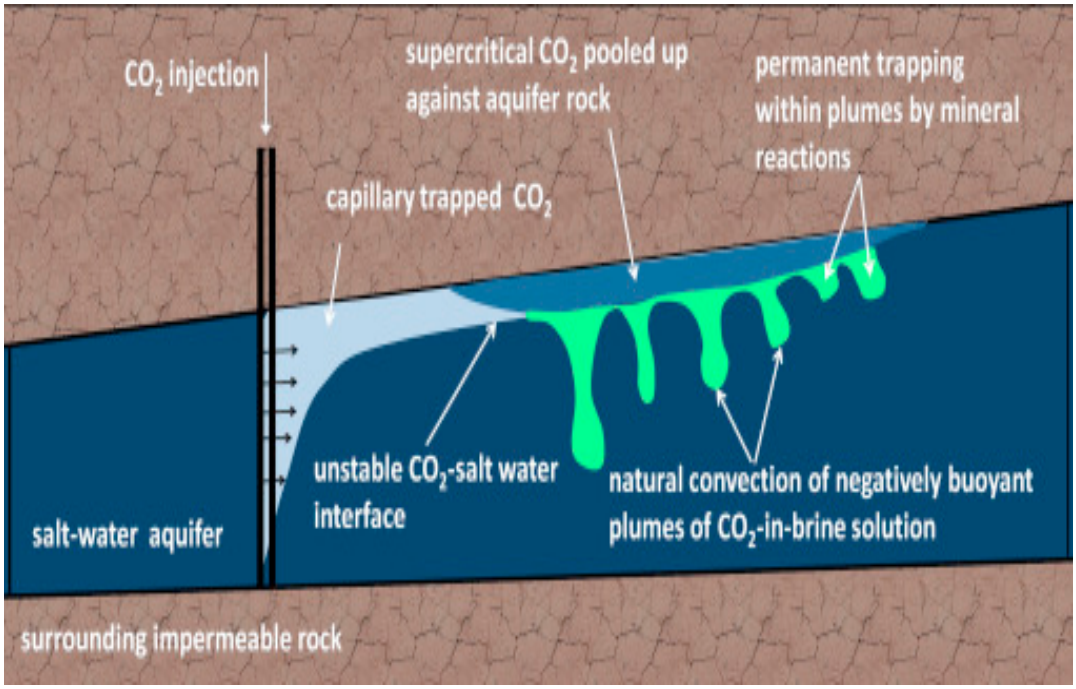

Figure 2-6 Injected CO_2 moves up-dip to develop interface and laterally distributed under the cape rock (such as shale) as a distinct phase, adapted from (Riaz & Cinar, 2014).

2.5.4 Mineral Trapping of CO_2

When CO_2 incorporate in a stable mineral phase via various reactions with different organic matters and minerals in the geological storage formation is called minerals trapping (D. Zhang & Song, 2014). On a geological time scale, dissolution of CO_2 will occur in formation waters initiating different geochemical reactions, forming a weak carbonic acid (Equations 2-1 to 2-2).

$$CO_2 + H_2O \longleftrightarrow H_2CO_3 \qquad \text{equation (2-1)}$$

$$H_2CO_3 \longleftrightarrow H^+ + HCO_3^- \qquad \text{equation (2-2)}$$

Thereafter, an increase in acidity will dissolve primary host rock mineral forming dissolved cations with the bicarbonate ions (Equation 2-3).

$$CaCO_3 + H^+ \longleftrightarrow Ca^{2+} + HCO_3^- \qquad \text{equation (2-3)}$$

Thereafter, dissolved bicarbonate ions will react with divalent cations (mainly Ca^{2+}, Fe^{2+}, and Mg^{2+}), forming precipitation of carbonaceous minerals (Ding, Xi, Jiang, & Liu, 2018) (Equations 2-4 to 2-6).

$$Ca^{2+} + HCO_3^- \longleftrightarrow CaCO_3(s) + H^+ \qquad \text{equation (2-4)}$$

$$Mg^{2+} + HCO_3^- \longleftrightarrow MgCO_3(s) + H^+ \qquad \text{equation (2-5)}$$

$$Fe^{2+} + HCO_3^- \longleftrightarrow FeCO_3(s) + H^+ \qquad \text{equation (2-6)}$$

This process will contain CO_2 in the form of carbonate mineral and will aid other trapping mechanisms for permanent immobilization of CO_2. However, these chemical reactions are highly dependent upon hydrogeology, mineralogy and structure of the formation (Rochelle, Czernichowski-Lauriol, & Milodowski, 2004). Therefore, it is better suited for CO_2 storage to select those geological formations which contains divalent cations (Ca^{2+}, Fe^{2+}, and Mg^{2+}) for mineral trapping purposes.

Pearce et al., have examined the drilled core samples and found the variation in the mineralogy of the rock samples which were exposed to CO_2 (J. Pearce, Underschultz, & La Croix, 2019). It was observed that natural chlorite and plagioclase formed ankerite and siderite after interaction with CO_2 (Figure 2-7 a to b). This process is well-matched with the natural system which is highly saturated with CO_2. The mineral

trapping and alternation in the porous media may provide an adequate environment for CO_2 storage (Figure 2-7 b, c and d).

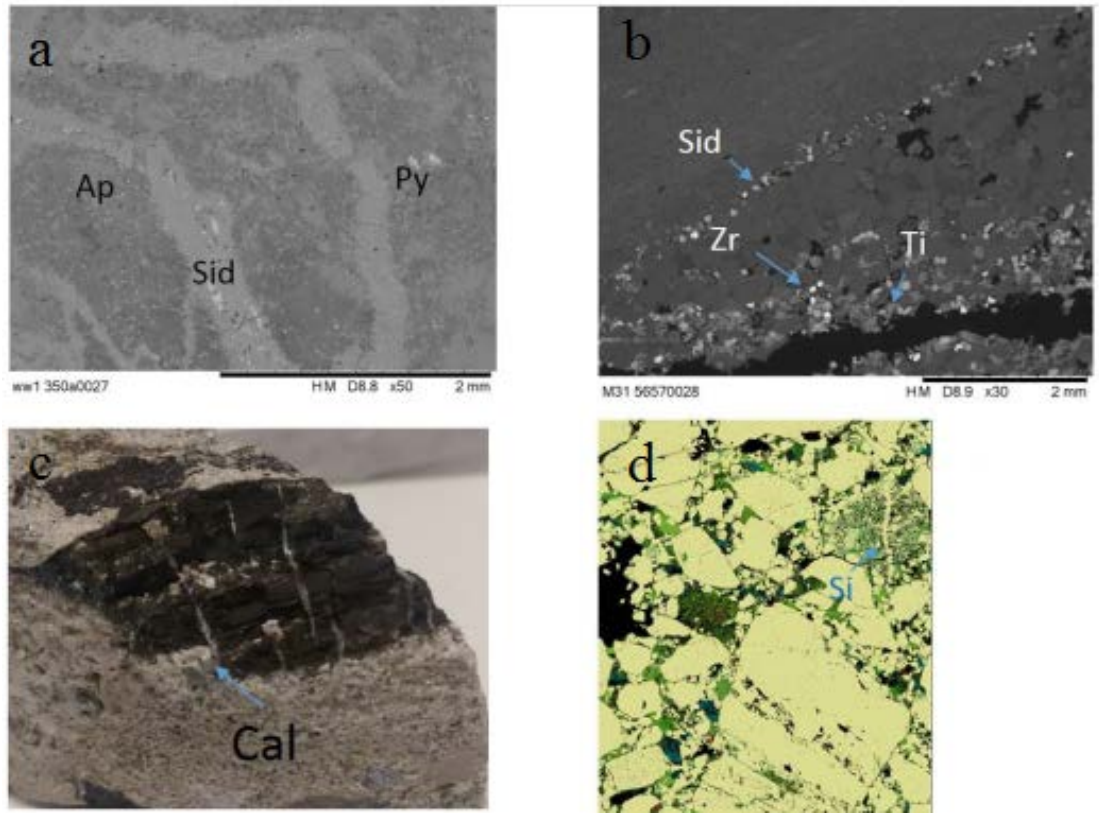

Figure 2-7 Process of natural fractures and mineral trapping in core samples of the well (Wandon), (a) seal rock (b, c and d) transition zone, Abbreviations: Apatite = Ap, Cement Ti-oxide = Ti, Calcite = Cal, Silica cement = Si, and Siderite = Sid, adapted from (J. Pearce et al., 2019).

Table 2-3 provides the minerals that are usually engaged with mineral trapping responses, including the sub-atomic weight, specific gravity limit, and possible load of CO_2 that is fixed by response with 1 m^3 to 1 kg of mineral. The second piece of the table records the connected response items.

Table 2-3 Mineral trapping and its reaction products, adapted from (Stephen A. Rackley, 2017).

CO_2 potential fixed					
Reactants minerals	Formula	Sp. gravity	Mol. weight	Kg/m^3 mineral	Kg/Kg mineral
Wollastonite	$CaSiO_3$	2.9–3.1	116.2	1140	0.38
Diopside	$MgCaSi_2O_6$	3.3–3.6	216.6	1400	0.41
Fayalite	Fe_2SiO_4	4.39	203.8	1890	0.43
Forsterite	Mg_2SiO_4	3.2–3.3	140.7	2020	0.62
Products of reaction					
Anhydrite	$CaSO_4$		Chalcedony	SiO_2	
Siderite	$FeCO_3$		Alunite	$KAl_3(OH)_6(SO_4)_2$	
Magnesite	$MgCO_3$		Ankerite	$CaMg_{0.3}Fe_{0.7}(CO_3)_2$	
Calcite	$CaCO_3$		Dawsonite	$NaAlCO_3(OH)_2$	

Regardless of whether these particles stay in the solution for the more extended term, or add to mineral trapping responses, will highly rely upon brine water pH and ionic loading, as demonstrated schematically in Figure 2-8.

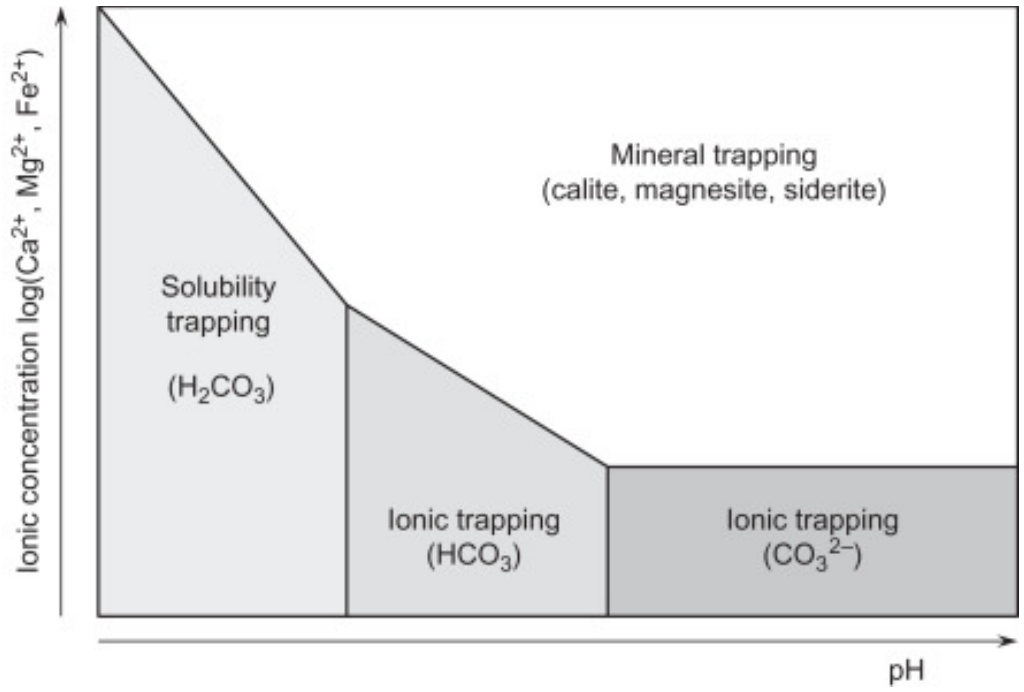

Figure 2-8 Dependencies of geochemical trapping on pH, adapted from (Stephen A. Rackley, 2017).

2.6 Application of Rock Wettability for CO_2 Geo-Storage Formation

CO_2 geological storage formations comprises a three-phase system that contains a non-aqueous phase liquid (NAPL) and an aqueous phase liquid (APL), which are denoted by hydrophobic and hydrophilic terminology, respectively. This terminology is used for the aqueous phase to cover the deep pore matrix (as hydrophilic) and non-aqueous phase to not cover (as hydrophobic) (Ali, Aftab, et al., 2020; Muhammad Ali et al., 2021; Ali, Sahito, et al., 2020). Wettability has a direct and strong impact on the crucial parameters such as, interfacial areas of the fluids and morphology (Iglauer, Fernø, Shearing, & Blunt, 2012; Christopher Holst Pentland, Iglauer, Gharbi, Okada, & Suekane, 2012), relative permeability (McCaffery & Bennion, 1974; Morrow, 1990), residual non-aqueous phase saturation (Chaudhary et al., 2013; Jadhunandan & Morrow, 1995; Morrow, 1990; Christopher H Pentland, El-Maghraby, Iglauer, & Blunt, 2011), and aqueous phase saturation (S_w) and capillary pressure (P_c) relationship ($S_w[P_c]$) which controls the ability of the reservoir fluids to statically distribute in buoyancy-capillary equilibrium force (E. C. Donaldson & Alam, 2013; Jackson, Valvatne, & Blunt, 2005). Therefore, it is of utmost importance to investigate the wettability in detail despite greater physiochemical complications. In CSS applications, wettability is directly responsible for the CO_2 distribution across the geo-storage formation and governs containment security, residual and structural trapping potential, fluid dynamics and injection rates. It is also indirectly responsible for mineral and dissolution trapping potential (via liquid-mineral and liquid-liquid interfaces). Thus, wettability should be investigated in a sufficient manner for accurate storage potential estimations and risk assessment.

Wettability can be defined as a fundamental surface property that is impacted by dynamic intermolecular interactions and controls the capability and relative attraction of one fluid on the solid surface in the presence of another fluid (G. P. De, 1985). When CO_2 is injected into geological storage formations, three immiscible phases, for instance, aqueous phase (brine), non-aqueous phase (supercritical CO_2 – $ScCO_2$), and rock formation intermingle with each other. In this scenario, the influence of three interfacial force tensions (γ) come into consideration; the interfacial force field between liquid and fluid (in this case brine and $ScCO_2$), and one of each liquid or fluid and the rock surface (for example, calcite represents the clean carbonate geological

formation). In this example, three different forces are induced by three different interfacial tensions acting in separate directions (Figure 2-9). These all interfacial forces are acting at the same time (assuming in the absence of all other external forces such as buoyancy and viscous forces) resulting in the final force which governs the precise fluid formation on the rock surface, and is calculated by the contact angle (θ), as depicted in Figure 2-9. The value of contact angle (θ) can be determined between 0°-180° and is completely derived due to intermolecular force balance as expressed by Young's equation (2-7).

$$\cos\theta = \gamma_{SL} - \gamma_{SF} / \gamma_{LF} \qquad \text{equation (2-7)}$$

Where, θ is the contact angle derived due to intermolecular force balance, γ is the interfacial tension force for the solid-liquid (mineral-brine) (SL), solid-fluid (mineral-$ScCO_2$) (SF), and liquid-fluid (brine-$ScCO_2$) (LF) interfaces, respectively. It is found from previous studies that γ_{LF} is experimentally derived which is the function of liquid-fluid intermolecular interactions and is influenced by geo-storage thermos-physical conditions (like temperature and pressure) (Al-Anssari, Arain, et al., 2018; Arif, Al-Yaseri, et al., 2016; Iglauer, Mathew, & Bresme, 2012; Sarmadivaleh et al., 2015). However, the other two interfacial tensions (γ_{SL} and γ_{SF}) cannot be measured (Butt, Graf, & Kappl, 2006) and can only be estimated via theoretical and indirect calculations like semi-empirical equations and molecular dynamic simulation (Good & Girifalco, 1960). Therefore, the contact angle (θ) from equation 2-7 cannot be calculated but requires experimental investigation.

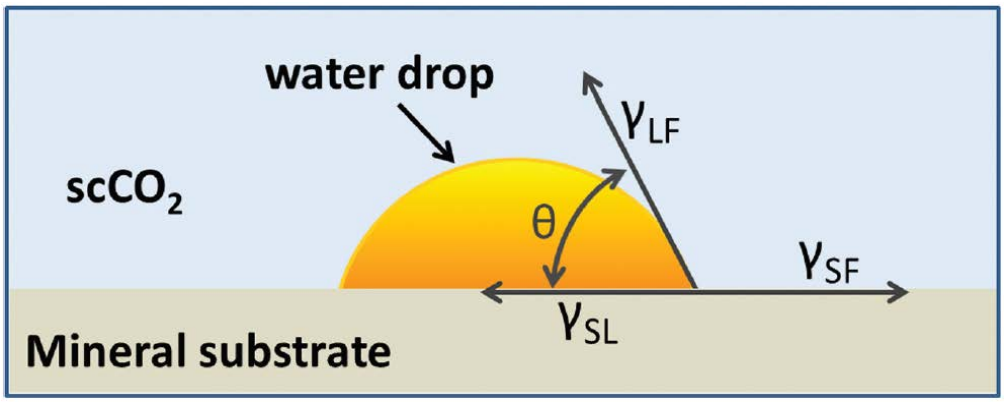

Figure 2-9 Three interfacial force tensions acting on a water drop on a rock surface in the presence of supercritical CO_2, adapted from (Iglauer, Pentland, et al., 2015).

Furthermore, this section also discusses the wettability (contact angle, θ) in detail, and how it behave in various thermos-physical conditions, liquid-fluid systems, and geo-storage formations. In the CSS context, wettability is directly related to structural and residual trapping capacities of geo-storage formation, which depends on the idea that upward movement of CO_2 can be retained via enough strength of capillary forces in subsurface formation (Arif et al., 2019b). These capillary forces are dependent on contact angle (θ) between rock-brine-CO_2 and non-wetting (CO_2) and wetting (formation brine) phase interfacial tension (γ), as shown in the below equations.

$$P_c = P_{CO2} - P_{water} \qquad \text{equation (2-8)}$$

$$\frac{2\gamma Cos(\theta)}{R} \qquad \text{equation (2-9)}$$

Where P_c = capillary pressure, Pco_2 = rock non-wetting phase pressure, P_{water} = rock wetting phase pressure, γ = interfacial forces between water and CO_2, R = radius of largest pore throat and θ = contact angle. Once CO_2 is injected into the geo-storage formation it displaces the wetting phase (formation water), which is related to receding contact angle (note: this assumption is based on the ideal pore matrix for determining the first approximation, however, in real situations pore matrix also plays a crucial role) (Broseta, Tonnet, & Shah, 2012; Iglauer, 2018; Iglauer, Al-Yaseri, et al., 2015). In CO_2-wet systems when the receding contact angle (θ_r) is more than 90° (note in equation 2-9, where $\cos\theta(90°) = 0$), capillary leakage can occur due to upward suction force in cap-rock causing a significant decrease in structural trapping. Thereafter, once CO_2 injection is stopped, the wetting phase (formation brine) will reinvade the pore matrix which is previously occupied by clusters of CO_2, this phenomenon is related to advancing contact angle ($\theta_{a)}$, where primary drainage is not affected by wettability if ($\theta_{a)}$ is less than 50° (Chiquet et al., 2007; Rahman et al., 2016). This process is crucial for providing containment security via additional trapping support called residual trapping. The classification of wettability in geo-storage formations is well defined by (Iglauer, Pentland, et al., 2015), where the rock is highly water-wet when the contact angle is smaller than 50°, poorly water-wet is ranging between 50° to 70°, and intermediate-water wet is raging between 70° to 110°. The wettability system transform into poorly CO_2-wet when the contact angle is ranging between 110° to 130°, highly CO_2-wet when contact angle range is between 130° to 180° and

completely non-wetting when contact angle is = 180°. All these classifications are physically proven on the rock-brine-mineral surfaces (Iglauer, 2017; Sarmadivaleh et al., 2015).

2.7 Wettability Determination Using Various Approaches

It is one of the pertinent factor to determine the wettability in CO_2 geo-storage calculations. Various direct (quantitative) and indirect (qualitative) methods have evolved for the classification of wettability in a given rock-fluid system at various thermos-physical geo-storage conditions. For instance, relative permeability and capillary pressure curve determination by typical core flooding (material balance method) (Haghighi et al., 2020), nuclear magnetic resonance imaging (wettability shift method using NMR technique) (Looyestijn, 2008), X-ray computed tomography (X-ray CT) (MacAllister, Miller, Graham, & Yang, 1993) and micro-computed tomography (μCT) imaging (dynamic saturation profile method) (Idowu et al., 2015) and interpreted via US Bureau of Mines (USBM) (E. C. Donaldson, Thomas, & Lorenz, 1969) and Amott-Harvey index (W. Anderson, 1986) can provide wettability assessment at macroscopic and microscopic level. In addition to this, 2-D micro models are used as a representative of geo-storage formations for determining the wetting characteristics at pore-scale in brine-CO_2 systems at high pressure and high-temperature conditions (Chalbaud et al., 2009). Molecular dynamics simulations are also used for CO_2-water interfaces at various thermos-physical geo-storage conditions (Iglauer, Mathew, et al., 2012). However, above all methods only provide indirect qualitative assessment of wettability and contact angle method is the only method which is used to determine direct quantitative wettability assessment (Ali, 2018; Lander, Siewierski, Brittain, & Vogler, 1993).

2.7.1 Wettability Determination Using Direct Quantitative Approaches

Direct quantitative assessment of wettability (via contact angle) in a given rock-fluid system is widely accepted (Al-Anssari et al., 2016; Ali, Sahito, et al., 2020; Arif, Barifcani, Lebedev, et al., 2016; Iglauer, Al-Yaseri, et al., 2015; Iglauer, Pentland, et al., 2015). This method involves several configurations for measuring the contact

angle, however, gas bubble (captive bubble), pendant drop (sessile drop) and tilted plate (advancing and receding contact angles) methods are mostly used in the oil and gas industry (Sarmadivaleh et al., 2015). In these methods, an IFT cell (goniometric cell) is used which is made of Stainless Steel or Hastelloy material (in case of CO_2). This IFT cell can sustain high temperature (up to 433 °K) and high pressure (up to 70 MPa) and contains a sample holder. The IFT cell is connected with two high precision syringe pumps supplying gas and fluid, the heating mechanism (for providing high temperature) and a mixing reactor (for providing equilibrium between gas and liquid). This mechanism offers a direct quantitative measurement of wettability on a rock substrate (Al-Anssari et al., 2016; Ali, Arif, et al., 2019; M. Ali et al., 2021). However, these methods are only used in the presence of rock-mineral substrates and pure fluids (Ahmed Al-Yaseri et al., 2015; Arif, Al-Yaseri, et al., 2016). Furthermore, this mechanism can conduct contact angle measurement at a wide variety of geo-storage conditions and thus, provides the wettability investigation as a function of salinity, surface roughness, ageing, temperature and pressure.

In a pendant drop (sessile drop) method for a typical CO_2-brine-mineral system, initially high precision syringe pumps are filled with CO_2 and brine (salinity can differ based on reservoir condition) at geo-storage conditions (note: syringe pumps used in this system can control the flow rate and pressure, i.e. Teledyne ISCO, Model D-500, pressure accuracy of 0.1%). The temperature of high precision syringe pumps is controlled by heating baths (i.e. heating bath model 900F, from Julabo). Thereafter, high precision syringe pumps are used to inject CO_2 and brine at high pressure and high temperature (HPHT) conditions in a mixing reactor (i.e. Parr mixing reactor, volume 500 ml) which already contains mineral substrates. These fluids are mixed at 1200 RPM for 1 hour with mineral substrates at (HPHT) until live brine is formed and equilibrium conditions are achieved. This equilibrium is important for avoiding mass transfer of brine and CO_2 during contact angle measurements on minerals substrates (El-Maghraby, Pentland, Iglauer, & Blunt, 2012). Afterwards, live brine is transferred to a high precision syringe pump and a clean mineral or polished rock surface is placed onto the sample holder followed by tightly closing the IFT cell. Thereafter, CO_2 is gradually introduced via a high precision syringe pump in an IFT cell until reservoir (HPHT) conditions are met. The temperature of the IFT cell is controlled via different mechanism like heating tape and controller (i.e. Model No. HTC101-002 from Omega

Company). Once the IFT cell is full with CO_2, a droplet (mean drop size was 4.5 µL (± 0.6 µL)) of live brine is introduced from another high precision syringe pump on the mineral substrate surrounded by CO_2 at HPHT conditions. Newly developed contact angle systems are equipped with high-performance video camera (i.e. Fujinon CCTV lens: HF35HA-1B; 1:1.6/35 mm, frame rate = 71 fps; pixel size = 7.4 µm; Basler SCA 640–70 fm) and contact angle interpreting software (like ImageJ), which are used to video record the complete procedure and to interpret the images for the measurement of contact angle, respectively. A schematic of the HPHT contact angle system is depicted in Figure 2-10.

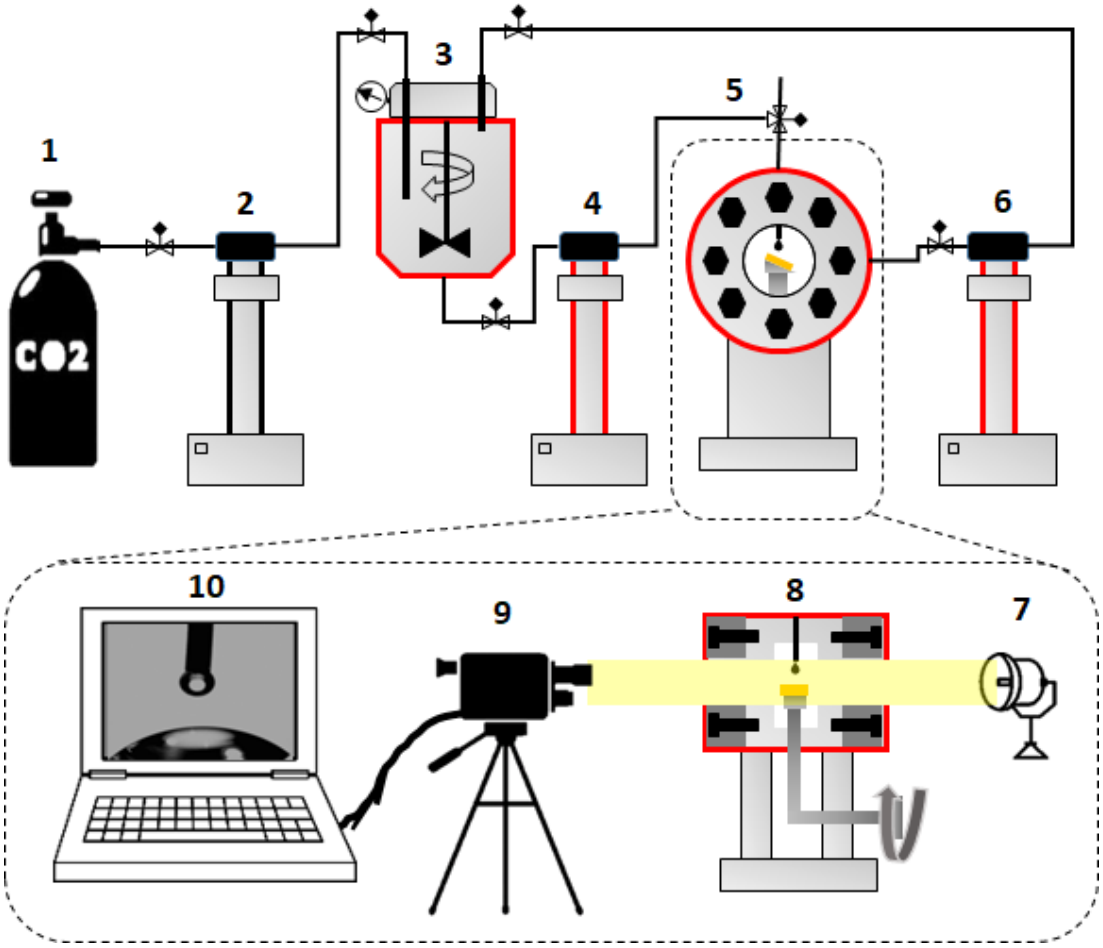

Figure 2-10 Schematic of HPHT contact angle system (1) CO_2 supply (2) high precision syringe pump for CO_2 (3) mixing reactor (4) high precision syringe pump for brine (5) IFT cell with sample holder, front view (6) high precision syringe pump for back pressure (7) brightness from light (8) IFT cell with sample holder, side view (9) video camera for recording the procedure (10) contact angle interpretation software, adapted from (Muhammad Ali et al., 2021).

However, other contact angle measurement configurations are almost the same with little variations in the method. For example, in the gas bubble (captive bubble) method, instead of liquid drop, a CO_2 bubble is dispensed from below the mineral substrate, whereas, IFT cell is filled with live brine at geo-storage conditions (HPHT). Similarly, in a tilted plate contact angle method, the IFT cell contains a sample holder in a tilted position and a droplet of live brine forms two angles (advancing and receding) at the leading and trailing corners of the droplet (Lander et al., 1993). Typically, receding contact angles are lesser than advancing contact angles and the difference between these angles lies due to the phenomenon called wettability hysteresis, which ranges between 5° to 20°. The wettability hysteresis is the function of different variables such as adsorption/absorption of molecules on reactive surfaces, structural or chemical heterogeneity, and surface roughness (Carré, Gastel, & Shanahan, 1996; Eral & Oh, 2013; Neumann & Good, 1972). An illustration of the wettability (contact angle) hysteresis is depicted in Figure 2-11.

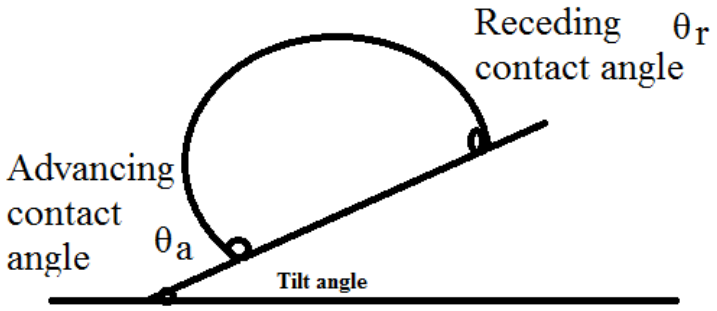

Figure 2-11 Wettability hysteresis.

2.8 Influencing Parameters on CO_2 Wettability in Ideal Geo-Storage Conditions

The parameters which impact CO_2 wettability in a given rock-fluid system for clean minerals or polished rock surfaces include geo-storage thermos-physical conditions [for instance, temperature (Abbaszadeh et al., 2020; Hamouda & Rezaei Gomari, 2006; Jing et al., 2021) and pressure (A. Z. Al-Yaseri et al., 2016; Fauziah et al., 2019; Hansen et al., 2000)], composition of brine in geo-storage formation (A. Z. Al-Yaseri et al., 2016; Arif, Barifcani, & Iglauer, 2016; Arif, Barifcani, Lebedev, et al., 2016; Saraji, Piri, & Goual, 2014), surface roughness (A. Z. Al-Yaseri et al., 2016; Marmur,

2006), and formation heterogeneity (Arif, Barifcani, & Iglauer, 2016). It is shown in previous studies that pressure has substantial effect on CO_2-wettability via shifting it towards more CO_2-wet conditions irrespective of formation type or wetting characteristics (A. Z. Al-Yaseri et al., 2016; Arif, Al-Yaseri, et al., 2016; Arif, Lebedev, et al., 2017a; Fauziah et al., 2019; Hansen et al., 2000; Sarmadivaleh et al., 2015), however, some studies have depicted little or no effect on contact angle due to the increase in pressure (Espinoza & Santamarina, 2010; Farokhpoor, Bjørkvik, Lindeberg, & Torsæter, 2013; Mills, Riazi, & Sohrabi, 2011). Whereas, temperature behaves differently in different formations, for instance, contact angle increase with the increase in temperature in sandstone formations (quartz mineral substrates) (Sarmadivaleh et al., 2015) and it decreases with the increase in temperature in carbonate (calcite mineral substrate) (Arif, Lebedev, et al., 2017a) or cap-rock (mica substrates) formations (Arif, Al-Yaseri, et al., 2016). Wetting characteristics have also shown different behaviour for the temperature, for example, contact angle decreases in hydrophobic dolomite with the increase in temperature and contact angle increases in hydrophilic dolomite with increase in temperature (AZ Al-Yaseri et al., 2017). Whereas, several other studies have also shown contradiction in this perspective (Al-Anssari, Arain, et al., 2018; Fauziah et al., 2019; Lu, Najafabadi, & Firoozabadi, 2017; D. Yang, Gu, & Tontiwachwuthikul, 2008). The composition of formation brine differs substantially in different geo-storage formations, however, the influence of salinity to contact angle has shown mixed behaviour, where some studies have shown that with the increase in salinity contact angle also increases (A. Z. Al-Yaseri et al., 2016; Iglauer, Pentland, et al., 2015), whereas, some studies have shown little or no effect in contact angle due to change in salinity (Mujahid Ali et al., 2021). In addition to this, geo-storage formation contains the mixture of monovalent ions (i.e. NaCl and KCl) and divalent cations (i.e. $CaCl_2$ and $MgCl_2$), where it is reported in previous studies that both salinities negatively affected hydrophilic surfaces, whereas, divalent cations compare to the monovalent ions affect more on the contact angle, owing to the cation screening effect (A. Z. Al-Yaseri et al., 2016; Iglauer, 2017). Another crucial parameter that impact the contact angle is the surface roughness of the rock mineral, therefore, mineral surfaces are polished before conducting contact angle measurements. This parameter can be denoted in various forms like roughness ratio (rs) (Tudek et al., 2017), or route mean square (RMS) (Mahesar, Ali, et al., 2020; Mahesar, Shar, et al., 2020; Memon et al., 2020), and can be measured via atomic

force microscopy (AFM). The effect of surface roughness on contact angle differs based on wetting characteristics, for instance, contact angle decreases in hydrophilic surfaces (calcite or quartz) with the increase in surface roughness and contrary to that, contact angle increases in hydrophobic surfaces with the increase in surface roughness (A. Z. Al-Yaseri et al., 2016; Arif, Lebedev, et al., 2017a). Moreover, contact angle studies comprises of various experimental techniques that can have substantial influence on wettability studies, for example, presence of surface contaminations (i.e. organic acids), equilibrium procedure of fluids, and substrate cleaning procedure (Ali, Aftab, et al., 2020; Ali, Al-Anssari, et al., 2019; Ali, Arif, et al., 2019). In addition to this, use of different chemicals and surfactants may also substantially change the surface coverage of the substrates, which in return will significantly affect the wetting behaviour of various minerals (Iglauer, 2017).

Arif et al., examined the CO_2/brine/rock system through measurement of contact angles (advancing and receding contact angle) relative to influencing factors like variable temperature (298 K to 343 K), pressure (0.1 MPa to 20 Mpa), surface roughness (contains minerals, shale and coal seams) and salinity (0 to 20 NaCl wt%) (Arif, Jones, Barifcani, & Iglauer, 2017). Additionally, the influence of both surface interfacial tension and wettability associated alteration were analysed relative to the principle of trapping mechanism (Iglauer, 2017). It was observed that with an increase in the pressure and salinity, both receding/advancing contact angles progressed. Further, it was indicated that the rock surface established significant de-wetting (less wet to water) when pressure was increased. In contrast to this, salinity de-wets the rock system very little. It was found that calcite illustrated slightly CO_2-wet behaviour however mica was intermediate-wet at 308 K and 20 MPa resulting considerable reduction in the geological storage potential of CO_2. Nevertheless, the extend of wettability variation increases relative to pressure is greater when compared to temperature resulting in the concept that the rock system becomes non-wetting relative to the depth (Arif, Barifcani, & Iglauer, 2016). Additionally, it was investigated that through information of variation in the wettability of the minerals (rock-forming such as mica and calcite) that high temperature, low salinity and low pressure are favourable factors for the underground geological storage of CO_2. In another study by Arif et al., it was depicted that total organic content (TOC) in shale formation have significant impact on the de-wetting of cap-rock. It was found that low/total organic content

(low/TOC) shale was water-wet, and high TOC shale was observed less water-wet (Arif, Lebedev, et al., 2017b). Thus, based on the wettability information low TOC shale was considered an adequate choice for CO_2 storage. Nevertheless, the effect of wettability enhancement on these formations have been rarely discussed in the real geo-storage conditions, which are anoxic (contain organic molecules), where reductive conditions succeed (Froelich et al., 1979; Townsend et al., 2003).

2.9 Presence of Organic Acids in Geo-Storage Formations

Since the advent of modern analytical methods like mass spectroscopy (MS) and gas chromatography (GC), research scientists have depicted a great geochemical interest in the separation of organic acids (carboxylic or fatty acids) from crude oil stream since the late 1960s (Kvenvolden, 1967). The occurrence of these fatty acids (recognizable fossils) have been found in numerous geological formations ranging from Precambrian age (before the development of geological formations) to recent age (Akob et al., 2015; Kvenvolden, 1967; Lundegard & Kharaka, 1994). The presence of organic acids in geological formations is hypothesized as possible ancestors for the development of hydrocarbons due to the presence of organics in biological substances, and similar molecular structure (Caballero, Trugo, & Finglas, 2003; Kvenvolden, 1967). These organic acids may comprise unsaturated straight-chain and branched-chain fatty acids and saturated straight chain monocarboxylic and dicarboxylic fatty acids (Lundegard & Kharaka, 1994; Waples, 1981). Many researchers have experimentally proved the presence of minute concentrations of organic acids in CO_2 geo-storage formations (i.e. deep saline aquifers) due to diagenesis of organic matter and fossil biodegradation (Akob et al., 2015; Bennett, Siegel, Baedecker, & Hult, 1993; Jones et al., 2008).

Lundegard et al., 1994 have found the abundance of monocarboxylic fatty acids in Cenozoic sedimentary basins, where, short-chain fatty acids (i.e. acetate) were commonly present between 80 °C to 140 °C (Lundegard & Kharaka, 1994). He has also depicted that organic acid anion concentrations in these geological formations were less than 3000 mg/L (note this is a very high concentration). He has further depicted that alkalinity of geological formation waters have the dominance of bicarbonate at temperatures less than 80 °C and more than 140 °C, whereas, in

Miocene reservoirs, organic alkalinity dominates the bicarbonate alkalinity. It was also discussed in this research that dicarboxylic acids are rarely found in geological formations, where, succinate and methyl-succinate are the most abundant dicarboxylic acids at concentrations less than 100 mg/L. Similarly, Akob et al., 2015 have conducted a detailed study on microbiology and composition of organic matter from Pennsylvania shale gas wells. He found that these geological formations have an abundance of organic acid anions (i.e. formate, pyruvate, and acetate) due to microbial activity ranging from (66-9400 cells/mL) (Akob et al., 2015).

Watson et al., 2002 have conducted an experimental study on hydrocarbon biodegradation in the laboratory, where he found significant production of organic acids ranging from (C_{10} to C_{20}) (Watson, Jones, Swannell, & Van Duin, 2002). Thereafter, further biodegradation of hydrocarbons have resulted in heavy molecular weight (> C_{20}) cyclic and branched-chain organic acids (note: geological formations have traces of hydrocarbons which can result in the production of these organic acids from a longer geological era). Whereas, Meredith et al., 2000 have conducted similar quantitative analysis on 33 crude oil samples from Italy, California and the UK, which depicted that crucial parameters responsible for the increased acidity in these hydrocarbons are the presence of organic acid fractions due to biodegradation (Meredith, Kelland, & Jones, 2000).

Cyr et al., 1984 have conducted a qualitative analysis of the Alberta (Canada) oil sands, where he found that monocarboxylic concentrations (1 - 14%) are chemisorbed on inorganic matrix (Cyr & Strausz, 1984). Further detailed study have revealed the presence of normal, iso, mono and di-unsaturated acids, cyclopropylalkanoic and cyclic terpenoid carboxylic acids, and anteiso alkenoic acids ranging from (C_{12} to C_{32}). It was also found that the majority of acyclic acids have similarity to those found in Alberta oil sands and petroleum bitumen as a by-product of biosynthesis (bacterial degradation). Similarly, McGowan et al., 1985 have conducted an experimental study for kerogen degradation from Green River oil shale for determining the structure of hydrocarbons and found the presence of branched-chain fatty acids (McGowan, Pearce, & Diehl, 1985).

The occurrence of these organic acids in fossils may range from C_2 to C_{26} (number of carbon atoms) (Caballero et al., 2003), where, odd carbon numbered organic acids are

rarely found compared to even carbon numbers (Kvenvolden, 1967), including but not limited to, acetic acid (C2), butanoic acid (C_4), hexanoic acid (C_6), caprylic acid (C_8), lauric acid (C_{12}), myristic acid (C_{14}), palmitic acid (C_{16}), stearic acid (C_{18}), behenic acid (C_{22}), lignoceric acid (C_{24}), and cerotic acid (C_{26}) (Amaya, Rana, & Hornof, 2002; Gomari & Hamouda, 2006; Hansen et al., 2000; Jardine, McCarthy, & Weber, 1989; Kharaka et al., 2009; Legens, Toulhoat, Cuiec, Villieras, & Palermo, 1999; Madsen & Ida, 1998; Stalker et al., 2013; L. Yang et al., 2015). Previously, all of the wettability studies in the presence of organic acids were related to rock/oil/brine systems for EOR applications. However, there is a serious lack of literature to comprehend the influence of these organics in a given rock/CO_2/brine systems.

2.9.1 Effect of Organic Acids on CO_2 Wettability in Real Geo-Storage Conditions

It is explained in the previous section that organic acids are widely present in the geo-storage formations (Akob et al., 2015; Ali, 2018; Lundegard & Kharaka, 1994), whereas, their influence on the wetting characteristics is rarely tested which can cause significant impact on the CO_2 trapping capacities (Akhondzadeh et al., 2020; Ali, Al-Anssari, et al., 2019; Ali, Arif, et al., 2019; Mujahid Ali et al., 2021; Legens et al., 1999). Previously, wettability studies were conducted on clean mineral surfaces for benchmarking the fundamental research for various influencing factors (pressure, temperature, salinity, and surface roughness) (A. Z. Al-Yaseri et al., 2016; Arif et al., 2019a; Fauziah et al., 2019). However, real geological conditions are anoxic (contains organic molecules), where reductive circumstances overcome the fundamental studies on clean mineral substrates (Froelich et al., 1979; Townsend et al., 2003). To fully understand and benchmark the real geological conditions, one should consider the organic effects on wetting characteristics at various physio-thermal conditions and how their minute concentrations may behave in various heterogeneous reservoir formations. In the beginning, a series of different studies by Anderson et al., have comprehended the wettability of geo-storage formations in detail which gave us an understanding of oil-wet surfaces (W. Anderson, 1986; W. G. Anderson, 1987a, 1987b, 1987c). These studies related the adsorption of polar compounds dissolved in crude oil to the oil-wet characteristics of reservoir rock (W. Anderson, 1986; W. G. Anderson, 1987a, 1987b, 1987c). Thereafter, researchers have used silanes to change

the wetting characteristics from hydrophilic conditions to hydrophobic conditions for understanding the oil-wet nature of reservoir rock (Araujo, Toledo, Leon, & Gonzalez, 1995; Grate et al., 2012; Vanithakumari, George, & Mudali, 2014), however, presence of silanes in real geo-storage conditions is not possible due to their highly reactive nature. Therefore, it is pertinent to gauge and simulate real conditions (presence of organic acids) at a laboratory scale for determining the thresholds of organics for wettability studies. Literature seriously lacks the information on this prospective and very few studies have gauge wettability characteristics in the presence of organic acids.

Therefore, we have conducted the stepwise experimental study for the applications of CO_2 geo-storage with various organic acids ranging from (C_6 to C_{24}) in various concentrations (10^{-2} – 10^{-10} mol/L) with various geo-storage formations (sandstone, carbonate, and cap-rock) (Ali, Aftab, et al., 2020; Ali, Al-Anssari, et al., 2019; Ali, Arif, et al., 2019). Our studies have depicted a substantial reduction in the CO_2 trapping potential in the presence of organic acids (further explained in chapter 3).

2.10 Effect of Nanomaterial on CO_2 Wettability in Real Geo-Storage Conditions

Recently, nanoparticles (NPs) are getting wide acceptance in a diversified range of industries including, biology (M. De, Ghosh, & Rotello, 2008), medicine (Lohse & Murphy, 2012), metal ions removal (H. Wang et al., 2012), heterogeneous catalysis (Johnson, 2003), food industry (Y. Wang et al., 2014), tissue penetration and drug delivery (Tong, Hemmati, Langer, & Kohane, 2012), and oil and gas industry (Alsaba, Al Dushaishi, & Abbas, 2020). In the petroleum industry nanoparticles are used for various applications of subsurface operations, which includes but not limited to, optimization of drilling fluids (Aftab, Ali, Arif, et al., 2020; Aftab, Ali, Sahito, et al., 2020; Ali & Aftab, 2020; Ali, Jarni, et al., 2020), enhanced oil recovery (Al-Anssari et al., 2021; Al-Anssari, Ali, et al., 2020; Al-Anssari, Arain, et al., 2018; Al-Anssari, Nwidee, et al., 2017; Nazarahari et al., 2021; Y. Yang et al., 2020), interfacial tension (IFT) reduction (Al-Anssari, Arain, et al., 2020; Cheraghian & Hendraningrat, 2016), chemical flooding (Akbar et al., 2020; Haghighi et al., 2020), low salinity water injection (N. Jha et al., 2018; N. K. Jha, Ali, et al., 2019; N. K. Jha et al., 2020),

wettability alteration (Al-Anssari et al., 2016; Ali, Sahito, et al., 2020; Naik, Malgaresi, You, & Bedrikovetsky, 2018), and optimizing fracturing fluids (Al-Muntasheri, Liang, & Hull, 2017; Awan et al., 2021; Fakoya & Shah, 2018). The nano-fluids (NFs) are formulated by adding nano-sized particles to the base fluid (deionized water or brine) at very low concentrations (Al-Anssari, Arif, Wang, et al., 2017b; Al-Anssari, Arif, et al., 2018). The effective subsurface applications of NPs in CO_2 geological formations are dependent on various factors, like stability, dispersion, inexpensiveness, and injectibility for providing constant migration of NFs in pore matrix (Al-Anssari, Arif, Wang, Barifcani, & Iglauer, 2017). However, the success ratio of NFs in CO_2 geo-storage formations is adversely affected by various parameters, like formation type, salinity, temperature, pressure, pH, zeta-potential and complex nature of porous medium (Salama, Negara, El Amin, & Sun, 2015). For instance, kinetic energy of nanoparticles is increased with increasing temperature causing constant collision between NPs, thus, reducing NFs stability (Liu et al., 2013). Another crucial parameter which affects the stability of NFs is salinity of CO_2 geological storage formations (i.e. deep saline aquifers), which varies considerably, thus causing the reduction in NP's repulsive forces due to the presence of electrolytes (i.e. brine). This phenomenon constantly increase coagulation and flocculation due to increased rate of coalescences and collisions in the nano-suspensions, thus, causing phase separation (El-sayed, Kamel, Morsy, & Taher, 2012). To avoid this challenge, surface active agents, like polymers (ShamsiJazeyi, Miller, Wong, Tour, & Verduzco, 2014), surfactants (Ahualli et al., 2011; Al-Anssari, Wang, Barifcani, & Iglauer, 2017) and their combinations (Sharma, Kumar, & Sangwai, 2015) are suggested in the base fluid (deionized water or brine) for controlling the properties and stability of NPs for specified subsurface applications. Therefore, selection of NP's type, base fluid, and concentrations should be considered carefully based on reservoir properties for achieving optimized conditions (Nwidee et al., 2016). It is reported in literature that nano-suspensions have the successful tendency for reducing the IFT (Al-Anssari, Arain, et al., 2018; Al-Anssari, Arain, et al., 2020; Al-Anssari, Barifcani, Keshavarz, & Iglauer, 2018) and altering the hydrophobic wettability to hydrophilic conditions (N. Jha et al., 2018; N. K. Jha, Ali, et al., 2019; N. K. Jha, Iglauer, et al., 2019). However, these studies were conducted on clean mineral surfaces in strong oxidizing conditions, whereas, real geo-storage conditions are reductive in nature (contains organic molecules). Literature seriously lacks the research in this perspective for

comprehending the effect of nanoparticles in the presence of organic acids and very few studies have gauge wettability characteristics of nanomaterials in reductive conditions.

Therefore, we have utilized various nanoparticles (SiO_2 and Al_2O_3) with various nano-concentrations (0.05, 0.1, 0.25, and 0.75 wt%) in the presence of various organic acids (C_6 to C_{24}) in various geo-storage formations (sandstone, and cap-rock). Our studies have shown that these nanomaterials have a significant ability to alter hydrophobic surfaces to hydrophilic for mitigating the effects of organic acids (further explained in chapter 4) (Muhammad Ali et al., 2021; Ali, Sahito, et al., 2020). Thus, it is necessary to understand the complex behaviour of wettability alteration relative to different types of organic acids found in realistic geological formations and there is an urgent need for using smart materials (i.e. nanoparticles) which can alter the CO_2-wettability to more water-wet conditions, thus, de-risking the CO_2 geological storage projects.

Chapter 3 Effect of Organic Acids on Geo-Storage Formations

OVERVIEW

This chapter is divided into three parts which are based on three published peer-reviewed journal articles which comprehends the influence of organic acids (hexanoic acid C_6, Lauric acid C_{12}, Stearic acid C_{18}, and lignoceric acid C_{24}) on CO_2-wettability of geo-storage formations (carbonate, sandstone, and cap-rock) at reservoir conditions. Wettability is a governing factor that determines reservoir injectivity, project feasibility, containment security, and CO_2 storage potential. Therefore, for comprehending the effect of organic acids for determining the thresholds of CO_2 trapping capacities (structural and residual), contact angle and analytical measurements were conducted at various concentrations of organic aged geo-storage samples. The details of each chapter is as follows:

Part 1: **Ali, M.**, Al-Anssari, S., Arif, M., Barifcani, A., Sarmadivaleh, M., Stalker, L., ... & Iglauer, S. (2019). Organic acid concentration thresholds for ageing of carbonate minerals: Implications for CO_2 trapping/storage. Journal of colloid and interface science, 534, 88-94.

In this article, the effect of organic acid (stearic acid C_{18}) was quantified by ageing calcite substrates (representing carbonate formation) with minute concentrations (10^{-2} – 10^{-10} mol/L) for 7 days. Thereafter, contact angle measurements were conducted at reservoir conditions (10 MPa, 25 MPa and 323 K) for providing the thresholds of structural and residual trapping capacities of CO_2 for carbonate formation. The calculated CO_2 column heights were also provided based on contact angle measurements. Further, organic aged calcite samples were characterized by analytical measurements (scanning electron microscopy SEM, energy dispersive spectroscopy EDS, and atomic force microscopy AFM).

Part 2: **Ali, M.**, Arif, M., Sahito, M. F., Al-Anssari, S., Keshavarz, A., Barifcani, A., ... & Iglauer, S. (2019). CO_2-wettability of sandstones exposed to traces

of organic acids: Implications for CO_2 geo-storage. International Journal of Greenhouse Gas Control, 83, 61-68.

In this article, the effect of various organic acids (hexanoic acid C_6, Lauric acid C_{12}, Stearic acid C_{18}, and lignoceric acid C_{24}) were quantified by ageing quartz substrates (representing sandstone formation) with minute concentrations (10^{-2} – 10^{-10} mol/L) for 7 days. Thereafter, contact angle measurements were conducted at reservoir conditions (0.1 MPa, 25 MPa and 323 K) for providing the thresholds of structural and residual trapping capacities of CO_2 for sandstone formation. Further, organic aged calcite samples were characterized by analytical measurements (scanning electron microscopy SEM, and energy dispersive spectroscopy EDS).

Part 3: **Ali, M**., Aftab, A., Arain, Z. U. A., Al-Yaseri, A., Roshan, H., Saeedi, A., ... & Sarmadivaleh, M. (2020). Influence of Organic Acid Concentration on Wettability Alteration of Cap-Rock: Implications for CO_2 Trapping/Storage. ACS Applied Materials & Interfaces, 12(35), 39850-39858.

In this article, the effect of various organic acids (hexanoic acid C_6, Lauric acid C_{12}, Stearic acid C_{18}, and lignoceric acid C_{24}) were quantified by ageing mica substrates (representing cap-rock formation) with minute concentrations (10^{-2} – 10^{-9} mol/L) for 7 days. Thereafter, contact angle measurements were conducted at reservoir conditions (0.1 MPa, 15 MPa, 25 MPa and 323 K) for providing the thresholds of structural trapping capacities of CO_2 for cap-rock formation. Further, organic aged calcite samples were characterized by analytical measurements (X-ray diffraction XRD, field emission scanning electron microscopy FESEM, energy dispersive spectroscopy EDS, total organic carbon TOC, fourier transform infrared spectroscopy FTIR, and atomic force microscopy AFM).

PART 1 Organic Acid Concentration Thresholds for Ageing of Carbonate Minerals: Implications for CO_2 Trapping/Storage

Muhammad Ali [a,*], Sarmad Al-Anssari [b,c], Muhammad Arif [a,d], Ahmed Barifcani [a,b], Mohammad Sarmadivaleh [a], Linda Stalker [e], Maxim Lebedev [f], Stefan Iglauer [a,g]

[a] Western Australia School of Mines, Minerals, Energy and Chemical Engineering, Curtin University, 26 Dick Perry Avenue, Kensington, 6151, WA, Australia

[b] Department of Chemical Engineering, Curtin University, Kent Street, 6102 Bentley, Western Australia

[c] Department of Chemical Engineering, University of Baghdad, Baghdad, 10071, Iraq

[d] Department of Petroleum Engineering, Khalifa University of Science & Technology, Abu Dhabi, UAE

[e] Commonwealth Scientific and Industrial Research Organisation (CSIRO), 26 Dick Perry Avenue, 6151 Kensington, Western Australia

[f] Department of Exploration Geophysics, Curtin University, 26 Dick Perry Avenue, 6151 Kensington, Western Australia

[g] School of Engineering, Edith Cowan University, 270 Joondalup Drive, Joondalup, WA 6027 Australia

[*] Corresponding author (Muhammad.ali7@postgrad.curtin.edu.au)

Abstract

Hypothesis: CO_2 geological storage (CGS) involves different mechanisms which can store millions of tonnes of CO_2 per year into depleted hydrocarbon reservoirs and deep saline aquifers. But their storage capacity is influenced by the presence of different carboxylic compounds in the reservoir. These molecules strongly affect the water wetness of the rock, which has a dramatic impact on storage capacities and containment security. However, a precise understanding of how these carboxylic acids influence the rock's CO_2-wettability is lacking.

Experiments: We thus systematically analysed these relationships as a function of pressure, temperature, storage depth and organic acid concentrations. A particular focus was on identifying organic acid concentration thresholds above which storage efficiency may get influenced significantly.

Findings: These thresholds (defined for structural trapping as a water contact angle $\theta > 90°$; and for capillary trapping when primary drainage is unaffected, i.e. $\theta > 50°$) were very low for structural trapping (~10^{-3} – 10^{-7} mol/L organic acid concentration $C_{organic}$) and extremely low for capillary trapping (10^{-7} mol/L to below 10^{-10} mol/L $C_{organic}$). Since minute organic acid concentrations are always present in deep saline aquifers and certainly, in depleted hydrocarbon reservoirs, significantly lower storage capacities and containment security than previously thought can be predicted in carbonate reservoirs, and reservoir-scale models and evaluation schemes need to account for these effects to de-risk CGS projects.

Highlights

- Carbonate aquifers (Calcite Surfaces)
- Dissolution of organic acid components in crude oil (Stearic Acid)
- CO_2 trapping in deep saline aquifers and depleted hydrocarbon reservoirs and their associated risk in the presence of organic acid components

Keywords

Wettability, CO_2 storage, Organic acids

3.1.1 Introduction

Depleted hydrocarbon reservoirs and deep saline aquifers are potential CO_2 sinks in which anthropogenic CO_2 emissions can be stored, thus mitigating global warming (III, 2013; Orr, 2009). Efficient and safe CO_2 geological storage involves a qualitative and quantitative assessment of the contribution of the different functional trapping

mechanisms which prevent the buoyant CO_2 from migrating back to the surface (III, 2013).

In this context, it has been shown that CO_2-wet surfaces drastically reduce structural (Iglauer, 2017; Iglauer, Pentland, et al., 2015; Jenkins et al., 2012) and capillary trapping capacities (Al-Khdheeawi et al., 2017a; Al-Menhali & Krevor, 2016; Chaudhary et al., 2013; Rahman et al., 2016). Furthermore, organic acid content on the rock surface is the main factor that renders (originally strongly water-wet) mineral surfaces to become CO_2-wet (Iglauer, 2017). While clean mineral surfaces are weakly, strongly or completely water-wet (Espinoza & Santamarina, 2010; Farokhpoor et al., 2013; Saraji et al., 2014), organic acid surfaces, e.g. alkylated or arylated minerals, minerals aged in crude oil or coal (Dickson, Gupta, Horozov, Binks, & Johnston, 2006; Iglauer, 2017; Iglauer, Pentland, et al., 2015; D. Yang et al., 2008) are weakly, strongly or even completely CO_2-wet depending on pressure, temperature and brine salinity (A. Z. Al-Yaseri et al., 2016; Chen, Wan, Li, & Song, 2015; Iglauer, 2017).

However, chemically clean mineral surfaces are artificial in the sense that they can only be prepared and persist in strongly oxidising environments (e.g. in an oxygen plasma or UV-ozone atmosphere) (Iglauer et al., 2014; Love et al., 2005), while it is well established that in the subsurface anoxic or reducing conditions prevail (Froelich et al., 1979; Townsend et al., 2003).

Besides, storage formations always contains traces of dissolved organic acid material (Jardine et al., 1989; Kharaka et al., 2009; Madsen & Ida, 1998; Stalker et al., 2013; Thurman, 2012; L. Yang et al., 2015), which is potentially sufficient to significantly change the rock's CO_2-wettability. Indeed a partial mono-molecular layer adsorbed to the mineral surface would be sufficient for this (Adamson & Gast, 1967; Gaines, 1966; Iglauer et al., 2014; Kuhn & Möbius, 1971; Maboudian & Howe, 1997; Shafrin & Zisman, 1962; Zasadzinski et al., 1994). Such organic acid contaminations thus has the potential to drastically reduce storage capacities and containment security (Al-Khdheeawi et al., 2017a; Al-Khdheeawi et al., 2017; Iglauer, Al-Yaseri, et al., 2015; Iglauer, Pentland, et al., 2015). It is therefore of vital importance to gauge this effect and to identify threshold concentrations of organic acid molecules at which CO_2 storage is significantly affected.

We thus systematically investigated such threshold values per clearly defined laboratory experiments, and we analysed the impact such minute organic acid concentrations have on CO_2 storage capacities and containment security.

3.1.2 Experimental Methodology

3.1.2.1 Materials

Nine pure calcite samples (Iceland spar, from WARD'S Natural Science, sample dimensions = 1 cm x 1 cm x 0.3 cm) were used as a model limestone storage formation. The surface roughness of all nine surfaces were measured via Atomic Forces Microscopy (AFM instrument model DSE 95-200, Semilab).

CO_2 (purity = 99.999 mol%; from BOC, gas code-082), N_2 (purity = 99.999 mol%; from BOC, gas code-234) and 10 wt% NaCl brine (NaCl purity ≥ 99.9 mol%; from Scharlab) were used. The NaCl was dissolved in deionized water (Ultrapure from David Gray; electrical conductivity = 0.02 mS/cm), which was equilibrated with calcite by rigorously mixing with calcite off-cuts while continuously monitoring the pH value (Alroudhan, Vinogradov, & Jackson, 2016; Venkatraman, Lake, & Johns, 2014). Subsequently, the NaCl brine was equilibrated with CO_2 at experimental conditions in a high pressure mixing reactor (El-Maghraby et al., 2012).

Acetone (99.9 mol%; from Rowe Scientific) was used as a surface cleaning agent, drops of hydrochloric acid (ACS reagent, concentration 37 vol%, Sigma Aldrich) were used to control the pH of the brine (see ageing procedure below for more details) and stearic acid (≥ 98.5 mol%; from Sigma Aldrich) was selected as a model for organic acid molecules present in the subsurface (Karoussi, Skovbjerg, Hassenkam, Stipp, & Hamouda, 2008; Madsen & Ida, 1998; Tabrizy, Denoyel, & Hamouda, 2011; Ulrich, Stumm, & Cosovic, 1988; Zullig & Morse, 1988).

3.1.2.2 Simulating real aquifer conditions

As mentioned above, real aquifers contain organic acid molecules which are partially adsorbed on the rock surface (Jardine et al., 1989; Kharaka et al., 2009; Madsen & Ida,

1998; Stalker et al., 2013; Thurman, 2012; L. Yang et al., 2015). It is thus vital to re-create such mineral surfaces to realistically mimic aquifer rock surfaces, particularly to their wettability characteristics (Adamson & Gast, 1967; J. A. Davis, 1982; Kleber et al., 2015; Ochs, Ćosović, & Stumm, 1994). Thus below the procedure for preparing such realistic aquifer surfaces is described, as it was used in this research work.

3.1.2.2.1 Calcite surface preparation

Initially, the mineral (calcite) substrates were cleaned with calcite-equilibrated DI-water to remove any dust or surface fragments from the surface. The sample was then dried in an oven at 90°C for 60 mins and exposed to air plasma (using a Diemer Yocto instrument) for 15 mins to remove any organic contamination (Iglauer et al., 2014; Love et al., 2005).

Ageing Procedure

To mimic a typical storage formation, where the rock pore surfaces were exposed to formation water over geological times (Birkholzer, Zhou, & Tsang, 2009; J. A. Davis, 1982; Hoeiland, Barth, Blokhus, & Skauge, 2001; Ji & Zhu, 2015; Karoussi et al., 2008; Kleber et al., 2015; Nordbotten, Celia, & Bachu, 2005; Ochs et al., 1994; Ulrich et al., 1988; White, Strazisar, Granite, Hoffman, & Pennline, 2003; Zullig & Morse, 1988), we adopted the following strategy:

The calcite samples were immersed for 30 mins in calcite-equilibrated 2 wt% NaCl brine (NaCl purity ≥ 99.9 mol%; from Scharlab) at ambient conditions, while the acidity was maintained at pH = 4 by adding drops of aqueous hydrochloric acid; this procedure increases the adsorption rate of stearic acid onto the substrate, and thus simulates adsorption of organic acid molecules over geological times (i.e. millions of years exposure time) (Birkholzer et al., 2009; J. A. Davis, 1982; Hoeiland et al., 2001; Ji & Zhu, 2015; Karoussi et al., 2008; Kleber et al., 2015; Nordbotten et al., 2005; Ochs et al., 1994; Ulrich et al., 1988; White et al., 2003; Zullig & Morse, 1988). Ultraclean N_2 was then used to mechanically clean (blow away) the remaining water from the surface to avoid contamination. Subsequently, the substrates were aged in stearic acid/n-decane solutions of prescribed molarity (10^{-2} M to 10^{-10} M stearic acid

concentration) for seven days to mimic exposure to formation fluid (which contains organic acid molecules) over geological times (Gomari & Hamouda, 2006; Hamouda & Rezaei Gomari, 2006; Karoussi et al., 2008; Tabrizy et al., 2011). Note that it is also shown that carboxylic acids and hydrocarbons both exist in deep saline aquifers (Bennett et al., 1993), as a result of biodegradation and organic matter diagenesis and subsequent migration into the water zones (Jones et al., 2008).

Mechanistically, the stearic acid esterifies the hydroxyl groups on the calcite surface in a condensation reaction (Scheme 3-1-1) (Z. Cao et al., 2016; Heberling et al., 2011; Mihajlović, Vučinić, Sekulić, Milićević, & Kolonja, 2013; Shi, Rosa, & Lazzeri, 2010; C. Wang, Sheng, Zhao, Pan, & Wang, 2006).

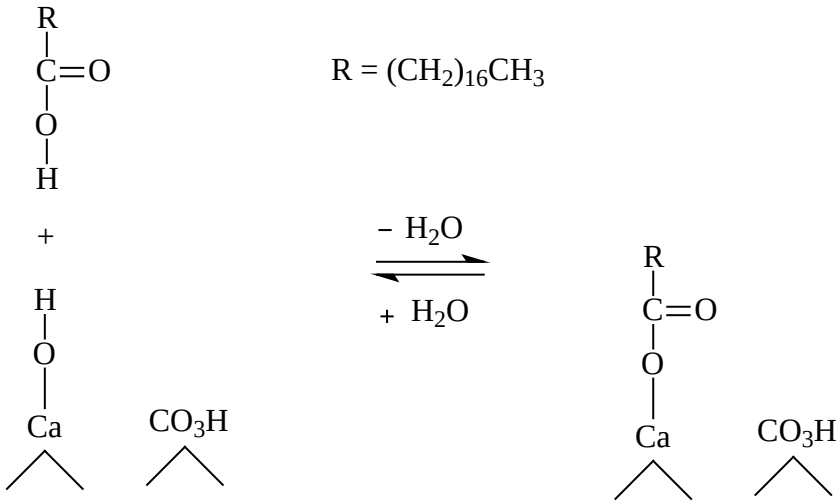

Scheme 3-1-1 Chemisorption of stearic acid ($CH_3(CH_2)_{16}$-COOH) on solid calcite surface (∧ indicates solid bulk) (Z. Cao et al., 2016; Heberling et al., 2011; Mihajlović et al., 2013; Shi et al., 2010; C. Wang et al., 2006).

Thus octadecanoic groups (C_{18} ester groups) were chemically (covalently) bonded to the calcite surface, rendering them strongly hydrophobic (Al-Anssari et al., 2016).

3.1.2.2.2 Surface characterization of pure and aged calcite surfaces

Pure Calcite

The surface properties of the calcite samples were investigated via energy-dispersive X-ray spectroscopy (EDS, Oxford X-act SSD X-ray detector with Inca and Aztec software), atomic force microscopy (AFM DSE 95-200, Semilab) and contact angle (θ) measurements. For pure calcite surfaces, the average atomic surface content was 24.7 wt% ± 4.9 wt% Ca, 20.5 wt% ± 3.3 wt% C and 54.8 wt% ± 6.3 wt% O, Table 3-1-1, Figure 3-1-2; these values are averages over 45 data points measured on five different surface sites for each of the nine samples. The average root mean square (RMS) surface roughness measured was 20.12 nm (± 16 nm), Table 3-1-2; which is very smooth. For such smooth surfaces, no significant influence on CO_2-wettability was observed (A. Z. Al-Yaseri et al., 2016). Furthermore, contact angles on these pure calcite samples were (advancing 0° and receding 0°) at ambient conditions, thus pure calcite was completely water-wet at ambient conditions. However, higher contact angles (advancing 48° and receding 40°) and (advancing 68° and receding 62°) were measured at reservoirs conditions on these pure calcite samples (323 K, 10 MPa and 25 MPa), consistent with literature data (Al-Anssari, Arif, Wang, et al., 2017a; Arif, Lebedev, et al., 2017a).

Aged Calcite

Ageing had no significant influence on surface roughness (20.58 nm ± 16 nm), Table 3-1-2. However, the atomic surface concentrations changed due to chemisorption of the carboxylic acids on the calcite surface, consistent with (Zullig & Morse, 1988). The new average surface atomic content of the treated samples was 22.7 wt% ± 5.1 wt% Ca, 22.9 wt% ± 3.6 wt% C and 54.4 wt% ± 5 wt% O, Table 3-1-1, Figure 3-1-2. Thus, a significant overall average increase in surface carbon concentration (+2.3 wt% C) was observed due to surface stearate adsorption (Table 3-1-1).

Furthermore, ageing of the calcite surfaces caused a significant change in contact angles and thus CO_2-wettability, this is discussed in detail below.

Table 3-1-1 Surface composition of pure and aged calcite and change due to ageing.

Stearic Acid Concentration (Molarity)	Pure calcite			After ageing			Change due to ageing			Estimated surface coverage (Dickson et al., 2006)
	wt% Ca	wt% C	wt% O	wt% Ca	wt% C	wt% O	wt% Ca	wt% C	wt% O	$\left(1-\frac{wt\%\ C_{before\ aging}}{wt\%\ C_{after\ aging}}\right)\times 100$
10^{-2}	24.9	18.8	56.3	23.2	22.3	54.5	-1.7	+3.5	-1.8	15.7
10^{-3}	25.8	18.4	55.9	23.2	21.5	55.3	-2.6	+3.1	-0.6	14.4
10^{-4}	25.1	21.3	53.6	24.8	24.5	50.7	-0.3	+3.2	-2.9	13.1
10^{-5}	22.0	20.0	58.0	21.6	22.9	55.5	-0.4	+2.9	-2.5	12.7
10^{-6}	28.0	24.9	47.2	22.1	27.9	50.0	-5.9	+3.0	+2.8	10.8
10^{-7}	24.0	20.4	55.7	22.5	22.0	55.5	-1.5	+1.6	-0.2	7.3
10^{-8}	25.6	20.0	54.4	20.9	21.4	57.8	-4.7	+1.4	+3.4	6.5
10^{-9}	28.3	19.6	52.1	28.2	20.8	51.0	-0.1	+1.2	-1.1	5.8
10^{-10}	18.6	21.5	59.8	18.0	22.6	59.4	-0.6	+1.1	-0.4	4.9
0	20.9	20.1	59.0	20.9	20.1	59.0	0	0	0	0

Table 3-1-2 Contact angle measurements and Surface Roughness (AFM*) at different stearic acid concentrations.

Stearic acid concentration (Molarity)	Initial RMS* surface roughness (nm), pure calcite	Final RMS* surface roughness (nm), treated calcite	CO_2/Calcite/brine contact angle (10 MPa and 323 K)		CO_2/Calcite/brine contact angle (25 MPa and 323 K)	
			θ_a	θ_r	θ_a	θ_r
10^{-2}	4.4	4.8	$126.0^{n=3}$	$98.6^{n=3}$	$141.2^{n=3}$	$131.8^{n=3}$
10^{-3}	13.4	13.9	$108.2^{n=3}$	$91.8^{n=3}$	$113.5^{n=3}$	$105.1^{n=3}$
10^{-4}	25.3	26.2	$100.9^{n=3}$	$86.5^{n=3}$	$108.5^{n=3}$	$101.8^{n=3}$
10^{-5}	37.1	37.6	$72.4^{n=3}$	$65.7^{n=3}$	$99.6^{n=3}$	$84.4^{n=3}$
10^{-6}	25.9	26.4	$63.9^{n=3}$	$53.5^{n=3}$	$95.4^{n=3}$	$81.7^{n=3}$
10^{-7}	27.2	27.5	$60.9^{n=3}$	$51.4^{n=3}$	$87.5^{n=3}$	$79.6^{n=3}$
10^{-8}	18.6	19.2	$56.4^{n=3}$	$49.7^{n=3}$	$78.2^{n=3}$	$68.8^{n=3}$
10^{-9}	7.2	7.5	$52.0^{n=3}$	$45.6^{n=3}$	$71.8^{n=3}$	$67.5^{n=3}$
10^{-10}	21.6	22.1	$50.2^{n=3}$	$43.1^{n=3}$	$70.1^{n=3}$	$64.3^{n=3}$

*RMS – Route Mean Square

*AFM - Atomic Force Microscopy

n - The number of repeated experiments at the conditions indicated

3.1.2.3 Contact angle measurements

CO_2-wettability was determined by contact angle measurements at reservoir conditions (i.e. 323 K, at 10 MPa and 25 MPa) using a tilted plate goniometric setup (Al-Anssari et al., 2016; Lander et al., 1993). The experimental setup consisted of a high pressure-high temperature cell that can operate at reservoir conditions. The substrate was placed at a tilted angle of (17º) inside the cell. Two separate high precision syringe pumps (Teledyne D-500, pressure accuracy of 0.1%) adjusted the CO_2 pressure or injected the brine. The detailed setup has been described earlier (Arif, Barifcani, Lebedev, et al., 2016; Arif, Lebedev, et al., 2017a).

Experimentally, the sample was placed inside the pressure cell on the tilted plate and the cell was heated to the desired temperature (323 K). Subsequently, the CO_2 pressure was raised to prescribed values (10 MPa and 25 MPa), and a droplet of degassed brine with an average volume of 6 µL (± 1 µL) was dispensed onto the calcite surface through a needle. The advancing (θ_a) and receding (θ_r) water contact angles were then measured at the leading and trailing edge of the droplet just before the drop started to move (Lander et al., 1993). A high-resolution video camera (Basler SCA 640–70 fm, pixel size = 7.4 µm; frame rate = 71 fps; Fujinon CCTV lens: HF35HA-1B; 1:1.6/35 mm) captured movies of these processes, and θ_a and θ_r were measured on images extracted from the movie files. The standard deviation of the measurements was ±3° based on replicated measurements.

3.1.3 Results and Discussion

CO_2-wettability of a storage formation is a key parameter that strongly influences CO_2 movement and distribution throughout the formation (Al-Khdheeawi et al., 2017a; Al-Khdheeawi et al., 2017), rate of injectivity (Iglauer, 2017; Iglauer, Pentland, et al., 2015), storage capacity and containment security (Arif, Barifcani, Lebedev, et al., 2016; Arif, Lebedev, et al., 2017b; Iglauer, Al-Yaseri, et al., 2015). It is thus vital to understand CO_2-wettability in detail. In this context, the water receding contact angle (i.e. CO_2 displacing water) is related to structural trapping (below an impermeable cap-rock) (Broseta et al., 2012). The advancing contact angle (water displacing CO_2) determines the capillary trapping capacity (Chiquet et al., 2007) and thus the amount

of residually trapped CO_2 (Al-Menhali & Krevor, 2016; Chaudhary et al., 2013; Rahman et al., 2016). It has also been shown in previous studies that dissolution trapping is significantly affected by the wettability, and it is thus necessary to know the wettability for accurate reservoir simulations and storage capacity predictions (Al-Khdheeawi et al., 2017a; Al-Khdheeawi et al., 2017).

We thus conducted contact angle measurements with different mineral surface chemistry scenarios at various thermo-physical conditions. The minute concentrations of stearic acid exposed to the substrates (which represents the small amounts of organic acid molecules in deep saline aquifer storage formations) had a highly significant influence on the water-wetness of the rock.

The results show that calcite rapidly loses its water-wetness with increasing stearic acid surface coverage (Figure 3-1-1), i.e. higher organic acid concentration led to significantly higher CO_2-wettability. For instance, at 323 K and 25 MPa, a carbonate storage formation having 10^{-10} M stearic acid is weakly water-wet (θ_r = 64.3°), while θ_r reached 90° at 10^{-4} M stearic acid exposure concentration (note that capillary leakage is possible at θ_r > 90°) (Arif, Lebedev, et al., 2017b; Iglauer, 2017; Iglauer, Pentland, et al., 2015; Naylor, Wilkinson, & Haszeldine, 2011).

The optimal capillary trapping limit, which we define here as the point where primary drainage is unaffected by wettability is at θ_a = 50° (Morrow, 1970). θ_a is even more affected by the concentration of the carboxylic acid; even at a relatively low pressure of 10 MPa (note that increasing pressure increases θ) (A. Z. Al-Yaseri et al., 2016; Iglauer, 2017) and 323 K, θ_a reaches 50° at 10^{-10} M carboxylic acids concentration (note that this is a very minute concentration, much higher carboxylic acids concentration are measured in deep saline aquifers (Jardine et al., 1989; Kharaka et al., 2009; Madsen & Ida, 1998; Stalker et al., 2013; Thurman, 2012; L. Yang et al., 2015) and for 25 MPa this organic threshold is even below 10^{-10} M (Figure 3-1-1).

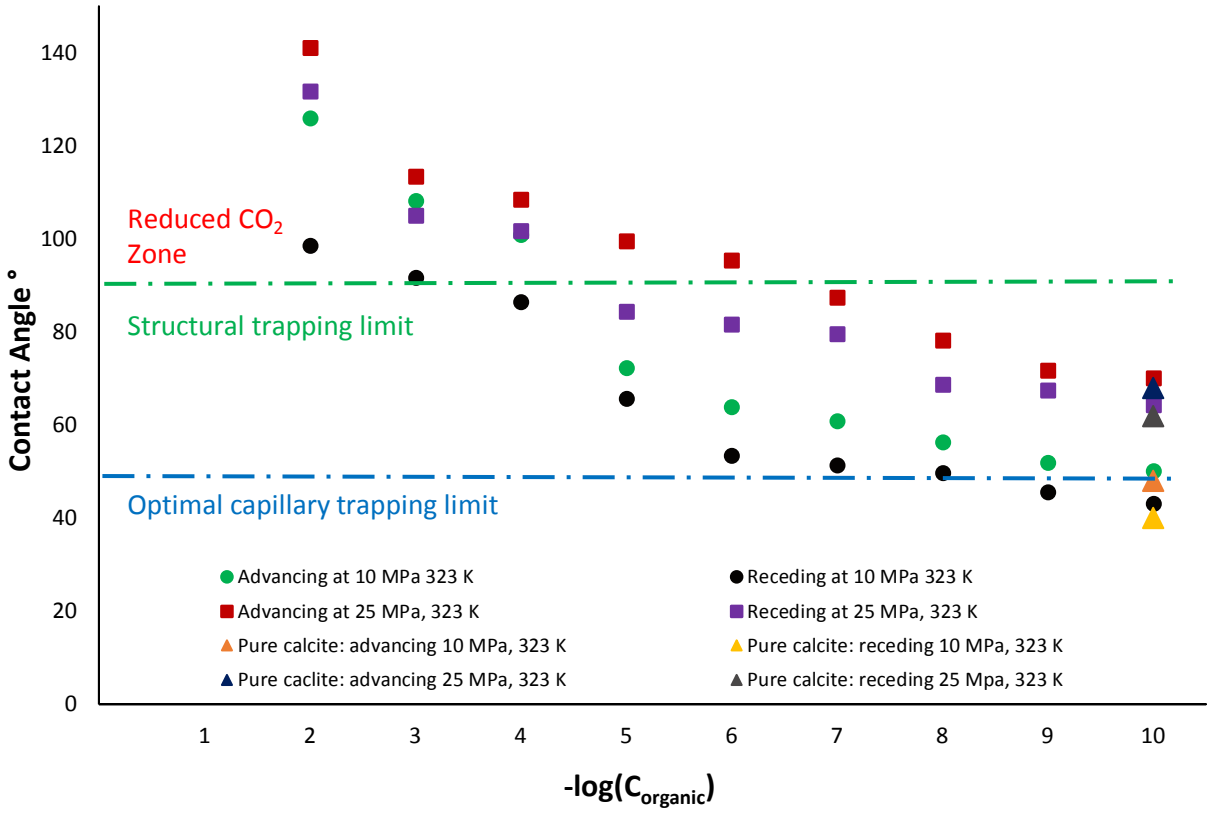

Figure 3-1-1 CO_2/calcite/brine (water) contact angles measured as a function of stearic acid concentration at 323 K and 10 MPa and 25 Mpa; $C_{organic}$ is the stearic acid concentration (molarity). The dotted green line represents the structural trapping limit, while the blue dotted line represents the optimal capillary trapping limit. The zone above the dotted green line indicates the reduced CO_2 zone.

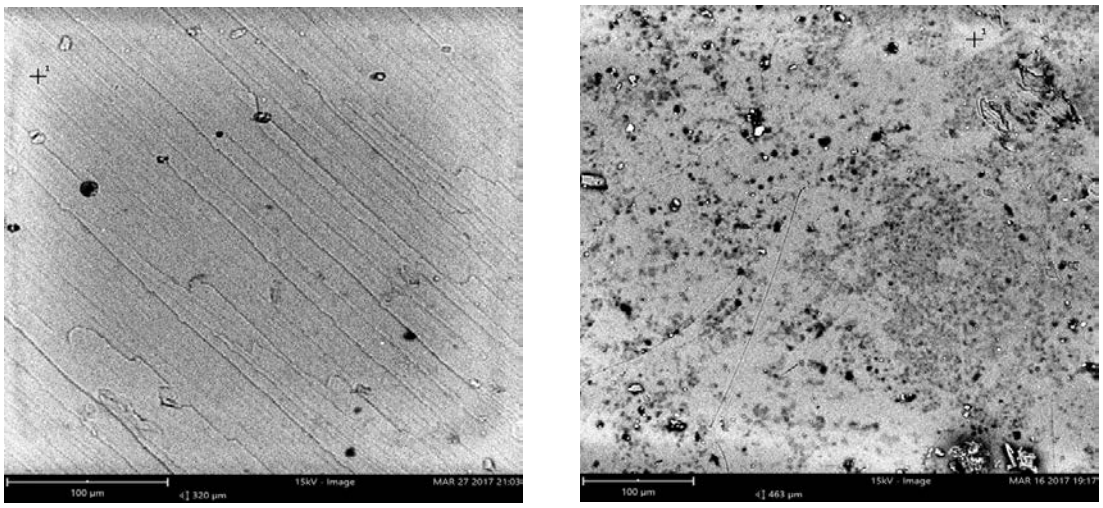

a) b)

Figure 3-1-2 SEM images before and after treatment with 10^{-2} M organic acid, (a) before treatment, (b) after treatment.

The SEM images of the calcite surfaces were acquired before and after treatment with stearic acid; two examples are shown in Figure 3-1-2. The texture of the image without stearic acid (Figure 3-1-2a) is quite transparent whereas a clear spread of organic acid on the calcite surface can be observed after surface treatment with 10^{-2} M stearic acid (Figure 3-1-2b). This stearic acid coverage of the calcite surface is responsible for the wettability change from strongly water-wet to weakly CO_2-wet.

Physically, the shape of the droplet spreading on the calcite surface observed during the contact angle measurement also indicates the wetting behaviour (Figure 3-1-3). It is clear that the brine droplet almost completely spread on the pure calcite surface at 10 MPa (Figure 3-1-3a), implying water-wet conditions. On the contrary, the brine droplet showed a maximum spread on the surface treated with 10^{-2} M stearic acid (measured at 25 MPa; Figure 3-1-3d) resulting in a higher water contact angle.

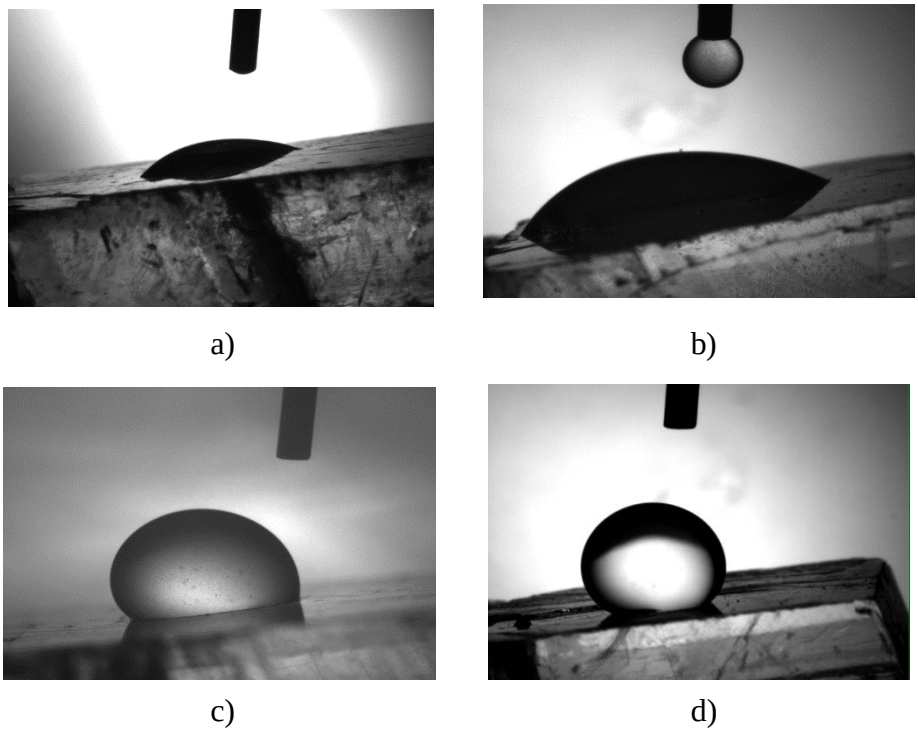

Figure 3-1-3 Contact angle images of different calcite surfaces, (a) pure calcite at 10 MPa, (b) pure calcite at 25 MPa, (c) aged calcite with 10^{-2} M organic acid at 10 MPa, (d) aged calcite with 10^{-2} M organic acid at 25 MPa.

The implications of the results can be investigated via a capillary force – buoyancy force balance (Arif, Jones, et al., 2017) as follows:

$$h = \frac{2\gamma cos\theta_r}{\Delta\rho g R} \qquad Eq.\ 3-1-1$$

where 'h' is the height of the CO_2 column immobilized beneath the seal layer, 'γ' is CO_2-brine interfacial tension, 'θ_r' is the receding contact angle, 'Δρ' is the CO_2-brine density difference, 'g' is the gravitational acceleration, and 'R' is the cap-rock's average pore throat radius.

Thus, for a limestone storage formation at 10 MPa and 323 K, three main scenarios can be distinguished: a) pure calcite, b) storage rock exposed to 10^{-6} M stearic acid, and c) storage rock exposed to 10^{-2} M stearic acid.

The corresponding 'θ_r' values under these conditions are 45°, 55° and 100° (Figure 3-1-1). The 'γ' and 'Δρ' values at 10 MPa and 323 K are 40 mN/m, from (Arif, Jones, et al., 2017) and 683 kg/m^3 interpolated, from (X. Li, Boek, Maitland, & Trusler, 2012) respectively; while a typical cap-rock pore radius is 0.01 µm, from (Nelson, 2009). CO_2 column heights 'h' calculated using Eq. (3-1-1) are thus 916 m for the case of pure calcite, 685 m for the case of 10^{-6} M stearic acid exposure, and -207 m for the calcite surface exposed to 10^{-2} M stearic acid (Figure 3-1-4). It is therefore clear that with increasing stearic acid concentration, the structural storage capacity reduces significantly. Moreover, the column height reached a negative value (-207 m) at 10^{-2} M stearic acid concentration, indicating CO_2 leakage due to wettability reversal (Figure 3-1-4).

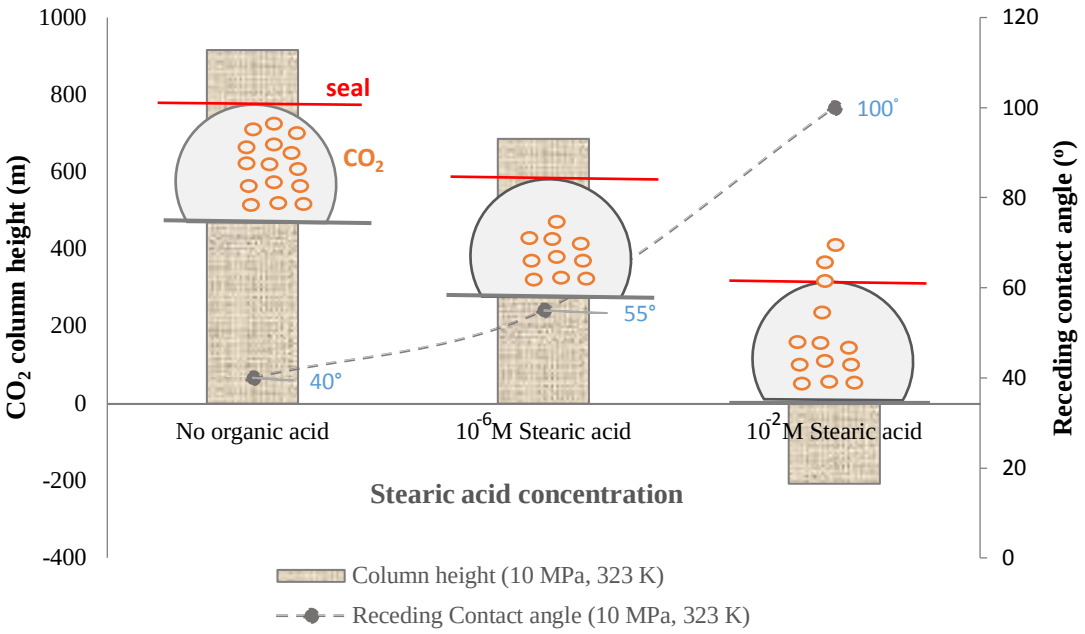

Figure 3-1-4 CO_2 column heights estimated as a function of stearic acid concentration at 10 MPa and 323 K. For 10^{-2} M stearic acid concentration, the height is negative which implies CO_2 leakage (column in negative y-axis). The graphic at the intersect of each column illustrates a hypothetical storage scenario where the black semi-circular region represents the storage rock, orange bubbles inside represent CO_2, and the red line at the top represents the seal layer. The left column (no organic present) shows CO_2 bubbles occupying a larger height as compared to the second column, which indicates a decrease in structural trapping due to the presence of organic acid, whereas the column on the right shows potential CO_2 leakage due to wetting alteration to weakly CO_2-wet at higher organic acid concentrations.

Furthermore, the wettability alteration found in this work can be explained by the interplay of the interfacial tensions ('γ') which are related by the Young's equation as follows (Arif, Barifcani, & Iglauer, 2016):

$$\cos\theta = \frac{\gamma_{sv} - \gamma_{sl}}{\gamma_{vl}} \qquad Eq.\ 3-1-2)$$

In Eq. (3-1-2), 'γ_{sv}' is the calcite-CO_2 interfacial tension, 'γ_{sl}' is the calcite-brine interfacial tension, and 'γ_{vl}' is the CO_2-brine interfacial tension. At a given pressure and temperature, the numerator in equation (3-1-2) decreases with increasing stearic

acid concentration as 'γ_{sv}' decreases with increasing stearic acid coverage (Arif, Jones, et al., 2017; Dickson et al., 2006). Thus, as 'γ_{vl}' is a constant at constant pressure and temperature, the adsorption of stearic acid on the calcite surface results in a higher water contact angle and de-wetting of the surface.

It is thus clear that a precise knowledge of the organic acid concentrations in a storage reservoir is essential for assessing the conditions for long-term geological storage. A pertinent limitation, however, is that current data applies to carbonate/limestone formations, and a broader consideration of various organic acid molecules and minerals may provide better insights. Moreover, We note that it has been previously shown for quartz surfaces that divalent cations result in further contact angle increase due to the stronger surface screening effect of the divalent ions (in comparison with the corresponding monovalent ions), thus reducing the surface potential and surface hydrophilicity – which results in higher contact angles (A. Z. Al-Yaseri et al., 2016; Iglauer, 2017).

3.1.4 Conclusions

Deep saline aquifers and depleted hydrocarbon reservoirs are the most important sinks for CO_2 geological storage (Firoozabadi & Myint, 2010; III, 2013). However, it has been shown that the CO_2-wettability of the storage and seal rock dramatically influences the injectivity, storage capacity, containment security (Al-Khdheeawi et al., 2017a; Al-Khdheeawi et al., 2017; Arif, Barifcani, Lebedev, et al., 2016; Arif, Lebedev, et al., 2017b; Iglauer, 2017; Iglauer, Al-Yaseri, et al., 2015; Iglauer, Pentland, et al., 2015), and thus project economics and technical feasibility.

Realistic subsurface conditions have, however, not been tested, and the focus was on clean mineral substrates, which, however, do not exist in the subsurface (as in the subsurface anoxic or reducing conditions prevail, while clean mineral surfaces can only exist in strongly oxidising conditions) (Froelich et al., 1979; Love et al., 2005).

We, therefore, measured the CO_2-wettability on carbonate mineral surfaces which mimic these subsurface storage conditions of carbonate reservoirs more realistically. This representativeness was achieved by exposure to highly diluted carboxylic acids

(10^{-2} – 10^{-10} M), and measurements were conducted at realistic storage conditions (10 MPa and 25 MPa and 323 K). Clearly, even minute exposure to traces of such organic acid molecules significantly increased the water contact angle (θ), and thus CO_2-wettability. This effect drastically increased with higher organic acid concentration and pressure.

We thus conclude that CO_2 geological storage capacities and containment security can be significantly lower than previously thought. Reservoir-scale models thus need to take these effects into account so that accurate storage predictions are obtained thus de-risking carbon geological storage (CGS) projects.

3.1.5 Graphical Abstract

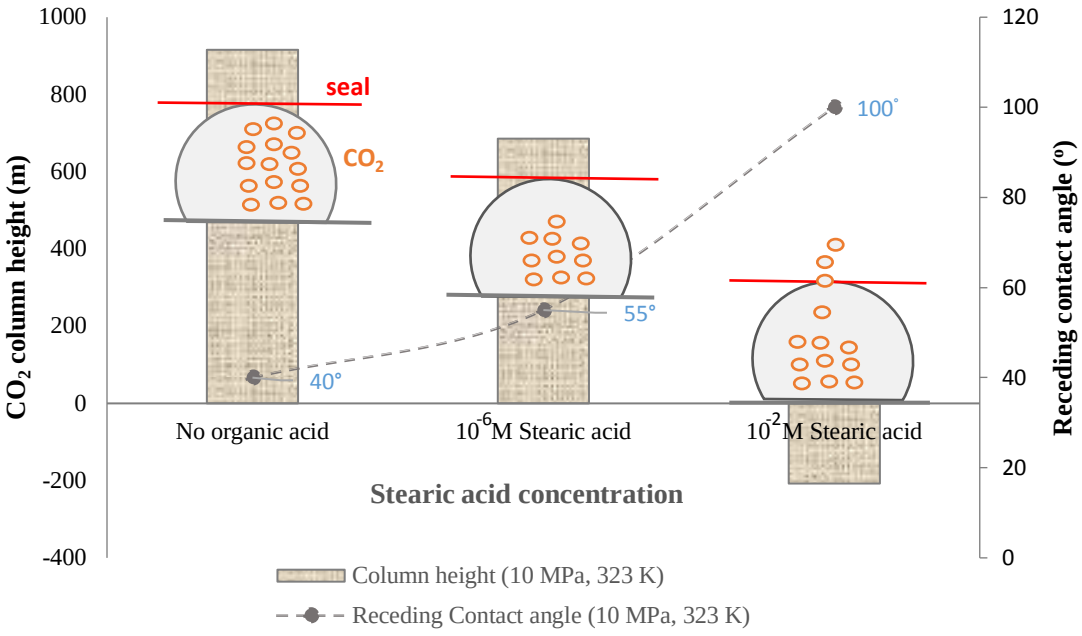

PART 2 CO_2-wettability of sandstones exposed to traces of organic acids; implications for CO_2 geo-storage

Muhammad Ali [a,*], , Muhammad Arif [a,b], Muhammad Faraz Sahito [c], Sarmad Al-Anssari [a,d], Alireza Keshavarz [e], Ahmed Barifcani [a], Linda Stalker [f], Mohammad Sarmadivaleh [a], Stefan Iglauer [a,e]

[a] Western Australia School of Mines, Minerals, Energy and Chemical Engineering, Curtin University, 26 Dick Perry Avenue, Kensington, 6151, WA, Australia

[b] Department of Petroleum Engineering, Khalifa University of Science & Technology, Abu Dhabi, UAE

[c] College of Engineering, King Fahd University of Petroleum and Minerals, Dhahran, 31261, Saudi Arabia

[d] Department of Chemical Engineering, College of Engineering, University of Baghdad, Baghdad, Iraq

[e] School of Engineering, Edith Cowan University, 270 Joondalup Drive, Joondalup, WA 6027 Australia

[f] CSIRO, 26 Dick Perry Avenue, Kensington, WA, 6151 Australia

[*] Corresponding author (Muhammad.ali7@postgrad.curtin.edu.au)

Abstract

The wettability of CO_2-brine-mineral systems plays a vital role during geological CO_2-storage. Residual trapping is lower in deep saline aquifers where the CO_2 is migrating through quartz-rich reservoirs but CO_2 accumulation within a three-way structural closure would have a high storage volume due to higher CO_2 saturation in hydrophobic quartz-rich reservoir rock. However, such wettability is only poorly understood at realistic subsurface conditions, which are anoxic or reducing. As a consequence of the reducing environment, the geological formations (i.e. deep saline aquifers) contain appreciable concentrations of various organic acids. We thus demonstrate here what

impact traces of organic acids exposed to storage rock have on their wettability. Technically, we tested hexanoic acid, lauric acid, stearic acid and lignoceric acid and measured wettability as a function of organic acid concentration at realistic storage conditions (i.e. 25 MPa and 323 K (50 °C)). Further, measurements were also conducted at ambient conditions to quantify the incremental pressure effect on wettability. Clearly, the quartz surface turned significantly less water-wet with increasing organic acid concentrations, even at trace concentrations. Importantly, we identified a threshold concentration at ~10^{-6} M organic acid, above which quartz wetting behaviour shifts from a strongly water-wet to an intermediate-wet state. This wettability shift may have important consequences for CO_2 residual trapping capacities, which may be significantly lower than for traditionally assumed water-wet conditions where CO_2 is migrating through quartz-rich reservoirs.

3.2.1 Introduction

CO_2 geological storage can significantly contribute towards a green environment via permanent CO_2 immobilization in deep underground formations, e.g. deep saline aquifers and depleted hydrocarbon reservoirs (Blunt et al., 1993; III, 2013; Orr, 2009). Efficient and safe CO_2 geological storage involves a qualitative and quantitative assessment of the contribution of the different functional trapping mechanisms which prevent the buoyant CO_2 from migrating back to the surface (III, 2013; Juanes, MacMinn, & Szulczewski, 2010). These trapping mechanisms include structural trapping (Arif, Al-Yaseri, et al., 2016; Arif, Barifcani, Lebedev, et al., 2016; Arif, Lebedev, et al., 2017a; Iglauer, Al-Yaseri, et al., 2015), capillary or residual trapping (Iglauer, Paluszny, Pentland, & Blunt, 2011; Iglauer, Wülling, et al., 2011; Juanes et al., 2010; S. C. Krevor et al., 2012; C. Pentland et al., 2011), mineral trapping (Gaus, 2010; Golding et al., 2011; J. K. Pearce et al., 2015) and dissolution trapping (Agartan et al., 2015; Iglauer, 2011). Also, adsorption trapping has been identified as another storage mechanism functional in coal seams and organic-rich shales (Arif, Barifcani, & Iglauer, 2016; Arif, Lebedev, et al., 2017b; Busch et al., 2008; Kaveh, Barnhoorn, & Wolf, 2016; Kaveh et al., 2012).

Structural and residual trapping are strongly influenced by the CO_2-brine-rock wettability (Al-Khdheeawi et al., 2017a; Al-Menhali & Krevor, 2016, 2017; Arif,

Lebedev, et al., 2017a; Chaudhary et al., 2013; Iglauer, 2017; Iglauer, Al-Yaseri, et al., 2015; Iglauer, Pentland, et al., 2015; Rahman et al., 2016; Wan et al., 2018), however, wettability is a complex parameter which is not well understood, particularly for realistic subsurface conditions. One key aspect of realistic subsurface conditions is their anoxic or reducing character, which results in the existence of organic molecules in target storage formations (Meredith et al., 2000; Watson et al., 2002).

It is shown in previous studies that the water receding contact angle on the cap-rock (i.e. CO_2 displacing water) is related to structural trapping (below an impermeable cap-rock) (Broseta et al., 2012). Whereas, the advancing water contact angle (water displacing CO_2) is related to capillary trapping in the reservoir rock (Chiquet et al., 2007) and thus the amount of residually trapped CO_2 (Al-Menhali & Krevor, 2016; Chaudhary et al., 2013; Rahman et al., 2016). Note further that dissolution trapping in the reservoir rock is significantly affected by the wettability and it is thus necessary to know the wettability for accurate reservoir simulations and storage capacity predictions (Al-Khdheeawi et al., 2017a; Al-Khdheeawi et al., 2017).

Although the concentrations of organic molecules in deep aquifers is normally low (Stalker et al., 2013), their prevailing concentrations are potentially sufficient to significantly influence the rock's wettability characteristics (Gomari & Hamouda, 2006; Iglauer et al., 2014; Standnes & Austad, 2003). Indeed, a partial mono-molecular layer adsorbed to the mineral surface would be sufficient for this (Adamson & Gast, 1967; Bikkina, Wan, Kim, Kneafsey, & Tokunaga, 2016; Gaines, 1966; Kuhn & Möbius, 1971; Maboudian & Howe, 1997; Mahadevan, 2012; Shafrin & Zisman, 1962; Zasadzinski et al., 1994).

These minute organic concentrations can adversely affect the storage capacities and containment security via their impact on CO_2 wettability (Al-Khdheeawi et al., 2017a; Al-Khdheeawi et al., 2017; Iglauer, Al-Yaseri, et al., 2015; Iglauer, Pentland, et al., 2015). It is therefore important to understand at what organic concentration the impact on CO_2/Water/Mineral wettability becomes significant for trapping capacities. Thus, this work aims to benchmark the influence of trace concentrations of such organics and the effect of their carbon chain length on CO_2-rock wettability.

3.2.2 Experimental Methodology

3.2.2.1 Materials

Nine pure quartz samples (Quartz (single crystals; testing chips from WARD'S Natural Science; sample range = 12 mm to 19 mm x 10 mm x 10 mm) were used as a model for sandstone storage formations. The surface roughness of all nine surfaces were provided by the supplier and the values ranged from 1 nm to 2 nm (root-mean-square (RMS) surface roughness, which is very smooth (Sarmadivaleh et al., 2015).

CO_2 (purity ≥ 99.999 mol%; from BOC, gas code-082), N_2 (purity ≥ 99.999 mol%; from BOC, gas code-234) and 10 wt% NaCl brine (NaCl purity ≥ 99.9mol%; from Scharlab) were used. The NaCl was dissolved in deionized water (Ultrapure from David Gray; electrical conductivity = 0.02 mS/cm). Subsequently, the NaCl brine was equilibrated with CO_2 at experimental conditions in a high pressure mixing reactor (according to the procedure described by (El-Maghraby et al., 2012). To represent organic compounds, organic acids were selected due to their presence in hydrocarbon reservoirs and aquifers; these included hexanoic acid, lauric acid, stearic acid, and lignoceric or oleic acid (Amaya et al., 2002; Hamouda & Rezaei Gomari, 2006; Hansen et al., 2000; Jardine et al., 1989; Kharaka et al., 2009; Legens et al., 1999; Madsen & Ida, 1998; Stalker et al., 2013; L. Yang et al., 2015), as shown in Table 3-2-1 (purchased from Sigma Aldrich, purity ≥ 98 mol%).

Table 3-2-1 Properties of organic acids used in this study.

Organic Acid	Physical state	Formula	Number of C atoms	Molar mass (g/mol)	Chemical Structure
Hexanoic acid	Liquid	$C_6H_{12}O_2$	6	116.158	
Lauric acid	solid	$C_{12}H_{24}O_2$	12	200.318	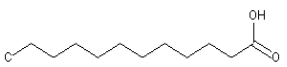
Stearic acid	solid	$C_{18}H_{36}O_2$	18	284.4772	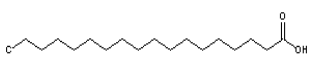
Lignoceric acid	solid	$C_{24}H_{48}O_2$	24	368.63	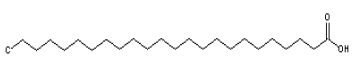

Acetone (≥ 99.9 mol%; from Rowe Scientific) was used as the surface cleaning agent, and drops of aqueous hydrochloric acid (ACS reagent, concentration 37 vol%, Sigma Aldrich) were used to control the pH of the brine (see ageing procedure below for more details).

3.2.2.2 Sample preparation

3.2.2.2.1 Quartz surface preparation

Initially, the mineral (quartz) substrates were cleaned with DI-water to remove any dust or surface fragments from the surface. The sample was then dried in an oven at 90°C for 60 mins and exposed to air plasma (using a Diemer Yocto instrument) for 15 mins to remove any organic contamination (Iglauer et al., 2014; Love et al., 2005).

3.2.2.2.2 Ageing procedure

To mimic a typical storage formation, where the rock pore surfaces were exposed to formation water over geological times we adopted the following strategy (Birkholzer et al., 2009; J. A. Davis, 1982; Hoeiland et al., 2001; Ji & Zhu, 2015; Karoussi et al., 2008; Kleber et al., 2015; Nordbotten et al., 2005; Ochs et al., 1994; Ulrich et al., 1988; White et al., 2003; Zullig & Morse, 1988):

The quartz samples were immersed for 30 mins in 2 wt% NaCl brine at ambient conditions, while the acidity was maintained at pH = 4 by adding drops of aqueous hydrochloric acid; this procedure increases the adsorption rate of organics onto the substrate, and thus simulates adsorption of organic molecules over geological times (i.e. millions of years' exposure time) (Jardine et al., 1989; Kharaka et al., 2009; Madsen & Ida, 1998; Stalker et al., 2013; Thurman, 2012; L. Yang et al., 2015). Ultraclean N_2 was then used to mechanically clean (blow away) the remaining water from the surface to avoid contamination. Subsequently, the substrates were aged in different organic acid/n-decane solutions of prescribed molarity (10^{-2} M to 10^{-10} M organic acid concentration) for seven days to mimic exposure to formation fluid (which contains organic molecules) over geological time (Jardine et al., 1989; Kharaka

et al., 2009; Madsen & Ida, 1998; Stalker et al., 2013; Thurman, 2012; L. Yang et al., 2015).

Previously, silanes were used to render the wettability of quartz surfaces oil-wet. Typically, different silanes have different impacts on surfaces hydrophilicity (Dickson et al., 2006; Grate et al., 2012; Hobeika et al., 2017). However, organic acids including stearic acids represent more realistically subsurface environments (Al-Anssari, Arif, et al., 2018; Al-Anssari et al., 2016; Gomari & Hamouda, 2006; Hamouda & Rezaei Gomari, 2006; Paterson et al., 2011); while silanes do not exist in the subsurface (due to their high reactivity).

It is vital to re-create such mineral surfaces to realistically mimic the subsurface behaviour, particularly to their wettability characteristics (Adamson & Gast, 1967; J. A. Davis, 1982; Kleber et al., 2015; Ochs et al., 1994). Note that it is proven that carboxylic acids and hydrocarbons both exist in deep saline aquifers (Bennett et al., 1993), as a result of biodegradation and organic matter diagenesis and subsequent migration into the water zones (Jones et al., 2008).

Mechanistically, the organic acid esterifies the hydroxyl groups on the quartz surface in a condensation reaction (Scheme 3-2-1).

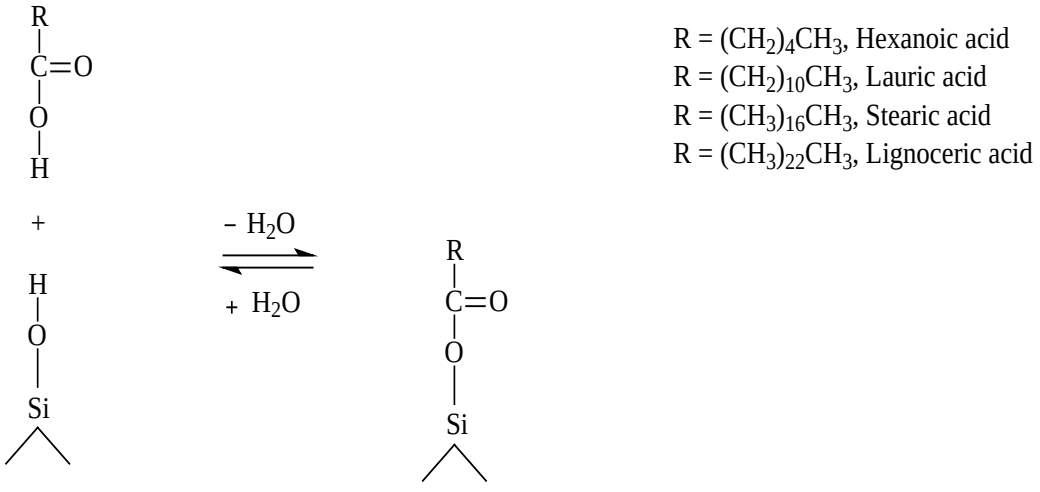

Scheme 3-2-1 Chemisorption of organic acids on solid quartz surface (⩚ indicates solid bulk).

Thus carboxylic components are chemically (covalently) bonded to the quartz surface, rendering them strongly hydrophobic (Al-Anssari et al., 2016).

3.2.2.3 Surface characterization of pure and aged quartz surfaces

The surface properties of the quartz samples were analysed via energy-dispersive X-ray spectroscopy (EDS, Oxford X-act SSD X-ray detector with Inca and Aztec software) and contact angle (θ) measurements. Table 3-2-2 lists the EDS results before and after ageing; these are average elemental surface concentrations (these are average over 45 data points: 5 data points measured on each sample, on nine different samples) for each acid tested. Surface coverages with organic acid are also given determined via the method defined by (Dickson et al., 2006).

Table 3-2-2 Surface composition of pure and aged quartz samples and associated surface coverage with all organic acids.

Concentration (Molarity)	Pure Quartz			After ageing			Change due to ageing			Estimated surface coverage, after (Dickson et al., 2006)
	wt% Si	wt% C	wt% O	wt% Si	wt% C	wt% O	wt% Si	wt% C	wt% O	$\left(1-\frac{wt\%\ C_{before\ aging}}{wt\%\ C_{after\ aging}}\right)\times 100$
Hexanoic Acid										
10^{-2}	31.9	2.3	65.8	38.1	4.8	57.1	+6.2	+2.5	-8.7	52.1
10^{-3}	33.3	4.1	62.6	30.3	7.5	62.2	-3.0	+3.4	-0.4	45.3
10^{-4}	35.4	2.8	61.8	37.0	4.9	58.1	+1.6	+2.1	-3.7	42.9
10^{-5}	34.7	3.2	62.1	34.2	5.1	60.7	-0.5	+1.9	-1.4	37.3
10^{-6}	29.0	3.5	67.5	32.9	5.2	61.9	+3.9	+1.7	-5.6	32.7
10^{-7}	29.5	4.2	66.3	29.0	5.8	65.2	-0.5	+1.6	-1.1	27.6
10^{-8}	32.8	1.8	65.4	48.0	2.3	49.7	+15.2	+0.5	-15.7	21.7
10^{-9}	29.9	3.4	66.7	33.1	4.1	62.8	+3.2	+0.7	-3.9	17.1
10^{-10}	31.8	2.6	65.6	32.0	2.9	65.1	+0.2	+0.3	-0.5	10.3
0	34.0	1.5	64.5	34.0	1.5	64.5	0	0	0	0
Lauric Acid										
10^{-2}	38.1	2.4	59.5	27.6	5.3	67.1	-10.5	+2.9	+7.6	54.7
10^{-3}	33.8	1.8	64.4	31.1	3.5	65.4	-2.7	+1.7	+1.0	48.6
10^{-4}	33.0	3.4	63.6	28.8	6.1	65.1	-4.2	+2.7	+1.5	44.3
10^{-5}	38.3	4.3	57.4	35.4	7.1	57.5	-2.9	+2.8	+0.1	39.4
10^{-6}	32.4	2.6	65.0	34.1	4.0	61.9	+1.7	+1.4	-3.1	35.0
10^{-7}	34.5	3.6	61.9	33.5	5.2	61.3	-1.0	+1.6	-0.6	30.8
10^{-8}	32.4	4.1	63.5	32.7	5.4	61.9	+0.3	+1.3	-1.6	24.1
10^{-9}	32.4	1.4	66.2	36.1	1.7	62.2	+3.7	+0.3	-4.0	17.6
10^{-10}	32.2	3.5	64.3	32.8	4.1	63.1	+0.6	+0.6	-1.2	14.6
0	31.6	2.3	66.1	31.6	2.3	66.1	0	0	0	0

Stearic Acid										
10^{-2}	35.4	1.3	63.3	32.2	3.1	64.7	-3.2	+1.8	+1.4	58.1
10^{-3}	34.3	3.7	62.0	26.8	7.6	65.6	-7.5	+3.9	+3.6	51.3
10^{-4}	37.0	4.5	58.5	26.7	8.4	64.9	-10.3	+3.9	+6.4	46.4
10^{-5}	36.8	1.6	61.6	32.3	2.8	64.9	-4.5	+1.2	+3.3	42.9
10^{-6}	35.8	2.4	61.8	41.7	3.8	54.5	+5.9	+1.4	-7.3	36.8
10^{-7}	36.0	4.3	59.7	22.0	6.3	71.7	-14.0	+2.0	+12	31.7
10^{-8}	38.2	2.9	58.9	23.8	4.0	72.2	-14.4	+1.1	+13.3	27.5
10^{-9}	34.1	4.2	61.7	23.5	5.2	71.3	-10.6	+1.0	+9.6	19.2
10^{-10}	36.5	4.1	59.4	45.4	4.9	49.7	+8.9	+0.8	-9.7	16.3
0	36.5	2.2	61.3	36.5	2.2	61.3	0	0	0	0
Lignoceric Acid										
10^{-2}	37.3	2.3	60.4	25.0	6.2	68.8	-12.3	+3.9	+8.4	62.9
10^{-3}	36.3	2.0	61.7	25.4	4.6	70.0	-10.9	+2.6	+8.3	56.5
10^{-4}	34.1	4.0	61.9	21.9	7.8	70.3	-12.2	+3.8	+8.4	48.7
10^{-5}	35.6	3.4	61.0	24.8	6.2	69.0	-10.8	+2.8	+8.0	45.2
10^{-6}	34.7	3.5	61.8	32.3	5.8	61.9	-2.4	+2.3	+0.1	39.7
10^{-7}	33.9	4.1	62.0	28.9	6.1	65.0	-5.0	+2.0	+3.0	32.8
10^{-8}	33.7	2.7	63.6	26.0	3.9	70.1	-7.7	+1.2	+6.5	30.8
10^{-9}	39.6	1.9	58.5	27.7	2.5	69.8	-11.9	+0.6	+11.3	24.0
10^{-10}	36.5	4.2	59.3	25.0	5.1	69.9	-11.5	+0.9	+10.6	17.6
0	34.0	3.6	62.4	34.0	3.6	62.4	0	0	0	0

Table 3-2-3 Average Elemental surface analysis of quartz samples before and after ageing.

Organic Acids	Before ageing			After ageing		
	Si (wt%)	C (wt%)	O (wt%)	Si (wt%)	C (wt%)	O (wt%)
Hexanoic acid	$32.2^{a} \pm 3.2^{b}$	$2.9^{a} \pm 1.4^{b}$	$64.8^{a} \pm 2.9^{b}$	$34.9^{a} \pm 9.5^{b}$	$4.4^{a} \pm 3.0^{b}$	$60.7^{a} \pm 7.8^{b}$
Lauric acid	$33.9^{a} \pm 3.4^{b}$	$2.9^{a} \pm 1.5^{b}$	$63.2^{a} \pm 4.4^{b}$	$32.4^{a} \pm 4.3^{b}$	$4.5^{a} \pm 2.7^{b}$	$63.2^{a} \pm 4.8^{b}$
Stearic acid	$36.1^{a} \pm 2.1^{b}$	$3.1^{a} \pm 1.6^{b}$	$60.8^{a} \pm 2.4^{b}$	$31.1^{a} \pm 11.7^{b}$	$4.8^{a} \pm 3.1^{b}$	$64.1^{a} \pm 11.3^{b}$
Lignoceric acid	$35.6^{a} \pm 3.0^{b}$	$3.2^{a} \pm 1.2^{b}$	$61.3^{a} \pm 2.6^{b}$	$27.1^{a} \pm 6.1^{b}$	$5.2^{a} \pm 2.7^{b}$	$67.7^{a} \pm 4.2^{b}$

[a] an average surface concentration is based on the arithmetic average of 45 data points measured on five different sites for each of the nine samples at all concentrations tested.
[b] '±' values are the standard deviations of these observations.

Clearly, ageing had a significant impact on the atomic surface concentrations irrespective of the type and concentration of organic acid (Table 3-2-3). A significant

overall average increase in surface carbon concentration (+1.6 wt% C for Hexanoic Acid, +1.7 wt% C for Lauric Acid, +1.9 wt% C for Stearic Acid and +2.2 wt% C for Lignoceric Acid) was measured. These changes in atomic coverage were caused by the chemisorption of the carboxylic acid on the quartz surface, consistent with (Zullig & Morse, 1988); see also section 3.2.2.2.2 and scheme 3-2-1 above.

Moreover, the brine contact angles on the pure quartz samples were 0° (advancing and receding) at ambient conditions, thus pure quartz was completely water-wet at ambient conditions. However, higher contact angles (advancing 56° and receding 54° ± 3°) were measured at reservoirs conditions on these pure quartz samples (323 K (50 °C), 25 MPa), consistent with literature data (A. Z. Al-Yaseri et al., 2016; Al-Yaseri et al., 2016; Arif, Barifcani, & Iglauer, 2016; Chiquet et al., 2007; Farokhpoor et al., 2013). However, the ageing of the quartz surfaces caused a significant change in contact angles and thus CO_2-wettability, this is discussed in section 3.2.3.

3.2.2.4 Contact angle measurements

Contact angle measurements are a standard technique for assessing the wettability behaviour of a given rock/fluid/fluid system. Here we used the tilted plate technique, which is regarded as the most effective contact angle measurement method as it can measure advancing and receding contact angles simultaneously (Lander et al., 1993).

The schematic of the experimental setup is shown in Figure 3-2-1. It consists of a high pressure-high temperature cell, which houses the sample inside on a tilted plate. The cell is connected to two pumps (Teledyne D-500, pressure accuracy of 0.1%) used for either discharging brine or CO_2. Furthermore, a CO_2 gas cylinder and the brine pump are both connected to a mixing reactor with which CO_2 and brine can be thermodynamically equilibrated (El-Maghraby et al., 2012).

Initially, the cell was charged with CO_2 at the desired measurement pressure and temperature (0.1 MPa, 25 MPa and 323 K (50 °C)). The temperature of the pumps was controlled through the heating bath and the cell temperature was controlled through heating tape around it. The brine pump was initially filled with CO_2-equilibrated brine (equilibrated at experimental conditions) and a droplet of equilibrated brine (average

drop volume was 6 µL (± 1 µL) was dispensed onto the quartz surface through a needle. The advancing (θ_a) and receding (θ_r) brine contact angles were then measured at the leading and trailing edge of the droplet just before the drop started to move (Lander et al., 1993). This process was recorded by a high-performance video camera (Basler SCA 640–70 fm, pixel size = 7.4 µm; frame rate = 71 fps; Fujinon CCTV lens: HF35HA-1B; 1:1.6/35 mm), which was connected to a computer system to display and analyse the results. The standard deviation of the measurements was ± 3° based on replicated measurements.

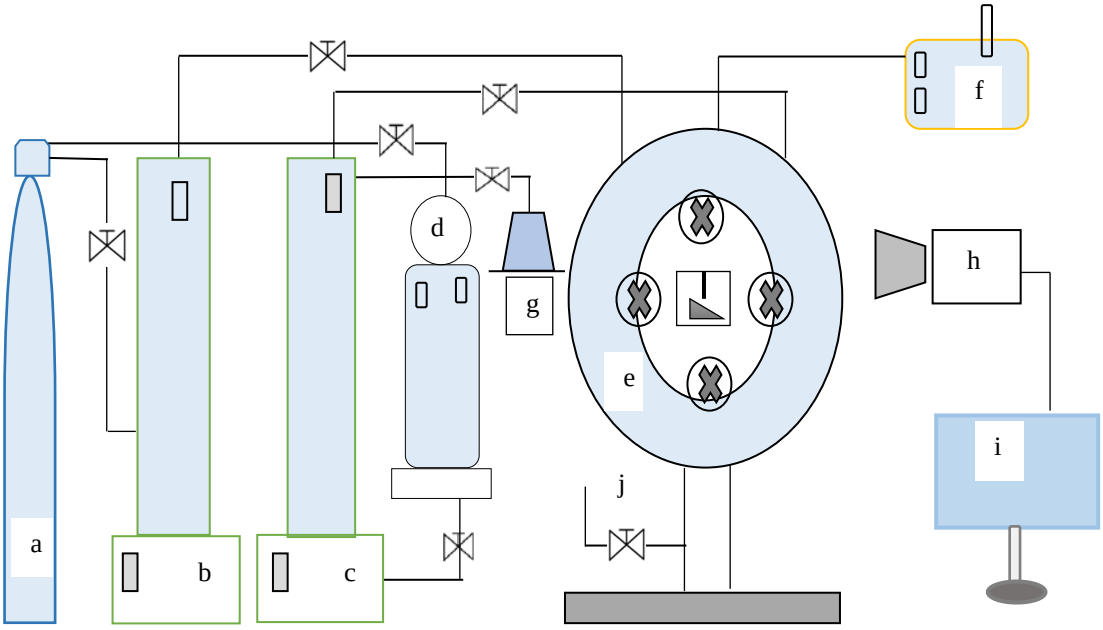

Figure 3-2-1 Experimental setting used in this study for measuring advancing and receding contact angles, modified after (Arif, Lebedev, et al., 2017a). (a) CO_2 cylinder (b) high precision syringe pump-CO_2, (c) high precision syringe pump-water, (d) High-pressure Parr reactor for fluid equilibration e) high-pressure cell with substrate housed on a tilted plate inside, (f) heating unit, (g) liquid feed/drain system, (h) high-resolution video camera, (i) image visualization and interpretation software, (j) pressure relief valve.

3.2.3 Results and Discussion

Our results show that the quartz surface loses its water-wetness with increasing organic acid concentration. However, at organic acid concentrations $\leq 10^{-6}$ M, contact angles were only minimally affected, Figure 3-2-6, and thus structural trapping is not

significantly affected (note: even at low concentrations ≤ 10^{-6} M optimal residual trapping capacities are significantly affected). However, for concentrations > 10^{-6} M, quartz wetting behaviour shifts from strongly water-wet to an intermediate-wet state (Iglauer, Pentland, et al., 2015). A recent study conducted on carbonate minerals (Ali, Al-Anssari, et al., 2019) showed that even at low organic concentrations (≤ 10^{-6} M organic acid), optimal residual trapping capacities could be affected, which is due to the surface coverage of the mineral with organic acid and its tendency to alter the formation more CO_2-wet. Such wettability alteration changes the primary drainage capillary pressure curve (W. G. Anderson, 1987a; Masalmeh, 2003; Morrow, 1970), and thus the initial CO_2 saturation directly influencing the residual CO_2 saturation (Akbarabadi & Piri, 2015; Heshmati & Piri, 2014; C. Pentland et al., 2011; S. Wang & Tokunaga, 2015).

3.2.3.1 Effect of acid concentration on quartz wettability

Advancing and receding brine contact angles increased significantly with an increase in organic acid concentration, as shown in Figures 3-2-2 to 3-2-5.

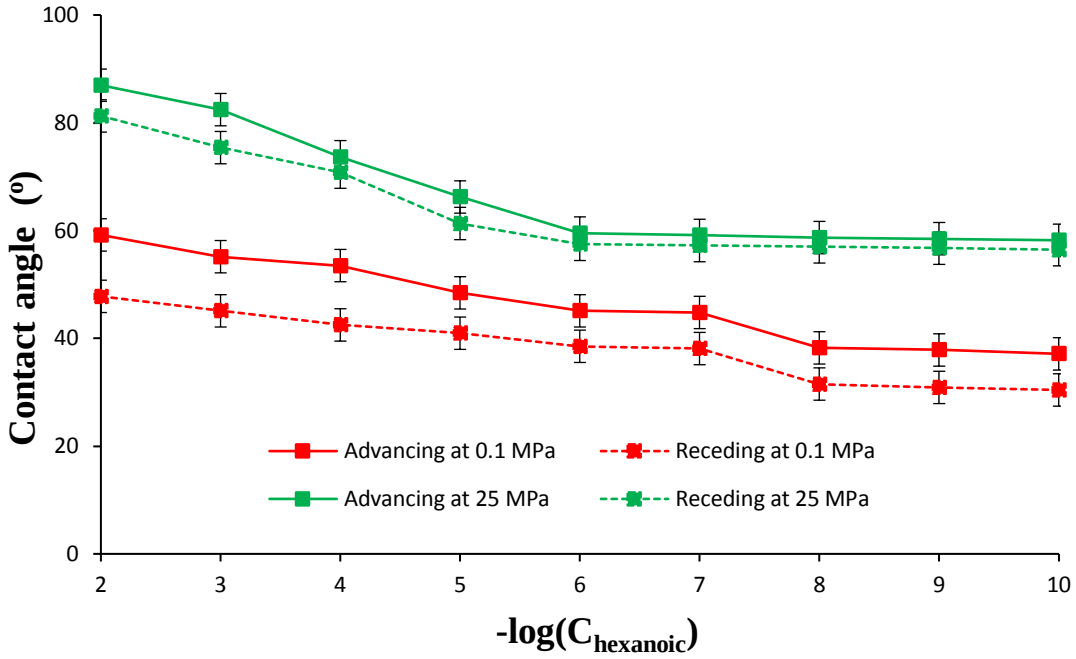

Figure 3-2-2 Quartz/CO_2/brine contact angles (measured through the water) as a function of hexanoic acid (C_6) concentration; $C_{hexanoic}$ is the hexanoic acid

concentration (molarity). Solid lines: advancing; dotted lines: receding. Red: ambient pressure; green: 25 MPa and 323 K (50 °C).

The contact angle was significantly higher at high pressure, consistent with literature data (A. Z. Al-Yaseri et al., 2016; Al-Yaseri et al., 2016; Broseta et al., 2012; Chen et al., 2015; Dickson et al., 2006; Espinoza & Santamarina, 2010; Iglauer, 2017; Iglauer, Al-Yaseri, et al., 2015; Iglauer, Pentland, et al., 2015; Kaveh et al., 2016; Kaveh et al., 2012). For example, at 25 MPa and 323 K (50 °C), for the quartz surface aged in 10^{-10} M hexanoic acid, θ_a was 58° and θ_r was 55° implying that the quartz surface is weakly water-wet under such conditions. With an increase in hexanoic acid concentration up to 10^{-6} M, there was an insignificant change in θ. However, further organic acid concentration increase resulted in a significant contact angle increase. For instance, when the hexanoic acid concentration increased to 10^{-2} M, at the same temperature and pressure (25 MPa, and 323 K (50 °C)), θ_a and θ_r increased to 87° and 82°, implying a wettability transformation from weakly water-wet to intermediate-wet. Such a reduction in water wettability of the surface potentially leads to a reduction in residual trapping capacities where CO_2 plume is migrating in storage formation (Al-Menhali & Krevor, 2016; Chaudhary et al., 2013; Iglauer, 2017; Rahman et al., 2016). Note for instance that lower residual CO_2 saturations have been measured in more hydrophobic rock by x-ray micro-tomography (Al-Menhali & Krevor, 2016; Chaudhary et al., 2013; Rahman et al., 2016).

Lauric acid followed somewhat similar trends. For the quartz surface aged in 10^{-10} M lauric acid, quartz/CO_2/water contact angles were significantly lower than those measured on surfaces aged in 10^{-2} M lauric acid. Thus higher organic concentrations render the surface more non-wetting to water. For example, at 25 MPa and 323 K (50 °C), for the quartz surface aged in 10^{-10} M lauric acid, θ_a measured as 61° and θ_r as 56°, which increased to θ_a = 89° and θ_r = 84° when lauric acid concentration increased to 10^{-2} M (Figure 3-2-3).

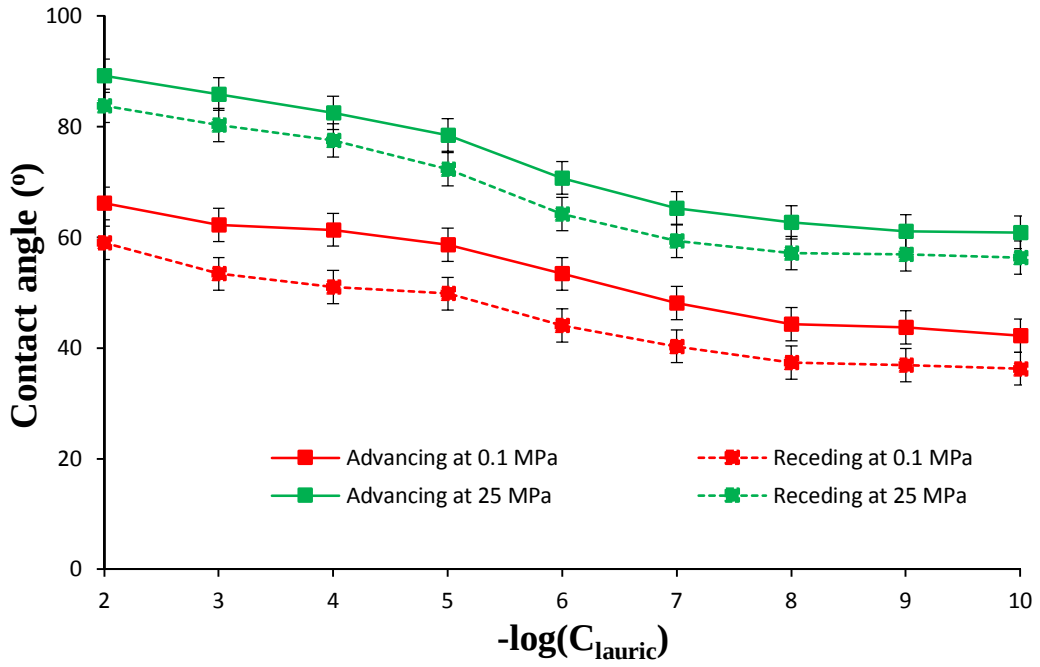

Figure 3-2-3 Quartz/CO_2/brine contact angles as a function of lauric acid (C_{12}) concentration; C_{lauric} is the lauric acid concentration (molarity). Solid lines: advancing; dotted lines: receding. Red: ambient pressure; green: 25 MPa and 323 K (50 °C).

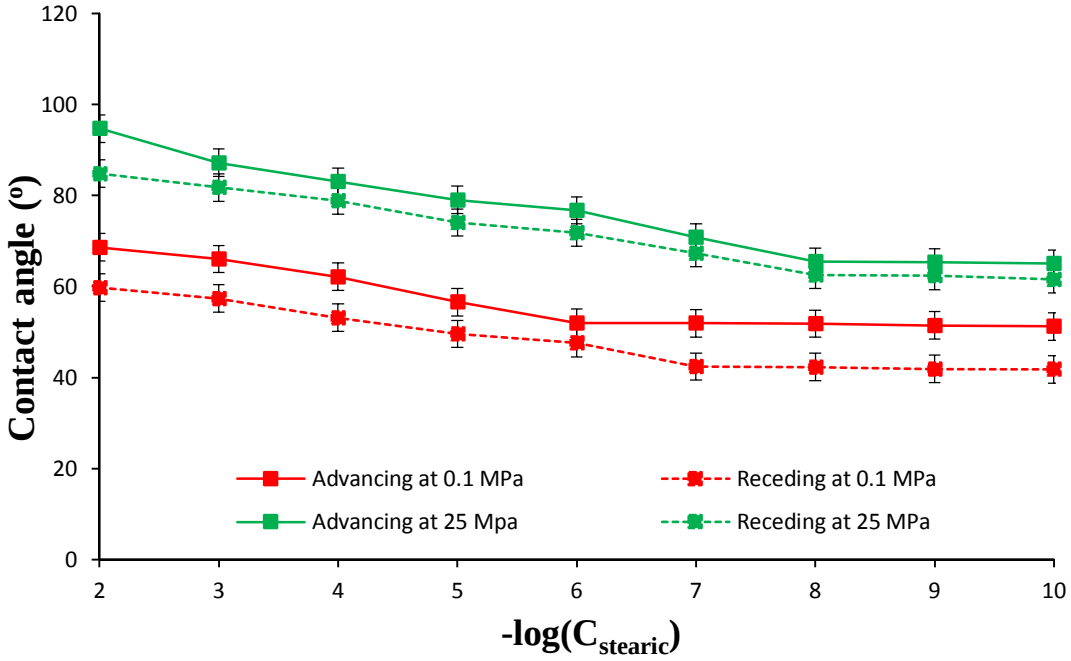

Figure 3-2-4 Quartz/CO_2/brine contact angles as a function of stearic acid (C_{18}) concentration; $C_{stearic}$ is the stearic acid concentration (molarity). Solid lines: advancing; dotted lines: receding. Red: ambient pressure; green: 25 MPa and 323 K (50 °C).

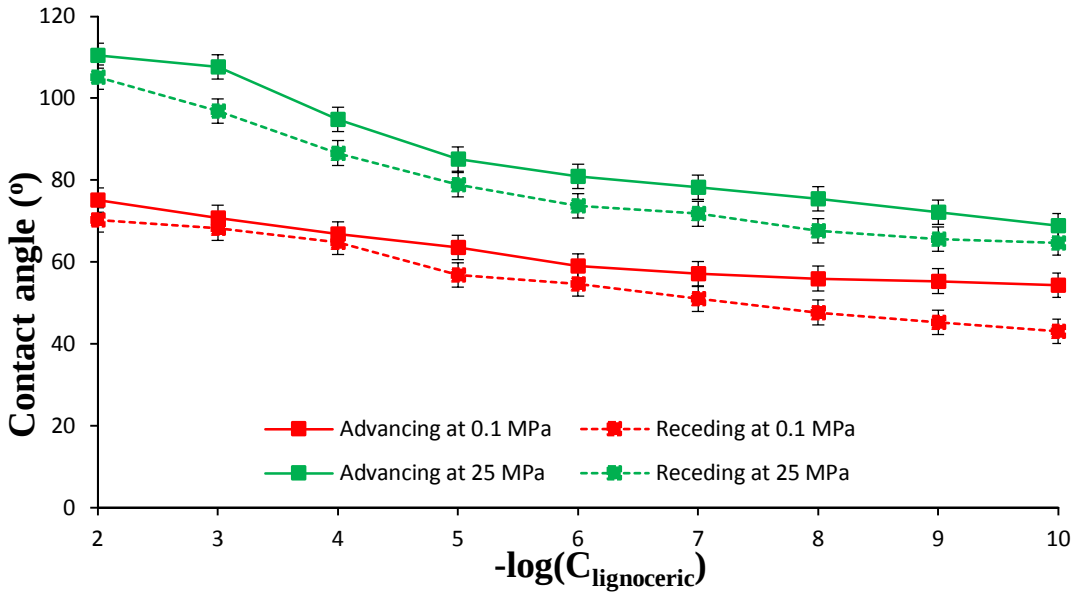

Figure 3-2-5 Quartz/CO_2/brine contact angles as a function of lignoceric acid (C_{24}) concentration; $C_{lignoceric}$ is the lignoceric acid concentration (molarity). Solid lines: advancing; dotted lines: receding. Red: ambient pressure; green: 25 MPa and 323 K (50 °C).

The results showed the same trend for quartz surfaces aged in stearic acid and lignoceric acid (Figures 3-2-4 and 3-2-5). In summary, the higher the organic acid concentration was, the higher were the values of both the advancing and receding water contact angles irrespective of the type of organic acid used for ageing. Our results are consistent with literature data on wettability of calcite/oil/brine systems in the presence of organic acids (Gomari & Hamouda, 2006; Hansen et al., 2000; Standnes & Austad, 2003). Mechanistically, carboxylic acid adsorbs onto the quartz surface leading to a wettability modification towards less water-wet surface conditions, see above in scheme 3-2-1.

When compared with the CO_2-wettability of pure quartz surfaces, we find that higher contact angles are found, even at the lowest organic acid concentration (10^{-10} M, which is very low). For instance, for pure quartz/CO_2/brine system, at 20 MPa and 323 K (50 °C), θ_a was reported to be approximately 40° (Sarmadivaleh et al., 2015), whereas the lowest θ_a in the presence of lowest chain organic acid (Hexanoic acid, C_6) was 57° (Figure 3-2-6). It is thus clear that even minute amounts of organic acid significantly

increase the CO_2-wettability of mineral surfaces. As such minute concentrations always exist in the subsurface, even in aquifers (Bennett et al., 1993; Jones et al., 2008; Stalker et al., 2013), lower residual trapping capacities than previously thought are expected (Ali, Al-Anssari, et al., 2019).

3.2.3.2 Influence of organic acid alkyl chain length on quartz wettability

It is clear that all organic acids similarly influence the quartz wettability i.e. both water advancing and receding contact angles increase with an increase in organic acid concentration and quartz rapidly loses its water-wetness, Figure 3-2-6. However, at a fixed organic acid concentration, the absolute values of contact angles were different for different acids (which differ in their alkyl chain length and their coverage on the quartz surface, as shown in Figure 3-2-6); surfaces aged in hexanoic acid (C_6) exhibited the lowest contact angles values, while surfaces aged in lignoceric acid (C_{24}) exhibited the highest contact angles values. Lauric acid and stearic acid fell in between. For instance, at 25 MPa and 323 K (50 °C), and a fixed organic concentration 10^{-2} M of hexanoic, lauric, stearic and lignoceric acid, $\theta_r = 81°$, $\theta_r = 84°$, $\theta_r = 85°$ and $\theta_r = 105°$, respectively. Such a wettability transformation from intermediate-wet to CO_2-wet is attributed to the number of carbon atoms present in the acid, Table 3-2-1. Clearly, longer alkyl chains in the organic acid renders the surface more hydrophobic.

These effects have a dramatic impact on the optimal residual trapping limit, which we consider here as the point where primary drainage is unaffected by wettability, i.e. at $\theta_a = 50°$ (Morrow, 1970, 1976). For example, at 25 MPa and 323 K (50 °C) and a fixed trace organic concentration of 10^{-10} M, $\theta_a > 50°$ for all acids (note that this is a very minute concentration, and much higher organic concentrations were measured in deep saline aquifers (Jardine et al., 1989; Kharaka et al., 2009; Madsen & Ida, 1998; Stalker et al., 2013; Thurman, 2012; L. Yang et al., 2015); Figure 3-2-6.

Overall it is clear that a detailed knowledge of organic acids and their relative concentrations in storage formations is very important for assessing the feasibility of long-term geological storage projects.

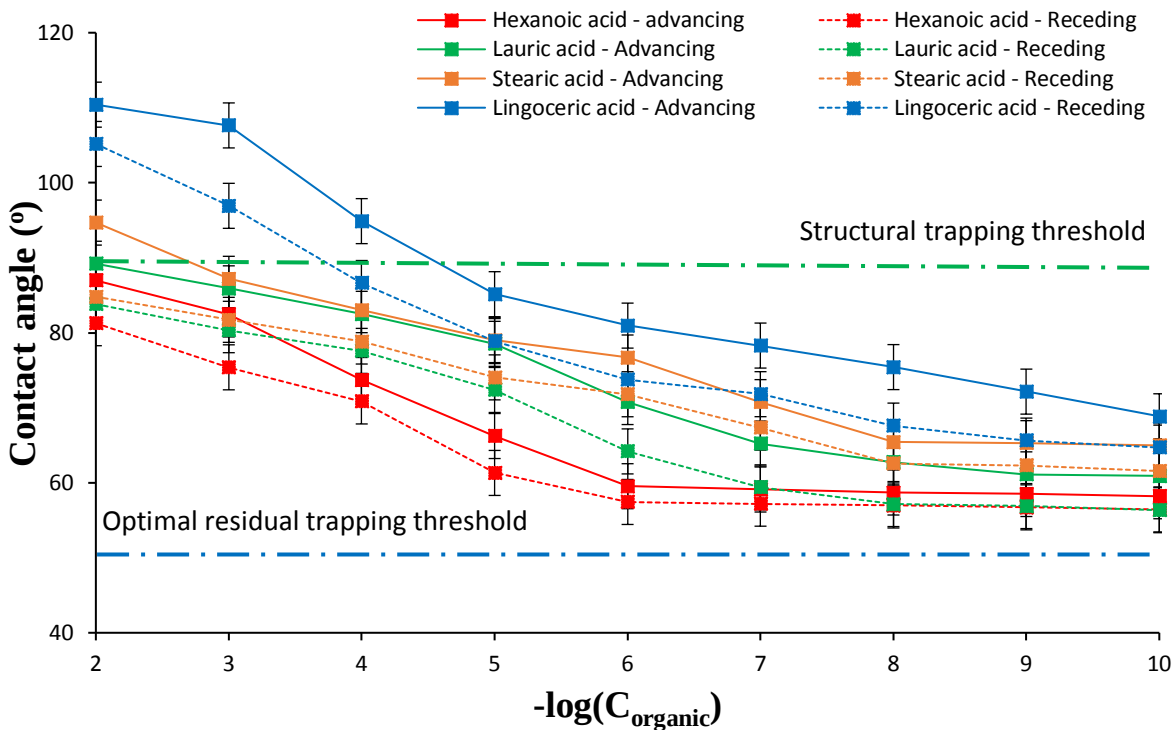

Figure 3-2-6 Quartz/CO_2/brine contact angles as a function of organic acid concentration and alkyl chain length at 25 MPa and 323 K (50 °C); $C_{organic}$ is the organic acid concentration (molarity). Dotted blue horizontal lines in the graph define the capillary trapping threshold ($\theta = 50°$), and dotted green horizontal lines in graph define the structural trapping ($\theta > 90°$) threshold.

3.2.4 Conclusions

Deep saline aquifers contain organic acids, which have a direct impact on the interfacial phenomena at the fluid/rock interface due to chemisorption. These effects are, however, only poorly understood; thus we measured the wettability of quartz/CO_2/brine systems in the presence of various organic acids. Four acids (hexanoic acid, lauric acid, stearic acid, lignoceric acid) were considered for a wide range of concentrations (10^{-9} M to 10^{-2} M) and advancing and receding contact angles were measured at typical storage conditions (25 MPa and 323 K (50 °C), as well as at ambient pressure) to mimic a realistic subsurface behaviour. We found that both advancing and receding contact angles increased with an increase in organic acid concentration throughout the tested experimental matrix. In addition, at a fixed organic acid concentration, the highest contact angles values were measured for lignoceric acid

(C_{24}), while the relatively least values were recorded for hexanoic acid (C_6). This behaviour is attributed to the number of carbon atoms in the organic acids alkyl chain, and hence a higher number of C atoms, resulting in more CO_2-wet/hydrophobic surfaces, which causes a reduction in residual trapping capacities.

We thus conclude that CO_2 geological storage capacities in certain geological scenarios (aquifers as an example) may be lower than previously thought. Reservoir-scale models thus need to take these effects into account so that accurate storage predictions are obtained thus de-risking carbon geological storage (CGS) projects.

PART 3 Influence of Organic Acid Concentration on Wettability Alteration of Cap-Rock: Implications for CO2 Trapping/Storage

Muhammad Ali [a,*], Adnan Aftab [b], Zain-Ul-Abedin Arain [a], Ahmed Al-Yaseri [c], Hamid Roshan [d], Ali Saeedi [a], Stefan Iglauer [a,c], Mohammad Sarmadivaleh [a],

[a] Western Australia School of Mines, Minerals, Energy and Chemical Engineering, Curtin University, 26 Dick Perry Avenue, Kensington, 6151, WA, Australia

[b] Petroleum Engineering Department, Mehran University of Engineering and Technology, Khairpur Mir's Campus, 66020, Sindh, Pakistan

[c] Petroleum Engineering Discipline, School of Engineering, Edith Cowan University, 270 Joondalup Dr, Joondalup, 6027, WA, Australia

[d] Petroleum Engineering Department, University of New South Wales, Sydney, 2052, NSW, Australia

[*] Corresponding author (Muhammad.ali7@postgrad.curtin.edu.au)

Abstract

Every year millions of tonnes of CO_2 are stored in CO_2-storage formations (deep saline aquifers) containing traces of organic acids including hexanoic acid C_6 (HA), lauric acid C_{12} (LuA), stearic acid C_{18} (SA) and lignoceric acid C_{24} (LiA). The presence of these molecules in deep saline aquifers is well documented in the literature, however their impact on structural trapping capacity and thus containment security is not yet understood. In this study, we, therefore, investigate how an increase in organic acid concentration can alter mica water wettability through an extensive set of experiments. The X-ray diffraction [(XRD) Figure S3-3-2], Field emission scanning electron microscopy (FESEM), Total organic carbon (TOC), Fourier transform infrared spectroscopy (FTIR), Atomic force microscopy (AFM) and Energy dispersive spectroscopy (EDS) were utilized to perceive variations in organic acid surface coverage with stepwise organic acid concentration increase and changes in surface roughness. Further, thresholds of wettability that may indicate limits for structural trapping potential ($\theta_r < 90°$) have been discussed. The experimental results show that

even minute concentration (~10^{-5} mol/L for structural trapping) of lignoceric acid is enough to affect CO_2 trapping capacity at 323 K and 25 MPa. Since higher concentrations exist in deep saline aquifers, it is necessary to account for these thresholds to de-risk CO_2-geological storage (CGS) projects.

3.3.1 Introduction

CO_2 capture and trapping in underground formations using CO_2-geological storage (CGS) is an inevitable option to mitigate the greenhouse gas effect (Metz et al., 2005). New methods are always discussed for capturing CO_2 (Buyukcakir, Je, Talapaneni, Kim, & Coskun, 2017; Ren et al., 2019; Sevilla, Al-Jumialy, Fuertes, & Mokaya, 2018), but its storage is limited. After capturing CO_2 at the surface, deep saline aquifers, coal beds, organic-rich shale reservoirs and depleted oil reservoirs are considered pertinent target formation for the storage of CO_2 (Ali, Dahraj, & Haider, 2015; M. Blunt, 1993; Metz et al., 2005). When CO_2 is stored deep underground, it is immobilized through four types of trapping mechanisms, which prevent upwards flow to the surface (Juanes et al., 2010). These mechanisms comprise structural trapping (Arif, Al-Yaseri, et al., 2016; Arif, Barifcani, Lebedev, et al., 2016; Iglauer, Al-Yaseri, et al., 2015), capillary or residual trapping (Iglauer, Wülling, et al., 2011; C. Pentland et al., 2011), dissolution trapping (Agartan et al., 2015; Al-Khdheeawi et al., 2017b) and mineral trapping (Golding et al., 2011; Matter et al., 2016). It is also noted that adsorption trapping plays an integral role in organic-rich shale formations and coal bed reservoirs (Arif, Lebedev, et al., 2017b; Golding et al., 2011; Kaveh et al., 2012).

It is highly backed by literature that structural and residual trapping mechanisms are the most pertinent storage mechanisms in a storage project (Iglauer, Al-Yaseri, et al., 2015; Iglauer, Pentland, et al., 2015; Iglauer, Wülling, et al., 2011). This is based on the relation of buoyancy to capillary forces. These capillary forces can be quantified by equation (3-3-1), as capillary pressure which is a function of contact angle between CO_2, brine and rock surface, and CO_2-brine interfacial tension (γ).

$$P_c = P_{CO2} - P_{water} = 2\gamma\cos(\theta)/r \quad \text{..... (3-3-1) (Arif, Al-Yaseri, et al., 2016)}$$

Where "P_c" represents capillary pressure, "P_{CO2}" represents CO_2 phase pressure, "P_{water}" represents pressure of water (brine) phase, "r" represents pore throat radius (in this case corresponding to the largest pore). When CO_2 moves upward due to capillary forces, it displaces brine with it, where the relevant angle "θ" is the water receding contact angle or equivalently CO_2 advancing contact angle (Broseta et al., 2012). It is important to mention here that equation (3-3-1) is valid for ideal capillaries, and thus can be presumed as a first estimate, whereas, in real situations, pore geometry is more complex and an important factor to be considered (Iglauer, Pentland, et al., 2015; Purcell, 1950). Theoretically, in the worst-case scenario (CO_2-wet rock), structural trapping is anticipated to fail due to upward-directed suction forces (Iglauer, Pentland, et al., 2015).

CO_2-brine-rock wettability has a profound effect on structural and residual trapping capacities (Abdulelah et al., 2021; Al-Khdheeawi et al., 2017a; Al-Menhali & Krevor, 2016; Iglauer, Al-Yaseri, et al., 2015; Iglauer, Pentland, et al., 2015; Rahman et al., 2016). Wettability is a crucial factor that is very complex in nature and to gauge this effect one should consider all the aspects at realistic subsurface conditions. However, accurate subsurface situations are reductive or anoxic in character and may present the presence of organics in CO_2 storage formations (Akob et al., 2015; Lundegard & Kharaka, 1994). Although the presence of organics in deep saline aquifer is very low (Stalker et al., 2013), but their minute concentrations are enough to alter the wettability to oil-wet (Ali, Al-Anssari, et al., 2019; Ali, Arif, et al., 2019; Gomari & Hamouda, 2006). This wettability alteration to oil-wet can severely impact the containment security and storage capacities of CO_2-storage formations (Al-Khdheeawi et al., 2017a, 2017b; Iglauer, Al-Yaseri, et al., 2015; Iglauer, Pentland, et al., 2015). Therefore, it is relevant to estimate organic concentration thresholds in cap-rock formations to assess the influence of their impact on CO_2 trapping capacities. Thus, in this study, we seek to understand as to what limits of organic concentrations and their carbon chain length may affect the CO_2/Water/Mineral wettability.

We have thus investigated wettability (advancing and receding water contact angles) of CO_2/brine on Mica (muscovite) samples at CO_2 storage conditions. Muscovite is a good cap-rock proxy as it has a chemical structure like to illite, and it is abundantly present in shale cap-rock formations (Arif, Al-Yaseri, et al., 2016; Arif, Barifcani,

Lebedev, et al., 2016; Chiquet et al., 2007). Muscovite chemical formula is $KAl_2(AlSi_3O_{10})(OH)_2$ (Arif, Al-Yaseri, et al., 2016; Arif, Barifcani, Lebedev, et al., 2016), and it is abundantly found in the mica family with others like biotite, phlogopite and illite (Bailey, 1984). In addition, the presence of muscovite is well noted in different metamorphic, sedimentary and igneous rocks (Guidotti, 1984). These minerals wettability has a profound effect on structural trapping capacities (Iglauer, Pentland, et al., 2015; Iglauer, Wülling, et al., 2011). The mica samples were then aged with different organic acids (with different carbon chain length) and different concentrations at a laboratory scale, to investigate the influence of these (tiny) concentrations on the CO_2 wettability of the Mica at subsurface conditions for containment security and CO_2 storage capacities. This information will assist in the broader-scale application of CGS projects and can assist with a reduction in project uncertainty.

3.3.2 Experimental Methodology

3.3.2.1 Materials

Pristine mica substrates (purchased from Ward's natural science; dimensions = 20 mm x 15 mm x 3 mm) were utilized as a proxy for cap-rocks. Atomic force microscopy (AFM instrument from Nano-surf, Flex-Axiom, Controller C3000, scan range XYZ 100x100x10µm) measurements were performed to quantify the surface roughness of all samples. NaCl (from Chemlab; purity ≥ 99.9 mol %) was dissolved in deionized water (electrical conductivity = 0.02 mS/cm, ultrapure from David Gray), for making 10 wt % brine solution for contact angle measurements.

It is widely reported in the literature that mica (muscovite) reacts in acidic environments (in the presence of CO_2) (Gaus, Azaroual, & Czernichowski-Lauriol, 2005; Hu & Jun, 2012). Muscovite chemical formula is $KAl_2(AlSi_3O_{10})(OH)_2$ and it is abundantly found with other clays, such as biotite, phlogopite and illite. While injecting CO_2 into geological formations, CO_2 dissolves in brine. Thereafter, CO_2 diffusion to lower cap-rock sections will trigger geochemical reactions which influence permeability, porosity and consequently perhaps the sealing capacity (Gaus et al., 2005). Gaus et al. (2005) have shown phlogopite reactivity in CO_2-rich brines

at Geo-sequestration conditions at Sleipner (North Sea) (Gaus et al., 2005), as well as Hu and Jun (2012) have shown dissolution of biotite in 1 mol % NaCl solution at various temperature and CO_2-pressure conditions (Hu & Jun, 2012).

Therefore, brine was equilibrated with the mica samples while constantly observing the pH of the brine solution (Venkatraman et al., 2014). In addition to this, CO_2 equilibration with brine was done at storage conditions in a high-temperature high pressure (HPHT) and high circulation (1200 RPM) mixing reactor (Mixing reactor from Parr instruments) to avoid mass transfer effects during the contact angle measurements (El-Maghraby et al., 2012). Four different organic acids (HA, LuA, SA, LiA or oleic acid) based on their carbon chain length were selected for this study due to their existence in depleted hydrocarbon reservoirs and deep saline aquifers to age the mica samples (Ali, Arif, et al., 2019; Ali, Sahito, et al., 2020; Jardine et al., 1989; Stalker et al., 2013), Table 3-3-1 (purity ≥ 98 mol%, from Sigma Aldrich).

Nitrogen (ultra-pure = 99.999 wt% from BOC, gas code-234) was used to clean the mica samples before and after ageing to dry and remove any contaminants from the surface. CO_2 (ultra-pure = 99.999 wt% from BOC, gas code-082) was used in the contact angle measurements at high pressure to simulate the CO_2 storage environment.

Table 3-3-1 Details of organic acids.

Name of Fatty Acid	Formula	Molar mass (g/mol)	Number of C atoms	pH (pKa)	Physical state	Chemical Structure
Hexanoic acid	$C_6H_{12}O_2$	116.158	6	4	Liquid	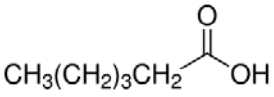
Lauric acid	$C_{12}H_{24}O_2$	200.318	12	5.3	solid	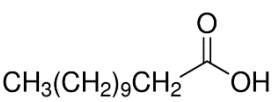
Stearic acid	$C_{18}H_{36}O_2$	284.4772	18	6	solid	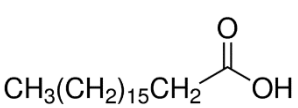
Lignoceric acid	$C_{24}H_{48}O_2$	368.63	24	7.4	solid	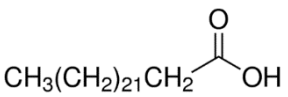

The hydrocarbon reservoirs are created from fossil, which contains fatty acids ranging from C_4 to C_{26} (Caballero et al., 2003). The presence of these fatty acids are well proven in depleted hydrocarbon reservoirs and deep saline aquifers (Akob et al., 2015; Lundegard & Kharaka, 1994; Stalker et al., 2013). Their acidity ranges from 4 to 7.5 pKa which makes them strong to weak acids.

The n-Decane (from Chem-supply; purity 99.9 mol %) was used as a base solution for formulating different organic acid concentrations. Toluene, methanol and acetone (from Rowe Scientific; 99.9 mol %) were utilized to clean the mica surfaces.

3.3.2.2 Procedure of Simulating Subsurface Conditions for Substrate's Surfaces

3.3.2.2.1 Cleaning Procedure of Mica Surfaces

It is important to clean the mica surfaces after they are received, as they will have some contaminants which may affect the experiments. The received mica samples were thus cleaned with deionized water to remove surface fragments and dust followed by blowing substrates with ultra-pure nitrogen and drying at 80 ℃ for 2 hours to remove thin water films after the initial cleaning process. Thereafter, samples were treated through air plasma (Diemer Yocto instrument) for 20 minutes to eliminate slightly remaining organic impurities (Iglauer et al., 2014; Love et al., 2005).

3.3.2.2.2 Ageing Procedure of Mica Surfaces

Deep underground storage formations contain formation connate waters over a long depositional time. To simulate cap-rock, we carried out the following procedure (J. A. Davis, 1982; Kleber et al., 2015; Ulrich et al., 1988; Zullig & Morse, 1988):

The mica surfaces were ionized by placing them in NaCl brine (2 wt %) for 30 minutes at room conditions, in addition to this brine pH was sustained at 4 by adding drops of aqueous hydrochloric acid (HCl, purity > 99%, concentration 37.5 %). This process increases the organic acid adsorption on the mica surfaces (Al-Anssari et al., 2019; Ali, Al-Anssari, et al., 2019; Ali, Arif, et al., 2019; Jardine et al., 1989; Madsen & Ida, 1998; Stalker et al., 2013). Thereafter, all modified surfaces were cleaned using ultra-

clean nitrogen to blow off the remaining brine from the mica surfaces. Afterwards, HCl/Brine ionized mica surfaces were placed in different n-decane/organic acid solutions of set concentrations (10^{-2}, 10^{-3}, 10^{-5}, 10^{-7} and 10^{-9} mol/L organic acid concentration). These mica surfaces were left for 7 days in organic solutions to mimic exposure to formation water for long geological times (Ali, Al-Anssari, et al., 2019; Ali, Arif, et al., 2019; Jardine et al., 1989; Madsen & Ida, 1998; Stalker et al., 2013).

To explore the effect of different organics on different formations, it is pertinent to reproduce these mineralogical formations for quantification of underground characteristics as a function of wettability features (J. A. Davis, 1982; Kleber et al., 2015). Literature lacks the information for effects of organics on different formations at storage conditions, whereas, previously silanes were used to alter the wettability from water-wet to oil-wet (Grate et al., 2012). But the presence of silanes is not possible in real storage formations due to their high reactivity. Deep saline aquifers contain organic acids and traces of hydrocarbons (Bennett et al., 1993) as an outcome of biodegradation of hydrocarbon mixtures where anaerobic conditions succeed and organic substance diagenesis (Akob et al., 2015; Jones et al., 2008). It is also depicted in previous research studies that many samples of different aquifers have shown similar organic acids (Akob et al., 2015; Lundegard & Kharaka, 1994; Stalker et al., 2013). Consequently, using organic acids for altering the wettability is more realistic due to their presence in storage formations (Al-Anssari et al., 2016; Gomari & Hamouda, 2006). This wettability change occurs due to the esterification of organics on the hydroxyl group of mineral surfaces by chemical bonding as shown in scheme 3-3-1. This renders the mineral surfaces strongly hydrophobic (Al-Anssari et al., 2016; Ali, Al-Anssari, et al., 2019; Ali, Arif, et al., 2019).

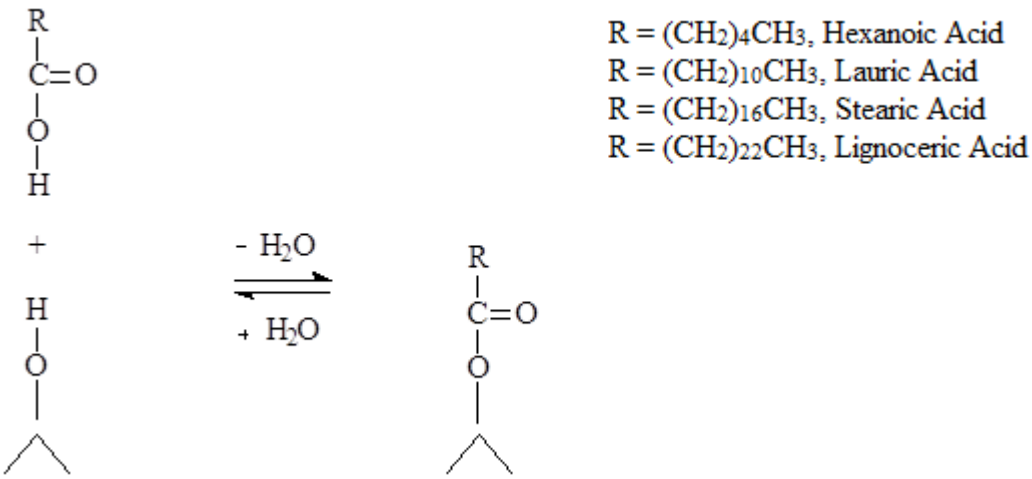

Scheme 3-3-1 Organic acids chemisorption on solid mica substrate (∧ shows mica solid bulk) (Ali, Arif, et al., 2019).

3.3.2.3 Characterization of Mica Surfaces

3.3.2.3.1 Total Organic Carbon Measurement

There are different methods to measure total organic carbon (TOC) (Arif, Lebedev, et al., 2017b; Yu et al., 2017). TOC analysis is widely used in different studies of cap-rock formations and the existence of organic carbon in cap-rock formation is well documented (Alshakhs & Rezaee, 2017). However, further investigation is required to quantify the effects of TOC on wettability and its implications on CO_2-storage formations (Arif, Lebedev, et al., 2017b).

To do this, we used mica samples which were free of organic carbon, to quantify the effects of organic acids on cap-rock formation (Arif, Barifcani, Lebedev, et al., 2016). Therefore, the pyrolysis technique (by Rock-Eval 6 instrument, from Vinci technologies) were used to measure the TOC in pure and aged mica substrates. It is clear from the graph (Figure S3-3-1) that pure mica samples have a negligible presence of TOC (500 ppm), which is due to air contaminations. Whereas, organic aged mica samples have shown a significant presence of TOC (1800 ppm) due to the chemisorption of organic acids. This ageing process is responsible for altering the wettability from a water-wet state to an oil-wet state.

3.3.2.3.2 Elemental composition and Surface Ageing of Mica Substrates

Elemental surface composition [in weight (wt) %] of the mica substrates, before and after ageing with organic acids was measured via energy dispersive spectroscopy (EDS) using a Field Emission Scanning Electron Microscope (FESEM) from Oxford Instruments. Further, scanning electron micrographs were taken for pure and aged mica substrates to show the effects of ageing with organics at different magnifications (Figure 3-3-1). It is clear that stearic acid uniformly covered the mica surface). A substantial total increase in average carbon surface concentration (+2.2 wt % C for LiA, +1.9 wt % C for SA, +1.5 wt% C for LuA and +1.2 wt% C for HA) was measured due to the chemisorption of organic acids on the mica surfaces (Zullig & Morse, 1988), (Table S3-3-1). Further, the mean elemental values of mica substrates are shown in Table 3-3-2. The mean elemental values are based on the calculated average of six mica substrates, five data points for each mica substrate, making it 30 data points in total for all concentrations tested and '±' shows the standard deviation values.

Table 3-3-2 Mean elemental values of mica substrates before and after ageing.

Organic Acids	Elemental mean Identification Before Aging					Elemental mean Identification After Aging				
	Si (wt%)	C (wt%)	O (wt%)	Al (wt%)	K (wt%)	Si (wt%)	C (wt%)	O (wt%)	Al (wt%)	K (wt%)
Hexanoic acid	21.8 ± 1.7	2.9 ± 0.7	48.2 ± 2.1	19.2 ± 0.8	7.9 ± 0.5	20.0 ± 1.4	3.9 ± 0.8	50.3 ± 2.8	18.5 ± 1.3	7.4 ± 1.1
Lauric acid	22.2 ± 0.9	3.1 ± 0.7	46.8 ± 2.0	19.6 ± 0.9	8.3 ± 0.7	21.0 ± 1.3	4.4 ± 1.7	48.2 ± 2.0	18.9 ± 1.0	7.6 ± 0.7
Stearic acid	22.3 ± 1.2	3.2 ± 0.6	46.1 ± 0.9	19.7 ± 0.8	8.7 ± 0.7	20.8 ± 1.3	4.8 ± 1.6	48.1 ± 1.7	19.2 ± 1.0	7.2 ± 0.9
Lignoceric acid	22.5 ± 1.0	3.2 ± 0.5	46.4 ± 1.5	19.2 ± 1.1	8.8 ± 0.7	20.6 ± 1.1	5.0 ± 1.6	47.8 ± 1.8	19.0 ± 1.0	7.7 ± 1.0

Five data points were examined on each substrate (before and after aged mica substrates) for five concentrations (10^{-2} mol/L, 10^{-3} mol/L, 10^{-5} mol/L, 10^{-7} mol/L, 10^{-9} mol/L) of four different organic acids (Hexanoic, Lauric, Stearic and Lignoceric acid).

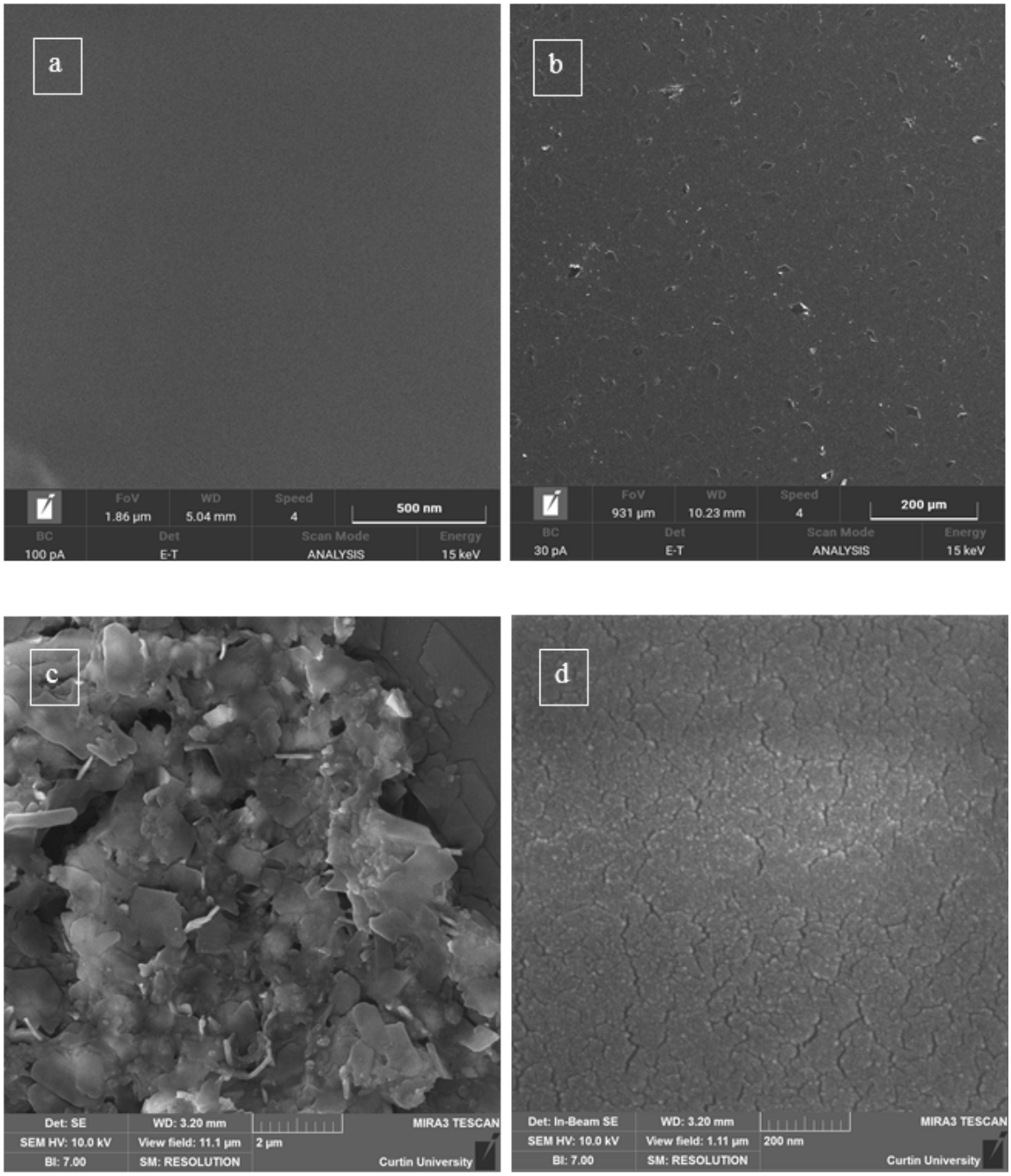

Figure 3-3-1 SEM Micrographs (a) Pure mica (b) organic aged mica surfaces with stearic acid at a magnification of 200 µm (c) organic aged mica surfaces with stearic acid at a magnification of 2 µm (d) organic aged mica surfaces with stearic acid at a magnification of 200 nm.

3.3.2.3.3 Fourier Transform Infrared Spectroscopy (FTIR) Measurements

To investigate the surface adsorption of organic acids, FTIR (from Perkin Elmer, Model FTIR Spectrum Two) analysis was conducted on pure and organic aged mica samples (Awan, Keshavarz, Akhondzadeh, Al-Anssari, Al-Yaseri, et al., 2020). The samples were exposed to 64 scans in the spectral range of 400-4000 cm^{-1}. The FTIR spectrum in (Figure 3-3-2) for pure mica (blue line) demonstrates crystalline illite/muscovite (Vaculikova & Plevova, 2005). Pure mica FTIR spectra showed broad OH-stretching near 3625 to 3670 cm^{-1} with 835 and 755 cm^{-1} doublets, which is an indication of illite crystals; note that literature spectra of illite and muscovite are very similar (Vaculikova & Plevova, 2005). Further, organic aged mica sample (red line) showed the same trend as the pure mica sample, except for sharp stretching doublets near 2850 to 2929 cm^{-1} which represents hydrogen bonding (C – H), as well as near 3630 cm^{-1}, which represents hydroxyl bonding (C – OH) (Mahamuda et al., 2014; Swapna et al., 2014). We conclude that the pure mica surface is covered with a (polar) hydroxyl group, which undergo chemical interaction with the hydroxyl groups in the organic acids, and thus chemically (covalently) bonding them to the mica surface, rendering them strongly hydrophobic (Al-Anssari et al., 2016; Ali, Al-Anssari, et al., 2019; Ali, Arif, et al., 2019).

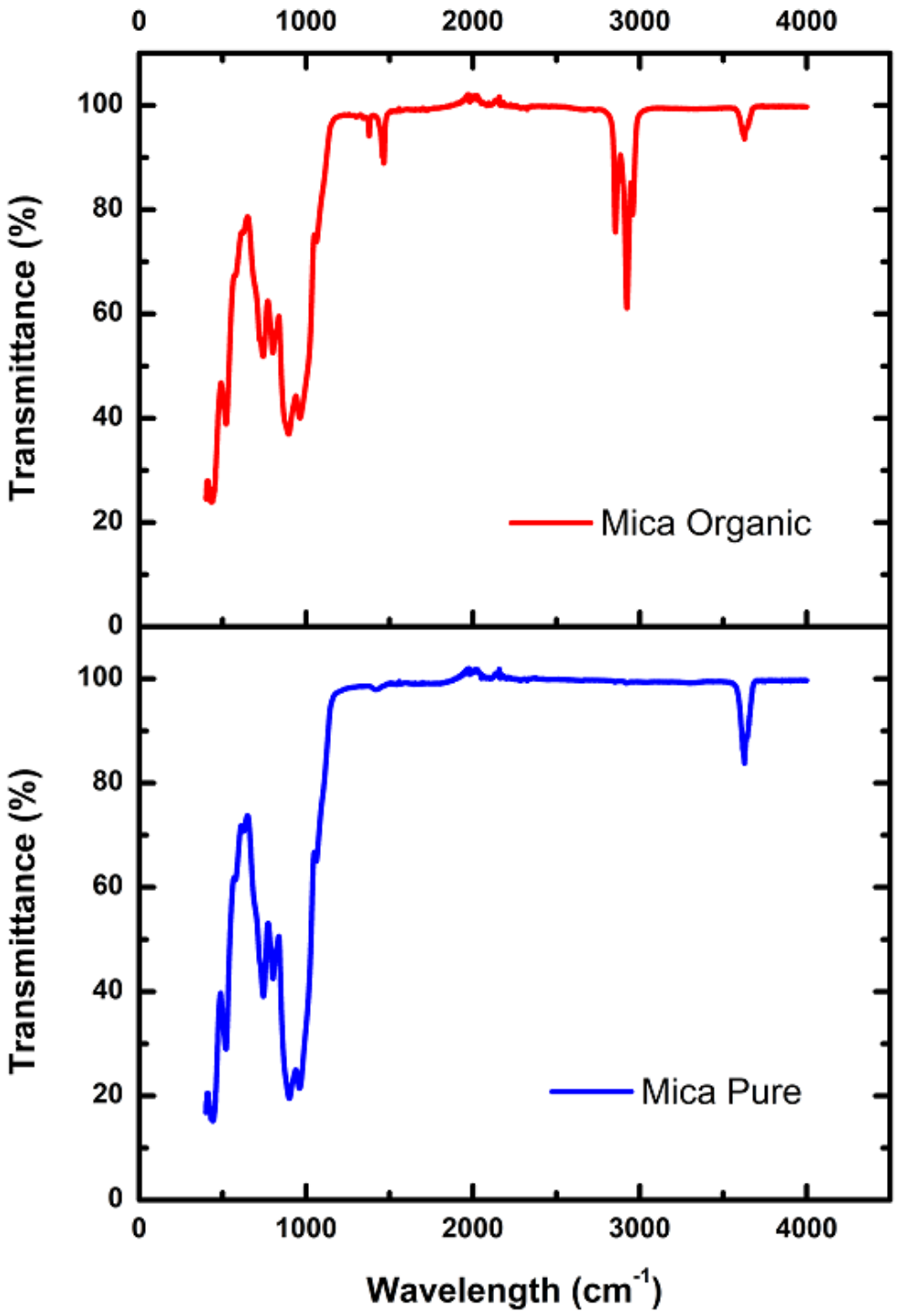

Figure 3-3-2 FTIR of Pure and Organic aged mica substrates.

3.3.2.3.4 Atomic Surface Microscopy (AFM) Measurements

Surface roughness is well known to influence wettability (Wenzel, 1936). Pure and organic aged mica substrates were thus characterised in terms of the surface roughness by atomic force microscopy technique (AFM instrument from Nano-surf, Flex-

Axiom, and Controller C3000). It was found that the pure mica sample's surface roughness ranged from 1 nm to 2 nm which is very smooth. In addition to that, organic aged mica surfaces were also homogeneous and very smooth with an average root mean square ranging from 200 to 460 nm. Thus, all surface roughness was less than 1 µm, and roughness, therefore, had no significant influence on contact angle measurements (A. Z. Al-Yaseri et al., 2016).

3.3.2.3.5 Contact Angle Measurements

Contact angle measurements are widely conducted to quantify the wettability alteration behaviour in a given CO_2/brine/mineral system (Al-Anssari et al., 2016; Ali, Sahito, et al., 2020; Arif, Barifcani, Lebedev, et al., 2016; Iglauer, Al-Yaseri, et al., 2015; Iglauer, Pentland, et al., 2015). This method involves the measurement of advancing (θ_a) and receding (θ_r) contact angles, which is here achieved through the tilted plate technique (Lander et al., 1993). These measurements can be performed at ambient and high pressure (HP) and high temperature (HT) conditions. The HPHT system used here contained a cell made up of Hastelloy material designed for sustaining high pressure (up to 60 MPa) and high temperature (up-to 423 °K), and it contained a sample holder at 17° tilted position. Two high precision ISCO syringe pumps (Teledyne ISCO D-260, pressure accuracy of 0.01%) were connected with the HPHT cell, which delivered CO_2 or CO_2 equilibrated brine during the measurement. HPHT mixing reactor (from Parr company, volume 500 ml) was also connected with a CO_2 gas bottle at the one end and a brine ISCO pump at the other end to achieve thermodynamic equilibrium between CO_2 and the brine solution (El-Maghraby et al., 2012). This brine equilibration is necessary to avoid mass transfer effects between CO_2 and brine during contact angle measurement on mica substrates. For this mica substrates were added into the mixing reactor followed by CO_2 and brine. They were mixed at 1200 RPM for 1 h until live brine was formed under the experimental high pressure and high temperature conditions. Thereafter, organic aged mica substrates were placed onto the sample holder in the tilted position and the cell was tightly closed followed by gradual CO_2 injection (controlled via CO_2 ISCO pump) until the required temperature and pressure [323 K, 15 and 25 MPa] were reached. The fluid temperature in ISCO pumps was governed with heating baths (from Julabo, Model 900F), and the

temperature of the cell was governed through a strip heating tape and controller (model no. HTC101-002 from Omega Company). Once the cell was filled with CO_2 at the required operating conditions, equilibrated brine was introduced from the mixing reactor to the brine ISCO pump. Thereafter, an equilibrated brine drop [mean drop size: 5 µL (± 0.75 µL)] was introduced (controlled via brine ISCO pump) onto the tilted mica substrate via high precision pointer. When a brine droplet touched the mica surface, advancing and receding contact angles were recorded at the trailing and leading edges of the droplet (Ali, 2018). A high-performance video camera (Fujinon CCTV lens: HF35HA-1B; 1:1.6/35 mm, frame rate = 71 fps; pixel size = 7.4 µm; Basler SCA 640–70 fm) was utilized to video record the procedure. Thereafter, Image J software was used to extract the contact angle values from the images. These measurements were performed three times for each experimental condition, and an average value of advancing and receding contact angle was calculated based on the mean (standard deviation of ± 3° for 0.1 MPa and 15 MPa; ± 5° for 25 MPa) of repeated measurements.

3.3.3 Results and Discussion

It is crucial to gauge the effects of CO_2-wettability for cap-rocks, which is a main aspect defining CO_2 movement and spreading throughout the CO_2-storage formation (Al-Khdheeawi et al., 2017a, 2017b), as well as, flow properties (Iglauer, 2017; Iglauer, Pentland, et al., 2015), containment security and CO_2 trapping quantity (Arif, Barifcani, Lebedev, et al., 2016; Arif, Lebedev, et al., 2017b; Iglauer, Al-Yaseri, et al., 2015). In this context, brine receding contact angle is related to structural trapping (capillary leakage can occur at $\theta_r > 90°$), when CO_2 is injected into the reservoir and displaces water (Broseta et al., 2012), while brine advancing contact angle is related to capillary trapping (where wettability do not affect primary drainage, $\theta_a < 50°$), when water is injected into the reservoir to capillary trap CO_2 (Al-Menhali & Krevor, 2016; Chiquet et al., 2007; Rahman et al., 2016). Note: It has been shown that changes in CO_2-wettability also significantly influence dissolution trapping (Al-Khdheeawi et al., 2017a, 2017b; Ali, 2018).

It is obvious from our results that the mica surfaces have lost water-wetness due to exposure to the organic acids. Initially, contact angle measurements were conducted

on pure mica substrates at ambient conditions which depicted strongly hydrophilic surfaces (in air) with θ = 0° (Arif, Barifcani, Lebedev, et al., 2016). Mica substrates at reservoir conditions (323 K, 15 and 25 MPa) were weakly hydrophilic (50.2° advancing, 44.9° receding at 15 MPa ± 3°; and 65.1° advancing, 60.4° receding at 25 MPa ± 5°) (Arif, Al-Yaseri, et al., 2016; Arif, Barifcani, Lebedev, et al., 2016).

3.3.3.1 Effect of Organic Acid Concentration on Wettability

It is very crucial to gauge the effect of organic acids on CO_2-wettability, until now quartz and calcite substrates as representative of sandstone and limestone storage formations have been tested. Whereas, these are storage rocks, but not cap-rock. Thus, quantification of CO_2-wettability in the existence of organic acids for cap-rock is very necessary for investigating structural trapping potential.

Clearly, the contact angles significantly raised with raising organic acid concentration as depicted in Figures 3-3-3 to 3-3-6.

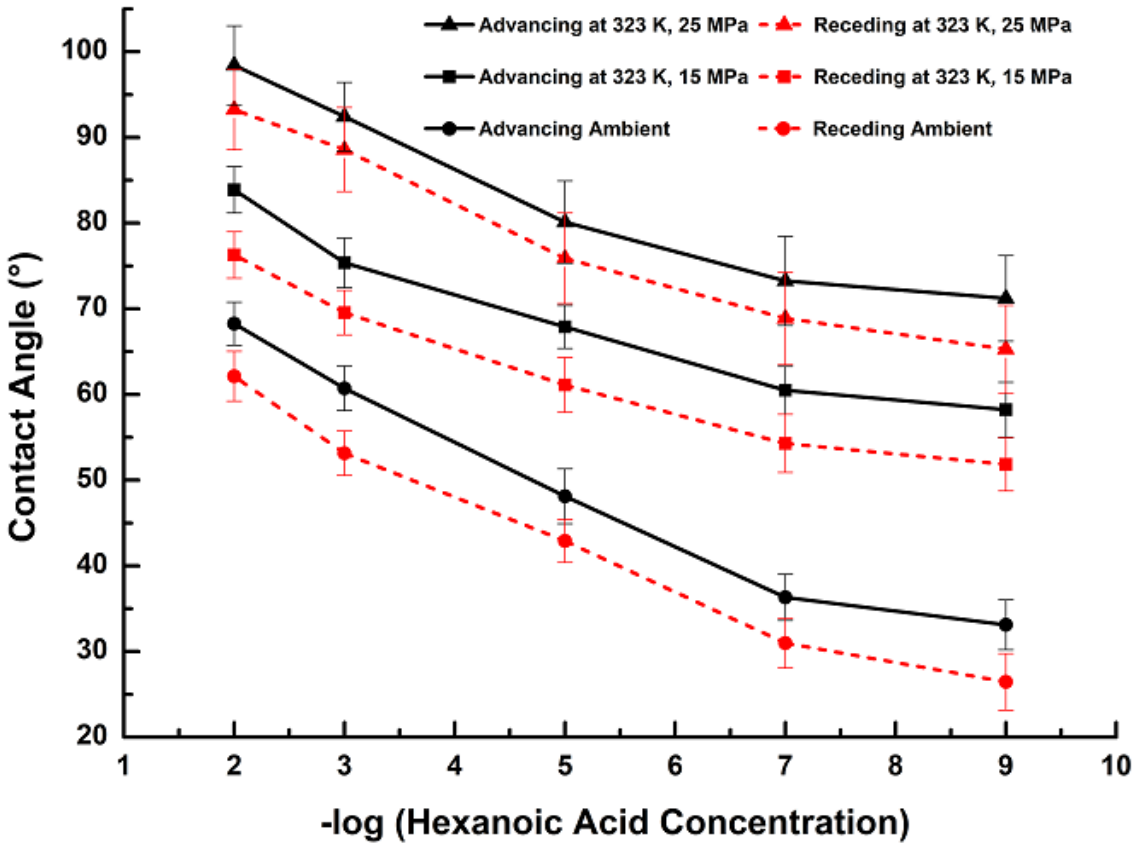

Figure 3-3-3 Mica/CO_2/Brine contact angles (advancing and receding) as a function of pressure and hexanoic acid (C_6) concentration (in mol/L).

For instance, for the mica substrate aged in 10^{-9} mol/L hexanoic acid concentration, at 323 K and 25 MPa, θ_a was 71.2° and θ_r was 65.3°, indicating that mica surface was weakly hydrophilic. Further, at 10^{-5} M hexanoic acid concentration, θ showed a small change, which is θ_a = 80.1° and θ_r = 75.9°. However, at the highest acid concentration (10^{-2} mol/L) of hexanoic acid, contact angles showed a significant change, which is θ_a = 98.4° and θ_r = 93.3° (Figure 3-3-3), indicating that mica surface transformed from weakly hydrophilic to intermediate-wet. Such reduced water wettability is potentially responsible for reduced structural trapping capacities ($\theta_r < 90°$) (Ali, Al-Anssari, et al., 2019; Ali, Arif, et al., 2019; Iglauer, Pentland, et al., 2015).

Mica substrates aged in lauric acid showed similar trends as observed for hexanoic acid aged substrates. For instance, at 10^{-2} mol/L lauric acid, mica/CO_2/brine contact angles were greater than those experimented for 10^{-9} mol/L lauric acid concentration. Thus, it is obvious that higher organic acid concentrations were responsible for shifting mica surfaces towards a more hydrophobic state. As an example, at 323 K and 25 MPa, for a 10^{-2} mol/L lauric acid concentration, θ_a was 110.1° and θ_r was 102.3°, which decreased to θ_a = 74.3° and θ_r = 68.1° when LuA concentration decreased to 10^{-9} mol/L (Figure 3-3-4).

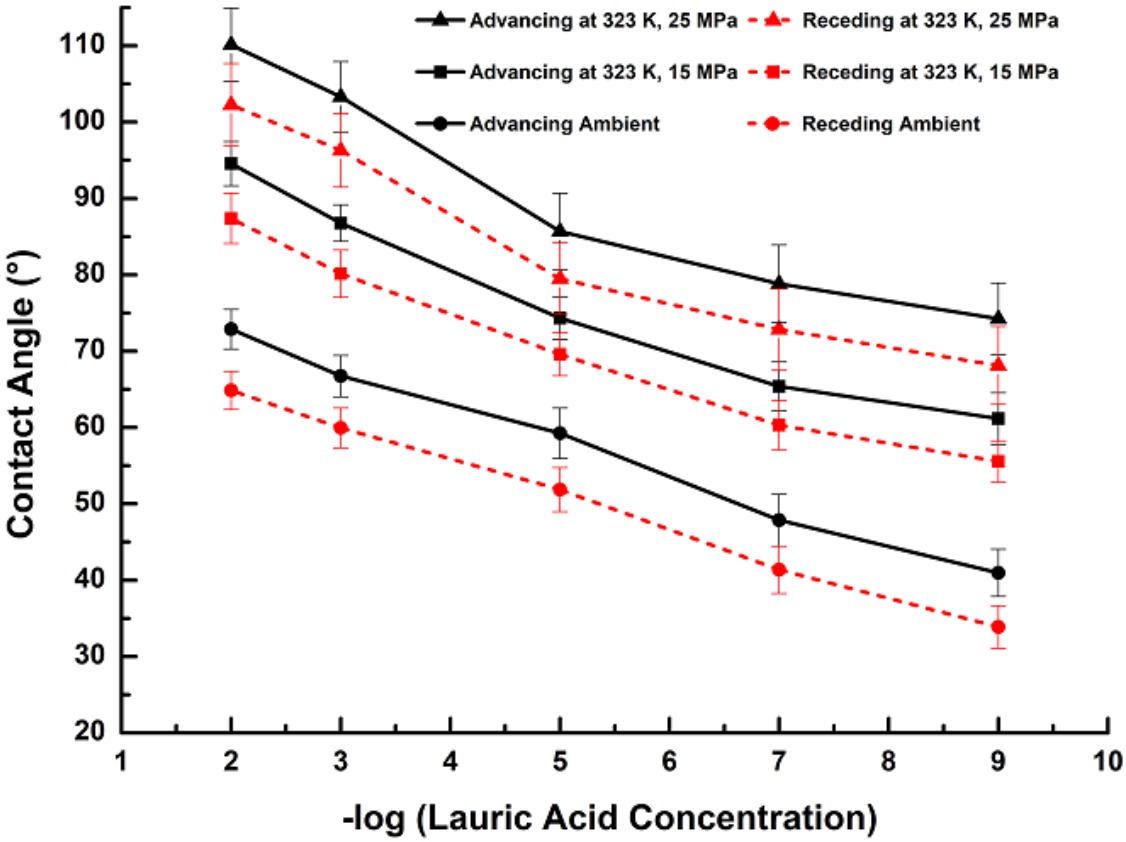

Figure 3-3-4 Mica/CO_2/Brine contact angles (advancing and receding) as a function of pressure and lauric acid (C_{12}) concentration (in mol/L).

For mica substrates aged in stearic and lignoceric acid, results also showed similar trends as those observed for hexanoic and lauric acid, however, the degree of wettability change was significantly enhanced (discussed more in section 3.3.3.3), due to the longer alkyl chain length (Ali, Arif, et al., 2019). For instance, at 10^{-2} mol/L of stearic and lignoceric acid, at 323 K, 25 MPa, θ_a was 121.2° and 133.0° and θ_r was 113.7° and 124.9° respectively. Whereas, at decreased concentration of stearic and lignoceric acid to 10^{-9} mol/L, θ_a decreased to 78.1° and 80.7° and θ_r = 70.9° and 74.4° respectively (Figures 3-3-5 and 3-3-6).

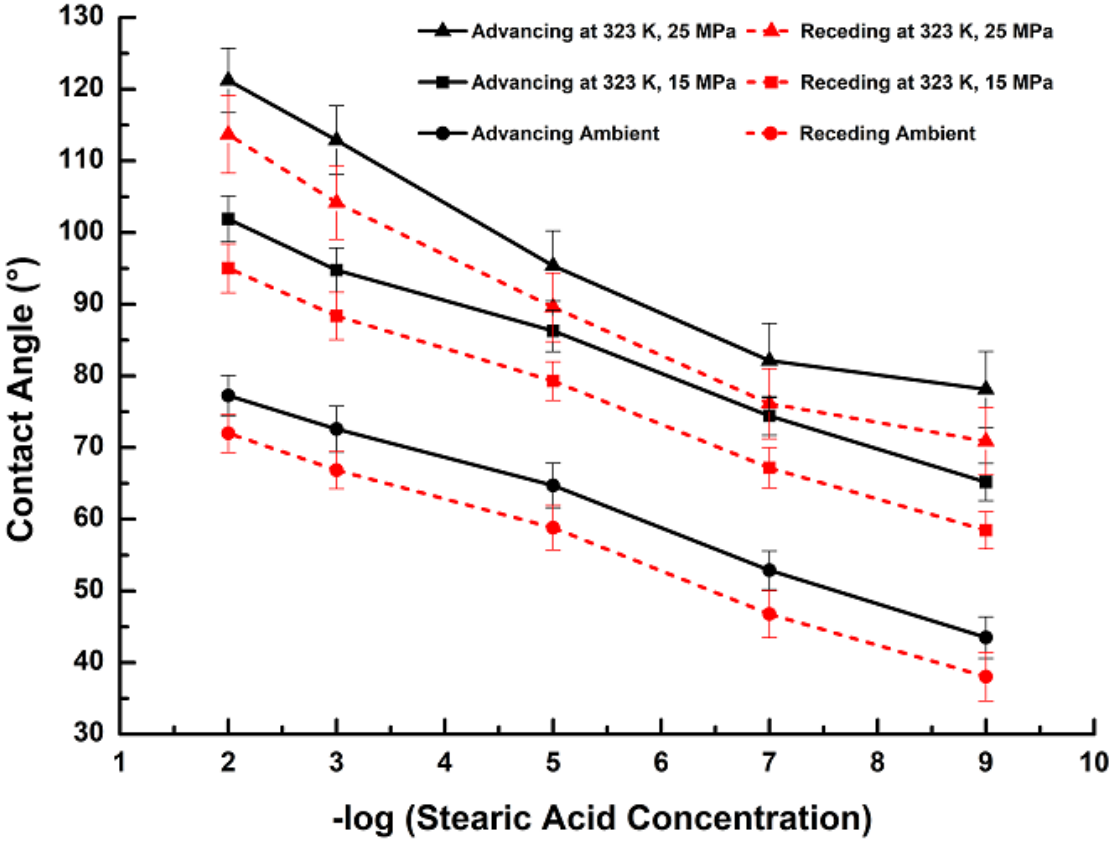

Figure 3-3-5 Mica/CO_2/Brine contact angles (advancing and receding) as a function of pressure and stearic acid (C_{18}) concentration (in mol/L).

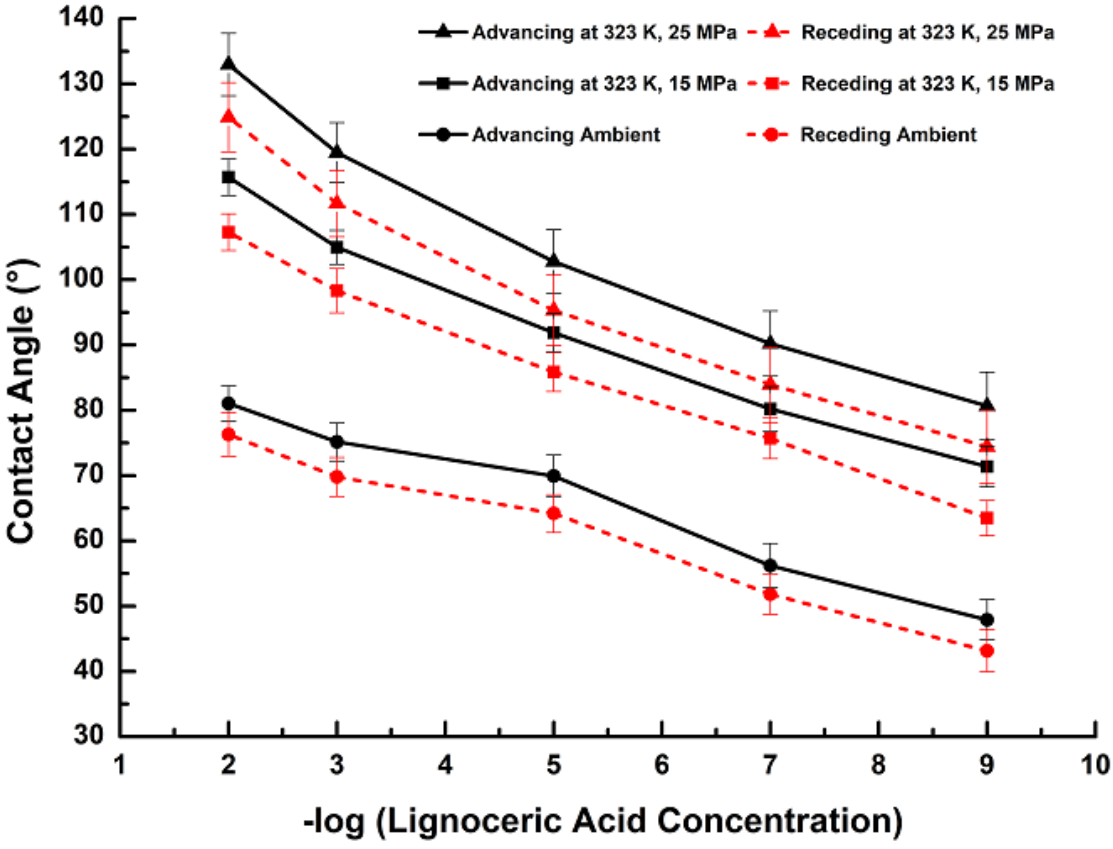

Figure 3-3-6 Mica/CO_2/Brine contact angles (advancing and receding) as a function of pressure and lignoceric acid (C_{24}) concentration (in mol/L).

Importantly, CO_2-wettability even at the lowest tested concentration (10^{-9} mol/L) are higher than pure mica substrates. For instance, for lignoceric acid, at the lowest concentration tested (10^{-9} mol/L), at 323 K and 15 MPa, θ_r was 63.5°, whereas, for pure mica substrates, at 323 K and 15 MPa, θ_r was 44.9° (Arif, Barifcani, Lebedev, et al., 2016). We conclude that even the smallest concentrations of organic acid significantly impact CO_2-wettability. Hence, as CO_2-storage formations always contain such small organic concentrations, structural trapping is significantly lower than that estimated for pure mica substrates (Ali, Al-Anssari, et al., 2019; Bennett et al., 1993; Jones et al., 2008; Stalker et al., 2013). In a nutshell, irrespective of the type of organic acid, the values of both contact angles (advancing and receding) raised with organic acid concentration (Ali, Al-Anssari, et al., 2019; Ali, Arif, et al., 2019; Gomari & Hamouda, 2006). This is due to increased chemisorption of carboxylic acid on the mica surfaces rendering the wettability more hydrophobic (Al-Anssari et al., 2016).

3.3.3.2 Effect of Pressure and Salinity on Wettability

It is well proven that pressure strongly influences the wettability of CO_2-storage formations (Al-Anssari, Arain, et al., 2018; Ali et al., 2017). Figures 3-3-3 to 3-3-6 show results for contact angle (advancing and receding) for mica substrates at 323 K and 0.1 MPa, 15 MPa, 25 MPa. Irrespective of the type of organic acid, pressure had a similar effect on the contact angles. This is due to the rise in intermolecular interactions between mica substrates and CO_2 with increasing pressure, as depicted for quartz substrates (Abramov et al., 2019).

For instance, for the organic acid with the smallest alkyl chain (hexanoic acid) at the lowest tested concentration of 10^{-9} mol/L, at 323 K and 0.1 MPa, θ_a was 33.1° and θ_r was 26.5°, whereas, at a higher pressure (25 MPa), contact angles increased significantly, θ_a = 71.2° and θ_r = 65.3°. This trend was also observed for lauric, stearic and lignoceric acid. For example, at the highest acid concentration (10^{-2} mol/L), for lauric, stearic and lignoceric acid, at 323 K and 0.1 MPa, θ_a were 72.9°, 77.3°, 81.0°

and θ_r were 64.8°, 72.0°, 76.3° respectively. Whereas, at a higher pressure (25 MPa), contact angles increased substantially to θ_a = 110.1°, 121.2°, 133.0° and θ_r = 102.7°, 113.7°, 124.9° respectively. Overall, a significant increase in CO_2-wettability was observed, caused by increasing pressure, which will cause a substantial reduction in structural trapping capacities of CO_2-storage formations.

It is widely reported in the literature that increased salinity of monovalent ions (NaCl and KCl brine formulations) reduces the surface hydrophilicity for cap-rock formations (Arif, Barifcani, Lebedev, et al., 2016). Moreover, it was previously reported that for quartz surfaces, divalent cations ($CaCl_2$ and $MgCl_2$) – in comparison with monovalent ions – further decrease surface hydrophilicity, due to the enhanced surface screening effect of divalent ions, and this reduces structural trapping capacities and containment security (A. Z. Al-Yaseri et al., 2016; Iglauer, 2017).

3.3.3.3 Effect of alkyl Chain Length on Wettability

CO_2 trapping is directly or indirectly affected by wettability in subsurface formation. In this context, wettability controls the capability of CO_2 to induce in above cap-rock formation, where buyout CO_2 apply force (antiparallel to gravity) on solid cap-rock and fluids itself. This mechanism drives everything of lower density than formation brine up-ward against the cap-rock. When the contact angle changes from hydrophilic to hydrophobic due to the presence of organic acids (i.e. to $\theta_r > 90°$), it can cause capillary leakage.

Our results have depicted that carboxylic acids have considerably impacted mica wettability by substantially increasing water contact angles, and mica has quickly lost its water-wetness (Figures 3-3-7 and 3-3-8). Even minute concentrations of 10^{-3} mol/L of lignoceric acid at 15 MPa and 10^{-5} mol/L of lignoceric acid at 25 MPa have altered the mica substrates to hydrophobic ($\theta_r > 90°$), causing reduced structural trapping capacities. Note that considerably greater organic acid concentrations are found in deep saline aquifers (Akob et al., 2015; Lundegard & Kharaka, 1994; Stalker et al., 2013).

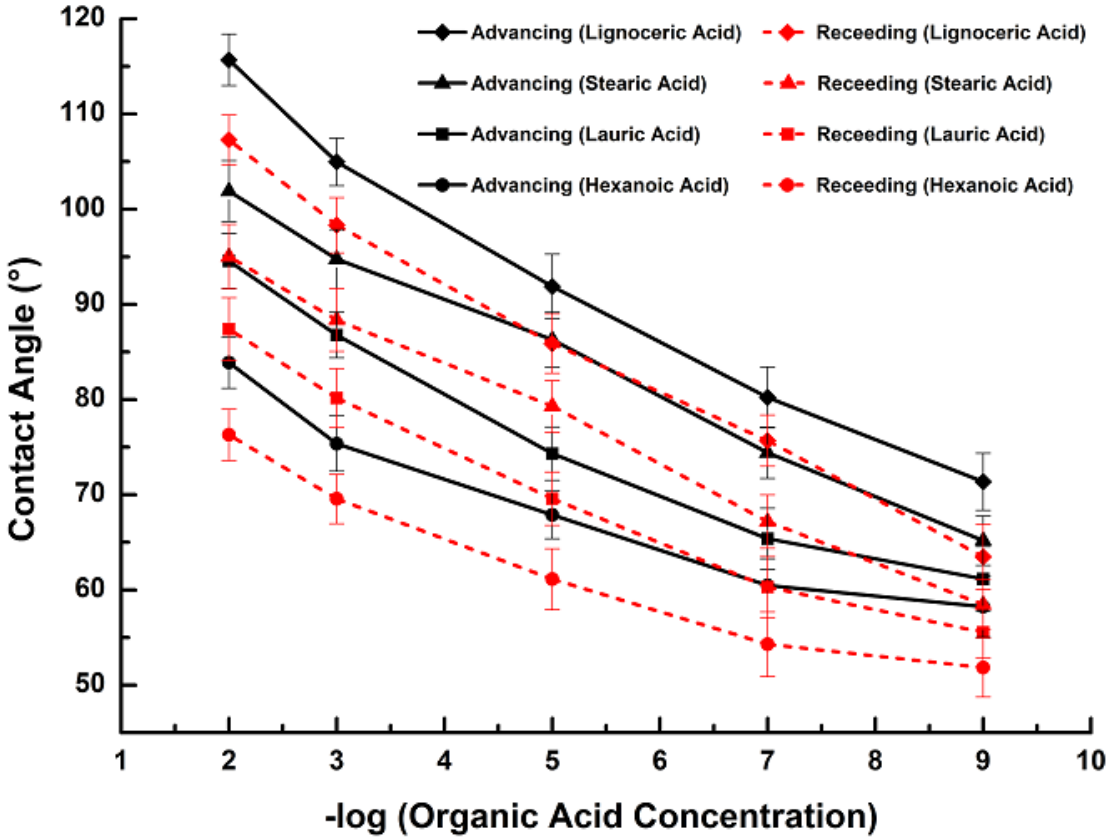

Figure 3-3-7 Mica/CO_2/Brine contact angles (advancing and receding) as a function of alkyl chain length and organic acid concentration (in mol/L) at 323 K and 15 MPa.

The above results show that at the same organic acid concentration for different organic acids, total values of contact angle (advancing and receding) were different (this is due to the presence of different alkyl chain length and surface coverage on mica substrates) as shown in Figures 3-3-7 and 3-3-8. Mica substrates aged in hexanoic acid (C_6) have depicted less contact angle (advancing and receding) values as compared to substrates aged in lignoceric acid (C_{24}). Gradual increase in contact angle (advancing and receding) values were seen with the increase in alkyl chain length (from C_6 to C_{24}). For instance, at the same organic acid concentration of 10^{-2} mol/L for all carboxylic acids, at 323 K and 15 MPa, the θ_r was 76.3°, 87.4°, 95.0° and 107.3° respectively (please note that at higher pressure of 25 MPa, these values are higher than 15 MPa). Such a transformation of intermediate hydrophilicity to strong hydrophobicity is credited to the presence of alkyl chain length in fatty acids. It is thus clear that the presence of more number of carbon atoms are accountable for shifting the mica wettability to further CO_2-wet.

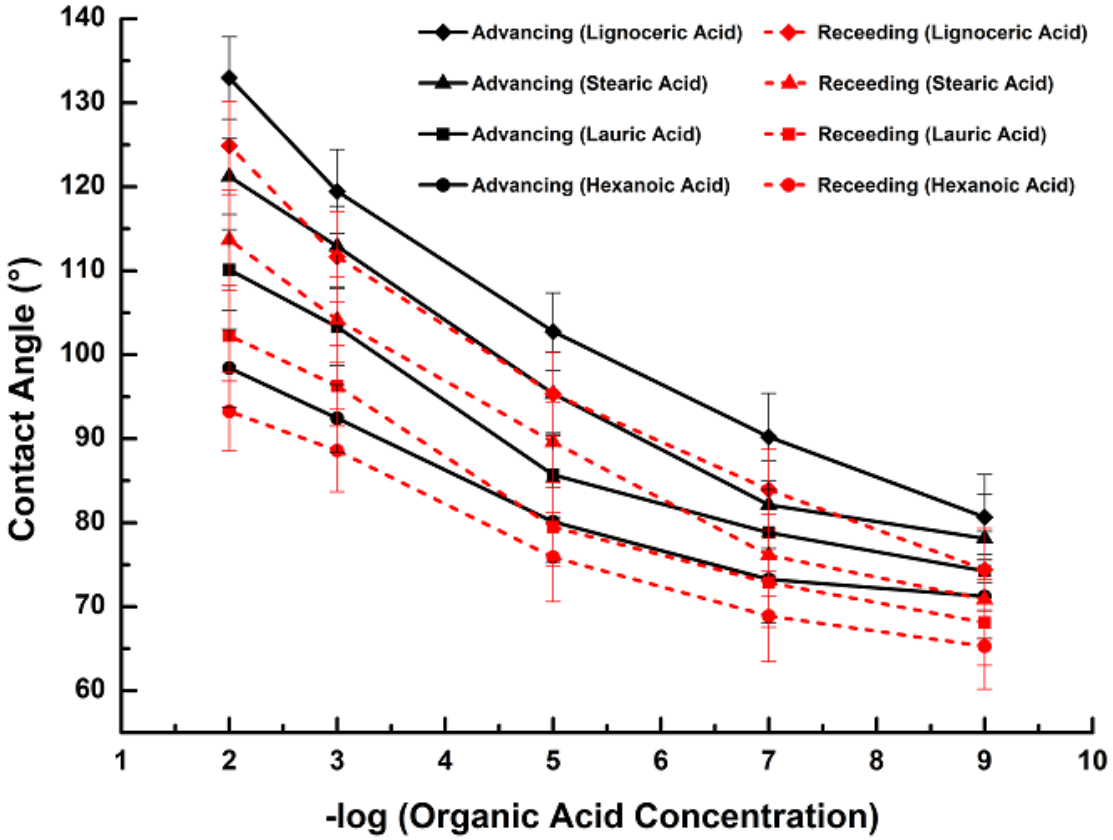

Figure 3-3-8 Mica/CO_2/Brine contact angles (advancing and receding) as a function of alkyl chain length and organic acid concentration (in mol/L) at 323 K and 25 MPa.

Thus it is clear from results that the presence of organic acids has a substantial impact on structural trapping capacities. It is therefore relevant to conduct thorough studies of different organics and their associated concentrations in storage formations to gauge these effect for the long term viability of CO_2-geological projects.

3.3.4 Conclusions

CO_2-wettability of storage formations (e.g. deep saline aquifers) is fundamentally dependant on many factors such as pressure, temperature, brine salinity and formation heterogeneity (Abramov et al., 2019; Ali, Arif, et al., 2019; Arif, Al-Yaseri, et al., 2016; Iglauer, 2017; N. Jha et al., 2018; N. K. Jha, Ali, et al., 2019; N. K. Jha et al., 2020). However, other factors like the presence of organics or nanoparticles may also drastically impact storage capacities at reservoir conditions (Al-Anssari, Nwidee, et al., 2017; Ali, Al-Anssari, et al., 2019; Ali, Sahito, et al., 2020). Literature lacks the

information on the presence of organic acids and their effects on CO_2-wettability in cap-rocks, which can reduce the structural trapping potential, technical feasibility, containment security and project economics (Al-Khdheeawi et al., 2017a; Al-Menhali & Krevor, 2016; Ali, 2018; Ali, Al-Anssari, et al., 2019; Ali, Arif, et al., 2019; Iglauer, Al-Yaseri, et al., 2015; Iglauer, Pentland, et al., 2015). However, the presence of such organics are well proven in storage formations (Akob et al., 2015; Ali, Al-Anssari, et al., 2019; Gomari & Hamouda, 2006; Jardine et al., 1989; Lundegard & Kharaka, 1994; Madsen & Ida, 1998; Stalker et al., 2013).

Therefore, we have investigated mica/CO_2/brine systems in the occurrence of four organic acids (hexanoic acid C_6, lauric acid $C_{12,}$ stearic acid C_{18} and lignoceric acid C_{24}) at various storage conditions (323 K, 0.1 MPa, 15 MPa and 25 MPa) by conducting contact angle (advancing and receding) measurements. It was found that pure mica surfaces which were initially water-wet turned into CO_2-wet ($\theta_a = 0°$ at 323 K, 0.1 MPa increased to $\theta_a = 133.0°$ at 323 K and 25 MPa for lignoceric acid concentration at 10^{-2} mol/L). In addition, lignoceric acid showed higher contact angle values and hexanoic acid have shown lower contact angle values, lauric and stearic acid have fell in between (at a fixed organic acid concentration). Such a change from completely water-wet to strongly CO_2-wet was caused by the presence of alkyl chain length in fatty acids, thus reducing structural trapping capacities (Abramov et al., 2019).

Overall, it is concluded that CO_2-storage formations (deep saline aquifers) may have a lower trapping potential than previously predicted due to the presence of organic acids. Therefore, it is desirable to include these effects in reservoir-scale models to obtain reliable CO_2 storage estimates and to thus avoid CGS project failure.

3.3.5 Graphical Abstract

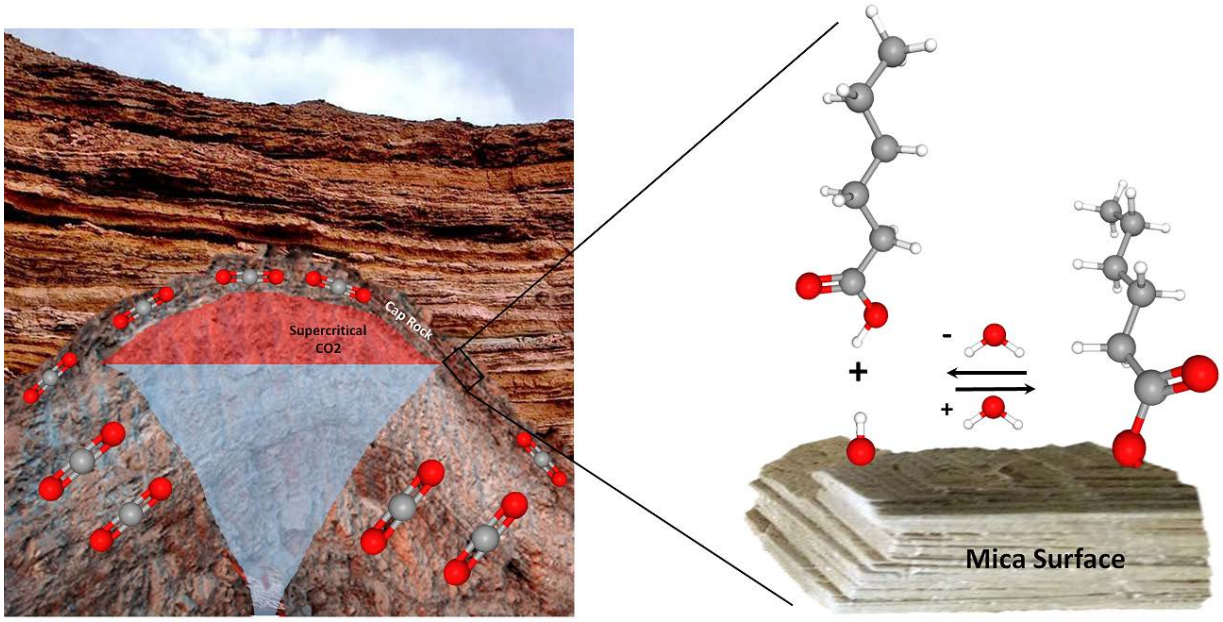

3.3.6 Supporting Information

Table S3-3-1 Surface analysis of mica substrates by EDS

Concentration (Molarity)	Pure Mica					After ageing					Change due to ageing				
	wt% Si	wt% C	wt% O	wt% Al	wt% K	wt% Si	wt% C	wt% O	wt% Al	wt% K	wt% Si	wt% C	wt% O	wt% Al	wt% K
Hexanoic Acid															
10^{-2}	20.4	2.8	50.1	18.8	7.9	19.8	4.9	51.8	17.2	6.3	-0.6	+2.1	+1.7	-1.6	-1.6
10^{-3}	22.1	2.4	49.6	18.2	7.7	18.7	3.9	52.4	18.3	6.7	-3.4	+1.5	+2.8	+0.1	-1.0
10^{-5}	23.7	3.1	46.0	19.4	7.8	20.2	4.2	50.5	17.9	7.2	-3.5	+1.1	+4.5	-1.5	-0.6
10^{-7}	21.7	2.6	47.6	19.7	8.4	18.9	3.3	51.7	18.5	7.6	-2.8	+0.7	+4.1	-1.2	-0.8
10^{-9}	21.1	2.9	49.2	19.3	7.5	20.7	3.4	48.4	19.1	8.4	-0.4	+0.5	-0.8	-0.2	+0.9
0	21.5	3.7	46.8	19.8	8.2	21.5	3.7	46.8	19.8	8.2	0	0	0	0	0
Lauric Acid															
10^{-2}	22.3	3.8	44.7	20.1	9.1	19.4	7.0	46.8	19.7	7.1	-2.9	+3.2	+2.1	-0.4	-2.0
10^{-3}	22.4	2.4	46.5	20.4	8.3	21.7	4.0	48.8	18.6	6.9	-0.7	+1.6	+2.3	-1.8	-1.4
10^{-5}	21.9	2.7	47.1	19.7	8.6	22.0	3.9	48.1	17.8	8.2	+0.1	+1.2	+1.0	-1.9	-0.4
10^{-7}	21.7	2.8	48.7	19.1	7.7	21.4	3.7	48.2	19.3	7.4	-0.3	+0.9	-0.5	+0.2	-0.3
10^{-9}	23.2	3.1	46.9	18.7	8.1	19.7	3.8	50.7	17.9	7.9	-3.5	+0.7	+3.8	-0.8	-0.2
0	21.5	3.7	46.8	19.8	8.2	21.5	3.7	46.8	19.8	8.2	0	0	0	0	0
Stearic Acid															
10^{-2}	21.1	3.3	46.7	20.2	8.7	20.2	6.7	47.1	19.3	6.7	-0.9	+3.4	+0.4	-0.9	-2.0
10^{-3}	22.2	3.4	45.3	20.3	8.8	22.1	6.1	46.4	18.9	6.5	-0.1	+2.7	+1.1	-1.4	-2.3
10^{-5}	22.6	2.9	45.4	19.5	9.6	20.8	4.4	47.8	19.7	7.3	-1.8	+1.5	+2.4	+0.2	-2.3
10^{-7}	23.4	2.6	47.0	18.7	8.3	20.5	3.6	50.2	17.9	7.8	-2.9	+1.0	+3.2	-0.8	-0.5
10^{-9}	23.1	3.1	45.2	19.9	8.7	19.6	4.0	50.0	19.5	6.9	-3.5	+0.9	+4.8	-0.4	-1.8
0	21.5	3.7	46.8	19.8	8.2	21.5	3.7	46.8	19.8	8.2	0	0	0	0	0
Lignoceric Acid															
10^{-2}	22.8	3.1	47.1	17.9	9.1	19.4	6.8	48.7	17.8	7.3	-3.4	+3.7	+1.6	-0.1	-1.8
10^{-3}	21.9	2.9	47.5	18.9	8.8	20.7	5.6	45.5	19.8	8.4	-1.2	+2.7	-2.0	+0.9	-0.4
10^{-5}	23.5	2.8	45.7	19.1	8.9	19.8	4.5	48.3	19.5	7.9	-3.7	+1.7	+2.6	+0.4	-1.0
10^{-7}	23.3	3.5	44.5	19.3	9.4	20.9	5.1	49.1	18.4	6.5	-2.4	+1.6	+4.6	-0.9	-2.9
10^{-9}	21.7	3.1	47.0	20.1	8.1	21.4	4.2	48.2	18.6	7.6	-0.3	+1.1	+1.2	-1.5	-0.5
0	21.5	3.7	46.8	19.8	8.2	21.5	3.7	46.8	19.8	8.2	0	0	0	0	0

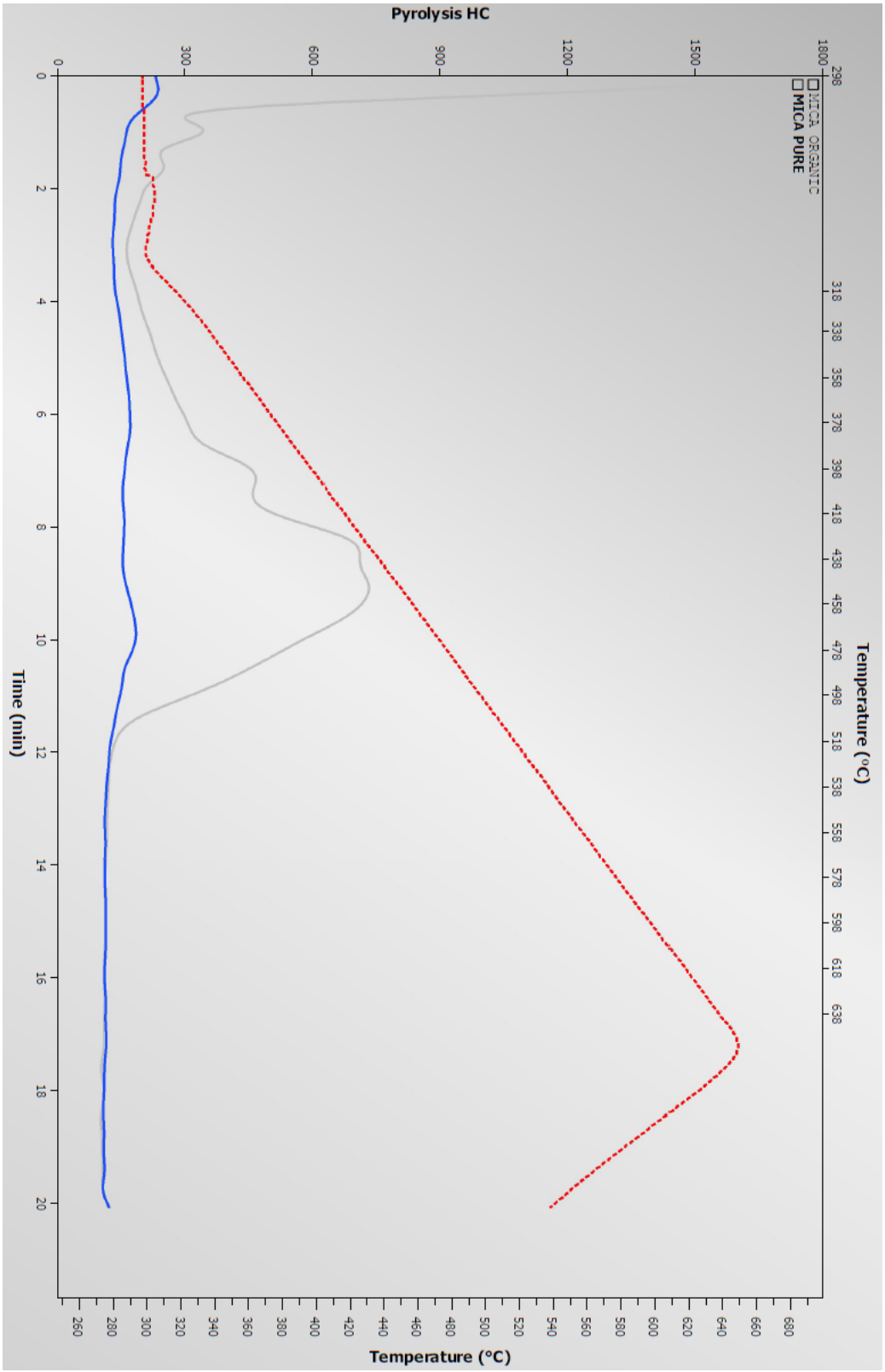

Figure S3-3-1 Total Organic Carbon (TOC) determination of pure and aged mica substrates (blue line represent the pure mica substrate and grey line represent the aged mica substrate)

3.3.6.1 X-ray Diffraction (XRD) Measurements

XRD is most commonly used to measure bulk mineralogy (Eskelinen, 1992). The XRD patterns of pure and organic aged mica samples are shown in Figure S3-3-2. The measured XRD spectra for (Mica Pure – blue line) showed oriented mica, silica and zeolite (Eskelinen, 1992); In addition to this, XRD spectra for (Mica Organic – red line) depicted oriented mica superimposed on muscovite/illite pattern with the presence of silica and zeolite crystals. These minerals are also abundantly found in shale cap-rock, which makes mica a perfect proxy for cap-rock in pristine form for investigating the effects of organics on wettability.

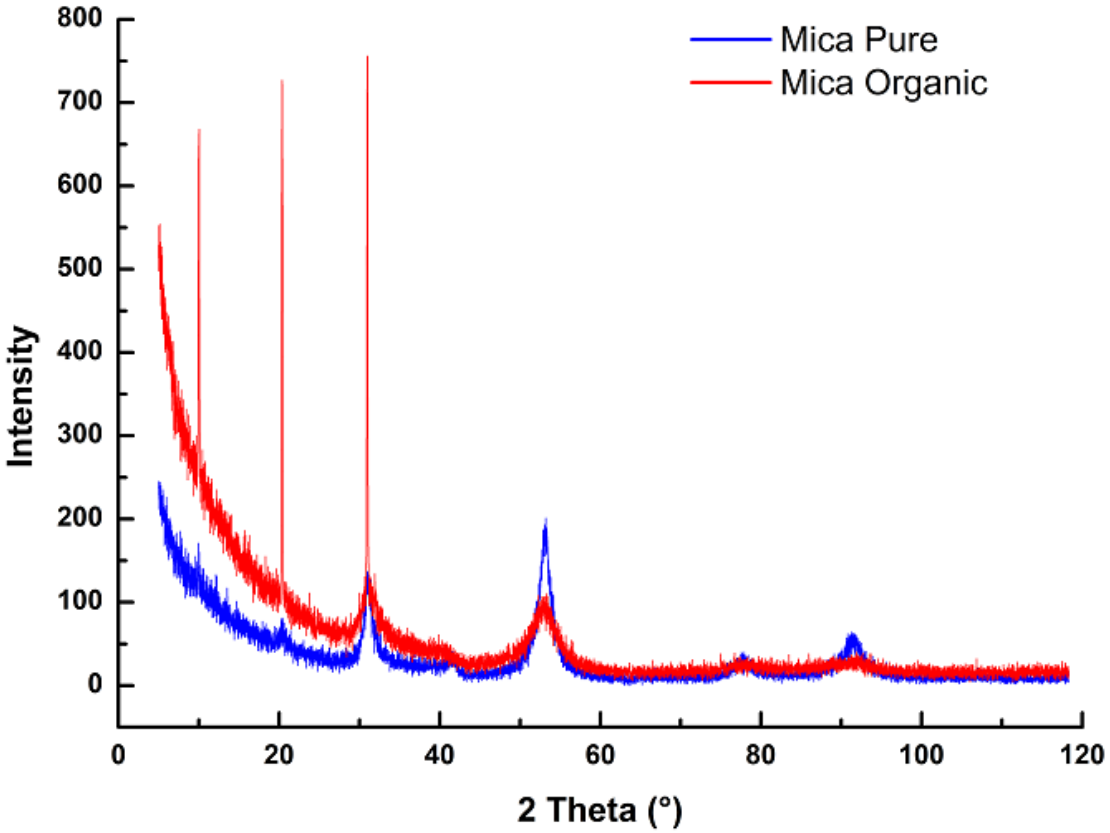

Figure S3-3-2 XRD spectra of Pure and Organic aged mica substrates.

Chapter 4 Effect of Nanoparticles on Geo-storage Formations

OVERVIEW

This chapter is divided into two parts which are based on two published peer-reviewed journal articles. In these journal articles, initially, the effect of organic acids (hexanoic acid C_6, Lauric acid C_{12}, Stearic acid C_{18}, and lignoceric acid C_{24}) is comprehended on CO_2-wettability of geo-storage formations (sandstone, and cap-rock) at reservoir conditions. Thereafter, the impact of nano-fluids (silica for sandstone and alumina for cap-rock) is quantified for the reversal of CO_2-wettability in geo-storage formations (sandstone, and cap-rock) at reservoir conditions. The result shows that the minute concentration of organic acids is enough to alter the CO_2-wettability from weakly water-wet to oil-wet, thus reduced CO_2 trapping capacities. Whereas, nano-fluid ageing have reversed the wettability from oil-wet to intermediate-wet conditions, thus increased CO_2 trapping potential. Therefore, for quantifying these effects, contact angle and analytical measurements were conducted at the highest concentration of organic-aged and various concentrations of nano-aged geo-storage samples. The details of each chapter is as follows:

Part 1: **Ali, M.**, Sahito, M. F., Jha, N. K., Arain, Z. U. A., Memon, S., Keshavarz, A., Iglauer, S., ... & Sarmadivaleh, M. (2020). Effect of nanofluid on CO_2-wettability reversal of sandstone formation; implications for CO_2 geo-storage. Journal of colloid and interface science, 559, 304-312.

In this article, initially, the effect of various organic acids (hexanoic acid C_6, Lauric acid C_{12}, Stearic acid C_{18}, and lignoceric acid C_{24}) were quantified by ageing quartz substrates (representing sandstone formation) with a minute concentration of 10^{-2} mol/L for 7 days and one year. Thereafter, organic-aged quartz substrates were aged with different silica nano-concentrations (0.75 wt%, 0.25 wt%, 0.1 wt%, 0.05 wt%) in deionized water for 5 hours to reverse the CO_2-wettability. Contact angle measurements were conducted at reservoir conditions (0.1 MPa, 25 MPa and 323 K) for providing the thresholds of structural and residual trapping capacities of CO_2 in a sandstone formation. Further, organic-aged and nano-aged quartz samples were

characterized by analytical measurements (scanning electron microscopy SEM, energy dispersive spectroscopy EDS, and atomic force microscopy AFM).

Part 2: **Ali, M**., Aftab, A., Awan, F. U. R., Akhondzadeh, H., Keshavarz, A., Saeedi, A., ... & Sarmadivaleh, M. (2021). CO_2-wettability reversal of cap-rock by alumina nanofluid: Implications for CO_2 geo-storage. Fuel Processing Technology, 214, 106722.

In this article, initially, the effect of various organic acids (hexanoic acid C_6, Lauric acid C_{12}, Stearic acid C_{18}, and lignoceric acid C_{24}) were quantified by ageing mica substrates (representing cap-rock formation) with a minute concentration of 10^{-2} mol/L for 7 days and one year. Thereafter, organic-aged mica substrates were aged with different alumina nano-concentrations (0.05 wt%, 0.1 wt%, 0.25 wt% and 0.75 wt%) in deionized water for 5 hours to reverse the CO_2-wettability. Contact angle measurements were conducted at reservoir conditions (0.1 MPa, 15 MPa, 25 MPa and 323 K) for providing the thresholds of structural trapping capacities of CO_2 in cap-rock formation. Further, organic-aged and nano-aged mica samples were characterized by analytical measurements (field emission scanning electron microscopy FESEM, energy dispersive spectroscopy EDS, and atomic force microscopy AFM).

PART 1 Effect of Nanofluid on CO_2-wettability reversal of sandstone formation; implications for CO_2 geo-storage

Muhammad Ali [a,*], Muhammad Faraz Sahito [b], Nilesh Kumar Jha [a,c], Zain-Ul-Abedin Arain [a], Shoaib Memon [a], Alireza Keshavarz [d], Stefan Iglauer [a,d], Ali Saeedi [a], Mohammad Sarmadivaleh [a]

[a] Western Australia School of Mines: Minerals, Energy and Chemical Engineering, Curtin University, 26 Dick Perry Avenue, 6151 Kensington, Australia

[b] College of Engineering, King Fahd University of Petroleum and Minerals, Dhahran, 31261, Saudi Arabia

[c] Petroleum Engineering Program, Department of Ocean Engineering, IIT Madras, Chennai, 600036, India

[d] School of Engineering, Edith Cowan University, 270 Joondalup Drive, Joondalup, WA 6027 Australia

[*] Corresponding author (Muhammad.ali7@postgrad.curtin.edu.au)

Abstract

Hypothesis: Nano-fluid treatment is a promising technique that can be used for wettability reversal of CO_2-brine-mineral systems towards a further favourable less CO_2-wet state in the existence of organic acids. However, literature requires more information and study for organic acids and nanoparticles' effect at reservoir (high pressure and high temperature) conditions.

Experiments: Therefore, we have measured in this study that what influence small amounts of organic acids exposed to quartz for the ageing time of (7 days and 1 year) have on their wettability and how this impact can be reduced by using different concentrations of nanoparticles at the reservoir conditions. Precisely, we have tested lignoceric acid (C_{24}), stearic acid (C_{18}), lauric acid (C_{12}) and hexanoic acid (C_6) at 10^{-2} Molarity, as well as, we have also used different concentrations (0.75 wt%, 0.25 wt%, 0.1 wt%, 0.05 wt%) of silica nanoparticles at realistic storage conditions.

Findings: The quartz surface turned significantly hydrophobic when exposed to organic acids for the longer ageing time of 1 year, and significantly hydrophilic after nano-fluid treatment at an optimum concentration of 0.1 wt%. It was observed that most nanoparticles were mechanistically irreversibly adsorbed on the surface of the quartz sample. This wettability shift thus may increase CO_2 storage capacities and containment security.

4.1.1 Introduction

CO_2 geological storage sequestration is one of the auspicious techniques used to immobilize CO_2 in deep underground formations thus contributing towards a green environment (Orr, 2009). Some of the important candidates for storing CO_2 underground are deep saline aquifers and depleted oil reservoirs (III, 2013; M. Blunt, 1993). CO_2 geological sequestration contains a quantitative and qualitative evaluation of diverse practical trapping mechanisms which preclude the floating CO_2 from travelling upward to the surface (III, 2013; Juanes et al., 2010). These trapping mechanisms include residual or capillary trapping (Iglauer, Paluszny, et al., 2011; Iglauer, Wülling, et al., 2011; S. C. Krevor et al., 2012; C. Pentland et al., 2011), mineral trapping (Gaus, 2010; Golding et al., 2011; J. K. Pearce et al., 2015), dissolution trapping (Agartan et al., 2015; Al-Khdheeawi et al., 2017a, 2017b; Iglauer, 2011) and structural trapping (Arif, Al-Yaseri, et al., 2016; Arif, Barifcani, Lebedev, et al., 2016; Arif, Lebedev, et al., 2017a; Iglauer, Al-Yaseri, et al., 2015). Further, it is being identified that adsorption trapping is an integral storage mechanism in organic rich shales and coal seams (Arif, Barifcani, & Iglauer, 2016; Arif, Lebedev, et al., 2017b; Iglauer, Pentland, et al., 2015; Kaveh et al., 2016; Kaveh et al., 2012).

Residual and structural trapping capacities are impacted by the wetting characteristics of rock and both are reduced in less water-wet environments (Al-Khdheeawi et al., 2017a; Al-Menhali, Menke, Blunt, & Krevor, 2016; Arif, Lebedev, et al., 2017a; Chaudhary et al., 2013; Iglauer, 2017; Iglauer, Al-Yaseri, et al., 2015; Iglauer, Pentland, et al., 2015; Rahman et al., 2016; Wan et al., 2018). However, there is a serious absence of information in the literature for the complex wettability behaviour at realistic reservoir conditions. Recent studies have depicted that geological formations (i.e. hydrocarbon reservoirs and also deep saline aquifers) comprehend

considerable amounts of various organic acids which can render the wettability more CO_2-wet, hence inducing lower trapping capacities (Ali, Al-Anssari, et al., 2019; Meredith et al., 2000; Watson et al., 2002).

Recent studies showed that nano-fluids can have beneficial effects in a range of applications for subsurface operations, like enhanced oil recovery (EOR) (Al-Anssari et al., 2016; Nwidee et al., 2016; Roustaei & Bagherzadeh, 2015), chemical flooding (ShamsiJazeyi et al., 2014; L. Wang & Mohanty, 2015; Zargartalebi, Kharrat, & Barati, 2015), water flooding (Hendraningrat, Li, & Torsæter, 2013; H. Zhang, Ramakrishnan, Nikolov, & Wasan, 2016), drilling (Ponmani, Nagarajan, & Sangwai, 2016) and CO_2 storage (including wettability) (Al-Anssari, Arif, Wang, et al., 2017a, 2017b). In this context, it is proven in literature that silica nanoparticles have intense effect on hydrophobic surfaces and their associated wetting behaviour to more water-wet making them suitable for CO_2 geo-sequestration (Al-Anssari, Arif, Wang, et al., 2017a, 2017b; Al-Anssari et al., 2016; Roustaei & Bagherzadeh, 2015).

Overall, this article is mainly based on advancing and receding contact angles of quartz surfaces aged in various organic acids and tested how nano-fluids can improve their wettability characteristics for the improvement of CO_2 geo-storage.

4.1.2 Methodology

4.1.2.1 Experimental Materials

Hydrophilic nanoparticles, Silicon dioxide (SiO_2) (from Sigma Aldrich; shape porous spherical; explained in Table 4-1-1) were utilized to formulate various nano-fluid compositions of 0.75 wt%, 0.25 wt%, 0.1 wt%, 0.05 wt% SiO_2 concentration with DI water. Deionized-water (Ultrapure of electrical conductivity = 0.02 mS/cm from David Gray) was utilized for the preparation of the nano-suspensions which were homogenized with an ultrasonic homogenizer for 15 mins (Frequency 20 kHz, Sonics and Materials Incorporation, USA).

Sixteen pure quartz crystals (from WARD'S Natural Science; single crystals; testing chips of sample size ranging from 10 mm to 20 mm x 11 mm x 11 mm) were utilized as quartz being a major constituent of sandstone formation (A. Z. Al-Yaseri et al.,

2016; Al-Yaseri et al., 2016; Garrido, Lafortune, Souli, & Dubujet, 2013; Scott & Barker, 2005; Worden & Morad, 2000).

Carbon dioxide (CO_2 from BOC, gas code-082, purity ≥ 99.999 mol%) was used for the contact angle measurements, and nitrogen (N_2 from BOC, gas code-234, purity ≥ 99.999 mol%) was used to dry the quartz surfaces. Sodium Chloride (NaCl from Scharlab, purity ≥ 99.9 mol%) was used to formulate 10 wt% NaCl brine by dissolving NaCl in deionized water. High pressure mixing reactor was used to equilibrate 10 wt% NaCl brine with CO_2 at experimental conditions described in this article (following the procedure described by (El-Maghraby et al., 2012) before dispensing the drop of brine into the high-pressure cell, see below in contact angle section. Organic acids having purity of ≥ 98 mol% from Sigma Aldrich was used in this study, including lignoceric acid (C_{24}), stearic acid (C_{18}), lauric acid (C_{12}) and hexanoic acid (C_6) were selected to study the effect of their associated concentration at 10^{-2} Molarity for mimicking their presence in storage formations (Amaya et al., 2002; Hamouda & Rezaei Gomari, 2006; Hansen et al., 2000; Jardine et al., 1989; Kharaka et al., 2009; Legens et al., 1999; Madsen & Ida, 1998; Stalker et al., 2013; L. Yang et al., 2015).

Aqueous hydrochloric acid (from Sigma Aldrich, concentration of 37 vol%) was used to control the pH of brine by adding its drops into the solution (see ageing procedure below). Acetone, methanol (from Rowe Scientific; purity ≥ 99.9 mol%) and toluene (≥ 99 mol%; from Chem-Supply) were utilized to clean the quartz surfaces from existing contaminations.

Table 4-1-1 Details of silicon dioxide (SiO_2) nanoparticles and organic acids

Purity [wt%]	≥ 99.50
Solubility in water	Insoluble
Density [kg m^{-3}]	2200-2600
Molecular mass [g mol^{-1}]	60.08
Surface area [m^2 g^{-1}]	140
Particle Size	100 to 130 nm

Organic Acid	Molar mass (g/mol)	Formula	Physical state	Number of C atoms	Chemical Structure
Lignoceric acid	368.63	$C_{24}H_{48}O_2$	solid	24	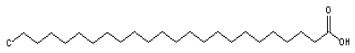
Stearic acid	284.4772	$C_{18}H_{36}O_2$	solid	18	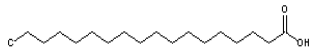
Lauric acid	200.318	$C_{12}H_{24}O_2$	solid	12	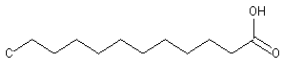
Hexanoic acid	116.158	$C_6H_{12}O_2$	liquid	6	

4.1.2.2 Preparation of Sample Procedure

4.1.2.2.1 Pure Quartz Samples Cleaning Procedure

It is of utmost importance to be careful during the surface preparation of quartz samples. A significant error can happen during contact angle measurements due to residual contaminations (Iglauer et al., 2014). Initially, ultrapure nitrogen was used to blow away any loose surface fragments from the quartz surfaces followed by toluene and DI water cleaning, to remove any inorganic or organic contaminations from the surface. Subsequently, plasma cleaning was done for 16 mins (using a Diemer Yocto instrument) to clean any remaining residues of impurities followed by drying the samples at 90 °C for 60 mins in a vacuum oven (Iglauer et al., 2014; Love et al., 2005).

4.1.2.2.2 Mimicking the Quartz as Representative of Storage Formation

Reservoir formations have existence of underground saline environment over a long deposition period; thus to simulate a representative underground formation, we adopted the following strategy (Birkholzer et al., 2009; J. A. Davis, 1982; Hoeiland et al., 2001; Ji & Zhu, 2015; Karoussi et al., 2008; Kleber et al., 2015; Nordbotten et al., 2005; Ochs et al., 1994; Ulrich et al., 1988; White et al., 2003; Zullig & Morse, 1988):

Initially, 2 wt% NaCl brine was used to ionize the cleaned quartz surfaces by submerging them in it for 30 mins at atmospheric conditions, at the same time drops

of aqueous hydrochloric acid were added to maintain a pH = 4; this process improves the rate of the organic adsorption on the quartz surfaces over long deposition period (i.e. millions of years' exposure time) (Al-Anssari et al., 2016; Jardine et al., 1989; Kharaka et al., 2009; Madsen & Ida, 1998; Stalker et al., 2013; Thurman, 2012; L. Yang et al., 2015). The remaining water from the surface was removed by using ultrapure nitrogen to avoid contamination. Subsequently, the brine and HCl treated quartz surfaces were placed in different organic acid/n-decane solutions (4 quartz surfaces in each acid for each nano-fluid) of prescribed molarity of 10^{-2} M at ambient pressure and elevated temperature (323 K), for 7 days and one year to provide sufficient exposure time for duplicating storage formation conditions (Jardine et al., 1989; Kharaka et al., 2009; Madsen & Ida, 1998; Stalker et al., 2013; Thurman, 2012; L. Yang et al., 2015). For the ageing of quartz minerals, different acrylic containers was used having sealed caps to avoid evaporation of n-decane. Note this evaporation may change the concentration of organic acid and it is very important to keep samples in a completely sealed environment. Later on, they were placed in a fume hood to avoid contamination for a year before doing contact angle measurements. It is of utmost importance to reproduce such rock surfaces to accurately simulate the formation behaviour, especially for their wettability characteristics (Adamson & Gast, 1967; J. A. Davis, 1982; Kleber et al., 2015; Ochs et al., 1994).

4.1.2.2.3 Formulation and Ageing Procedure of Nano-fluids

Nano-fluid Preparation

Different nano-fluid concentrations were analysed to investigate their competence for wettability modification of CO_2/brine/quartz organisms. For this nano-fluids were formulated by sonication method. Ultrasonic homogenizer (Frequency 20 kHz, Sonics and Materials Incorporation, USA) was used for 15 mins to sonicate DI water and SiO_2 nanoparticles (Table 4-1-1). Technically, sonication is obtained by a microtip of 9.5 mm dia (titanium material) to formulate 30 ml sets of nano-suspensions having sonication amplitude of (40 %) and energy (9500 J) (Al-Anssari, Wang, Barifcani, Lebedev, & Iglauer, 2017). Note that magnetic stirring is incapable to disperse nanoparticles in DI water homogeneously (Mahdi Jafari, He, & Bhandari, 2006).

Stability of Nano-fluids

It is of key importance to measure the nano-fluid stability, which is an important factor in nano-fluid application. To do this, we have measured the average solid particle size (nm), zeta potential (mV) and pH of each nano-fluid. Nano-suspensions with lower zeta-potential are more electrically unstable and can precipitate and flocculate more quickly (El-sayed et al., 2012). Moreover, electrolytes significantly decrease the repulsive forces among nanoparticles and thus accelerate particle coagulation and flocculation. Surfactants such as SDS can lower the zeta potential (to below ≤ -25 mV) of silica nano-suspensions due to nanoparticle adsorption on the solid surface creating supercharged particles (Ahualli et al., 2011). We have used a Zeta sizer (Nano ZS instrument, Malvern Instruments, UK) to measure the nano-fluid phase behaviour and average particle sizes for each nano-fluid concentration. The pH of each nano-suspension was measured with a pH meter (resolution 0.01 pH, Ohaus, Australia). The data shows that with increasing concentration of nano-fluids, average particle size have increased whereas, pH and zeta potential have decreased. Table 4-1-2 shows the details of nano-suspensions.

Table 4-1-2 Details of nano-suspensions

No.	Nanoparticle Concentration (%)	pH (pH)	Zeta-potential (mV)	Average particle size agglomeration (nm)
1	0.05	8.20	-57.00	223.60
2	0.10	8.05	-39.90	498.80
3	0.25	7.96	-38.00	516.57
4	0.75	7.48	-31.20	888.03

Ageing of Quartz in Different Nano-fluids

The nano-alteration conditions have a substantial outcome on wettability modification efficiency (Al-Anssari, Arif, Wang, et al., 2017a, 2017b). To test this, nano-modified quartz substrates were formed by submerging different organic/n-decane treated samples in different nano-fluids at ambient pressure and elevated temperature (323 K). Physically, the aged quartz surfaces were vertically submerged in nano-fluid for 5 hours (testing different compositions; 0.75 wt%, 0.25 wt%, 0.1 wt%, 0.05 wt% SiO_2

in DI water), while closely tightening the container's lid to avoid contamination. The substrates were arranged vertically to avoid gravitational nanoparticle deposition on the quartz surfaces. Further, the perpetual weight ratio of (5 gm of nano-emulsion for each 1 gm of quartz sample) was used to deliver the same adaptation field for each quartz sample.

Zeta-potential measurements were done to find out the surface charge of nano-fluids and all results came into negative values, as shown in Table 4-1-2. Since SiO_2 is one of the most stable compounds, therefore this surface charge is attributed to induced charge on the surface due to the presence of the hydroxyl group. When the hydroxyl group of quartz surface and nano-fluids suspension are aged together than they make a very strong chemical reaction which causes irreversible adsorption of nanoparticles on the quartz surface. This interaction showed an increase in water-wetness with silica-suspensions. Previously, organic acids aged quartz surfaces were submerged into negatively charged SiO_2 and ZrO_2 nano-fluids which showed enhancement of oil wettability of quartz surfaces (Al-Anssari, Arif, Wang, et al., 2017a, 2017b; Al-Anssari et al., 2016; Nwidee et al., 2016).

Mechanistically, the organic acid esterifies the hydroxyl groups on the quartz surface in a condensation reaction and then nanoparticles irreversibly adsorbed on the surface of the organo-aged quartz sample (Scheme 4-1-1).

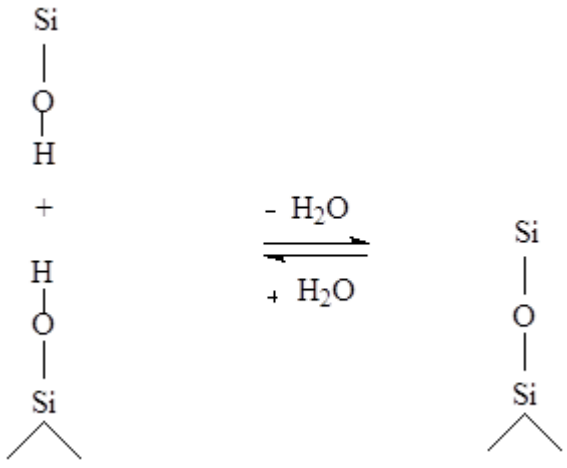

Scheme 4-1-1 Chemical bonding between organo-aged quartz surface and silica nano-fluids ($\wedge$ indicates solid bulk).

4.1.2.3 Classification of Clean, Organic-aged and Nano-aged Quartz Samples

The classification of quartz samples was done with three different methods including energy-dispersive X-ray spectroscopy (EDS, Oxford X-act SSD X-ray detector with Inca and Aztec software), contact angle (θ) measurements and atomic force microscopy (AFM, DSE 95-200, Semilab).

4.1.2.3.1 Quartz Surface Roughness

The surface roughness of clean quartz samples were characterized by atomic force microscopy (AFM, DSE 95-200, Semilab) with an average root mean square of 1 nm to 2 nm, which is ultra-smooth (Sarmadivaleh et al., 2015). Surface roughness was also measured for the samples aged in organic acids and nano-fluids. The surface roughness data shows that samples were very smooth and homogeneous ranging from 160 to 330 nm; Figure 4-1-1. Note that high surface roughness (> 1 µm) is influential during contact angle measurements (Marmur, 2006). Thus, as surface roughness is significantly lower than 1 µm, hence it does not affect CO_2-wettability measurements (A. Z. Al-Yaseri et al., 2016).

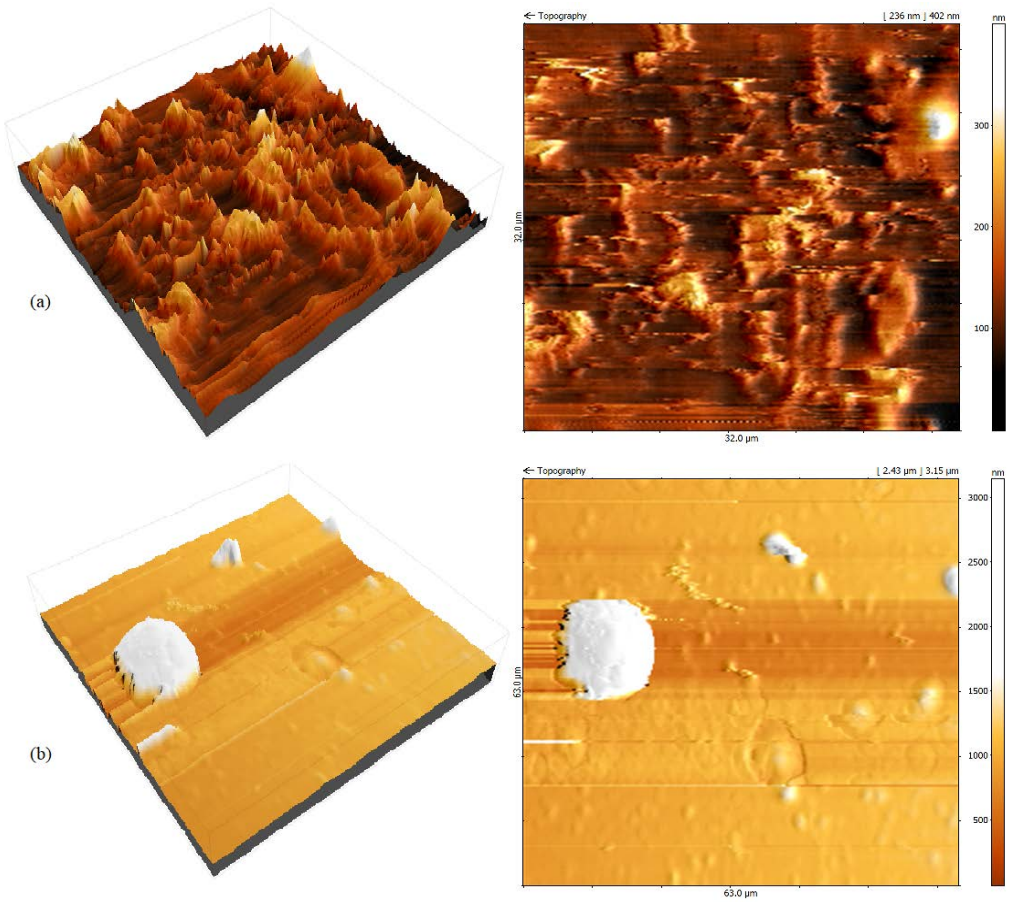

Figure 4-1-1 Topographical images of quartz surfaces (a) aged with stearic acid (10^{-2} M) (b) aged with 0.1% SiO_2 nano-fluid.

4.1.2.3.2 Elemental Identification Measurements

Atomic surface compositions (in wt% concentrations) of each quartz sample in pure and aged conditions with organic acids and nano-fluids were measured by energy dispersive spectroscopy (EDS). Clearly, ageing had a substantial influence on surface composition due to organic acids and nano-fluids (Table 4-1-3). A noteworthy cumulative rise in surface carbon concentration (+4.2 wt% C for Lignoceric Acid, +3.1 wt% C for Stearic Acid, +2.8 wt% C for Lauric Acid and +3.2 wt% C for Hexanoic Acid) due to organic acids in pure quartz samples and surface silica concentration (+22.2 wt% Si for Hexanoic-aged surface, +21.6 wt% Si for Lauric-aged surface, +22.9 wt% Si for Stearic-aged surface and +31.5 wt% Si for Lignoceric-aged surface) due to nanoparticles was measured on the organic-aged samples. This variation in atomic surface composition is caused by the chemisorption of the organic acids, consistent with (Zullig & Morse, 1988) and irreversible adsorption of nano-fluids on

quartz surfaces (Al-Anssari, Arif, Wang, et al., 2017a, 2017b). These measurements were taken at 5 different points of each sample and was repeated 3 times to get the average value of each sample. Table S4-1-1 in the supplementary file explains the detail atomic surface concentration. Whereas Table 4-1-3 is the cumulative average data of all samples. SEM images were acquired after treatment with nanoparticle suspension to show the adsorption of nanoparticles on the quartz surface; four example pictures at different resolutions are presented in Figure 4-1-2. The spread of nanoparticles is visible on quartz surface after the surface treatment with 0.1 wt% nanoparticle concentration. Such a coverage of quartz surface by nanoparticles causes wettability reversal from strongly CO_2-wet to weakly water-wet, see below.

Table 4-1-3 Average energy dispersive spectroscopy (EDS) measurements for pure and aged (organic acids and nano-fluids) quartz samples.

Organic Acids	Pure Quartz			After ageing with 10^{-2} M of different organic acids			After ageing with nano-fluids		
	wt% Si	wt% C	wt% O	wt% Si	wt% C	wt% O	wt% Si	wt% C	wt% O
Hexanoic Acid	$33.1^a \pm 1.2^b$	$3.3^a \pm 0.7^b$	$63.9^a \pm 1.9^b$	$30.0^a \pm 1.9^b$	$6.5^a \pm 1.7^b$	$63.6^a \pm 3.5^b$	$52.2^a \pm 6.3^b$	$6.3^a \pm 2.0^b$	$41.6^a \pm 6.4^b$
Lauric acid	$36.5^a \pm 1.6^b$	$2.5^a \pm 0.7^b$	$61.1^a \pm 1.6^b$	$29.6^a \pm 2.0^b$	$5.3^a \pm 1.4^b$	$65.4^a \pm 1.8^b$	$51.2^a \pm 6.9^b$	$7.0^a \pm 1.4^b$	$42.6^a \pm 6.3^b$
Stearic acid	$34.6^a \pm 2.2^b$	$2.2^a \pm 0.9^b$	$62.6^a \pm 1.9^b$	$32.2^a \pm 1.8^b$	$5.3^a \pm 2.2^b$	$62.2^a \pm 2.5^b$	$55.1^a \pm 5.8^b$	$6.6^a \pm 1.3^b$	$38.8^a \pm 6.8^b$
Lignoceric acid	$35.5^a \pm 1.8^b$	$2.6^a \pm 0.3^b$	$62.0^a \pm 1.6^b$	$24.8^a \pm 2.0^b$	$6.8^a \pm 0.6^b$	$68.3^a \pm 2.5^b$	$56.3^a \pm 5.1^b$	$7.5^a \pm 0.6^b$	$36.7^a \pm 5.0^b$

[a] This value is based on the arithmetic average of four samples at all nanoparticle concentrations measured on five different sites equalising 20 data points tested.
[b] This value is showing the standard deviation for all data points.

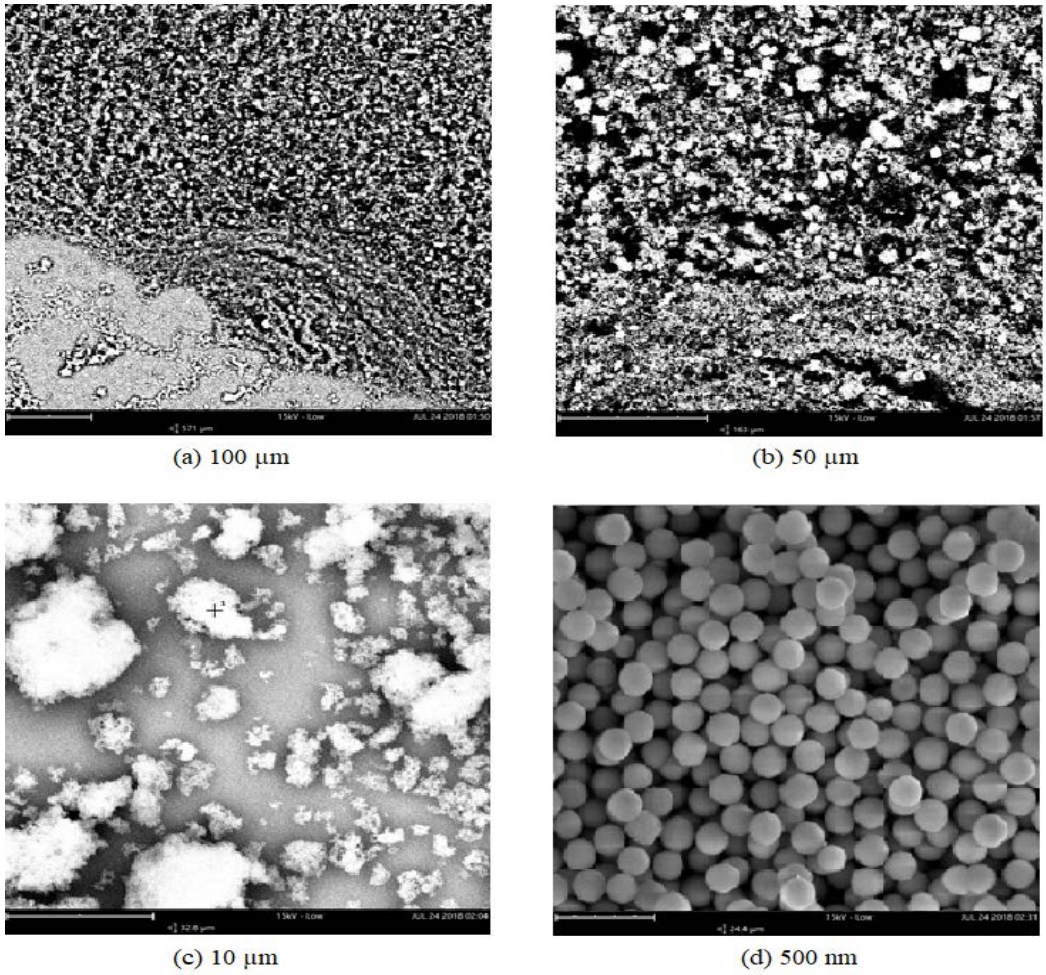

Figure 4-1-2 SEM images after treatment with 0.1% SiO_2 nano-fluid, (a) lowest magnification at 100 µm (d) highest possible magnification at 500 nm.

4.1.2.4 Contact Angle Measurements

Contact angle measurements technique is used to assess the wettability modification behaviour of a given CO_2/brine/rock (Iglauer, 2017), which involves a tilted plate technique for calculating advancing and receding tangent angles simultaneously (Lander et al., 1993). The contact angle mechanism comprises a high temperature and high-pressure cell (Hestalloy wetted material) which accommodates a plate on 17° for placing the samples inside. Two manually operated individual high precision syringe pumps (Teledyne D-500, pressure accuracy of 0.1%) are connected with the cell for discharging CO_2 or brine. In addition to this, the mixing reactor is connected with both pumps for formulating thermodynamically equilibrated live brine with CO_2 (El-

Maghraby et al., 2012). The procedure for the experiment is already described in our previous studies (Ali, Al-Anssari, et al., 2019).

4.1.3 Results and Discussion

It is very significant to apprehend the CO_2-wettability of a storage reservoirs as it considerably affects CO_2 distribution and movement across the formation (Al-Khdheeawi et al., 2017a, 2017b; Al-Khdheeawi et al., 2017), injection flow rate (Iglauer, 2017; Iglauer, Pentland, et al., 2015), storage volume and security (Arif, Barifcani, Lebedev, et al., 2016; Arif, Lebedev, et al., 2017b; Iglauer, Al-Yaseri, et al., 2015). Thus, structural trapping (underneath the cap-rock) is related to CO_2 displacing water (water receding contact angle) (Broseta et al., 2012) and water displacing CO_2 (water advancing contact angle) defines the residual trapping capacity of CO_2 (Al-Menhali et al., 2016; Chaudhary et al., 2013; Chiquet et al., 2007; Rahman et al., 2016). Dissolution trapping is also well connected and considerably impacted by the change in wettability (Al-Khdheeawi et al., 2017a, 2017b; Al-Khdheeawi et al., 2017).

Our results explain that quartz formations lose their water-wetness with increasing organic exposure, which, however, can be recovered by nano-fluid treatment. To quantify these effects, a droplet of 10 wt% NaCl brine was dispensed on quartz surfaces at ambient and reservoir conditions (25 MPa, 323 K) (Note: 10 wt% NaCl brine was thermodynamically equilibrated with CO_2 by using high-pressure autoclave mixing Parr reactor at reservoir conditions for 24 hours before transferring it to ISCO pump for dispensing the drop of brine on the substrate). Initially, pure quartz substrates were tested at ambient conditions which resulted in completely water-wet characteristics having 0° (advancing and receding) tangent angles, consistent with literature data (Iglauer et al., 2014; Sarmadivaleh et al., 2015). However, at reservoir conditions (25 MPa, 323 K) pure quartz surfaces depicted weakly water-wet characteristics having (advancing 56° and receding 54° ± 3°) tangent angles, consistent with literature data (A. Z. Al-Yaseri et al., 2016; Al-Yaseri et al., 2016; Arif, Barifcani, & Iglauer, 2016; Chiquet et al., 2007; Farokhpoor et al., 2013).

4.1.3.1 Effect of Organic Acids

Effect of organic acids on CO_2-wettability was investigated by, organic-aged quartz surfaces exposed to 10^{-2} M of Lignoceric Acid, Stearic Acid, Lauric Acid and Hexanoic Acid were used for contact angle measurements. Clearly, quartz surfaces showed a considerable change in contact angles at reservoir conditions (25 MPa, 323 K), thus rendering them more hydrophobic, from weakly water-wet to CO_2-wet, Figures 4-1-3 & 4-1-4. These measurements were taken at different ageing times (7 days and 1 year), to also assess the ageing effect on quartz surfaces.

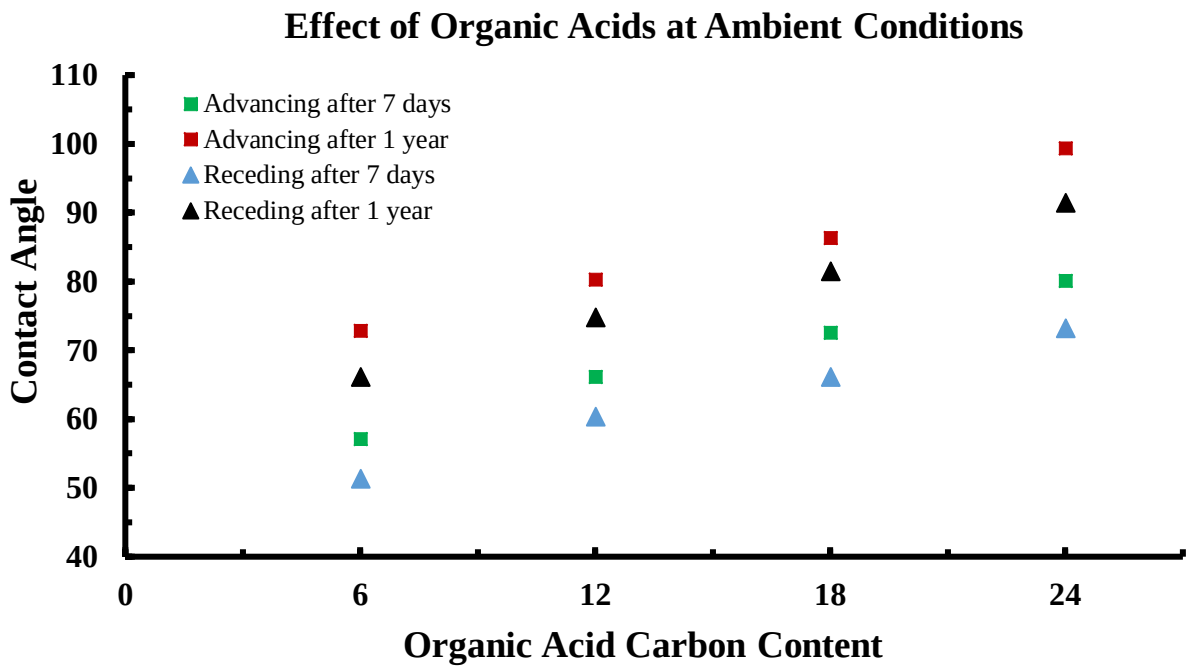

Figure 4-1-3 Quartz/CO_2/brine advancing and receding contact angles as a function of ageing effect and various organic acids at ambient conditions.

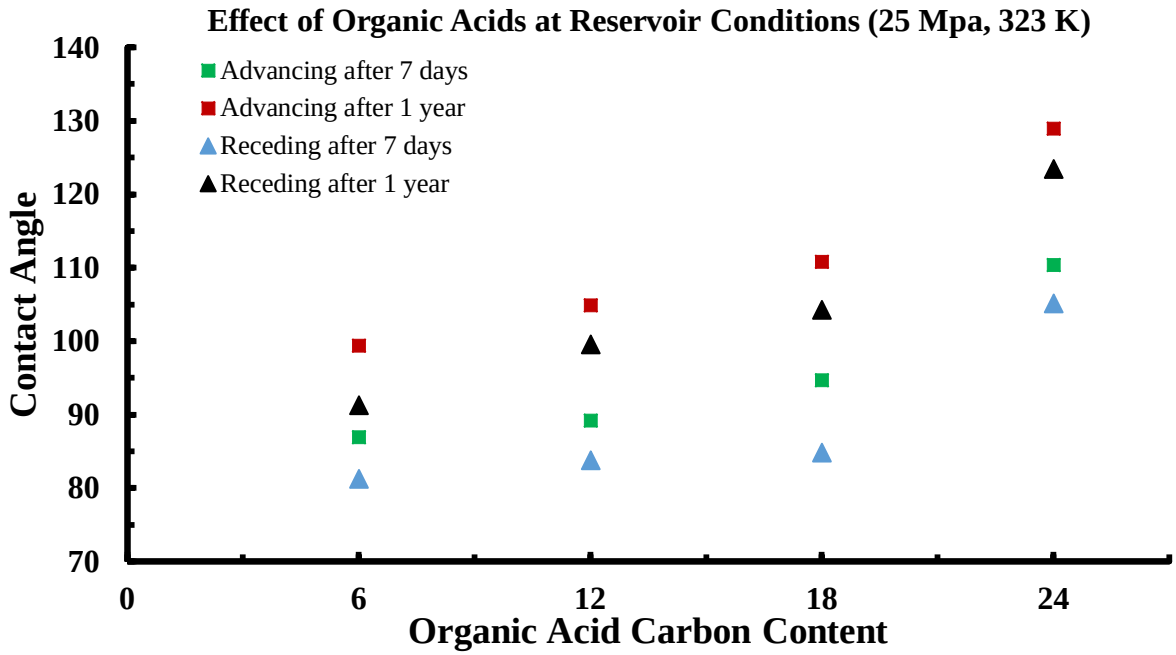

Figure 4-1-4 Quartz/CO_2/brine advancing and receding contact angles as a function of ageing effect and various organic acids at reservoir conditions (25 MPa and 323 K).

It is obvious while looking at results that, increased ageing time have an increasing effect on both water receding and advancing tangent angles. However, longer alkyl chains altered the surface more hydrophobic (Ali, Al-Anssari, et al., 2019), therefore hexanoic acid (C_6) displayed a relatively low contact angle while surfaces placed in lignoceric acid (C_{24}) induced the highest contact angle. For instance, with an ageing time of 1-year, at 323 K and 25 MPa, lignoceric, stearic, lauric and hexanoic acid, receding contact angle values were, θ_r = 123.44°, θ_r = 104.28°, θ_r = 99.56° and θ_r = 91.3°, respectively. As a result, structural trapping capacities are considerably reduced (structural leakage is possible at $\theta_r > 90°$ (Arif, Lebedev, et al., 2017b; Iglauer, 2017; Iglauer, Pentland, et al., 2015; Naylor et al., 2011). Such a wettability change and difference in receding contact angle values is accredited to the alkyl chains (number of carbon atoms) existing in the organic acid, which chemisorbed on the quartz surface (Ali, Al-Anssari, et al., 2019).

The optimal residual trapping limit is severely affected by ageing the quartz surfaces in organic acids, where wettability does not affect primary drainage i.e. at $\theta_a = 50°$ (Morrow, 1970, 1976). For example, at 323 K and 25 MPa, all organic acids at concentrations of 10^{-2} M showed higher advancing contact angles than the optimal

residual trapping limit (i.e. at $\theta_a > 50°$). Thus, the presence of these organic molecules will decrease the capillary trapping capacities (Ali, Al-Anssari, et al., 2019; Iglauer, Wülling, et al., 2011; Morrow, 1970, 1976). Note that carboxylic acids and hydrocarbons both exist in deep saline aquifers as a result of biodegradation and organic matter diagenesis and subsequent migration into the water zones (Ali, Al-Anssari, et al., 2019; Bennett et al., 1993; Gomari & Hamouda, 2006; Hamouda & Rezaei Gomari, 2006; Jones et al., 2008; Stalker et al., 2013). Similar organic fatty acids are found in many samples from different aquifers (Bennett et al., 1993; Gomari & Hamouda, 2006; Jones et al., 2008; Paterson et al., 2011; Stalker et al., 2013). It is well proven that organics reduces structural and residual CO_2-trapping capacities, and carbon geo-sequestration (CGS) projects need to account for the effects of organic acids.

It is also noticeable in previous studies (Ali, Al-Anssari, et al., 2019; Ali, Arif, et al., 2019) that with lower organic acids concentrations, its effect of altering wettability to more oil-wet reduces significantly.

4.1.3.2 Effects of Nano-fluids on Trapping Capacities

Literature provides the information that pressure, temperature and brine salinity have considerable influence on CO_2-storage capacities (Arif, Al-Yaseri, et al., 2016; Arif, Barifcani, Lebedev, et al., 2016; Iglauer, 2017). However, nano-fluid treatment (concentration and type) still needs to be investigated at high pressure and high-temperature conditions to find out the effect of these tiny particles for CO_2 trapping capacities in storage formations. The nano-fluid concentration and its associated adsorption of silica particles drives the efficiency of nano-treatment on quartz surfaces. It is clear from (Figure 4-1-5 and 4-1-6) that nano-fluids have considerably reversed the wettability of organic-aged hydrophobic quartz surfaces to hydrophilic, but nano-fluid concentration is mainly responsible for the degree of reversal (Roustaei & Bagherzadeh, 2015). For example, with hexanoic-aged quartz surface, at 25 MPa and 323 K, water receding contact angle for 0.05%, 0.1%, 0.25%, and 0.75% are $\theta_r = 35.16°$, $\theta_r = 26.87°$, $\theta_r = 40.92°$ and $\theta_r = 49.36°$ respectively (recall structural trapping limit $\leq 90°$). It is visible from data that each nano-fluid concentration is setting a similar trend in all organic-aged surfaces while nano-fluid concentration at 0.1 wt%

have showed optimum wetting conditions where contact angle is minimised comparing to other nano-fluid concentrations (Al-Anssari, Arif, Wang, et al., 2017a, 2017b).

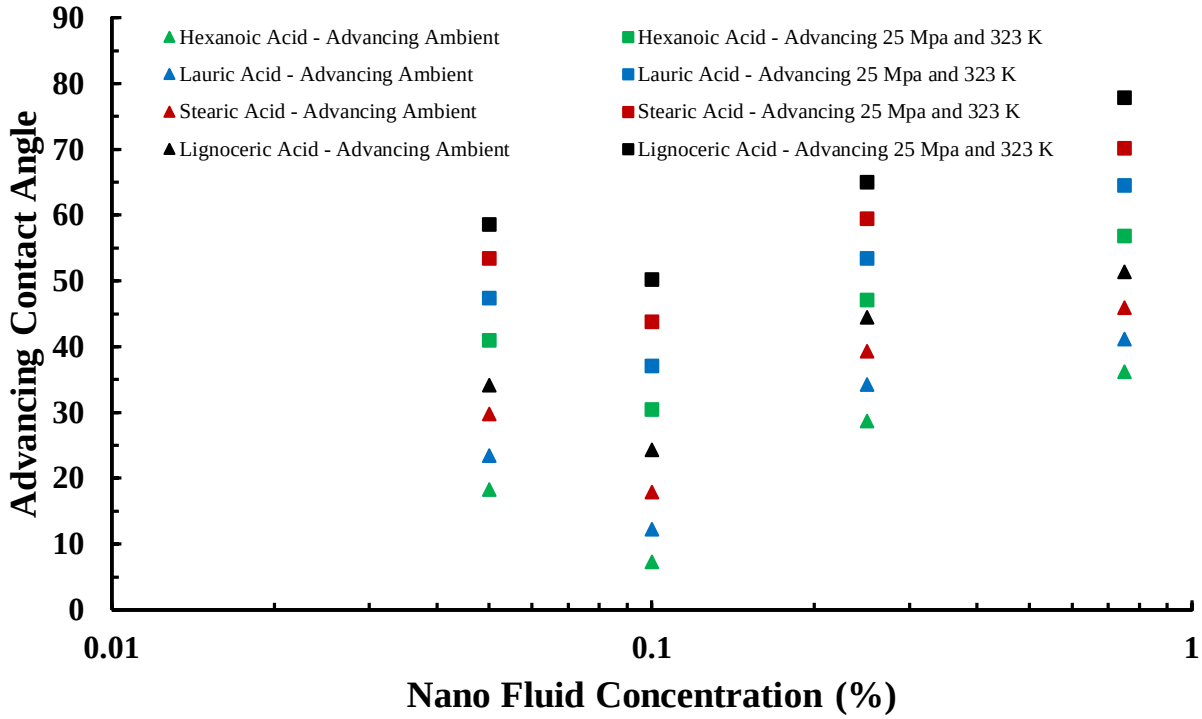

Figure 4-1-5 Quartz/CO_2/brine advancing contact angles as a function of various nano-fluid concentrations at ambient and reservoir conditions (25 MPa and 323 K).

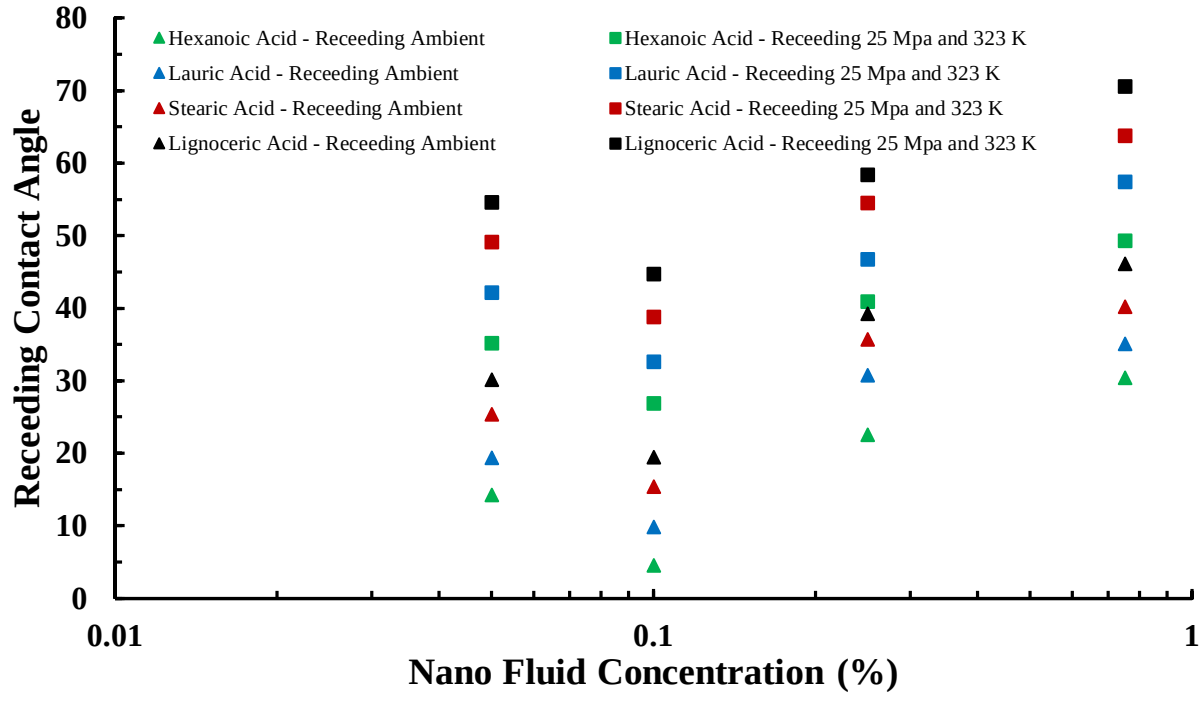

Figure 4-1-6 Quartz/CO_2/brine receding contact angles as a function of various nano-fluid concentrations at ambient and reservoir conditions (25 MPa and 323 K).

4.1.4 Implications

The measured contact angle data have established that presence of organic acids into storage formations will turn them hydrophobic at typical storage conditions which causes a reduction in structural and residual trapping capacities (Al-Menhali et al., 2016; Iglauer, Pentland, et al., 2015; Rahman et al., 2016). Thus, recommended nano-fluid treatment (in this case is 0.1 wt% SiO_2 in DI water) will significantly increase trapping capacities, which is due to wettability reversal from hydrophobic to hydrophilic conditions. Subsequently, injection of nanoparticle suspensions as part of CO_2-sequestration schemes in storage formations will composite an integral part for mitigating anthropogenic greenhouse gas emissions by significantly de-risking CO_2 storage projects.

4.1.5 Conclusions

It is very well proven in literature that depleted hydrocarbon reservoirs and deep saline aquifers are the utmost important candidates for CO_2-sequestration projects (Firoozabadi & Myint, 2010; III, 2013) and CO_2-wettability of these candidates drastically impacts its associated capacity, contamination security, injectivity, technical feasibility and thus project economics (Al-Khdheeawi et al., 2017a; Al-Menhali et al., 2016; Ali et al., 2017; Arif, Lebedev, et al., 2017a; Broseta et al., 2012; Iglauer, Al-Yaseri, et al., 2015; Iglauer, Pentland, et al., 2015; N. Jha et al., 2018; N. K. Jha, Ali, et al., 2019; Wan et al., 2018). However, these storage formations have presence of organic acids (Jardine et al., 1989; Kharaka et al., 2009; Madsen & Ida, 1998; Stalker et al., 2013; L. Yang et al., 2015), which reduces the trapping limits (Ali, Al-Anssari, et al., 2019; Ali, Arif, et al., 2019). Literature lacks the information to rectify these effects; thus we have investigated that in quartz/CO_2/brine systems, how the presence of various organic acids increases the wettability (Ali, Al-Anssari, et al., 2019; Ali, Arif, et al., 2019) and this change can be reversed by using different nano-fluids (Al-Anssari et al., 2019; Al-Anssari, Arain, et al., 2018; Al-Anssari, Arif, Wang,

et al., 2017a, 2017b; Al-Anssari et al., 2016; Al-Anssari, Nwidee, et al., 2017; Al-Anssari, Wang, Barifcani, Lebedev, et al., 2017).

Four organic acids (lignoceric acid, stearic acid, lauric acid and hexanoic acid) were used at (10^{-2} M concentration) and various concentrations (0.75%, 0.25%, 0.1% and 0.05%) of silica nanoparticle were formed. Initially, the effect of organic acids on CO_2-wettability were measured at (0.1 MPa, 25 MPa and 323 K) on organic aged quartz surfaces (ageing time 7 days and 1 year) by measuring advancing and receding tangent angles. Subsequently, contact angle measurements were done on reservoir conditions on organic-aged nano-treated surfaces to quantify the reversal effect of nano-fluids.

We found that contact angles have significantly increased on pure quartz samples which are completely water-wet to oil-wet (θ_a = 128.94° at 25 MPa and 323 K for lignoceric acid quartz surface at 1-year ageing time) and nano-fluids have shown a promising effect to reverse the wettability to intermediate-wet (θ_a = 50.21° at 25 MPa and 323 K at 0.1% nano-fluid concentration for lignoceric acid quartz surface at 1 year ageing time) (F. Huang, Kang, You, You, & Xu, 2017; Naik, You, & Bedrikovetsky, 2018).

In a nutshell, to correctly assess the viability of long-term geo-sequestration projects, it is very important to quantify the comprehensive understanding of organic acids, nano-fluids and their effective relative concentrations in storage formations. We thus conclude that injecting nano-fluids into storage reservoirs before CO_2 injection may be helpful to increase geological storage capacities and thus may reduce the risk of CO_2 geo-storage.

4.1.6 Graphical Abstract

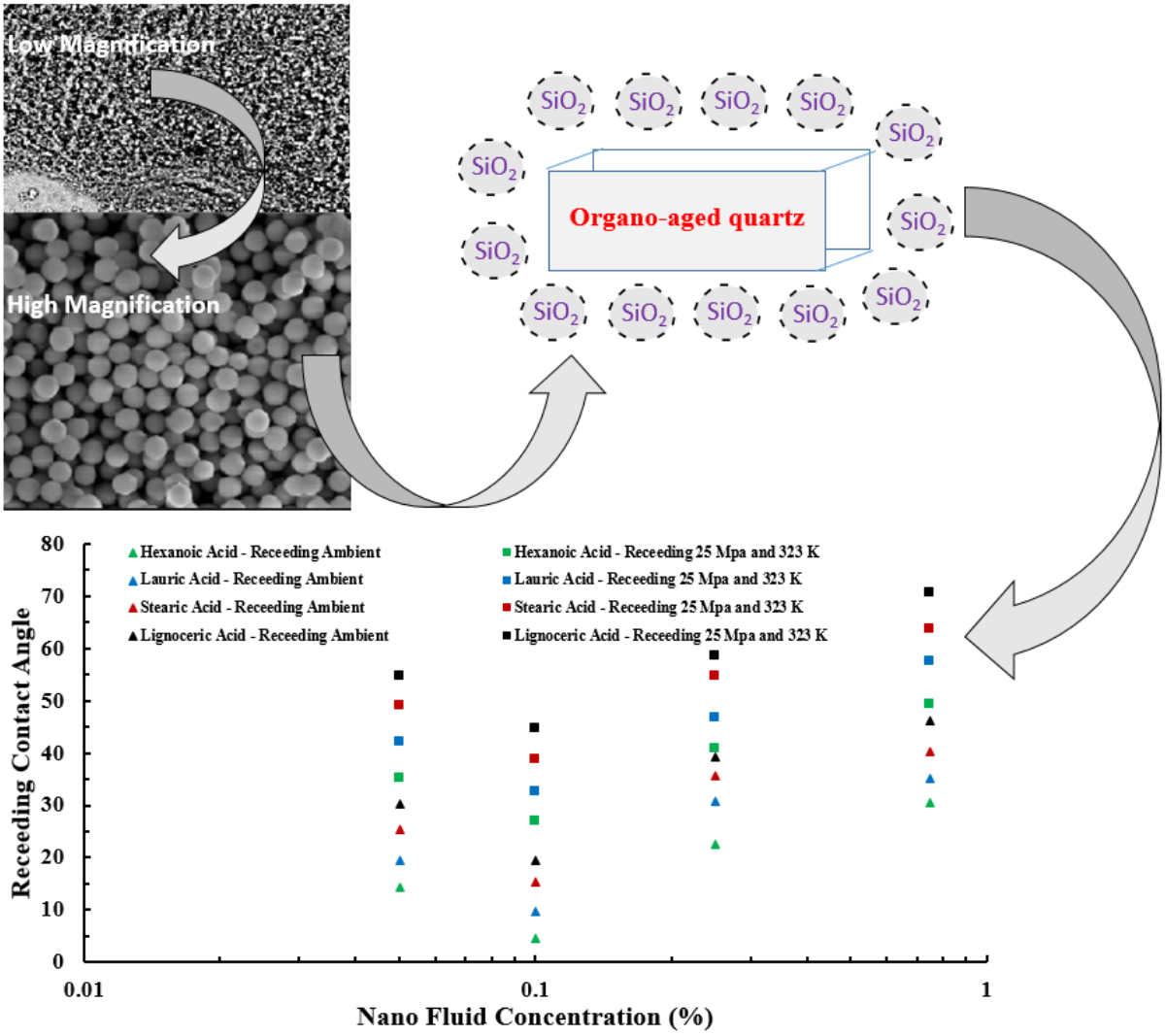

4.1.7 Supporting Information

Table S4-1-1 Surface composition of pure and aged quartz samples with all organic acids and nano-fluids.

Concentration of Nano-fluids	Pure Quartz			After ageing with 10^{-2} M (Hexanoic Acid)			After ageing with nano-fluids		
	wt% Si	wt% C	wt% O	wt% Si	wt% C	wt% O	wt% Si	wt% C	wt% O
0.05% SiO_2	31.9	2.3	65.8	28.1	4.8	67.1	45.9	6.1	48.0
0.10% SiO_2	34.2	3.9	61.9	31.8	8.1	60.1	49.7	6.3	44.0
0.25% SiO_2	33.8	2.6	63.6	30.9	5.3	63.8	52.8	6.4	40.8
0.75% SiO_2	32.9	3.3	63.8	28.4	6.9	64.7	58.5	6.3	35.2
Concentration of Nano-fluids	Pure Quartz			After ageing with 10^{-2} M (Lauric Acid)			After ageing with nano-fluids		
	wt% Si	wt% C	wt% O	wt% Si	wt% C	wt% O	wt% Si	wt% C	wt% O
0.05% SiO_2	38.1	2.4	59.5	27.6	5.3	67.1	44.3	6.8	48.9
0.10% SiO_2	37.4	2.6	60.0	30.4	5.8	63.8	50.2	7.4	42.4
0.25% SiO_2	34.9	3.1	62.0	29.7	6.7	63.6	54.7	8.3	37.0
0.75% SiO_2	35.6	1.8	62.6	31.5	3.9	64.6	58.1	5.6	36.3
Concentration of Nano-fluids	Pure Quartz			After ageing with 10^{-2} M (Stearic Acid)			After ageing with nano-fluids		
	wt% Si	wt% C	wt% O	wt% Si	wt% C	wt% O	wt% Si	wt% C	wt% O
0.05% SiO_2	35.4	1.3	63.3	32.2	3.1	64.7	49.3	5.2	45.5
0.10% SiO_2	36.7	2.6	60.7	33.7	6.3	60.0	52.3	7.8	39.9
0.25% SiO_2	32.4	3.1	64.5	30.4	7.4	62.2	57.6	7.6	37.8
0.75% SiO_2	35.1	2.7	62.2	33.9	6.4	59.7	60.8	7.2	32.0
Concentration of Nano-fluids	Pure Quartz			After ageing with 10^{-2} M (Lignoceric Acid)			After ageing with nano-fluids		
	wt% Si	wt% C	wt% O	wt% Si	wt% C	wt% O	wt% Si	wt% C	wt% O
0.05% SiO_2	37.3	2.3	60.4	25.0	6.2	68.8	51.2	7.1	41.7
0.10% SiO_2	34.5	2.8	62.7	26.8	7.4	65.8	53.7	7.8	38.5
0.25% SiO_2	33.7	2.7	63.6	23.7	7.0	69.3	58.4	8.1	33.5
0.75% SiO_2	35.1	2.4	62.5	22.8	6.4	70.8	61.4	6.9	31.7

PART 2 CO_2-Wettability Reversal of Cap-Rock by Alumina Nano-fluid; Implications for CO_2 Geo-Storage

Muhammad Ali [a,*], Adnan Aftab [b], Faisal Ur Rahman Awan [c,d], Hamed Akhondzadeh [c], Alireza Keshavarz [c], Ali Saeedi [a], Stefan Iglauer [a,c], Mohammad Sarmadivaleh [a]

[a] Western Australia School of Mines, Minerals, Energy and Chemical Engineering, Curtin University, 26 Dick Perry Avenue, Kensington, 6151, WA, Australia

[b] Petroleum Engineering Department, Mehran University of Engineering and Technology, Khairpur Mir's Campus, 66020, Sindh, Pakistan

[c] Petroleum Engineering Discipline, School of Engineering, Edith Cowan University, 270 Joondalup Dr, Joondalup, 6027, WA, Australia

[d] Department of Petroleum and Gas Engineering, New M. A. Jinnah Road Ext., Dawood University of Engineering and Technology, Karachi 74800, Pakistan

[*] Corresponding author (Muhammad.ali7@postgrad.curtin.edu.au)

Highlights

- Wettability is directly or indirectly related to CO_2 structural trapping potential in cap-rock formation.
- Organic acids have a substantial effect on altering the wettability to CO_2-wet, thus reduced CO_2 trapping potential.
- Alumina Nanoparticles have significantly reversed the wettability to water-wet, thus increased CO_2 trapping potential.

Abstract

The usage of nano-fluids is vast in different applications of nano-energy. These minute nanoparticles can be used to alter the hydrophobicity into hydrophilicity for CO_2-brine-mineral systems in the presence of organic acids. Nonetheless, the literature lacks information for the behaviour of nanoparticles and their associated concentrations in the presence of organic acids at the reservoir (high temperature and

high pressure) conditions. In this study, we have investigated that how different alkyl chain organic acids impact the wettability of mica muscovite for different ageing times (7 days and one year) and how this impact can be reversed by nano-fluid priming at different concentrations. To do that, we have used different organic acids with different alkyl chain lengths (hexanoic acid C_6, lauric acid C_{12}, stearic acid $C_{18,}$ and lignoceric acid C_{24}) at 10^{-2} mol/L. We have also used different Al_2O_3 nanoparticle suspensions (0.05 wt%, 0.1 wt%, 0.25 wt% and 0.75 wt%) in deionised water. When mica substrates were exposed to organic acids for a longer ageing time of 1 year, it has lost its water-wetness rapidly at maximum. Whereas this effect was optimally reduced by 0.25 wt% of alumina nano-formulation and mechanical irreversible adsorption of alumina nanoparticles was noted on mica substrates. This reversal of wettability may raise the containment security and CO_2 structural trapping potential.

Keywords

Alumina Nanoparticles, Organic Acids, Wettability, CO_2 Geo-storage, Deep Saline Aquifers, Cap-rock Formation

4.2.1 Introduction

CO_2 geo-storage (CGS) sequestration is one of the auspicious technique used to immobilize CO_2 in deep underground formations, thus contributing towards a green environment (Metz et al., 2005). To do that, CO_2 is captured from the environment and is stored in deep underground formations. Many methods have been previously discussed for CO_2 capture (Abdolahi-Mansoorkhani & Seddighi, 2020; Dietrich, Schöny, Fuchs, & Hofbauer, 2018; H. Li, Qu, & Hu, 2020; N. Wang, Feng, Liu, & Guo, 2018), but storing CO_2 deep underground formation is an only viable option for permanent CO_2 storage (Ali, Aftab, et al., 2020; Ali, Al-Anssari, et al., 2019; Ali, Sahito, et al., 2020). The projection of global CO_2 emissions in 2020 was 36.8 billion tons, which has now decreased by 8% (2.94 billion tons) due to the novel COVID-19 pandemic. This pandemic has caused the global industry to shut down, which has led to the sharpest fall of CO_2 emissions since World War II (IEA, 2020). However, future projection depicts that CO_2 emissions will gain momentum towards 43.08 billion tons

by 2050 (Newell et al., 2019). The projected amount of CO_2 emissions is at an alarming situation, and if its large portion is not stored in underground formations may lead to accelerated global warming and irreversible climate change (Metz et al., 2005; Orr, 2009).

Some of the prime candidates for CO_2 storage are deep saline aquifers, depleted petroleum oil reservoirs, coal beds, basaltic formations, and organic shale reservoirs (Al-Menhali & Krevor, 2016; Ji & Zhu, 2015; Metz et al., 2005). These formations have vast storage capacities and can act as a barrier for CO_2 mobilization after its storage to mitigate global warming (Ali, Aftab, et al., 2020; Ali, Al-Anssari, et al., 2019; Ali, Arif, et al., 2019; Ali, Sahito, et al., 2020; Metz et al., 2005). After CO_2 injection in underground formations, it is restrained by different mechanisms, which comprises structural trapping (in cap-rock, sandstone, and carbonate formations) (Ali, Aftab, et al., 2020; Arif, Al-Yaseri, et al., 2016; Arif, Barifcani, Lebedev, et al., 2016; Iglauer, Al-Yaseri, et al., 2015; Iglauer, Pentland, et al., 2015), residual or capillary trapping (in sandstone and carbonate formations) (M. Ali et al., 2021; Iglauer, Wülling, et al., 2011; C. Pentland et al., 2011), dissolution and mineral trapping (in basaltic, sandstone and carbonate formations) (Agartan et al., 2015; Al-Khdheeawi et al., 2020; Al-Khdheeawi et al., 2017b; Iglauer, 2011), diffusion and adsorption trapping (in coal bed and organic shale formations) (Arif, Lebedev, et al., 2017b; Busch et al., 2008; Golding et al., 2011; Kaveh et al., 2012).

In this context, wetting characteristics (wettability) of CO_2 geo-storage formation govern the storage trapping capacities, containment security, production enhancement, and fluid dynamics (W. G. Anderson, 1987a; Broseta et al., 2012; E. Donaldson & Alam, 2008; Naik, You, & Bedrikovetsky, 2015; Naik, You, et al., 2018). It is shown in previous studies that less water-wet conditions have shown the reduced potential for CO_2 storage (Al-Khdheeawi et al., 2017a; Arif, Lebedev, et al., 2017a; Chaudhary et al., 2013; Iglauer, Al-Yaseri, et al., 2015; Rahman et al., 2016). However, there is a serious lack of data that can comprehend complex wettability phenomena at realistic storage cap-rock environments. It is proven in the literature that subsurface realistic storage environments are reductive or anoxic, which contains highly diluted amounts of organic molecules (Akob et al., 2015; Lundegard & Kharaka, 1994; Stalker et al., 2013). These minute organic concentrations are sufficient to alter wettability from

water-wet to oil-wet (Ali, 2018; Gomari & Hamouda, 2006; Iglauer et al., 2020), thus, reducing storage capacities and containment security (Ali, Al-Anssari, et al., 2019; Ali, Arif, et al., 2019).

In this perspective, alumina nano-fluid suspensions can be a vital solution to diminish the effect of reductive conditions in subsurface cap-rock storage formations. It is shown in the literature that nano-fluids are positively used for versatile applications of subsurface operations (Gu, Qiu, Liu, You, & Qin, 2020), like chemical flooding (Haghighi et al., 2020), enhanced oil recovery (Al-Anssari et al., 2019; Al-Anssari, Arain, et al., 2018; Al-Anssari, Nwidee, et al., 2017; Y. Yang et al., 2020), drilling (Aftab, Ali, Arif, et al., 2020; Aftab, Ali, Sahito, et al., 2020; Ali & Aftab, 2020; Ali, Jarni, et al., 2020), low salinity water flooding (N. Jha et al., 2018; N. K. Jha, Ali, et al., 2019; N. K. Jha et al., 2020), IFT reduction (Al-Anssari, Arain, et al., 2020), and wettability alteration (Al-Anssari et al., 2016; Ali, Sahito, et al., 2020; Naik, Malgaresi, et al., 2018).

We have thus experimented CO_2/brine/Mica (muscovite, cap-rock proxy) contact angles (advancing and receding) to investigate rock wetting characteristics (in the presence of organic acids and alumina nano-fluids) for determining CO_2 structural trapping capacities in cap-rock formations. Shale cap-rock formations contains an abundant mineral called illite that has a similar mineralogical structure like to mica (muscovite), which can be represented as a good cap-rock proxy (Arif, Al-Yaseri, et al., 2016; Arif, Barifcani, Lebedev, et al., 2016; Chiquet et al., 2007). It is already proven in many previous studies that shale samples already contain existing organics in them which has a profound impact on wettability studies (Arif, Lebedev, et al., 2017b; Yu et al., 2017). Therefore, we have used clean mica muscovite samples (as a proxy of cap-rock) to obtain the correct thresholds for organic acids. It is also depicted in various previous wettability studies, where mica has been used as a proxy of cap-rock formation (Ali, Aftab, et al., 2020; Arif, Al-Yaseri, et al., 2016; Arif, Barifcani, Lebedev, et al., 2016). Muscovite chemically represented as $KAl_2(AlSi_3O_{10})(OH)_2$ (Arif, Al-Yaseri, et al., 2016; Arif, Barifcani, Lebedev, et al., 2016), and it is commonly present in the mica family with other members like phlogopite, illite, and biotite, (Bailey, 1984). Further, the existence of muscovite is well proven in various sedimentary, metamorphic, and sedimentary formations (Guidotti, 1984). Previous

studies have proven that these minerals wetting state is closely related to structural trapping capacities (Iglauer, Pentland, et al., 2015; Iglauer, Wülling, et al., 2011).

This information will shed light that how mica substrates aged in organic acids alter the wettability to oil-wet, hence reduced CO_2 structural trapping capacity (Ali, Aftab, et al., 2020) and how these effects can be reversed by ageing organic-aged mica substrates in alumina nano-fluids, hence increased CO_2 structural trapping capacity (similar trends were found in sandstone and carbonate formations by using silica nano-fluids) (Al-Anssari et al., 2016; Ali, Sahito, et al., 2020). It is vital for CGS projects to account for these organic and alumina nano-fluid thresholds for determining project feasibility and reduced uncertainty.

4.2.2 Experimental

4.2.2.1 Materials

Hydrophilic alumina nanoparticles (Al_2O_3) were acquired from Sigma Aldrich (details are given in Table 4-2-1) for formulating different nano-fluid suspensions (0.05 wt%, 0.1 wt%, 0.25 wt%, and 0.75 wt%) in de-ionized (DI) water (Ultrapure of electrical conductivity = 0.02 mS/cm from David Gray). Pure mica crystals (dimensions = 15 mm x 20 mm x 3 mm, from Ward's natural science) were used as the proxy of cap-rocks. Ten wt% brine solution was prepared by mixing NaCl (purity ≥ 99.9 mol%, from Rowe Scientific) and deionized water as a proxy of formation water for contact angle measurements.

It is proven in the literature that petroleum and gas reservoirs were the by-product of fossils, which comprise organic acids (from C_4 to C_{26}) (Caballero et al., 2003). These organic acids are in abundant quantity in depleted oil reservoirs and also occurs in deep saline aquifers due to organic substance diagenesis and biodegradation of fossil mixtures where anaerobic situations flourish (Akob et al., 2015; Lundegard & Kharaka, 1994; Stalker et al., 2013). To mimic the real reservoir situation for depicting the presence of organic acids in storage formations, we have used four different organic acids (hexanoic acid, lauric acid, stearic acid, and lignoceric acid) ranging from C_6 to C_{24} (purity ≥ 98 mol%, from Sigma Aldrich) for ageing mica substrates, details are explained in Table 4-2-1. The reason for choosing an equal amount of

difference in alkyl chain length of organic acids was to see the effect of alkyl chain length on wettability (explained in detail in section 4.2.3.1).

Drops of hydrochloric acid (HCl, the concentration of 37 vol%, from Sigma Aldrich) was introduced in 2 wt% NaCl solution for controlling its pH to 4 pKa and to ionize the mica substrates for speeding the ageing process of organic acids (details are given in section 4.2.2.2.2). For removal of contaminants from mica substrates before and after the ageing process, Ultra-pure nitrogen (purity = 99.999 wt%, from BOC, gas code-234) was utilized. Contact angle (advancing and receding) measurements were conducted in CO_2 (purity = 99.999 wt%, from BOC, gas code-082) atmosphere at high pressure and high-temperature environments for simulating CO_2 geo-storage conditions. Methanol, toluene, acetone (purity ≥ 99.9 mol%, from Chemlab), and DI water were used to clean away pre-existing contaminations on mica substrates. n-Decane solution (purity ≥ 99.9 mol%, from Sigma Aldrich) was used to formulate various organic acid concentrations as the base liquid.

Table 4-2-1 Aluminum Oxide (Al_2O_3) nanoparticles and organic acids details.

Solubility in water				Insoluble		
Molar weight (gm/mol)				101.96		
Surface area (m^2/gm)				85-115		
Particle Size				13 nm		
Density (g/cm^3]				3.987		
Purity (wt%)				≥ 99.8		
Name of Organic Acid	pH (pKa)	Physical state	Formula	Molar mass (g/mol)	Number of C atoms	Chemical Structure
Hexanoic acid	4	Liquid	$C_6H_{12}O_2$	116.158	6	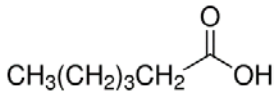
Lauric acid	5.3	solid	$C_{12}H_{24}O_2$	200.318	12	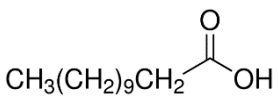
Stearic acid	6	solid	$C_{18}H_{36}O_2$	284.477	18	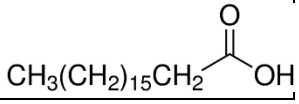

Lignoceric acid	7.4	solid	$C_{24}H_{48}O_2$	368.63	24	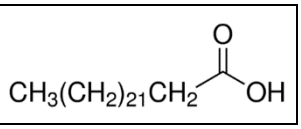

4.2.2.2 The procedure of Mimicking Geo-Storage Environments for Mica Surfaces

4.2.2.2.1 Initial Cleaning Procedure of Pristine Mica

Pristine mica substrates contain impurities that may affect the experimental results. To avoid this, it is pertinent to clean pure mica substrates as they are received. We thus cleaned pure mica samples with deionized water and acetone to eliminate any in-organic or organic surface impurities. This procedure was followed by a blow of ultra-pure nitrogen on the substrate's surfaces; as well as a vacuum oven was used for the drying process (80 °C, time = 120 minutes) for removal of any remaining fluid after preliminary cleaning. Afterwards, air plasma (Diemer Yocto instrument) was used to treat the mica substrates for 20 minutes to eliminate any residual fragments after the drying procedure (Iglauer et al., 2014).

4.2.2.2.2 Simulating Mica Substrates as Geo-Storage Formation

CO_2 storage formations are anoxic which contains organic impurities that lie in the exposure of formation waters (note this exposure can be for millions of years). Therefore, it is pertinent to simulate a similar mineralogical situation in-order to fully comprehend the underground physiognomies for the contact angle experiments (J. A. Davis, 1982; Kleber et al., 2015). There is a serious lack of data in the literature for comprehending the effects of organics on various types of storage formations at various geophysical conditions. However, to do this, silanes were utilized earlier for modifying the hydrophilic surfaces (Grate et al., 2012), but real reductive conditions for storage formations do not contain silanes (note silanes are highly reactive in reductive conditions). It is previously proven that deep saline aquifers contain enough volume of organics to alter their wettability from water-wet to oil-wet (Akob et al., 2015; Ali, Aftab, et al., 2020; Lundegard & Kharaka, 1994; Stalker et al., 2013), and their presence is possible due to organic substance diagenesis and biodegradation of fossil mixtures where anaerobic situations flourish (Bennett et al., 1993; Jones et al.,

2008). Therefore, it is more realistic to use organic acids for modifying the wettability of the rock matrix, instead of using silanes at laboratory scale (Al-Anssari et al., 2016; Gomari & Hamouda, 2006). This modification of mineral hydrophobicity happens due to chemical bonding between hydroxyl groups of mineralogical surfaces and organic esterification (Al-Anssari et al., 2016; Ali, Aftab, et al., 2020; Ali, Al-Anssari, et al., 2019; Ali, Arif, et al., 2019). Thus we followed the subsequent approach (J. A. Davis, 1982; Kleber et al., 2015; Madsen & Ida, 1998; Zullig & Morse, 1988).

Initially, NaCl brine (2 wt%) was formulated with deionized water, and drops of aqueous HCl were added for maintaining the pH at four pKa. Afterwards, pristine mica substrates were aged with a solid/liquid ratio of 1:5 in pH-controlled two wt% NaCl brine. This process ionizes the pristine mica substrates to increase the adsorption rate of organic acids for mimicking the millions of year's formation water exposure (Al-Anssari et al., 2016; Ali, 2018; Ali, Aftab, et al., 2020; Ali, Al-Anssari, et al., 2019; Ali, Arif, et al., 2019; Jardine et al., 1989). Thereafter, a blow of ultra-pure nitrogen was used to remove the brine solution from sample surfaces to elude impurities. Consequently, ionized mica substrates were aged in different organic acid/n-decane solutions of prescribed concentration of 10^{-2} mol/L (note four mica substrates were aged in each organic acid for each nano-fluid suspension). Our mica substrates remained in organic acid/n-decane solutions for seven days (initial contact angle measurement as a function of ageing) and one year (subsequent contact angle measurement as a function of ageing). This variation in ageing is due to provide enough interval for mimicking formation performance to accurately comprehend wettability characteristics (Adamson & Gast, 1967; Ali, Sahito, et al., 2020; J. A. Davis, 1982; Kleber et al., 2015). However, ageing with 7 days and one year does not show a significant difference in contact angle measurements (explained in section 4.2.3.1), this is due to the optimum ageing effect was already achieved in 7 days and longer interval ageing of one year has only caused an insignificant forced ageing resulting in less contact angle differences between 7 days aged samples and one-year aged samples.

In-order to contain exact organic acid concentration (10^{-2} mol/L in our case), acrylic containers with tightly sealed caps were used for the ageing process (especially useful in 1-year ageing) to elude n-decane evaporation. This evaporation can cause a change

in organic concentration and subsequent error in comprehending the exact wettability threshold. Afterwards, acrylic containers were stored in a closed environment (fume hood) to elude impurities for a year.

4.2.2.3 Ageing of Organic Aged Mica Substrates in Alumina Nano-fluids

4.2.2.3.1 Formulation of Alumina Nano-Fluid

Various concentrations (0.05 wt%, 0.1 wt%, 0.25 wt%, and 0.75 wt%) of alumina nano-formulations were formulated (nano-fluid formulation was done by sonication method) to comprehend their competence for wettability reversal of CO_2/brine/mica systems. The prescribed weight of Al_2O_3 nanoparticles (for various concentrations) was added to deionized water and sonicated (Ultrasonic homogenizer, Frequency 20 kHz, Sonics and Materials Incorporation, USA) for 15 minutes (note that homogeneous stirring is not possible with a magnetic stirrer) (Mahdi Jafari et al., 2006). This process is conducted with a microtip (titanium material) of 9.5 mm diameter with a sonication amplitude of (40 %) and energy of (9500 Joules).

4.2.2.3.2 Alumina Nano-Fluid's Stability

It is crucial to determine the stability of nano-formulations, which is a pertinent aspect to comprehend its competence for the reversal of wettability (Ali, Sahito, et al., 2020). To do this, nano-fluid electrical stability phase behaviour, i.e., Zeta-potential (mV) and average particle size (nm) results for alumina nanoparticles were measured from pH level of 6 to 12 (note same range has been noted in deep saline aquifers (Dupraz, Parmentier, Ménez, & Guyot, 2009). Zeta-sizer Nano (Malvern, ZS ZEN 3600, Malvern Instruments, UK) was employed for each nano-fluid concentration (0.05 to 0.75 wt%), while pH was measured using a pH meter (resolution 0.01 pH, Ohaus, Australia).

Lower Zeta-potential values (+ 10 to -10 mV) of the nano-formulation are incipiently electrically stable and are prone to aggregate quicker than as compared to higher values (i.e., Absolute zeta potential > 35 mV) (Awan, Keshavarz, Akhondzadeh, Al-Anssari, & Iglauer, 2020; El-sayed et al., 2012). Furthermore, the repulsive forces

(positive or negative charged) are significantly decreased, resulting in acceleration of the nanoparticle coagulation process that yields sedimentation in the presence of the electrolyte. Cationic and anionic surfactants can alter the electrical stability (i.e., zeta potential) of the particles (in the present case, alumina nanoparticles) by coating particle's surface with their counter-ion head group, hence resulting in supercharged particles (Ahualli et al., 2011; Awan, Keshavarz, Akhondzadeh, Al-Anssari, Al-Yaseri, et al., 2020).

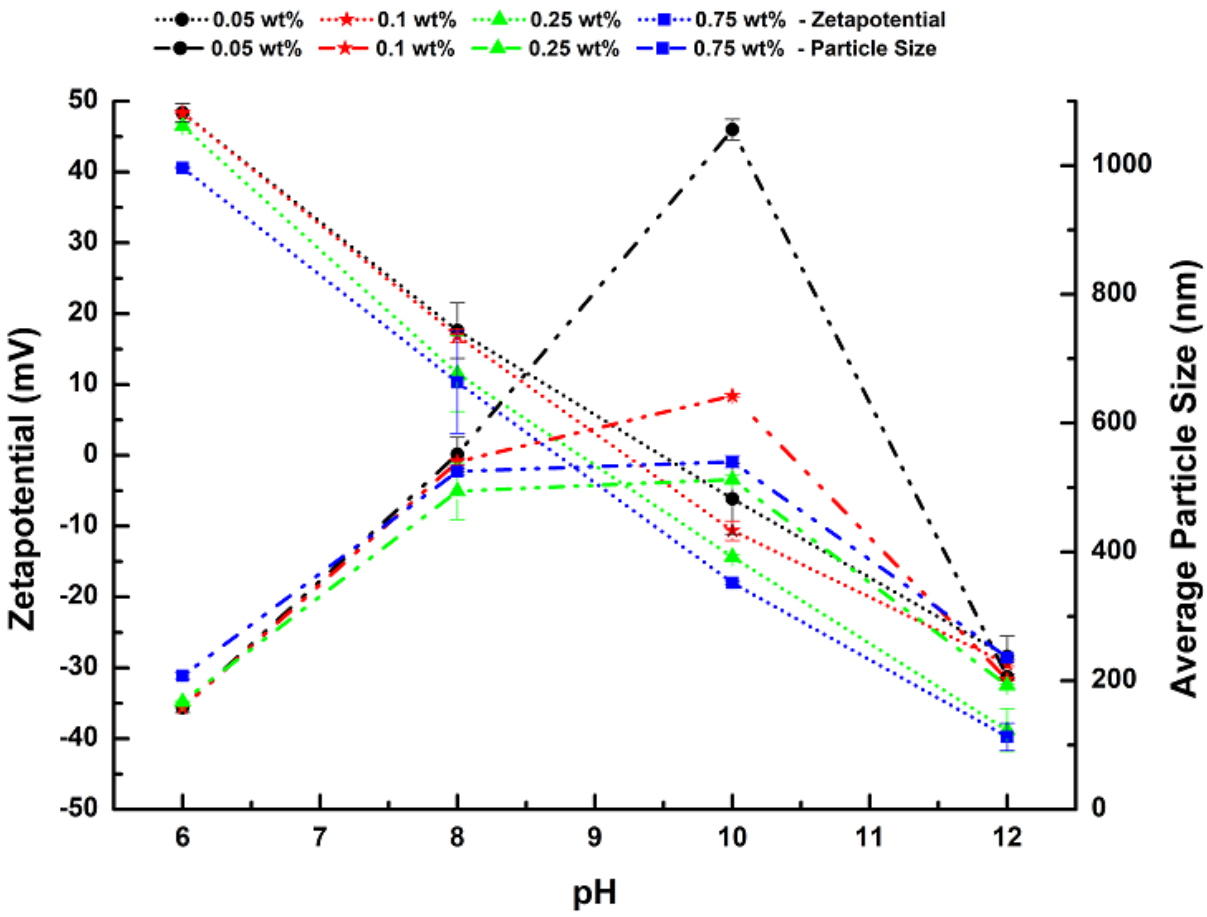

Figure 4-2-1 Zeta-potential and average particle size measurements of various alumina nanoparticles concentration (0.05, 0.1, 0.25 and 0.75 wt%) as a function of pH.

The zeta-potential measurement depicts that the alumina nanoparticles have an isoelectric point (IEP, i.e., $\zeta=0$) at a pH level of 8 to 10 in DI water, as shown in Figure 4-2-1. It is noteworthy to mention here that, as the weight percentage is increased from 0.05 to 0.75, a decline in zeta-potential on the positive side is observed (e.g., at pH =

6), however when we observe on the highly alkaline side (i.e., pH = 12) an inverse phenomenon is observed. This change of behaviour is due to OH^- ions added to the nano-formulation. As more alumina nanoparticle adsorptive sites at more significant loading (i.e., 0.75 wt%), the more OH^- gets attached to the nanoparticle surface, hence resulting in higher dispersion stability (Awan, Keshavarz, Akhondzadeh, Al-Anssari, & Iglauer, 2020). Generally, the data shows that with increasing concentration of nano-fluids, the average particle size (d_{av}) has increased (up to 10 pH). However, upon a further increase in pH, the d_{av} has decreased owing to the enhancement of electrostatic repulsion due to the absorption of OH^- ions, also resulting in a higher zeta-potential value (on the positive side).

Alumina nano-fluid is an excellent candidate for muscovite owing to its broad spectrum of zeta-potential (i.e., from 48 to -40 mV) and its associated stability across a wide pH range (i.e., from 6 to 12 pH), as can be seen in Figure 4-2-1. The absolute difference in surface roughness owing to the presence of nanoparticles can be examined quantitatively, as can be seen in Table 4-2-2. It is hypothesized that alumina nanoparticles are chemisorbed onto the muscovite surface due to their surface activity, as can be seen in Figure 4-2-1, for which the presence of OH^- charges plays a vital role in interacting with positively charge mica surface.

4.2.2.3.3 Ageing Procedure of Organic Aged Mica Substrate's in Alumina Nano-Fluids

It is proven in the literature that nano-fluids have considerable competence in comprehending wettability reversal (Al-Anssari et al., 2019; Al-Anssari, Arain, et al., 2018; Al-Anssari, Nwidee, et al., 2017; Ali, Sahito, et al., 2020). To do this, organic/n-decane aged mica substrates were vertically submerged (note vertical submerging of mica samples reduces gravitational deposition of nanoparticles) for 5 hours in various alumina nano-formulations (0.05 wt%, 0.1 wt%, 0.25 wt%, and 0.75 wt%) at elevated temperature 323 K and atmospheric pressure to form nano-modified mica surfaces. This ageing is obtained with a solid/nano-fluid ratio of 1:5 (1 gram of mica substrate for 5 grams of nano-formulation) for delivering the same coverage for each mica surface (Al-Anssari et al., 2016; Ali, Sahito, et al., 2020).

Mechanistically, the nano-fluid ageing process provides a very strong chemical reaction by the ageing of the hydroxyl group of nano-formulation with a hydroxyl group of mica substrate (note this chemical reaction is the reason for irreversible adsorption of nanoparticles on mica substrates). This irreversible adsorption of nanoparticles on organic/n-decane aged mica substrates is responsible for shifting the hydrophobicity into hydrophilicity. Previously, quartz substrates aged in organic acids were placed in negatively charges SiO_2 nanoparticle solutions, which has shown similar significant wettability reversal to water-wet (Al-Anssari et al., 2016; Ali, Sahito, et al., 2020).

Overall, the hydroxyl group of mica substrates is esterified with organic acids in a condensation reaction (shifting the wettability to CO_2-wet), and nanoparticles cause irreversible adsorption on organic/n-decane aged mica substrates in a chemical reaction (reversing the wettability to weakly water-wet).

4.2.2.4 Characterization of Nano-aged, Organic-aged, and Pristine Mica substrates

4.2.2.4.1 Surface Chemistry

Surface elemental analysis (in wt%) of each mica sample was carried out using a Field Emission Scanning Electron Microscope (FESEM) from Oxford Instruments via energy dispersive spectroscopy (EDS) technique. These measurements were done on all pure, organic/n-decane aged and nano-aged mica substrates. It is clear from our results that the ageing of organic acids and nano-formulations have a significant effect on the surface elemental analysis (average elemental values of pure, organic-aged, and nano-aged mica substrates are depicted in Table 4-2-2). A significant average increase in surface alumina concentration (+19.1 wt% Al, for Hexanoic-aged surface, +17.4 wt% Al, for Lauric-aged surface, +21.4 wt% Al, for Stearic-aged surface, and +18.5 wt% Al, for Lignoceric-aged surface) due to adsorption of nanoparticles (Ali, Sahito, et al., 2020) and in surface carbon concentration (+6.1 wt% C, for Lignoceric Acid, +4.5 wt% C, for Stearic Acid, +3.8 wt% C, for Lauric Acid and +2.6 wt% C, for Hexanoic Acid) due to chemisorption of carboxylic acids was noted on mica substrates (Ali, Aftab, et al., 2020; Zullig & Morse, 1988). These values are the average of 5 data points for each, pure, organic-aged, and nano-aged mica substrates (A detailed surface

elemental analysis is given in Table S4-2-1). Further, high magnification scanning electron micrographs (SEM) were acquired on pure and nano-aged mica substrates for depicting the irreversible adsorption of nano-formulations (Figure 4-2-2, it is clearly shown that 0.25 wt% Alumina nano-formulation have uniformly adsorbed on mica substrate). Such uniform adsorption of nano-formulation is responsible for wettability reversal from a strongly hydrophobic surface to a weakly hydrophilic surface. "±" shows standard deviation in all mica substrates tested in that particular range (Table 4-2-2).

Table 4-2-2 Average surface elemental analysis of pristine, organic-aged, and nano-aged mica substrates*.

Organic Acids	Average elemental values of pristine mica					Average elemental values after organic-aged mica (10^{-2} mol/L)					Average elemental values after nano-aged mica (0.05 wt%, 0.1 wt%, 0.25 wt% and 0.75 wt%)				
	wt% Al	wt% Si	wt% C	wt% O	wt% K	wt% Al	wt% Si	wt% C	wt% O	wt% K	wt% Al	wt% Si	wt% C	wt% O	wt% K
Hexanoic acid	19.4 ± 0.8	21.9 ± 1.0	3.2 ± 0.4	46.9 ± 0.5	8.7 ± 0.6	18.7 ± 1.1	20.5 ± 1.7	5.7 ± 0.4	47.8 ± 3.0	7.4 ± 0.7	37.8 ± 7.4	13.2 ± 3.8	4.8 ± 0.5	38.4 ± 3.0	5.8 ± 0.5
Lauric acid	19.3 ± 0.9	22.3 ± 0.7	2.8 ± 0.3	47.1 ± 1.3	8.5 ± 0.6	18.6 ± 0.6	19.9 ± 1.4	6.6 ± 0.3	47.6 ± 1.0	7.4 ± 1.0	35.9 ± 8.9	13.3 ± 3.3	5.3 ± 0.4	39.9 ± 5.5	5.6 ± 0.6
Stearic acid	19.5 ± 0.8	22.2 ± 1.5	3.2 ± 0.7	46.6 ± 0.8	8.6 ± 0.8	18.5 ± 0.9	20.5 ± 1.5	7.7 ± 0.3	45.8 ± 1.5	7.5 ± 0.7	40.0 ± 8.6	11.7 ± 3.2	5.9 ± 0.2	36.5 ± 5.2	6.0 ± 0.5
Lignoceric acid	19.4 ± 0.7	22.4 ± 1.2	3.1 ± 0.6	46.4 ± 1.2	8.8 ± 0.5	18.8 ± 1.1	20.3 ± 0.5	9.1 ± 0.2	44.6 ± 1.8	7.2 ± 0.7	37.3 ± 8.9	13.2 ± 2.6	6.8 ± 0.4	37.1 ± 5.4	5.7 ± 0.6

* An average of 5 data points of each, pure, organic-aged, and nano-aged mica substrates of four different organic acids (hexanoic, lauric, stearic, and lignoceric acid) and four different nano-formulations (0.05 wt%, 0.1 wt%, 0.25 wt%, and 0.75 wt%).

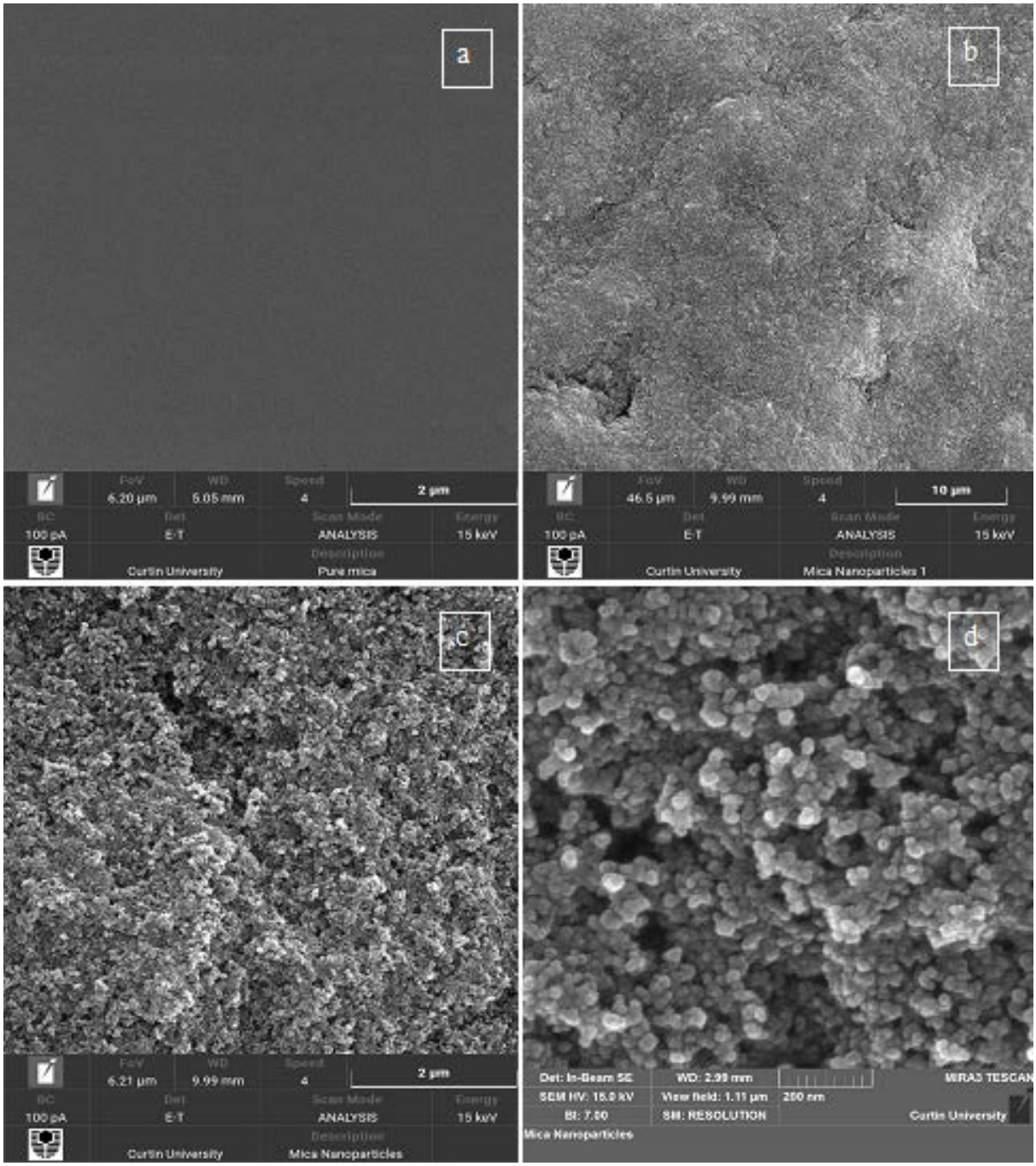

Figure 4-2-2 Different magnifications of SEM Micrographs (a) Pristine mica at a magnification of 2 µm (b) 0.25 wt% Alumina nano-aged mica surface at a magnification of 10 µm (c) 0.25 wt% Alumina nano-aged mica surface at a magnification of 2 µm (d) 0.25 wt% Alumina nano-aged mica surface at a magnification of 200 nm.

4.2.2.4.2 Surface Roughness

Surface roughness has a substantial impact on contact angle measurements, hence wettability (Wenzel, 1936). Therefore, all substrates (pristine mica, organic-aged mica, and nano-aged mica) were characterized by conducting surface topography (Atomic force microscopy by Flex-Axiom, Controller C3000 AFM instrument from Nano-surf) measurements. Topographic experiments have revealed that pristine mica substrates have a very smooth surface (route mean square, RM), ranging from 1 to 2 nm (Ali, Aftab, et al., 2020). Further, the topography of organic-aged and nano-aged mica substrates have also depicted homogenous and smooth surfaces with an average root mean square ranging from 200 to 460 nm (for organic-aged mica) (Ali, Aftab, et al., 2020) and 340 to 620 nm (for nano-aged mica). It is proven in the literature that surfaces with average route mean square roughness for more than 1 µm has a considerable effect on wettability measurements (A. Z. Al-Yaseri et al., 2016). Hence, all mica substrate's surface roughness resulted in less than 1 µm value; therefore, roughness has no impact on contact angle experiments (Marmur, 2006).

4.2.2.5 Contact Angle Experiments

There are several methods to quantify wettability behaviour, like, capillary pressure and relative permeability curve, nuclear magnetic resonance (NMR) technique, spinning drop technique, Wilhelmy balance, and capillary rise method, Amott-Harvey index, and US Bureau of Mines (USBM) core flood method. All these methods can give indirect wettability calculation, whereas, contact angle method is the only method that gives direct quantitative wettability calculation in a given rock fluid system (Al-Anssari et al., 2016; Ali, Sahito, et al., 2020; Arif, Barifcani, Lebedev, et al., 2016; Iglauer, Al-Yaseri, et al., 2015; Iglauer, Pentland, et al., 2015). This method contains a tilted surface technique for the calculation of advancing (θ_a) and receding (θ_r) contact angles (Lander et al., 1993).

In this technique (Figure 4-2-3), a flat mineral sample surface (mica in our case) is placed inside the high pressure and high-temperature cell (HPHT, Hastelloy material made) on a tilted plate. For a relative rock fluid system, it is pertinent to obtain a thermodynamically equilibrated brine solution with CO_2 and mica substrates. Mica is

a reactive surface that can react in acidic environments due to the presence of CO_2 (Gaus et al., 2005; Hu & Jun, 2012), causing errors in wettability experiments. Therefore, brine solution is introduced in Parr reactor mixed with CO_2 and mica substrates at desired experimental (high pressure and high temperature) conditions to obtain thermodynamic equilibration before the contact angle measurements (El-Maghraby et al., 2012). Thereafter, gas (CO_2 in our case) is introduced into the HPHT cell at desired reservoir conditions (323 K, 0.1 MPa, 15 MPa, and 25 MPa in our case) controlled by a high precision syringe pump (Teledyne ISCO, Model D-500, pressure accuracy of 0.1%). Afterwards, a drop of thermodynamically equilibrated brine (average drop size was 4.5 µL ± 0.75 µL) is dispensed (controlled by another high precision syringe pump) on the tilted mineral surface. This process is video recorded for determining advancing (θ_a) and receding (θ_r) contact angles at the front and back edges of the brine droplet (Ali, 2018). The schematic of the HPHT contact angle system is depicted in (Figure 4-2-3). A further detailed description of this process is given in our previous articles (Ali, Aftab, et al., 2020; Ali, Al-Anssari, et al., 2019; Ali, Arif, et al., 2019; Ali, Sahito, et al., 2020).

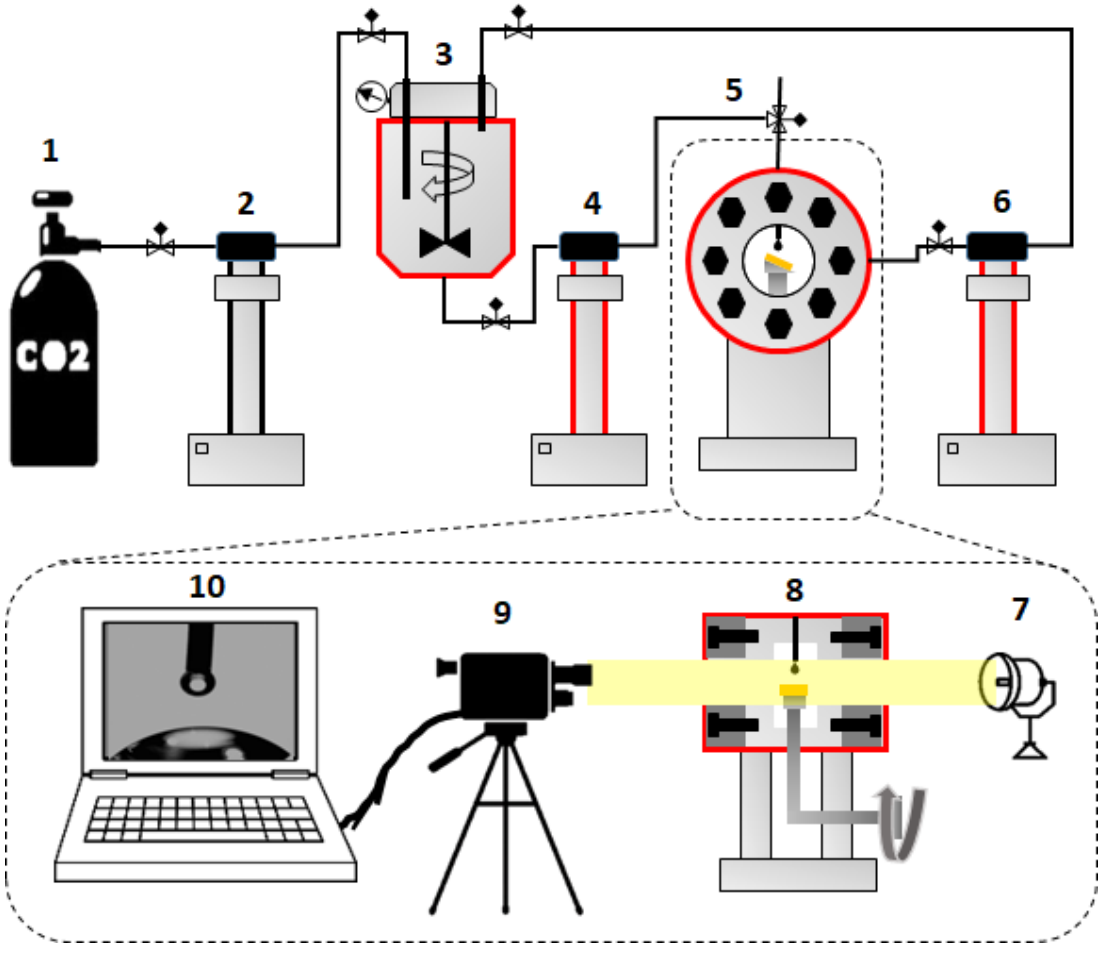

Figure 4-2-3 Schematic of HPHT contact angle system (1) CO_2 bottle (2) ISCO syringe pump for CO_2 (3) High-pressure Parr reactor for live brine formulation (4) ISCO syringe pump for live brine (5) HPHT Hastelloy cell with tilted plate housing, front view (6) ISCO syringe pump for wet CO_2 (7) Light projection (8) HPHT Hastelloy cell with tilted plate housing, side view (9) High-resolution video camera (10) ImageJ software for interpretation.

4.2.3 Results and Discussion

It is pertinent to comprehend the quantitative assessment of CO_2-wettability for cap-rock formations (mica in our case). This assessment is crucial for determining the CO_2 drive and its distribution across the storage formation (Al-Khdheeawi et al., 2017a, 2017b), storage capacities (Arif, Barifcani, Lebedev, et al., 2016; Iglauer, Al-Yaseri, et al., 2015), flow properties (Iglauer, 2017; Iglauer, Pentland, et al., 2015), and containment security (Arif et al., 2019b). In this regard, capillary outflow can happen when the receding contact angle of brine (10 wt% NaCl in our case) is greater than 90° (this phenomenon represents CO_2 injection into the storage formation while displacing water), thus reduced structural trapping capacity (Broseta et al., 2012). Whereas, wettability have no impact on primary drainage when the advancing contact angle of brine is less than 50° (this phenomenon represents water injection into the storage formation to capillary trap CO_2) (Chiquet et al., 2007; Rahman et al., 2016). It is also proven that dissolution trapping is substantially impacted by CO_2-wettability alteration (Agartan et al., 2015; Iglauer, 2011).

It is clear from our contact angle measurements that hydrophilic mica surfaces were greatly affected by the presence of organic acids and rapidly lost their water-wetness. This wettability alteration can greatly affect the structural trapping capacities of mica cap-rock, whereas this wettability shift can be reversed by alumina nano-fluid treatment. Initially, pristine mica substrates were tested at atmospheric pressure and elevated temperature (323 K), which resulted in a completely hydrophilic state with $\theta = 0°$ (Ali, Aftab, et al., 2020; Arif, Al-Yaseri, et al., 2016; Arif, Barifcani, Lebedev, et al., 2016). Whereas, reservoir conditions (323 K, 15 MPa and 25 MPa) have depicted a weakly water-wet state ($\theta_a = 50.2° \pm 3°$ and $\theta_r = 44.9° \pm 3°$ at 15 MPa; and $\theta_a = 65.1°$

± 5° and θ_r = 60.4° ± 5° at 25 MPa) (Ali, Aftab, et al., 2020; Arif, Al-Yaseri, et al., 2016; Arif, Barifcani, Lebedev, et al., 2016).

4.2.3.1 Effect of Organic Acids as a function of Ageing Time, alkyl chain length and Pressure on CO_2 Geo-Storage Capacities

CO_2-wettability of cap-rock formation is directly or indirectly related to CO_2 structural trapping capacity. In ideal situations, wettability drives the ability of CO_2 to displace the water and induce below the cap-rock formation. This happens when CO_2 move upward (due to buoyancy factor) and apply force on solid cap-rock formation; thus, structurally trapping itself. However, in real situations, organic fatty acids are present in the storage formation, which can significantly affect the wettability, thus, causing capillary leakage (Akob et al., 2015; Ali, Aftab, et al., 2020; Lundegard & Kharaka, 1994).

Our results have shown that at a constant organic acid (hexanoic acid C_6, lauric acid C_{12}, stearic acid $C_{18,}$ and lignoceric acid C_{24}) concentration of 10^{-2} mol/L with different ageing times (7 days and one year), mica has greatly lost its water-wetness. For instance, at a constant pressure of 15 MPa and 323 K for lignoceric acid with one-year ageing time, mica/CO_2/brine contact angles were strongly hydrophobic (θ_a = 131.3° and θ_r = 123.6°) and at similar conditions, with seven days ageing time contact angle values were (θ_a = 115.7° and θ_r = 107.3°) compared to pristine mica (θ_a = 50.2° and θ_r = 44.9°), which may have serious consequences in structural trapping capacities due to prolonged exposure of organic acids (Figure 4-2-4).

However, irrespective of ageing time, longer alkyl chain (higher number of carbon atoms) organic acids have a more negative effect on structural trapping (increased contact angle values) compared to shorter alkyl chains (fewer number of carbon atoms) organic acids. Therefore, mica substrates aged in lignoceric acid (C_{24}) have shown higher contact angle values compared to mica substrates aged in hexanoic acid (C_6). For instance, at 25 MPa and 323 K, with an ageing time of one year, of all organic acids (hexanoic acid C_6, lauric acid C_{12}, stearic acid $C_{18,}$ and lignoceric acid C_{24}), receding contact angle values were, θ_r = 105.7°, 116.2°, 127.6°, and 136.2°, respectively (Figure 4-2-4). Such higher contact angle values can significantly reduce

structural trapping capacities (note structural leakage is possible at $\theta_r > 90°$) (Ali, Aftab, et al., 2020; Arif, Barifcani, Lebedev, et al., 2016; Iglauer, Al-Yaseri, et al., 2015; Iglauer, Pentland, et al., 2015).

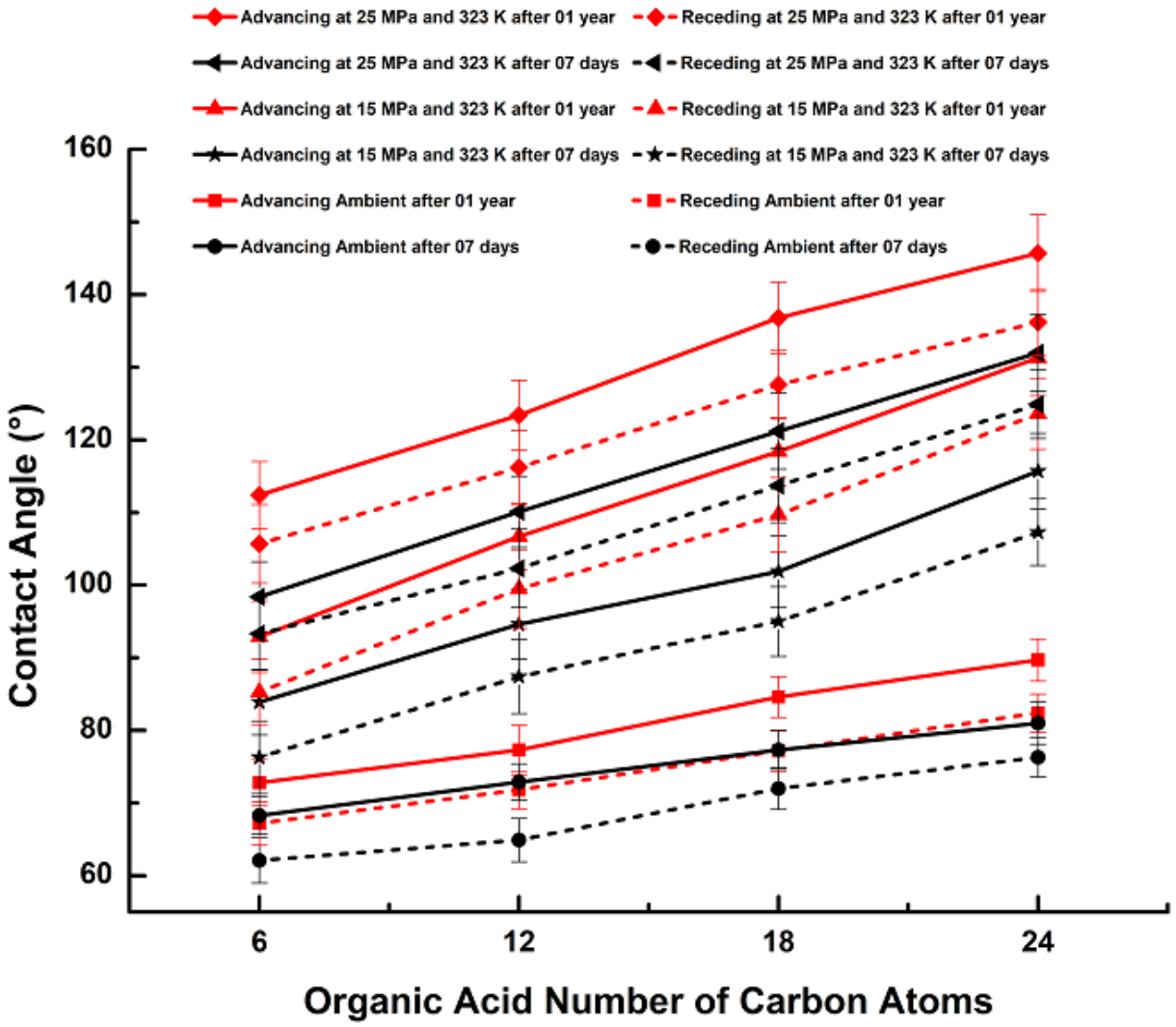

Figure 4-2-4 Mica/CO_2/Brine advancing and receding contact angles as a function of ageing time, different organic acids, and pressure.

Further, irrespective of ageing time and type of organic acid, higher pressure (deep saline aquifers > 15 MPa) may cause a higher threat (increasing contact angle values) for structural trapping capacities due to an increase in intermolecular forces between solid (mica in our case) and gas (CO_2 in our case) with increasing pressure (Abramov et al., 2019). For example, mica substrates aged in stearic acid at atmospheric pressure and elevated temperature (323 K) with seven days ageing time have shown weakly

intermediate-wet state θ_a = 72.9° and θ_r = 64.9°, whereas, at similar conditions with higher pressure of 25 MPa, mica/CO_2/brine contact angle values turned in CO_2-wet θ_a = 110.1° and θ_r = 102.3° (Figure 4-2-4). Hence, such minute concentrations of organic acids and higher pressures are always present in storage formations; lower structural trapping capacities may be encountered than estimated (Ali, Al-Anssari, et al., 2019; Bennett et al., 1993; Jones et al., 2008; Stalker et al., 2013).

4.2.3.2 Effect of Nano-Fluids on CO_2 Geo-Storage Capacities

It is shown in the literature that various parameters like temperature, pressure, brine salinity, and organic acids have a substantial impact on CO_2 geo-storage (Arif, Al-Yaseri, et al., 2016; Arif, Barifcani, Lebedev, et al., 2016; Iglauer, 2017). However, there is a serious lack of data for comprehending the effect of nanoparticles (type and concentration) at HPHT reservoir conditions for CO_2-wettability, hence CO_2-storage capacities. To do that, we have used different concentrations of alumina nanoparticles (0.05 wt%, 0.1 wt%, 0.25 wt%, and 0.75 wt%) in deionized water for the reversal of hydrophobic mica surfaces. Organic-aged mica substrates were aged vertically in these nano-fluid concentrations for 5 hours, followed by contact angle measurements at reservoir conditions (323 K, 0.1 MPa, 15 MPa, and 25 MPa in our case). This nano-treatment of mica substrates is achieved by the adsorption efficiency of alumina nanoparticles and their associated concentrations. It is depicted from our results (figure 4-2-5 and 4-2-6, advancing and receding contact angles with alumina nano-fluid) that the wettability of organic-aged CO_2-wet mica substrates have substantially reduced by alumina nano-fluid ageing (note the degree of wettability reversal was different for different alumina nano-fluid concentrations) (Nowrouzi, Manshad, & Mohammadi, 2020).

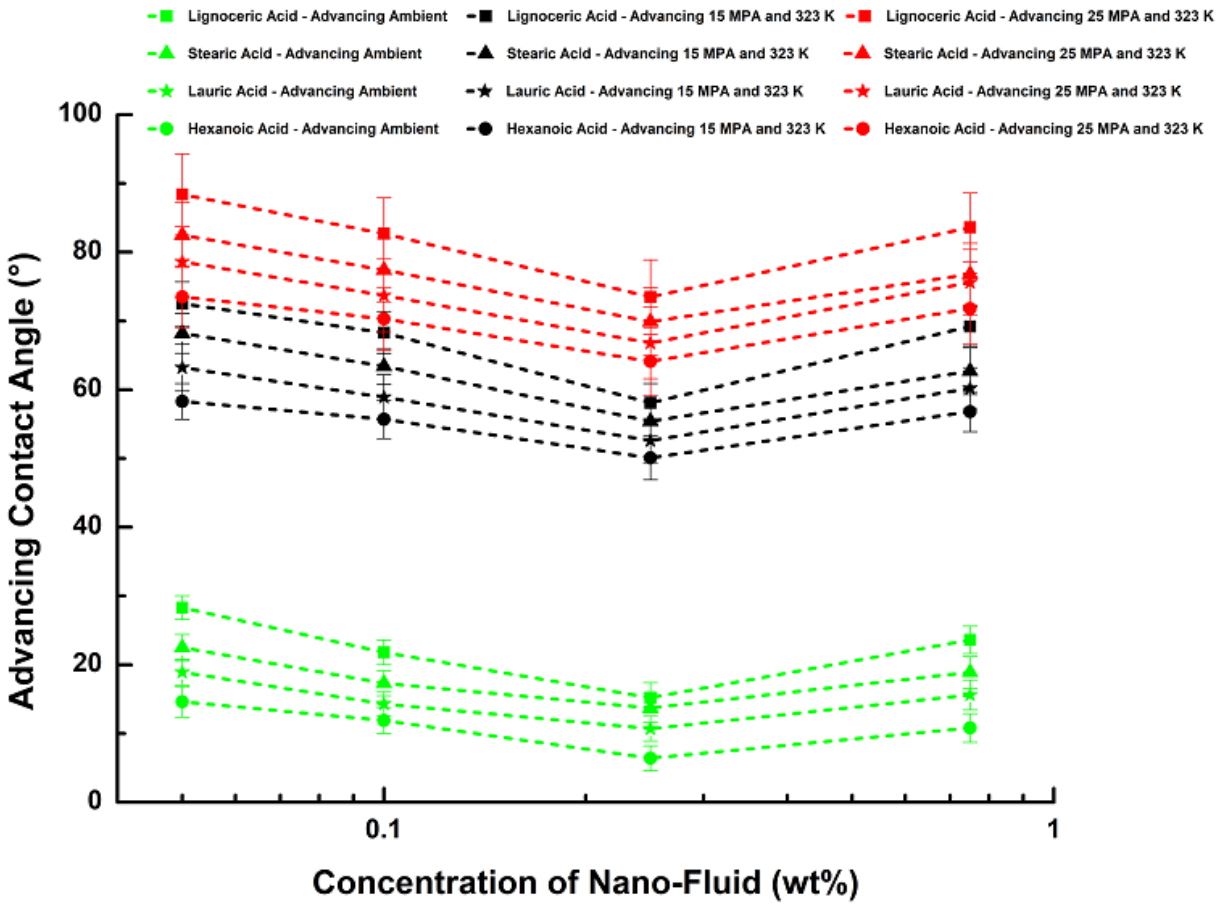

Figure 4-2-5 Mica/CO_2/Brine contact angles (advancing) as a function of pressure and different alumina nano-fluid concentrations.

For instance, with lignoceric-aged mica substrates at 323 K and 25 MPa for 0.05 wt%, 0.1 wt%, 0.25 wt%, and 0.75 wt% nano-fluid alumina concentrations, brine receding contact angles were θ_r = 81.6°, 75.8°, 68.9°, and 76.9°, respectively (note structural trapping limit is ≤ 90°), which has reduced from θ_r = 136.2° for lignoceric-aged mica substrates at 323 K and 25 MPa for one-year ageing. It can be seen from the acquired data that each concertation of alumina nano-fluid is setting the same trend for other organic-aged mica substrates; however, 0.25 wt% alumina nano-fluid concentration has shown the optimum reversal of wettability as compare to other alumina nano-fluid concentrations tested.

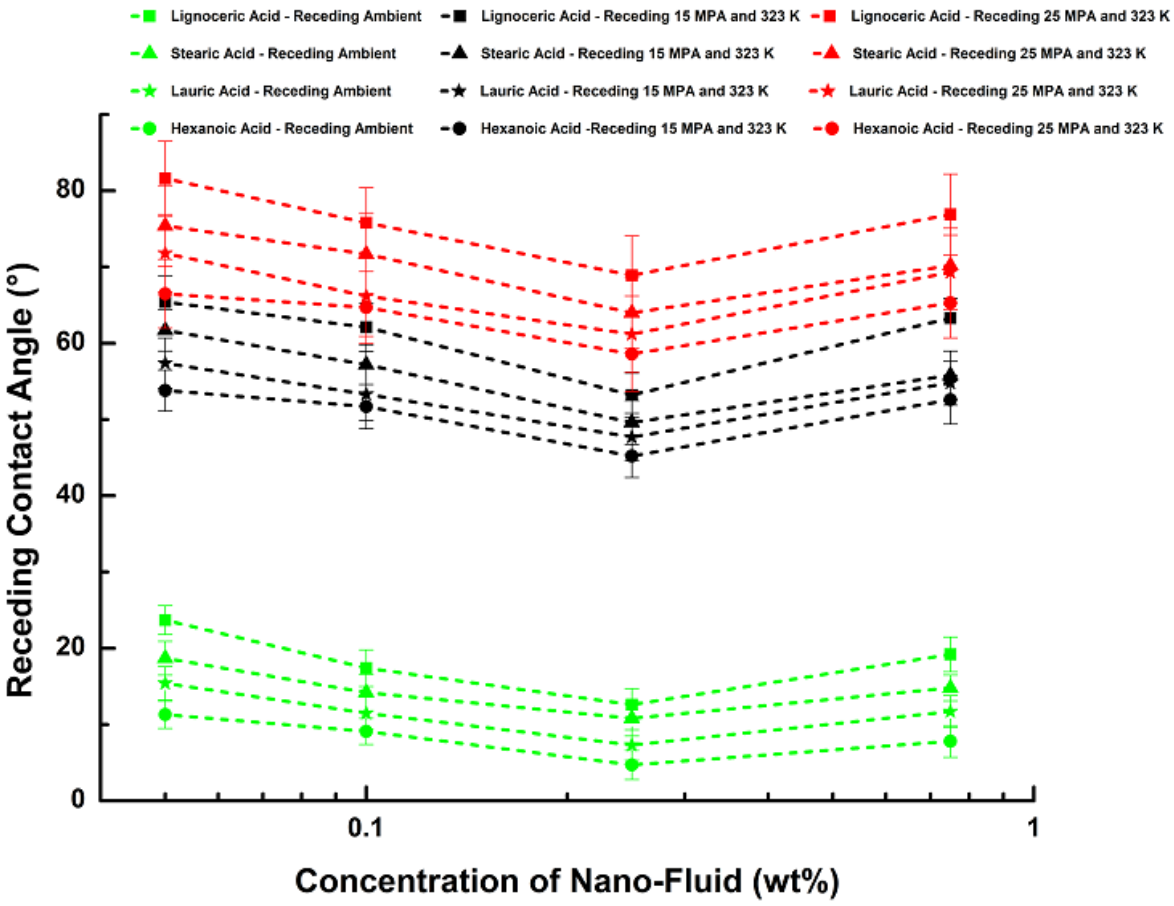

Figure 4-2-6 Mica/CO_2/Brine contact angles (receding) as a function of pressure and different alumina nano-fluid concentrations.

4.2.4 Implications

The conducted contact angle experiments have depicted that the existence of organic acids into CO_2 geo-storage formations (mica in our case) is responsible for shifting the wettability to more CO_2-wet, thus, reduced structural trapping capacities (Ali, Aftab, et al., 2020; Iglauer, Pentland, et al., 2015). Therefore, optimum alumina nano-fluid concentration (0.25 wt% in deionized water) is recommended for the reversal of wettability from hydrophobicity to hydrophilicity, hence, increased structural trapping capacities, as depicted in similar studies for applications of SiO_2 nanoparticles in quartz formation (Ali, Sahito, et al., 2020). This can be achieved by the following two processes.

1. Initially, by injecting optimum nano-fluid suspension (0.25 wt% in deionized water) in CO_2-geo storage formation to alter the wettability, which is CO_2-wet

due to the presence of organic acids (hence less CO_2 structural trapping potential). This will change its wetting characteristics to Intermediate-wet (hence greater CO_2 structural trapping potential).

2. Finally, when wetting characteristics are shifted towards intermediate-wet, CO_2 will be injected at above supercritical pressure, which will exert the pressure on the wetting phase (formation water) and free CO_2 will move upward due to the buoyancy force and will accumulate below the impermeable layer, where it will be structurally trapped below the cap-rock formation.

Consequently, alumina nano-fluid injection may play an integral part as part of CO_2 geo-storage feasibility. Therefore, CO_2 geo-storage projects should account for the strategies where leakage risk can be minimized.

4.2.5 Conclusion

Various factors such as formation heterogeneity, brine salinity, temperature, surface roughness, and pressure are crucial fundamentals that drive CO_2-wettability of storage formations (A. Z. Al-Yaseri et al., 2016; Ali et al., 2017; Ali, Arif, et al., 2019; Ali et al., 2015; Arif, Barifcani, Lebedev, et al., 2016; Iglauer, 2017; N. Jha et al., 2018; N. K. Jha, Ali, et al., 2019; N. K. Jha et al., 2020). Nonetheless, organic acids' existence in storage formation is well-proven, which may significantly reduce structural trapping capacities (Ali, 2018; Ali, Aftab, et al., 2020; Ali, Al-Anssari, et al., 2019; Ali, Arif, et al., 2019), and this may be reduced with different concentrations of nano-fluids in nano-energy applications (Al-Anssari et al., 2019; Al-Anssari, Arain, et al., 2018; Al-Anssari et al., 2016; Al-Anssari, Nwidee, et al., 2017; Ali, Sahito, et al., 2020). There is a serious lack of data in the literature that can account for the CO_2-wettability in the existence of organic acids for mitigating project achievability, technical injection problems, containment security, and structural trapping feasibility in cap-rock formation (Al-Khdheeawi et al., 2017a; Al-Menhali & Krevor, 2016; Ali, 2018; Ali, Al-Anssari, et al., 2019; Ali, Arif, et al., 2019; Iglauer, Al-Yaseri, et al., 2015; Iglauer, Pentland, et al., 2015). In contrast, many studies of storage formations have already shown the presence of organics at a larger scale (Akob et al., 2015; Ali, Al-Anssari, et al., 2019; Gomari & Hamouda, 2006; Jardine et al., 1989; Lundegard & Kharaka, 1994; Madsen & Ida, 1998; Stalker et al., 2013).

To properly address this issue. We have used four organic acids (hexanoic, lauric, stearic, and lignoceric acid) at a fixed organic acid/n-decane concentration of 10^{-2} mol/L with different exposure durations (7 days and one year) for ageing pure mica substrates. Thereafter, different concentrations (0.05 wt%, 0.1 wt%, 0.25 wt%, and 0.75 wt%) of alumina nano-fluids were formulated with deionized water for ageing (5-hour duration) organic-aged mica substrates. Contact angle measurements (advancing and receding) were conducted at various storage conditions (323 K, 0.1 MPa, 15 MPa, and 25 MPa) in-order to fully comprehend the wetting characteristics of organic-aged and nano-aged mica substrates, thus, determining structural trapping limits (leakage can occur at > 90°) in the presence of organic acids and nano-fluids.

Our results depict that pristine mica substrates were weakly water-wet (θ_a = 65.1° and θ_r = 60.4°) at typical storage conditions (323 K, 25 MPa), which turned strongly hydrophobic (θ_a = 145.7° and θ_r = 136.2°) in the presence of 10^{-2} mol/L lignoceric acid concentration (longer alkyl chain) at similar conditions of 1-year ageing duration (such a change is attributed to chemisorption of organic acids, thus reduced structural trapping potential). However, optimum alumina nano-fluid concentration (0.25 wt%) have shown a significant reduction in CO_2-wettability and turned them weakly water-wet (θ_a = 73.5° and θ_r = 68.9°), thus, increased structural trapping potential.

In a nutshell, it is crucial to fully comprehend the CO_2-wettability of cap-rock storage formations in the presence of organic acids and nano-fluids at typical storage conditions, as lower structural trapping potential may be predicted, which can affect the feasibility of long term CO_2 geo-storage projects. We thus recommend that CO_2 geo-schemes and simulation strategies should account for the benefits of nano-energy applications into CO_2 geo-storage formations to further de-risking the project viability of CO_2 geo-sequestration.

4.2.6 Graphical Abstract

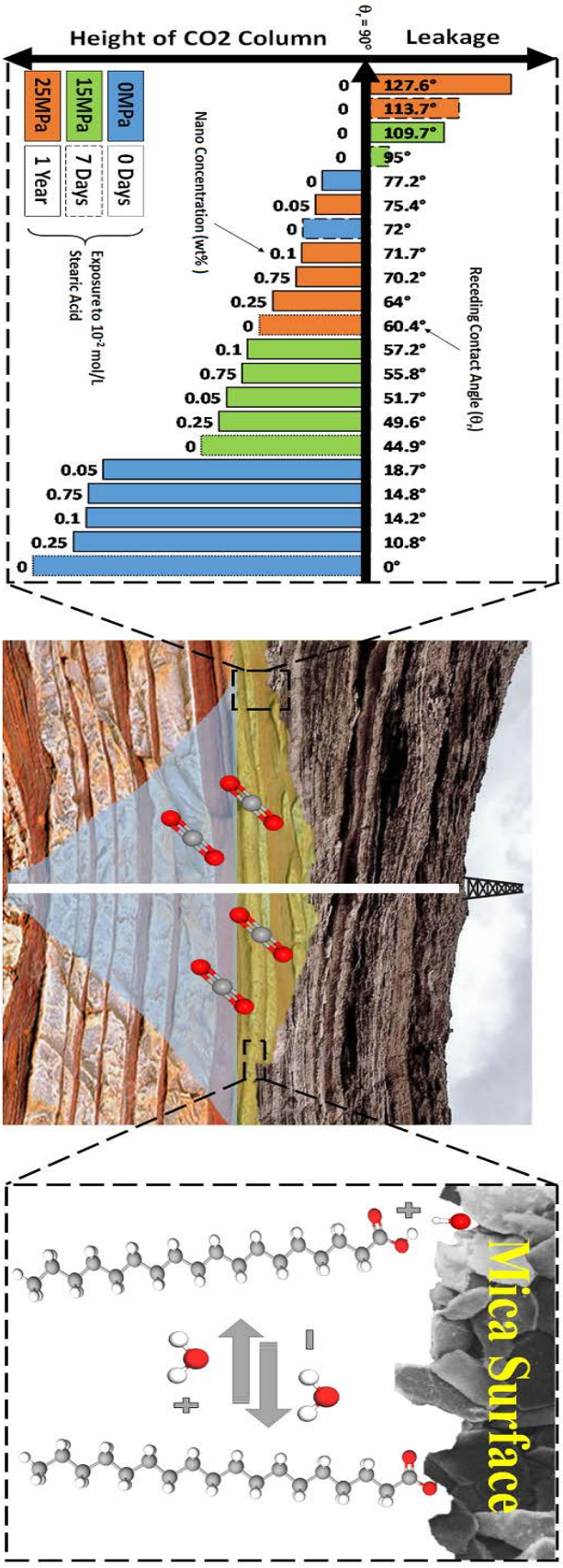

4.2.7 Supporting Information

Table S4-2-1 Surface elemental analysis of pristine, organic-aged and nano-aged mica substrates.

Nano-fluid Concentration (wt%)	Pristine Mica					After ageing with 10^{-2} mol/L (Hexanoic Acid)					After ageing with nano-fluids				
	wt% Al	wt% Si	wt% C	wt% O	wt% K	wt% Al	wt% Si	wt% C	wt% O	wt% K	wt% Al	wt% Si	wt% C	wt% O	wt% K
0.05% Al_2O_3	20.3	20.7	3.6	47.5	7.9	19.7	18.9	5.6	49.0	6.8	30.7	17.2	5.2	41.0	5.9
0.10% Al_2O_3	19.7	21.9	3.2	46.6	8.6	17.6	18.8	5.4	51.3	6.9	35.9	14.3	4.2	39.4	6.2
0.25% Al_2O_3	18.7	22.4	3.1	46.8	9.0	18.6	22.0	5.8	45.4	8.2	39.2	11.7	5.0	38.3	5.8
0.75% Al_2O_3	18.9	22.7	2.8	46.5	9.1	18.9	22.1	6.1	45.4	7.5	45.4	9.6	4.7	35.0	5.3
Nano-fluid Concentration (wt%)	Pristine Mica					After ageing with 10^{-2} mol/L (Lauric Acid)					After ageing with nano-fluids				
	wt% Al	wt% Si	wt% C	wt% O	wt% K	wt% Al	wt% Si	wt% C	wt% O	wt% K	wt% Al	wt% Si	wt% C	wt% O	wt% K
0.05% Al_2O_3	20.1	22.4	2.4	47.3	7.8	19.0	19.6	6.8	47.3	7.3	26.9	16.8	5.4	45.5	5.4
0.10% Al_2O_3	20.0	23.1	2.8	45.6	8.5	19.1	19.4	6.5	48.6	6.4	33.4	13.9	5.7	41.9	5.1
0.25% Al_2O_3	18.3	22.0	2.9	48.2	8.6	18.2	18.9	6.7	47.9	8.3	38.7	12.3	5.3	37.5	6.2
0.75% Al_2O_3	18.9	21.8	3.0	47.4	8.9	17.9	21.7	6.3	46.7	7.4	44.6	10.2	4.9	34.6	5.7
Nano-fluid Concentration (wt%)	Pristine Mica					After ageing with 10^{-2} mol/L (Stearic Acid)					After ageing with nano-fluids				
	wt% Al	wt% Si	wt% C	wt% O	wt% K	wt% Al	wt% Si	wt% C	wt% O	wt% K	wt% Al	wt% Si	wt% C	wt% O	wt% K
0.05% Al_2O_3	19.4	23.7	3.4	45.8	7.7	17.5	21.6	7.4	45.6	7.9	31.4	14.5	6.1	41.6	6.4
0.10% Al_2O_3	19.7	20.8	3.1	47.3	9.1	18.6	21.8	7.9	44.4	7.3	37.6	12.6	6.0	37.7	6.1
0.25% Al_2O_3	18.6	21.5	3.8	46.9	9.2	18.7	19.7	7.6	47.3	6.7	42.3	11.3	5.7	35.3	5.4
0.75% Al_2O_3	20.2	22.6	2.5	46.3	8.4	19.3	18.9	8.0	45.7	8.1	48.5	8.2	5.9	31.2	6.2
Nano-fluid Concentration (wt%)	Pristine Mica					After ageing with 10^{-2} mol/L (Lignoceric Acid)					After ageing with nano-fluids				
	wt% Al	wt% Si	wt% C	wt% O	wt% K	wt% Al	wt% Si	wt% C	wt% O	wt% K	wt% Al	wt% Si	wt% C	wt% O	wt% K
0.05% Al_2O_3	20.0	22.6	2.9	45.9	8.6	19.8	19.8	9.2	43.2	8.0	28.5	15.6	7.1	42.5	6.3
0.10% Al_2O_3	19.4	22.9	2.6	46.8	8.3	19.7	20.6	9.0	43.7	7.0	35.6	13.9	6.7	37.8	6.0
0.25% Al_2O_3	19.6	23.2	3.0	45.3	8.9	18.2	20.8	9.3	44.8	6.9	38.9	12.7	6.9	36.1	5.4
0.75% Al_2O_3	18.7	20.8	3.7	47.6	9.2	17.6	20.0	8.9	46.8	6.7	46.3	10.4	6.4	31.8	5.1

CHAPTER 5 Conclusions and Future Recommendations

5.1 Conclusion

Depleted oil and gas reservoirs and deep saline aquifers are pivotal sinks for underground CO_2 geological storage. In-order to explore their potential, influencing parameters should be investigated for CO_2 geo-storage formations. Wetting and non-wetting properties of geological formations are important factors that are directly related to storage capacity estimations and reduce the uncertainties in the large scale EOR and CO_2 geological storage operations. Previously, many important parameters related to wettability were investigated, like temperature, pressure, salinity, formation type, and surface roughness. However, these investigations were conducted on clean mineral surfaces and CO_2 geological storage formations contain organic fatty acids which have a substantial impact on the wetting characteristics of reservoir rock in a given CO_2/brine and oil/brine systems due to the chemisorption mechanism. Therefore, to gauge this effect we have systematically experimented with various organic acids (hexanoic acid C_6, lauric acid C_{12}, stearic acid C_{18}, and lignoceric acid C_{24}) based on equal difference in their alkyl chain length in various geo-storage formations (sandstone, carbonate and cap-rock) for wettability studies. In addition to this, a novel new procedure were experimented by using various nanomaterials (silica and alumina) in various geo-storage formations (sandstone, and cap-rock) to mitigate the effect caused by organic acids. Significant findings of this work are concluded below:

5.2 Effect of Organic Acids on Carbonate Geo-Storage Formation (Chapter 3, Part 1)

In this research, we have aged calcite substrates as a representative of carbonate formation in minute concentrations (10^{-2} – 10^{-10} mol/L) of stearic acid (C_{18}) at various physio-thermal geo-storage conditions (323 K, 10 MPa, and 25 MPa). In addition to this, acquired data were interpreted for CO_2 column height estimations. Our results show that, at highest physio-thermal conditions and acidic concentration (323 K, 25 MPa, and 10^{-2} mol/L) (note: the highest concentration of organic acid used in our

studies is the possible lowest concentration in geo-storage formations), pure calcite samples, whose advancing contact angle was 68° have shifted to 141°, and receding contact angle, which was 62°, have shifted to 132°. Thus, reduced structural and residual trapping limit beyond 90° and 50°, respectively. Further, CO_2 column height estimations have determined that structural and residual trapping limits are substantially reduced in the presence of organic acids.

5.3 Effect of Organic Acids on Sandstone Geo-Storage Formation (Chapter 3, Part 2)

In this research, we have aged quartz substrates as a representative of sandstone formation in minute concentrations (10^{-2} – 10^{-10} mol/L) of various organic acids (hexanoic acid C_6, lauric acid C_{12}, stearic acid C_{18}, and lignoceric acid C_{24}) at various physio-thermal geo-storage conditions (323 K, 0.1 MPa, and 25 MPa). Our results show that, at highest physio-thermal conditions and longer alkyl chain length (number of carbon atoms) acidic concentration (323 K, 25 MPa, and 10^{-2} mol/L of lignoceric acid C_{24}), pure quartz samples, whose advancing contact angle was 56° have shifted to 110°, and receding contact angle, which was 54°, have shifted to 105°, thus reduced structural and residual trapping limit. All organic acids have shown the wettability effect similarly, however, the degree of change in contact angle was different for each organic acid due to shorter and longer alkyl chain length in a sandstone formation.

5.4 Effect of Organic Acids on Cap-Rock Geo-Storage Formation (Chapter 3, Part 3)

In this research, we have aged mica substrates as a representative of cap-rock formation in minute concentrations (10^{-2} – 10^{-9} mol/L) of various organic acids (hexanoic acid C_6, lauric acid C_{12}, stearic acid C_{18}, and lignoceric acid C_{24}) at various physio-thermal geo-storage conditions (323 K, 0.1 MPa, 15 MPa and 25 MPa). Our results show that, at highest physio-thermal conditions and longer alkyl chain length (number of carbon atoms) acidic concentration (323 K, 25 MPa, and 10^{-2} mol/L of lignoceric acid C_{24}), pure mica samples, whose advancing contact angle was 65° have shifted to 133°, and receding contact angle, which was 60°, have shifted to 125°, thus reduced structural trapping limit. Similarly, as quartz substrates, all organic acids have

shown a negative effect on mica substrates for determining the wetting behaviour. However, the degree of change was solely dependent on alkyl chain length (number of carbon atoms).

5.5 Effect of Silica Nano-Fluid on Organic-Aged Sandstone Geo-Storage Formation (Chapter 4, Part 1)

In this research, we have reversed the wettability of various organic aged (hexanoic acid C_6, lauric acid C_{12}, stearic acid C_{18}, and lignoceric acid C_{24}, at 10^{-2} mol/L) quartz substrates (as representative of sandstone formation) with various silica (SiO_2) nano-suspensions (0.05, 0.1, 0.25, and 0.75 wt%) at various physio-thermal geo-storage conditions (323 K, 0.1 MPa, and 25 MPa). Moreover, the effect of organic acids was also quantified at different ageing times (7 days and 1 year) for mimicking the geo-storage formations for a longer geological era. Our results show that, at highest physio-thermal conditions, longer alkyl chain length (number of carbon atoms) acidic concentration, and longer ageing time (323 K, 25 MPa, and 10^{-2} mol/L of lignoceric acid C_{24}, 1-year ageing time), pure quartz samples, whose advancing contact angle was 56° have shifted to 129°, and receding contact angle, which was 54°, have shifted to 123°. Whereas, at same conditions with optimum silica nano-suspension (0.1 wt%), organic aged CO_2-wet quartz surface, whose advancing contact angle was 129° have shifted to 62°, and receding contact angle, which was 123°, have shifted to 58°, thus, increased structural trapping capacities. All silica nano-suspension have similarly depicted the wettability reversal, however, among all silica nano-concentrations, 0.1 wt% was the optimum concentration which have reversed the CO_2-wettability at maximum.

5.6 Effect of Alumina Nano-Fluid on Organic-Aged Cap-rock Geo-Storage Formation (Chapter 4, Part 2)

In this research, we have reversed the wettability of various organic aged (hexanoic acid C_6, lauric acid C_{12}, stearic acid C_{18}, and lignoceric acid C_{24}, at 10^{-2} mol/L) mica substrates (as representative of cap-rock formation) with various alumina (Al_2O_3) nano-suspensions (0.05, 0.1, 0.25, and 0.75 wt%) at various physio-thermal geo-storage conditions (323 K, 0.1 MPa, 15 MPa, and 25 MPa). In addition to that, mica

substrates were aged in various organic acids at various ageing times (7 days and 1 year) to comprehend the ageing effect in cap-rock geo-storage formations for simulating longer geological times. Our results show that, at highest physio-thermal conditions, longer alkyl chain length (number of carbon atoms) acidic concentration, and longer ageing time (323 K, 25 MPa, and 10^{-2} mol/L of lignoceric acid C_{24}, 1-year ageing time), pure mica samples, whose advancing contact angle was 65° have shifted to 146°, and receding contact angle, which was 60°, have shifted to 136°. Thereafter, at same conditions with optimum alumina nano-suspension (0.25 wt%), organic aged CO_2-wet mica surface, whose advancing contact angle was 146° have shifted to 74°, and receding contact angle, which was 136°, have shifted to 69°, thus, increased structural trapping capacities. Similarly, as silica nano-suspensions in quartz substrates, alumina nano-suspension have depicted the positive effect on mica substrates for determining the wetting characteristics. However, among all alumina nano-concentrations, 0.25 wt% was the optimum concentration which have reversed the CO_2-wettability at maximum.

5.7 Future Recommendations

This research recommends following the future outlook in determining the detailed scenarios for the effects of organics and nanomaterials.

- The current research is conducted on a variety of subjective organic acids and their associated concentrations for benchmarking the development in science, however, the actual composition of organic acids may differ and large scale analysis of real geological formations may determine detailed understandings.
- The current research is conducted on synthetic rock thin sections (calcite, quartz, and mica), however, real geological storage formations are heterogeneous and their composition may differ. Subsequently, the reported investigations and their applications will be restricted. Therefore, it is recommended to conduct wettability studies for determining CO_2 geo-storage potential in realistic geological rock thin sections.
- The experimental part of this research comprises of direct quantitative assessment (contact angle measurements) for determining the wettability

behaviour. However, these measurements are representative of surface chemistry and therefore, other qualitative methods (like capillary pressure curve, relative permeability etc.) should also be used for determining the complex wetting characteristics of pore matrix in the presence of organic acids.

- The two types of nanomaterials (silica and alumina) were used in this research for the reversal of wettability from CO_2-wet conditions. It is recommended to formulate several other nanomaterials (like TiO, ZrO, ZnO, FeO etc.) for quantifying their effects on wetting characteristics of geo-storage formations in the presence of organic acids.
- In several studies, surface-active agents (like surfactants and polymers) have also depicted a great potential in the reversal of wettability. Therefore, it is recommended to use these chemicals comparatively with nanoparticles for quantifying the wetting characteristics of geo-storage formations in the presence of organic acids.
- It is clear from these studies that detailed research is required for determining the effect of organic acids and nanomaterials for safe and long-term CO_2 geo-storage projects. It is also recommended that reservoir models and simulation studies that calculate CO_2 storage capacities should account for the thresholds of organic acids.
- At a field scale, it is recommended to inject optimum nano-suspensions with formation water before supercritical CO_2 injection, which will reverse the wetting characteristics of geo-storage formation towards the intermediate-wet for increased CO_2 storage potential.

References

Abbaszadeh, M., Shariatipour, S., & Ifelebuegu, A. (2020). The influence of temperature on wettability alteration during CO2 storage in saline aquifers. *International Journal of Greenhouse Gas Control, 99*, 103101.

Abdolahi-Mansoorkhani, H., & Seddighi, S. (2020). CO2 capture by modified hollow fiber membrane contactor: Numerical study on membrane structure and membrane wettability. *Fuel Processing Technology, 209*, 106530.

Abdulelah, H., Al-Yaseri, A., Ali, M., Giwelli, A., Negash, B. M., & Sarmadivaleh, M. (2021). CO2/Basalt's Interfacial Tension and Wettability Directly from Gas Density: Implications for Carbon Geo-Sequestration. *Journal of Petroleum Science and Engineering*, 108683. doi:10.1016/j.petrol.2021.108683

Abdulla, A., Alessio, S., Lin, Q., Raeini, A. Q., Branko, B., & Blunt, M. J. (2020). Pore-scale mechanisms of CO 2 storage in oilfields. *Scientific Reports (Nature Publisher Group), 10*(1).

Abramov, A., Keshavarz, A., & Iglauer, S. (2019). Wettability of Fully Hydroxylated and Alkylated (001) α-Quartz Surface in Carbon Dioxide Atmosphere. *The Journal of Physical Chemistry C, 123*(14), 9027-9040.

Adamson, A. W., & Gast, A. P. (1967). *Physical chemistry of surfaces* (Vol. 150): Interscience publishers New York.

Administration, U. E. I. (2011). *Annual Energy Outlook 2011: With Projections to 2035*: Government Printing Office.

Aftab, A., Ali, M., Arif, M., Panhwar, S., Saady, N. M. C., Al-Khdheeawi, E. A., . . . Iglauer, S. (2020). Influence of tailor-made TiO2/API bentonite nanocomposite on drilling mud performance: Towards enhanced drilling operations. *Applied Clay Science, 199*, 105862.

Aftab, A., Ali, M., Sahito, M. F., Mohanty, U. S., Jha, N. K., Akhondzadeh, H., . . . Iglauer, S. (2020). Environmental Friendliness and High Performance of Multifunctional Tween 80/ZnO-Nanoparticles-Added Water-Based Drilling Fluid: An Experimental Approach. *ACS Sustainable Chemistry & Engineering*.

Agartan, E., Trevisan, L., Cihan, A., Birkholzer, J., Zhou, Q., & Illangasekare, T. H. (2015). Experimental study on effects of geologic heterogeneity in enhancing dissolution trapping of supercritical CO2. *Water resources research, 51*(3), 1635-1648.

Aguilar, E., Allende, L., del Toro, F. J., Chung, B.-N., Canto, T., & Tenllado, F. (2015). Effects of elevated CO2 and temperature on pathogenicity determinants and virulence of Potato virus X/Potyvirus-associated synergism. *Molecular Plant-Microbe Interactions, 28*(12), 1364-1373.

Ahualli, S., Iglesias, G., Wachter, W., Dulle, M., Minami, D., & Glatter, O. (2011). Adsorption of anionic and cationic surfactants on anionic colloids: supercharging and destabilization. *Langmuir, 27*(15), 9182-9192.

Ajayi, T., Awolayo, A., Gomes, J. S., Parra, H., & Hu, J. (2019). Large scale modeling and assessment of the feasibility of CO2 storage onshore Abu Dhabi. *Energy, 185*, 653-670.

Akbar, I., Zhou, H., Liu, W., Tahir, M. U., Memon, A., Ansari, U., & Lv, F. (2020). Experimental Investigation of Chemical Flooding Using Nanoparticles and Polymer on Displacement of Crude Oil for Enhanced Oil Recovery. *International Journal of Chemical Engineering, 2020*.

Akbarabadi, M., & Piri, M. (2015). Co-sequestration of SO2 with supercritical CO2 in carbonates: An experimental study of capillary trapping, relative permeability, and capillary pressure. *Advances in Water Resources, 77*, 44-56.

Akhondzadeh, H., Keshavarz, A., Al-Yaseri, A. Z., Ali, M., Awan, F. U. R., Wang, X., . . . Lebedev, M. (2020). Pore-scale analysis of coal cleat network evolution through liquid nitrogen treatment: A Micro-Computed Tomography investigation. *International Journal of Coal Geology, 219*, 103370.

Akob, D. M., Cozzarelli, I. M., Dunlap, D. S., Rowan, E. L., & Lorah, M. M. (2015). Organic and inorganic composition and microbiology of produced waters from Pennsylvania shale gas wells. *Applied Geochemistry, 60*, 116-125.

Al-Anssari, S., Ali, M., Alajmi, M., Akhondzadeh, H., Khaksar Manshad, A., Kalantariasl, A., . . . Keshavarz, A. (2021). Synergistic Effect of Nanoparticles and Polymers on the Rheological Properties of Injection Fluids: Implications for Enhanced Oil Recovery. *Energy & Fuels*.

Al-Anssari, S., Ali, M., Memon, S., Bhatti, M. A., Lagat, C., & Sarmadivaleh, M. (2019). Reversible and irreversible adsorption of bare and hybrid silica nanoparticles onto carbonate surface at reservoir condition. *Petroleum*.

Al-Anssari, S., Ali, M., Memon, S., Bhatti, M. A., Lagat, C., & Sarmadivaleh, M. (2020). Reversible and irreversible adsorption of bare and hybrid silica nanoparticles onto carbonate surface at reservoir condition. *Petroleum, 6*(3), 277-285.

Al-Anssari, S., Arain, Z.-U.-A., Barifcani, A., Keshavarz, A., Ali, M., & Iglauer, S. (2018). *Influence of Pressure and Temperature on CO2-Nanofluid Interfacial Tension: Implication for Enhanced Oil Recovery and Carbon Geosequestration.* Paper presented at the Abu Dhabi International Petroleum Exhibition & Conference.

Al-Anssari, S., Arain, Z.-U.-A., Shanshool, H. A., Ali, M., Keshavarz, A., Iglauer, S., & Sarmadivaleh, M. (2020). *Effect of Nanoparticles on the Interfacial Tension of CO-Oil System at High Pressure and Temperature: An Experimental Approach.* Paper presented at the SPE Asia Pacific Oil & Gas Conference and Exhibition.

Al-Anssari, S., Arif, M., Wang, S., Barifcani, A., & Iglauer, S. (2017). Stabilising nanofluids in saline environments. *Journal of colloid and interface science, 508*, 222-229.

Al-Anssari, S., Arif, M., Wang, S., Barifcani, A., Lebedev, M., & Iglauer, S. (2017a). CO2 geo-storage capacity enhancement via nanofluid priming. *International Journal of Greenhouse Gas Control, 63*, 20-25.

Al-Anssari, S., Arif, M., Wang, S., Barifcani, A., Lebedev, M., & Iglauer, S. (2017b). Wettability of nano-treated calcite/CO2/brine systems: Implication for enhanced CO2 storage potential. *International Journal of Greenhouse Gas Control, 66*, 97-105.

Al-Anssari, S., Arif, M., Wang, S., Barifcani, A., Lebedev, M., & Iglauer, S. (2018). Wettability of nanofluid-modified oil-wet calcite at reservoir conditions. *Fuel, 211*, 405-414.

Al-Anssari, S., Barifcani, A., Keshavarz, A., & Iglauer, S. (2018). Impact of nanoparticles on the CO2-brine interfacial tension at high pressure and temperature. *Journal of colloid and interface science, 532*, 136-142.

Al-Anssari, S., Barifcani, A., Wang, S., Maxim, L., & Iglauer, S. (2016). Wettability alteration of oil-wet carbonate by silica nanofluid. *Journal of colloid and interface science, 461*, 435-442.

Al-Anssari, S., Nwidee, L., Ali, M., Sangwai, J. S., Wang, S., Barifcani, A., & Iglauer, S. (2017). *Retention of silica nanoparticles in limestone porous media.* Paper presented at the SPE/IATMI Asia Pacific Oil & Gas Conference and Exhibition.

Al-Anssari, S., Wang, S., Barifcani, A., & Iglauer, S. (2017). Oil-water interfacial tensions of silica nanoparticle-surfactant formulations. *Tenside Surfactants Detergents, 54*(4), 334-341.

Al-Anssari, S., Wang, S., Barifcani, A., Lebedev, M., & Iglauer, S. (2017). Effect of temperature and SiO2 nanoparticle size on wettability alteration of oil-wet calcite. *Fuel, 206*, 34-42.

Al-Bayati, D., Saeedi, A., Myers, M., White, C., & Xie, Q. (2019). Insights into immiscible supercritical CO2 EOR: An XCT scanner assisted flow behaviour in layered sandstone porous media. *Journal of CO2 Utilization, 32*, 187-195.

Al-Khdheeawi, E. A., Mahdi, D. S., Ali, M., Fauziah, C. A., & Barifcani, A. (2020). *Impact of Caprock Type on Geochemical Reactivity and Mineral Trapping Efficiency of CO.* Paper presented at the Offshore Technology Conference Asia.

Al-Khdheeawi, E. A., Mahdi, D. S., Ali, M., Iglauer, S., & Barifcani, A. (2021). Reservoir Scale Porosity-Permeability Evolution in Sandstone due to CO2 Geological Storage. *Available at SSRN 3818887*.

Al-Khdheeawi, E. A., Vialle, S., Barifcani, A., Sarmadivaleh, M., & Iglauer, S. (2017a). Impact of reservoir wettability and heterogeneity on CO2-plume migration and trapping capacity. *International Journal of Greenhouse Gas Control, 58*, 142-158.

Al-Khdheeawi, E. A., Vialle, S., Barifcani, A., Sarmadivaleh, M., & Iglauer, S. (2017b). Influence of injection well configuration and rock wettability on CO2 plume behaviour and CO2 trapping capacity in heterogeneous reservoirs. *Journal of Natural Gas Science and Engineering, 43*, 190-206.

Al-Menhali, A. S., & Krevor, S. (2016). Capillary trapping of CO2 in oil reservoirs: Observations in a mixed-wet carbonate rock. *Environmental science & technology, 50*(5), 2727-2734.

Al-Menhali, A. S., & Krevor, S. (2017). Pore-scale Analysis of In Situ Contact Angle Measurements in Mixed-wet Rocks: Applications to Carbon Utilization in Oil Fields. *Energy Procedia, 114*, 6919-6927.

Al-Menhali, A. S., Menke, H. P., Blunt, M. J., & Krevor, S. C. (2016). Pore scale observations of trapped CO2 in mixed-wet carbonate rock: applications to storage in oil fields. *Environmental science & technology, 50*(18), 10282-10290.

Al-Muntasheri, G. A., Liang, F., & Hull, K. L. (2017). Nanoparticle-enhanced hydraulic-fracturing fluids: a review. *SPE Production & Operations, 32*(02), 186-195.

Al-Rubaye, A., Al-Yaseri, A., Ali, M., & Mahmud, H. B. (2021). Characterization and analysis of naturally fractured gas reservoirs based on stimulated reservoir volume and petro-physical parameters. *Journal of Petroleum Exploration and Production*, 1-11.

Al-Yaseri, A., & Jha, N. K. (2021). On Hydrogen Wettability of Basaltic Rock. *Journal of Petroleum Science and Engineering*, 108387.

Al-Yaseri, A., Roshan, H., Zhang, Y., Rahman, T., Lebedev, M., Barifcani, A., & Iglauer, S. (2017). Effect of the temperature on CO2/brine/dolomite

wettability: Hydrophilic versus hydrophobic surfaces. *Energy & Fuels*, *31*(6), 6329-6333.

Al-Yaseri, A., Sarmadivaleh, M., Saeedi, A., Lebedev, M., Barifcani, A., & Iglauer, S. (2015). N2+ CO2+ NaCl brine interfacial tensions and contact angles on quartz at CO2 storage site conditions in the Gippsland basin, Victoria/Australia. *Journal of Petroleum Science and Engineering*, *129*, 58-62.

Al-Yaseri, A. Z., Lebedev, M., Barifcani, A., & Iglauer, S. (2016). Receding and advancing (CO2+ brine+ quartz) contact angles as a function of pressure, temperature, surface roughness, salt type and salinity. *The Journal of Chemical Thermodynamics*, *93*, 416-423.

Al-Khdheeawi, E. A., Vialle, S., Barifcani, A., Sarmadivaleh, M., & Iglauer, S. (2017). Influence of CO2-wettability on CO2 migration and trapping capacity in deep saline aquifers. *Greenhouse Gases: Science and Technology*, *7*(2), 328-338.

Al-Yaseri, A. Z., Roshan, H., Lebedev, M., Barifcani, A., & Iglauer, S. (2016). Dependence of quartz wettability on fluid density. *Geophysical Research Letters*, *43*(8), 3771-3776.

Ali, M. (2018). *Effect of Organic Surface Concentration on CO2-Wettability of Reservoir Rock*. Curtin University.

Ali, M., & Aftab, A. (2020). Topic review Unconventional Reservoirs Subjects: Energy & Fuel Technology. doi:10.32545/encyclopedia202007.0023.v3

Ali, M., Aftab, A., Arain, Z. U., Al-Yaseri, A., Roshan, H., Saeedi, A., . . . Sarmadivaleh, M. (2020). Influence of Organic Acid Concentration on Wettability Alteration of Cap-Rock: Implications for CO2 Trapping/Storage. *ACS Appl Mater Interfaces*, *12*(35), 39850-39858. doi:10.1021/acsami.0c10491

Ali, M., Aftab, A., Awan, F. U. R., Akhondzadeh, H., Keshavarz, A., Saeedi, A., . . . Sarmadivaleh, M. (2021). CO2-wettability reversal of cap-rock by alumina nanofluid: Implications for CO2 geo-storage. *Fuel Processing Technology*, *214*, 106722.

Ali, M., Al-Anssari, S., Arif, M., Barifcani, A., Sarmadivaleh, M., Stalker, L., . . . Iglauer, S. (2019). Organic acid concentration thresholds for ageing of carbonate minerals: Implications for CO2 trapping/storage. *Journal of colloid and interface science*, *534*, 88-94.

Ali, M., Al-Anssari, S., Shakeel, M., Arif, M., Dahraj, N. U., & Iglauer, S. (2017). *Influence of Miscible CO 2 Flooding on Wettability and Asphaltene Precipitation in Indiana Lime Stone*. Paper presented at the SPE/IATMI Asia Pacific Oil & Gas Conference and Exhibition.

Ali, M., Arif, M., Sahito, M. F., Al-Anssari, S., Keshavarz, A., Barifcani, A., . . . Iglauer, S. (2019). CO2-wettability of sandstones exposed to traces of organic acids: Implications for CO2 geo-storage. *International Journal of Greenhouse Gas Control*, *83*, 61-68.

Ali, M., Awan, F. U. R., Ali, M., Al-Yaseri, A., Arif, M., Sanchez-Roman, M., . . . Iglauer, S. (2021). Effect of humic acid on CO2-wettability in sandstone formation. *J Colloid Interface Sci*, *588*, 315-325. doi:10.1016/j.jcis.2020.12.058

Ali, M., Awan, F. U. R., Ali, M., Al-Yaseri, A., Arif, M., Sánchez-Román, M., . . . Iglauer, S. (2021). Effect of humic acid on CO2-wettability in sandstone formation. *Journal of colloid and interface science*, *588*, 315-325.

Ali, M., Dahraj, N. U., & Haider, S. A. (2015). *Study of Asphaltene Precipitation during CO2 Injection in Light Oil Reservoirs*. Paper presented at the SPE/PAPG Pakistan section Annual Technical Conference.

Ali, M., Jarni, H. H., Aftab, A., Ismail, A. R., Saady, N. M. C., Sahito, M. F., . . . Sarmadivaleh, M. (2020). Nanomaterial-based drilling fluids for exploitation of unconventional reservoirs: A review. *Energies, 13*(13), 3417.

Ali, M., Sahito, M. F., Jha, N. K., Arain, Z. U., Memon, S., Keshavarz, A., . . . Sarmadivaleh, M. (2020). Effect of nanofluid on CO2-wettability reversal of sandstone formation; implications for CO2 geo-storage. *J Colloid Interface Sci, 559*, 304-312. doi:10.1016/j.jcis.2019.10.028

Ali, M., Sahito, M. F., Jha, N. K., Memon, S., Keshavarz, A., Iglauer, S., . . . Sarmadivaleh, M. (2020). Effect of nanofluid on CO2-wettability reversal of sandstone formation; implications for CO2 geo-storage. *Journal of colloid and interface science, 559*, 304-312.

Alroudhan, A., Vinogradov, J., & Jackson, M. (2016). Zeta potential of intact natural limestone: Impact of potential-determining ions Ca, Mg and SO4. *Colloids and Surfaces A: Physicochemical and Engineering Aspects, 493*, 83-98.

Alsaba, M. T., Al Dushaishi, M. F., & Abbas, A. K. (2020). A comprehensive review of nanoparticles applications in the oil and gas industry. *Journal of Petroleum Exploration and Production Technology, 10*(4), 1389-1399.

Alshakhs, M., & Rezaee, M. R. (2017). A new method to estimate total organic carbon (TOC) Content, an example from Goldwyer Shale Formation, the Canning Basin. *The Open Petroleum Engineering Journal, 10*, 118-133.

Amaya, J., Rana, D., & Hornof, V. (2002). Dynamic interfacial tension behavior of water/oil systems containing in situ-formed surfactants. *Journal of solution chemistry, 31*(2), 139-148.

Ampomah, W., Balch, R., Cather, M., Rose-Coss, D., Dai, Z., Heath, J., . . . Mozley, P. (2016). Evaluation of CO2 storage mechanisms in CO2 enhanced oil recovery sites: Application to Morrow sandstone reservoir. *Energy & Fuels, 30*(10), 8545-8555.

Anderson, W. (1986). Wettability literature survey-part 2: Wettability measurement. *Journal of Petroleum Technology, 38*(11), 1,246-241,262.

Anderson, W. G. (1987a). Wettability literature survey-part 4: Effects of wettability on capillary pressure. *Journal of Petroleum Technology, 39*(10), 1,283-281,300.

Anderson, W. G. (1987b). Wettability literature survey-part 6: the effects of wettability on waterflooding. *Journal of Petroleum Technology, 39*(12), 1,605-601,622.

Anderson, W. G. (1987c). Wettability literature survey part 5: the effects of wettability on relative permeability. *Journal of Petroleum Technology, 39*(11), 1,453-451,468.

Araujo, Y. C., Toledo, P. G., Leon, V., & Gonzalez, H. Y. (1995). Wettability of silane-treated glass slides as determined from X-ray photoelectron spectroscopy. *Journal of colloid and interface science, 176*(2), 485-490.

Arif, M., Abu-Khamsin, S., & Iglauer, S. (2019a). Wettability of rock/CO2/brine and rock/oil/CO2-enriched-brine systems: Critical parametric analysis and future outlook. *Advances in colloid and interface science*.

Arif, M., Abu-Khamsin, S. A., & Iglauer, S. (2019b). Wettability of rock/CO2/brine and rock/oil/CO2-enriched-brine systems: Critical parametric analysis and future outlook. *Advances in colloid and interface science, 268*, 91-113.

Arif, M., Abu-Khamsin, S. A., Zhang, Y., & Iglauer, S. (2020). Experimental investigation of carbonate wettability as a function of mineralogical and thermo-physical conditions. *Fuel, 264*, 116846.

Arif, M., Al-Yaseri, A. Z., Barifcani, A., Lebedev, M., & Iglauer, S. (2016). Impact of pressure and temperature on CO2–brine–mica contact angles and CO2–brine interfacial tension: Implications for carbon geo-sequestration. *Journal of colloid and interface science, 462*, 208-215.

Arif, M., Barifcani, A., & Iglauer, S. (2016). Solid/CO2 and solid/water interfacial tensions as a function of pressure, temperature, salinity and mineral type: Implications for CO2-wettability and CO2 geo-storage. *International Journal of Greenhouse Gas Control, 53*, 263-273.

Arif, M., Barifcani, A., Lebedev, M., & Iglauer, S. (2016). Structural trapping capacity of oil-wet caprock as a function of pressure, temperature and salinity. *International Journal of Greenhouse Gas Control, 50*, 112-120.

Arif, M., Jones, F., Barifcani, A., & Iglauer, S. (2017). Electrochemical investigation of the effect of temperature, salinity and salt type on brine/mineral interfacial properties. *International Journal of Greenhouse Gas Control, 59*, 136-147.

Arif, M., Lebedev, M., Barifcani, A., & Iglauer, S. (2017a). CO2 storage in carbonates: Wettability of calcite. *International Journal of Greenhouse Gas Control, 62*, 113-121.

Arif, M., Lebedev, M., Barifcani, A., & Iglauer, S. (2017b). Influence of shale-total organic content on CO2 geo-storage potential. *Geophysical Research Letters, 44*(17), 8769-8775.

Awan, F. U. R., Keshavarz, A., Akhondzadeh, H., Al-Anssari, S., Al-Yaseri, A., Nosrati, A., . . . Iglauer, S. (2020). Stable Dispersion of Coal Fines during Hydraulic Fracturing Flowback in Coal Seam Gas Reservoirs—An Experimental Study. *Energy & Fuels, 34*(5), 5566-5577.

Awan, F. U. R., Keshavarz, A., Akhondzadeh, H., Al-Anssari, S., & Iglauer, S. (2020). A novel approach for using silica nanoparticles in a proppant pack to fixate coal fines. *The APPEA Journal, 60*(1), 88-96. doi:https://doi.org/10.1071/AJ19031

Awan, F. U. R., Keshavarz, A., Azhar, M. R., Akhondzadeh, H., Ali, M., Al-Yaseri, A., . . . Iglauer, S. (2021). Adsorption of nanoparticles on glass bead surface for enhancing proppant performance: A systematic experimental study. *Journal of Molecular Liquids*, 115398.

Bachu, S. (2008). CO2 storage in geological media: Role, means, status and barriers to deployment. *Progress in energy and combustion science, 34*(2), 254-273.

Bachu, S., & Adams, J. (2003). Sequestration of CO2 in geological media in response to climate change: capacity of deep saline aquifers to sequester CO2 in solution. *Energy Conversion and Management, 44*(20), 3151-3175.

Bachu, S., Gunter, W., & Perkins, E. (1994). Aquifer disposal of CO2: hydrodynamic and mineral trapping. *Energy Conversion and Management, 35*(4), 269-279.

Bailey, S. (1984). Classification and structures of the micas. *Reviews in Mineralogy and Geochemistry, 13*(1), 1-12.

Bennett, P. C., Siegel, D., Baedecker, M. J., & Hult, M. (1993). Crude oil in a shallow sand and gravel aquifer—I. Hydrogeology and inorganic geochemistry. *Applied Geochemistry, 8*(6), 529-549.

Berger, P. M., Yoksoulian, L., Freiburg, J. T., Butler, S. K., & Roy, W. R. (2019). Carbon sequestration at the Illinois Basin-Decatur Project: experimental

results and geochemical simulations of storage. *Environmental Earth Sciences, 78*(22), 646.

Bikkina, P., Wan, J., Kim, Y., Kneafsey, T. J., & Tokunaga, T. K. (2016). Influence of wettability and permeability heterogeneity on miscible CO2 flooding efficiency. *Fuel, 166*, 219-226.

Birkholzer, J. T., Zhou, Q., & Tsang, C.-F. (2009). Large-scale impact of CO2 storage in deep saline aquifers: A sensitivity study on pressure response in stratified systems. *International Journal of Greenhouse Gas Control, 3*(2), 181-194.

Blunt, M., Fayers, F. J., & Orr Jr, F. M. (1993). Carbon dioxide in enhanced oil recovery. *Energy Conversion and Management, 34*(9-11), 1197-1204.

Boden, T. A., Marland, G., & Andres, R. (1995). Estimates of global, regional, and national annual CO 2 emissions from fossil-fuel burning, hydraulic cement production, and gas flaring: 1950-- 1992.

Broseta, D., Tonnet, N., & Shah, V. (2012). Are rocks still water-wet in the presence of dense CO2 or H2S? *Geofluids, 12*(4), 280-294.

Budisa, N., & Schulze-Makuch, D. (2014). Supercritical carbon dioxide and its potential as a life-sustaining solvent in a planetary environment. *Life, 4*(3), 331-340.

Busch, A., Alles, S., Gensterblum, Y., Prinz, D., Dewhurst, D. N., Raven, M. D., . . . Krooss, B. M. (2008). Carbon dioxide storage potential of shales. *International Journal of Greenhouse Gas Control, 2*(3), 297-308.

Butt, H., Graf, K., & Kappl, M. (2006). Physics and Chemistry of Interfaces Wiley: Weinheim.

Buyukcakir, O., Je, S. H., Talapaneni, S. N., Kim, D., & Coskun, A. (2017). Charged covalent triazine frameworks for CO2 capture and conversion. *ACS Applied Materials & Interfaces, 9*(8), 7209-7216.

Caballero, B., Trugo, L. C., & Finglas, P. M. (2003). *Encyclopedia of food sciences and nutrition*: Academic.

Cao, C., Liu, H., Hou, Z., Mehmood, F., Liao, J., & Feng, W. (2020). A review of CO2 storage in view of safety and cost-effectiveness. *Energies, 13*(3), 600.

Cao, Z., Daly, M., Clémence, L., Geever, L. M., Major, I., Higginbotham, C. L., & Devine, D. M. (2016). Chemical surface modification of calcium carbonate particles with stearic acid using different treating methods. *Applied Surface Science, 378*, 320-329.

Carré, A., Gastel, J.-C., & Shanahan, M. E. (1996). Viscoelastic effects in the spreading of liquids. *Nature, 379*(6564), 432-434.

Chahal, P. (2020). Global Warming and Greenhouse Effect. *Conservation, Sustainability, and Environmental Justice in India*, 95.

Chalbaud, C., Robin, M., Lombard, J., Martin, F., Egermann, P., & Bertin, H. (2009). Interfacial tension measurements and wettability evaluation for geological CO2 storage. *Advances in Water Resources, 32*(1), 98-109.

Chang, Y.-B., Coats, B. K., & Nolen, J. S. (1996). *A compositional model for CO 2 floods including CO 2 solubility in water*. Paper presented at the Permian Basin Oil and Gas Recovery Conference.

Chaturvedi, K. R., & Sharma, T. (2020). Single-step silica nanofluid for improved carbon dioxide flow and reduced formation damage in porous media for carbon utilization. *Energy*, 117276.

Chaudhary, K., Bayani Cardenas, M., Wolfe, W. W., Maisano, J. A., Ketcham, R. A., & Bennett, P. C. (2013). Pore-scale trapping of supercritical CO2 and the role

of grain wettability and shape. *Geophysical Research Letters, 40*(15), 3878-3882.

Chen, C., Wan, J., Li, W., & Song, Y. (2015). Water contact angles on quartz surfaces under supercritical CO2 sequestration conditions: Experimental and molecular dynamics simulation studies. *International Journal of Greenhouse Gas Control, 42*, 655-665.

Cheraghian, G., & Hendraningrat, L. (2016). A review on applications of nanotechnology in the enhanced oil recovery part A: effects of nanoparticles on interfacial tension. *International Nano Letters, 6*(2), 129-138.

Chiquet, P., Broseta, D., & Thibeau, S. (2007). Wettability alteration of caprock minerals by carbon dioxide. *Geofluids, 7*(2), 112-122.

Chu, S., & Majumdar, A. (2012). Opportunities and challenges for a sustainable energy future. *Nature, 488*(7411), 294-303.

Cyr, T., & Strausz, O. (1984). Bound carboxylic acids in the Alberta oil sands. *Organic Geochemistry, 7*(2), 127-140.

Dahraj, N. U., Ali, M., & Khan, M. N. (2016). *End of Linear Flow Time Picking in Long Transient Hydraulically Fractured Wells to Correctly Estimate the Permeability, Fracture Half-Length and Original Gas in Place in Liquid Rich Shales.* Paper presented at the PAPG/SPE Pakistan Section Annual Technical Conference and Exhibition.

Dake, L. P. (1983). *Fundamentals of reservoir engineering*: Elsevier.

Davis, J. A. (1982). Adsorption of natural dissolved organic matter at the oxide/water interface. *Geochimica et Cosmochimica Acta, 46*(11), 2381-2393.

Davis, S., Williams, S., & Boundy, R. (2016). Transportation energy data book: Edition 35 (No. ORNL/TM-2016/470). *Oak Ridge National Laboratory (ORNL), Oak Ridge*.

Davis, S. J., Caldeira, K., & Matthews, H. D. (2010). Future CO2 emissions and climate change from existing energy infrastructure. *Science, 329*(5997), 1330-1333.

De, G. P. (1985). Wetting: statics and dynamics. *Rev Mod Phys, 57*(3), 827.

De, M., Ghosh, P. S., & Rotello, V. M. (2008). Applications of nanoparticles in biology. *Advanced Materials, 20*(22), 4225-4241.

dell'energia, A. i. (2010). *Energy technology perspectives 2010: scenarios & strategies to 2050*: ill.

Dickson, J. L., Gupta, G., Horozov, T. S., Binks, B. P., & Johnston, K. P. (2006). Wetting phenomena at the CO2/water/glass interface. *Langmuir, 22*(5), 2161-2170.

Dietrich, F., Schöny, G., Fuchs, J., & Hofbauer, H. (2018). Experimental study of the adsorber performance in a multi-stage fluidized bed system for continuous CO2 capture by means of temperature swing adsorption. *Fuel Processing Technology, 173*, 103-111.

Ding, S., Xi, Y., Jiang, H., & Liu, G. (2018). CO2 storage capacity estimation in oil reservoirs by solubility and mineral trapping. *Applied Geochemistry, 89*, 121-128.

Donaldson, E., & Alam, W. (2008). Wettability Gulf Publishing Company. *Original edition*.

Donaldson, E. C., & Alam, W. (2013). *Wettability*: Elsevier.

Donaldson, E. C., Thomas, R. D., & Lorenz, P. B. (1969). Wettability determination and its effect on recovery efficiency. *Society of Petroleum Engineers Journal, 9*(01), 13-20.

Dullien, F. (1991). Structure of porous media *Transport Processes in Porous Media* (pp. 3-41): Springer.

Dupraz, S., Parmentier, M., Ménez, B., & Guyot, F. (2009). Experimental and numerical modeling of bacterially induced pH increase and calcite precipitation in saline aquifers. *Chemical Geology, 265*(1-2), 44-53.

Durand, B. (2005). Carbon dioxide capture and storage.

Ebrahimi, A. N., Jamshidi, S., Iglauer, S., & Boozarjomehry, R. B. (2013). Genetic algorithm-based pore network extraction from micro-computed tomography images. *Chemical Engineering Science, 92*, 157-166.

El-Maghraby, R., Pentland, C., Iglauer, S., & Blunt, M. (2012). A fast method to equilibrate carbon dioxide with brine at high pressure and elevated temperature including solubility measurements. *The Journal of Supercritical Fluids, 62*, 55-59.

El-sayed, G. M., Kamel, M., Morsy, N., & Taher, F. (2012). Encapsulation of nano Disperse Red 60 via modified miniemulsion polymerization. I. Preparation and characterization. *Journal of Applied Polymer Science, 125*(2), 1318-1329.

Eral, H., & Oh, J. (2013). Contact angle hysteresis: a review of fundamentals and applications. *Colloid and polymer science, 291*(2), 247-260.

Eskelinen, P. (1992). X-ray diffraction study of TiO2 thin films on mica. *Journal of solid state chemistry, 100*(2), 356-362.

Espinoza, D. N., & Santamarina, J. C. (2010). Water-CO2-mineral systems: Interfacial tension, contact angle, and diffusion—Implications to CO2 geological storage. *Water resources research, 46*(7).

Fakoya, M. F., & Shah, S. N. (2018). Effect of silica nanoparticles on the rheological properties and filtration performance of surfactant-based and polymeric fracturing fluids and their blends. *SPE Drilling & Completion, 33*(02), 100-114.

Farokhpoor, R., Bjørkvik, B. J., Lindeberg, E., & Torsæter, O. (2013). Wettability behaviour of CO2 at storage conditions. *International Journal of Greenhouse Gas Control, 12*, 18-25.

Fauziah, C. A., Al-Khdheeawi, E. A., Barifcani, A., & Iglauer, S. (2019). *Wettability measurements of mixed clay minerals at elevated temperature and pressure: implications for CO 2 geo-storage*. Paper presented at the SPE Gas & Oil Technology Showcase and Conference.

Firoozabadi, A., & Myint, P. C. (2010). Prospects for subsurface CO2 sequestration. *AIChE journal, 56*(6), 1398-1405.

Froelich, P. N., Klinkhammer, G., Bender, M. L., Luedtke, N., Heath, G. R., Cullen, D., . . . Maynard, V. (1979). Early oxidation of organic matter in pelagic sediments of the eastern equatorial Atlantic: suboxic diagenesis. *Geochimica et Cosmochimica Acta, 43*(7), 1075-1090.

Gaines, G. L. (1966). Insoluble monolayers at liquid-gas interfaces.

Garcia, S., Kaminska, S., & Mercedes Maroto-Valer, M. (2010). *Underground carbon dioxide storage in saline formations.* Paper presented at the Proceedings of the Institution of Civil Engineers-Waste and Resource Management.

Garrido, D. R. R., Lafortune, S., Souli, H., & Dubujet, P. (2013). Impact of supercritical CO2/water interaction on the caprock nanoporous structure. *Procedia Earth and Planetary Science, 7*, 738-741.

Gaus, I. (2010). Role and impact of CO2–rock interactions during CO2 storage in sedimentary rocks. *International Journal of Greenhouse Gas Control, 4*(1), 73-89.

Gaus, I., Azaroual, M., & Czernichowski-Lauriol, I. (2005). Reactive transport modelling of the impact of CO2 injection on the clayey cap rock at Sleipner (North Sea). *Chemical Geology, 217*(3-4), 319-337.

Gauteplass, J., Almenningen, S., Ersland, G., Barth, T., Yang, J., & Chapoy, A. (2020). Multiscale investigation of CO2 hydrate self-sealing potential for carbon geo-sequestration. *Chemical Engineering Journal, 381*, 122646.

Gerber, P. J., Henderson, B., & Makkar, H. P. (2013). *Mitigation of greenhouse gas emissions in livestock production: a review of technical options for non-CO2 emissions*: Food and Agriculture Organization of the United Nations (FAO).

Gislason, S. R., & Oelkers, E. H. (2014). Carbon storage in basalt. *Science, 344*(6182), 373-374.

Gíslason, S. R., Sigurdardóttir, H., Aradóttir, E. S., & Oelkers, E. H. (2018). A brief history of CarbFix: Challenges and victories of the project's pilot phase. *Energy Procedia, 146*, 103-114.

Godec, M. L., Kuuskraa, V. A., & Dipietro, P. (2013). Opportunities for using anthropogenic CO2 for enhanced oil recovery and CO2 storage. *Energy & Fuels, 27*(8), 4183-4189.

Golding, S., Uysal, I., Boreham, C., Kirste, D., Baublys, K., & Esterle, J. (2011). Adsorption and mineral trapping dominate CO2 storage in coal systems. *Energy Procedia, 4*, 3131-3138.

Gomari, K. R., & Hamouda, A. (2006). Effect of fatty acids, water composition and pH on the wettability alteration of calcite surface. *Journal of Petroleum Science and Engineering, 50*(2), 140-150.

Good, R. J., & Girifalco, L. (1960). A theory for estimation of surface and interfacial energies. III. Estimation of surface energies of solids from contact angle data. *The Journal of Physical Chemistry, 64*(5), 561-565.

Goodman, A., Sanguinito, S., Kutchko, B., Natesakhawat, S., Cvetic, P., & Allen, A. J. (2020). Shale pore alteration: Potential implications for hydrocarbon extraction and CO2 storage. *Fuel, 265*, 116930.

Grate, J. W., Dehoff, K. J., Warner, M. G., Pittman, J. W., Wietsma, T. W., Zhang, C., & Oostrom, M. (2012). Correlation of oil–water and air–water contact angles of diverse silanized surfaces and relationship to fluid interfacial tensions. *Langmuir, 28*(18), 7182-7188.

Grim, C. (2017). Cape Grim Greenhouse Gas Web Data.

Gu, C., Qiu, R., Liu, S., You, Z., & Qin, R. (2020). Shear thickening effects of drag-reducing nanofluids for low permeability reservoir. *Advances in Geo-Energy Research, 4*(3), 317-325.

Guidotti, C. V. (1984). Micas in metamorphic rocks. *Micas, reviews in mineralogy, 13*, 357-467.

Gunning, J., Ennis-King, J., LaForce, T., Jenkins, C., & Paterson, L. (2020). Bayesian well-test 2D tomography inversion for CO2 plume detection. *International Journal of Greenhouse Gas Control, 94*, 102804.

Gunter, W. D., Bachu, S., & Benson, S. (2004). The role of hydrogeological and geochemical trapping in sedimentary basins for secure geological storage of carbon dioxide. *Geological Society, London, Special Publications, 233*(1), 129-145.

Gutiérrez, F., & Lizaga, I. (2016). Sinkholes, collapse structures and large landslides in an active salt dome submerged by a reservoir: The unique case of the Ambal ridge in the Karun River, Zagros Mountains, Iran. *Geomorphology, 254*, 88-103.

Haghighi, O. M., Zargar, G., Khaksar Manshad, A., Ali, M., Takassi, M. A., Ali, J. A., & Keshavarz, A. (2020). Effect of Environment-Friendly Non-Ionic Surfactant on Interfacial Tension Reduction and Wettability Alteration; Implications for Enhanced Oil Recovery. *Energies, 13*(15), 3988.

Hamouda, A. A., & Rezaei Gomari, K. A. (2006). *Influence of temperature on wettability alteration of carbonate reservoirs.* Paper presented at the SPE/DOE Symposium on Improved Oil Recovery.

Hansen, G., Hamouda, A., & Denoyel, R. (2000). The effect of pressure on contact angles and wettability in the mica/water/n-decane system and the calcite+ stearic acid/water/n-decane system. *Colloids and Surfaces A: Physicochemical and Engineering Aspects, 172*(1-3), 7-16.

Heberling, F., Trainor, T. P., Lützenkirchen, J., Eng, P., Denecke, M. A., & Bosbach, D. (2011). Structure and reactivity of the calcite–water interface. *Journal of colloid and interface science, 354*(2), 843-857.

Hendraningrat, L., Li, S., & Torsæter, O. (2013). A coreflood investigation of nanofluid enhanced oil recovery. *Journal of Petroleum Science and Engineering, 111*, 128-138.

Herrero, M., Henderson, B., Havlík, P., Thornton, P. K., Conant, R. T., Smith, P., . . . Gill, M. (2016). Greenhouse gas mitigation potentials in the livestock sector. *Nature Climate Change, 6*(5), 452-461.

Heshmati, M., & Piri, M. (2014). Experimental investigation of dynamic contact angle and capillary rise in tubes with circular and noncircular cross sections. *Langmuir, 30*(47), 14151-14162.

Hinkle, H., Hargett, T., & Bailon, W. (2017). BamCore and Global Warming: Windsor: BamCore.

Hobeika, N., Bouriat, P., Touil, A., Broseta, D., Brown, R., & Dubessy, J. (2017). Help from a hindrance: Using astigmatism in round capillaries to study contact angles and wetting layers. *Langmuir, 33*(21), 5179-5187.

Hoeiland, S., Barth, T., Blokhus, A., & Skauge, A. (2001). The effect of crude oil acid fractions on wettability as studied by interfacial tension and contact angles. *Journal of Petroleum Science and Engineering, 30*(2), 91-103.

Holloway, S. (2007). Carbon dioxide capture and geological storage. *Philosophical Transactions of the Royal Society A: Mathematical, Physical and Engineering Sciences, 365*(1853), 1095-1107.

Hu, Y., & Jun, Y.-S. (2012). Biotite dissolution in brine at varied temperatures and CO2 pressures: Its activation energy and potential CO2 intercalation. *Langmuir, 28*(41), 14633-14641.

Huang, F., Kang, Y., You, Z., You, L., & Xu, C. (2017). Critical conditions for massive fines detachment induced by single-phase flow in coalbed methane reservoirs: modeling and experiments. *Energy & Fuels, 31*(7), 6782-6793.

Huang, W., Chen, W., & Anandarajah, G. (2017). The role of technology diffusion in a decarbonizing world to limit global warming to well below 2 C: An assessment with application of Global TIMES model. *Applied energy, 208*, 291-301.

Hussain, M., Butt, A. R., Uzma, F., Ahmed, R., Islam, T., & Yousaf, B. (2019). A comprehensive review of sectorial contribution towards greenhouse gas emissions and progress in carbon capture and storage in Pakistan. *Greenhouse Gases: Science and Technology, 9*(4), 617-636.

Idowu, N., Long, H., Øren, P.-E., Carnerup, A. M., Fogden, A., Bondino, I., . . . AS, D. N. (2015). *Wettability analysis using micro-CT, FESEM and QEMSCAN,*

and its applications to digital rock physics. Paper presented at the International Symposium of the Society of Core Analysts.

IEA. (2020). Global Energy Review 2020. *IEA, Paris*.

Iglauer, S. (2011). Dissolution trapping of carbon dioxide in reservoir formation brine–a carbon storage mechanism *Mass transfer-advanced aspects*: InTechOpen.

Iglauer, S. (2017). CO2–water–rock wettability: variability, influencing factors, and implications for CO2 geostorage. *Accounts of Chemical Research, 50*(5), 1134-1142.

Iglauer, S. (2018). Optimum storage depths for structural CO2 trapping. *International Journal of Greenhouse Gas Control, 77*, 82-87.

Iglauer, S., Al-Yaseri, A. Z., Rezaee, R., & Lebedev, M. (2015). CO2 wettability of caprocks: Implications for structural storage capacity and containment security. *Geophysical Research Letters, 42*(21), 9279-9284.

Iglauer, S., Ali, M., & Keshavarz, A. (2020). Hydrogen Wettability of Sandstone Reservoirs: Implications for Hydrogen Geo-Storage. *Geophysical Research Letters*. doi:10.1029/2020GL090814

Iglauer, S., Fernø, M., Shearing, P., & Blunt, M. (2012). Comparison of residual oil cluster size distribution, morphology and saturation in oil-wet and water-wet sandstone. *Journal of colloid and interface science, 375*(1), 187-192.

Iglauer, S., Mathew, M., & Bresme, F. (2012). Molecular dynamics computations of brine–CO2 interfacial tensions and brine–CO2–quartz contact angles and their effects on structural and residual trapping mechanisms in carbon geo-sequestration. *Journal of colloid and interface science, 386*(1), 405-414.

Iglauer, S., Paluszny, A., Pentland, C. H., & Blunt, M. J. (2011). Residual CO2 imaged with X-ray micro-tomography. *Geophysical Research Letters, 38*(21).

Iglauer, S., Paluszny, A., Rahman, T., Zhang, Y., Wülling, W., & Lebedev, M. (2019). Residual trapping of CO2 in an oil-filled, oil-wet sandstone core: Results of three-phase pore-scale imaging. *Geophysical Research Letters, 46*(20), 11146-11154.

Iglauer, S., Pentland, C., & Busch, A. (2015). CO2 wettability of seal and reservoir rocks and the implications for carbon geo-sequestration. *Water resources research, 51*(1), 729-774.

Iglauer, S., Salamah, A., Sarmadivaleh, M., Liu, K., & Phan, C. (2014). Contamination of silica surfaces: Impact on water–CO2–quartz and glass contact angle measurements. *International Journal of Greenhouse Gas Control, 22*, 325-328.

Iglauer, S., Wülling, W., Pentland, C. H., Al-Mansoori, S. K., & Blunt, M. J. (2011). Capillary-trapping capacity of sandstones and sandpacks. *SPE Journal, 16*(04), 778-783.

III, I. P. o. C. C. W. G. (2013). *IPCC special report on carbon dioxide capture and storage*: Published for the Intergovernmental Panel on Climate Change, Cambridge ….

Ingrosso, F., & Ruiz-López, M. F. (2017). Modeling solvation in supercritical CO2. *ChemPhysChem, 18*(19), 2560-2572.

Jackson, M. D., Valvatne, P. H., & Blunt, M. J. (2005). Prediction of wettability variation within an oil/water transition zone and its impact on production. *SPE Journal, 10*(02), 185-195.

Jadhunandan, P., & Morrow, N. R. (1995). Effect of wettability on waterflood recovery for crude-oil/brine/rock systems. *SPE reservoir engineering, 10*(01), 40-46.

Jardine, P., McCarthy, J., & Weber, N. (1989). Mechanisms of dissolved organic carbon adsorption on soil. *Soil Science Society of America Journal, 53*(5), 1378-1385.

Jenkins, C. R., Cook, P. J., Ennis-King, J., Undershultz, J., Boreham, C., Dance, T., . . . Hortle, A. (2012). Safe storage and effective monitoring of CO2 in depleted gas fields. *Proceedings of the National Academy of Sciences, 109*(2), E35-E41.

Jha, N., Ali, M., Sarmadivaleh, M., Iglauer, S., Barifcani, A., Lebedev, M., & Sangwai, J. (2018). *Low salinity surfactant nanofluids for enhanced CO2 storage application at high pressure and temperature*. Paper presented at the Fifth CO2 Geological Storage Workshop.

Jha, N. K., Ali, M., Iglauer, S., Lebedev, M., Roshan, H., Barifcani, A., . . . Sarmadivaleh, M. (2019). Wettability alteration of quartz surface by low-salinity surfactant nanofluids at high-pressure and high-temperature conditions. *Energy & Fuels, 33*(8), 7062-7068.

Jha, N. K., Iglauer, S., Barifcani, A., Sarmadivaleh, M., & Sangwai, J. S. (2019). Low-salinity surfactant nanofluid formulations for wettability alteration of sandstone: role of the SiO2 nanoparticle concentration and divalent cation/SO42–ratio. *Energy & Fuels, 33*(2), 739-746.

Jha, N. K., Iglauer, S., & Sangwai, J. S. (2017). Effect of monovalent and divalent salts on the interfacial tension of n-heptane against aqueous anionic surfactant solutions. *Journal of Chemical & Engineering Data, 63*(7), 2341-2350.

Jha, N. K., Lebedev, M., Iglauer, S., Ali, M., Roshan, H., Barifcani, A., . . . Sarmadivaleh, M. (2020). Pore scale investigation of low salinity surfactant nanofluid injection into oil saturated sandstone via X-ray micro-tomography. *Journal of colloid and interface science, 562*, 370-380.

Ji, X., & Zhu, C. (2015). CO2 storage in deep saline aquifers *Novel materials for carbon dioxide mitigation technology* (pp. 299-332): Elsevier.

Jing, J., Yang, Y., & Tang, Z. (2021). Assessing the influence of injection temperature on CO2 storage efficiency and capacity in the sloping formation with fault. *Energy, 215*, 119097.

Johnson, B. F. (2003). Nanoparticles in catalysis. *Topics in Catalysis, 24*(1), 147-159.

Jones, D., Head, I., Gray, N., Adams, J., Rowan, A., Aitken, C., . . . Bowler, B. (2008). Crude-oil biodegradation via methanogenesis in subsurface petroleum reservoirs. *Nature, 451*(7175), 176-180.

Juanes, R., MacMinn, C. W., & Szulczewski, M. L. (2010). The footprint of the CO 2 plume during carbon dioxide storage in saline aquifers: storage efficiency for capillary trapping at the basin scale. *Transport in porous media, 82*(1), 19-30.

Juanes, R., Spiteri, E., Orr Jr, F., & Blunt, M. (2006). Impact of relative permeability hysteresis on geological CO2 storage. *Water Resources Research, 42*(12).

Kalam, S., Olayiwola, T., Al-Rubaii, M. M., Amaechi, B. I., Jamal, M. S., & Awotunde, A. A. (2020). Carbon dioxide sequestration in underground formations: review of experimental, modeling, and field studies. *Journal of Petroleum Exploration and Production Technology*, 1-23.

Kang, S. M., Fathi, E., Ambrose, R. J., Akkutlu, I. Y., & Sigal, R. F. (2011). Carbon dioxide storage capacity of organic-rich shales. *SPE J, 16*(4), 842-855.

Karl, T. R., Melillo, J. M., Peterson, T. C., & Hassol, S. J. (2009). *Global climate change impacts in the United States*: Cambridge University Press.

Karoussi, O., Skovbjerg, L. L., Hassenkam, T., Stipp, S. S., & Hamouda, A. A. (2008). AFM study of calcite surface exposed to stearic and heptanoic acids. *Colloids and Surfaces A: Physicochemical and Engineering Aspects, 325*(3), 107-114.

Kaveh, N. S., Barnhoorn, A., & Wolf, K.-H. (2016). Wettability evaluation of silty shale caprocks for CO2 storage. *International Journal of Greenhouse Gas Control, 49*, 425-435.

Kaveh, N. S., Wolf, K., Ashrafizadeh, S., & Rudolph, E. (2012). Effect of coal petrology and pressure on wetting properties of wet coal for CO2 and flue gas storage. *International Journal of Greenhouse Gas Control, 11*, S91-S101.

Kazemifar, F., Blois, G., Kyritsis, D. C., & Christensen, K. T. (2016). Quantifying the flow dynamics of supercritical CO2–water displacement in a 2D porous micromodel using fluorescent microscopy and microscopic PIV. *Advances in Water Resources, 95*, 352-368.

Kharaka, Y. K., Thordsen, J. J., Hovorka, S. D., Nance, H. S., Cole, D. R., Phelps, T. J., & Knauss, K. G. (2009). Potential environmental issues of CO2 storage in deep saline aquifers: Geochemical results from the Frio-I Brine Pilot test, Texas, USA. *Applied Geochemistry, 24*(6), 1106-1112.

King, M., & Bott, T. R. (2012). *Extraction of natural products using near-critical solvents*: Springer Science & Business Media.

Kleber, M., Eusterhues, K., Keiluweit, M., Mikutta, C., Mikutta, R., & Nico, P. S. (2015). Mineral–organic associations: formation, properties, and relevance in soil environments *Advances in agronomy* (Vol. 130, pp. 1-140): Elsevier.

Klutse, N. A. B., Ajayi, V. O., Gbobaniyi, E. O., Egbebiyi, T. S., Kouadio, K., Nkrumah, F., . . . Abiodun, B. J. (2018). Potential impact of 1.5 C and 2 C global warming on consecutive dry and wet days over West Africa. *Environmental Research Letters, 13*(5), 055013.

Krevor, S., Blunt, M. J., Benson, S. M., Pentland, C. H., Reynolds, C., Al-Menhali, A., & Niu, B. (2015). Capillary trapping for geologic carbon dioxide storage–From pore scale physics to field scale implications. *International Journal of Greenhouse Gas Control, 40*, 221-237.

Krevor, S. C., Pini, R., Zuo, L., & Benson, S. M. (2012). Relative permeability and trapping of CO2 and water in sandstone rocks at reservoir conditions. *Water resources research, 48*(2).

Kuhn, H., & Möbius, D. (1971). Systems of monomolecular layers—Assembling and physico-chemical behavior. *Angewandte Chemie International Edition in English, 10*(9), 620-637.

Kumar, A., Malik, G., Goyal, K., Sardana, N., Chandra, R., & Mulik, R. S. (2020). Controllable synthesis of tunable aspect ratios novel h-BN nanorods with an enhanced wetting performance for water repellent applications. *Vacuum*, 109927.

Kumar, A., Noh, M., Pope, G., Sepehrnoori, K., Bryant, S., & Lake, L. (2004). *Reservoir simulation of CO2 storage in deep saline aquifers.* Paper presented at the SPE/DOE Symposium on Improved Oil Recovery.

Kvenvolden, K. A. (1967). Normal fatty acids in sediments. *Journal of the American Oil Chemist's Society, 44*(11), 628-636.

Lackner, K. S. (2003). A guide to CO2 sequestration. *Science, 300*(5626), 1677-1678.

Lander, L. M., Siewierski, L. M., Brittain, W. J., & Vogler, E. A. (1993). A systematic comparison of contact angle methods. *Langmuir, 9*(8), 2237-2239.

Legens, C., Toulhoat, H., Cuiec, L., Villieras, F., & Palermo, T. (1999). Wettability change related to adsorption of organic acids on calcite: Experimental and ab initio computational studies. *SPE Journal, 4*(04), 328-333.

Lemonnier, P., & Ainsworth, E. A. (2018). Crop responses to rising atmospheric [CO2] and global climate change *Food security and climate change* (pp. 51-69): John Wiely & Sons Ltd. Chichester.

Li, H., Qu, M., & Hu, Y. (2020). High-temperature CO2 capture by Li4SiO4 adsorbents: Effects of pyroligneous acid (PA) modification and existence of CO2 at desorption stage. *Fuel Processing Technology, 197*, 106186.

Li, W., Nan, Y., Zhang, Z., You, Q., & Jin, Z. (2020). Hydrophilicity/Hydrophobicity Driven CO2 Solubility in Kaolinite Nanopores in Relation to Carbon Sequestration. *Chemical Engineering Journal*, 125449.

Li, W., Zhang, M., Nan, Y., Pang, W., & Jin, Z. (2020). Molecular Dynamics Study on CO2 Storage in Water-Filled Kerogen Nanopores in Shale Reservoirs: Effects of Kerogen Maturity and Pore Size. *Langmuir*.

Li, X., Boek, E., Maitland, G. C., & Trusler, J. M. (2012). Interfacial Tension of (Brines+ CO2):(0.864 NaCl+ 0.136 KCl) at Temperatures between (298 and 448) K, Pressures between (2 and 50) MPa, and Total Molalities of (1 to 5) mol· kg–1. *Journal of Chemical & Engineering Data, 57*(4), 1078-1088.

Li, Z., Dong, M., Li, S., & Huang, S. (2006). CO2 sequestration in depleted oil and gas reservoirs—caprock characterization and storage capacity. *Energy Conversion and Management, 47*(11-12), 1372-1382.

Lindeberg, E., & Wessel-Berg, D. (1997). Vertical convection in an aquifer column under a gas cap of CO2. *Energy Conversion and Management, 38*, S229-S234.

Liu, Y., Sun, C., Bolin, T., Wu, T., Liu, Y., Sternberg, M., . . . Lin, X.-M. (2013). Kinetic pathway of palladium nanoparticle sulfidation process at high temperatures. *Nano letters, 13*(10), 4893-4901.

Lohse, S. E., & Murphy, C. J. (2012). Applications of colloidal inorganic nanoparticles: from medicine to energy. *Journal of the American Chemical Society, 134*(38), 15607-15620.

Looyestijn, W. J. (2008). Wettability index determination from NMR logs. *Petrophysics-The SPWLA Journal of Formation Evaluation and Reservoir Description, 49*(02).

Louk, K., Ripepi, N., Luxbacher, K., Gilliland, E., Tang, X., Keles, C., . . . Amante, J. (2017). Monitoring CO2 storage and enhanced gas recovery in unconventional shale reservoirs: Results from the Morgan County, Tennessee injection test. *Journal of Natural Gas Science and Engineering, 45*, 11-25.

Love, J. C., Estroff, L. A., Kriebel, J. K., Nuzzo, R. G., & Whitesides, G. M. (2005). Self-assembled monolayers of thiolates on metals as a form of nanotechnology. *Chemical reviews, 105*(4), 1103-1170.

Lu, Y., Najafabadi, N. F., & Firoozabadi, A. (2017). Effect of temperature on wettability of oil/brine/rock systems. *Energy & Fuels, 31*(5), 4989-4995.

Lundegard, P. D., & Kharaka, Y. K. (1994). Distribution and occurrence of organic acids in subsurface waters *Organic acids in geological processes* (pp. 40-69): Springer.

M. Blunt, F. J. F., Jr. F. M. Orr. (1993). Carbon dioxide in enhanced oil recovery. *Energy Conversion Management, 34*, 9-11.

Maboudian, R., & Howe, R. T. (1997). Critical review: Adhesion in surface micromechanical structures. *Journal of Vacuum Science & Technology B:*

Microelectronics and Nanometer Structures Processing, Measurement, and Phenomena, 15(1), 1-20.

Mac Dowell, N., Fennell, P. S., Shah, N., & Maitland, G. C. (2017). The role of CO 2 capture and utilization in mitigating climate change. *Nature Climate Change, 7*(4), 243-249.

MacAllister, D. J., Miller, K. C., Graham, S. K., & Yang, C.-T. (1993). Application of X-ray CT scanning to determine gas/water relative permeabilities. *SPE formation evaluation, 8*(03), 184-188.

Mackay, E. J. (2013). Modelling the injectivity, migration and trapping of CO2 in carbon capture and storage (CCS) *Geological Storage of Carbon Dioxide (CO2)* (pp. 45-70e): Elsevier.

Madsen, L., & Ida, L. (1998). Adsorption of carboxylic acids on reservoir minerals from organic and aqueous phase. *SPE Reservoir Evaluation & Engineering, 1*(01), 47-51.

Mahadevan, J. (2012). Comments on the paper titled "Contact angle measurements of CO2–water-quartz/calcite systems in the perspective of carbon sequestration": A case of contamination? *International Journal of Greenhouse Gas Control*(7), 261-262.

Mahamuda, S., Swapna, K., Venkateswarlu, M., Rao, A. S., Shakya, S., & Prakash, G. V. (2014). Spectral characterisation of Sm3+ ions doped Oxy-fluoroborate glasses for visible orange luminescent applications. *Journal of luminescence, 154*, 410-424.

Mahdi Jafari, S., He, Y., & Bhandari, B. (2006). Nano-emulsion production by sonication and microfluidization—a comparison. *International Journal of Food Properties, 9*(3), 475-485.

Mahesar, A. A., Ali, M., Shar, A. M., Memon, K. R., Mohanty, U. S., Akhondzadeh, H., . . . Keshavarz, A. (2020). Effect of Cryogenic Liquid Nitrogen on the Morphological and Petrophysical Characteristics of Tight Gas Sandstone Rocks from Kirthar Fold Belt, Indus Basin, Pakistan. *Energy & Fuels, 34*(11), 14548-14559.

Mahesar, A. A., Shar, A. M., Ali, M., Tunio, A. H., Uqailli, M. A., Mohanty, U. S., . . . Keshavarz, A. (2020). Morphological and petro physical estimation of eocene tight carbonate formation cracking by cryogenic liquid nitrogen; a case study of Lower Indus basin, Pakistan. *Journal of Petroleum Science and Engineering*, 107318.

Marmur, A. (2006). Soft contact: measurement and interpretation of contact angles. *Soft Matter, 2*(1), 12-17.

Masalmeh, S. K. (2003). The effect of wettability heterogeneity on capillary pressure and relative permeability. *Journal of Petroleum Science and Engineering, 39*(3-4), 399-408.

Matter, J. M., & Kelemen, P. B. (2009). Permanent storage of carbon dioxide in geological reservoirs by mineral carbonation. *Nature Geoscience, 2*(12), 837-841.

Matter, J. M., Stute, M., Snæbjörnsdottir, S. Ó., Oelkers, E. H., Gislason, S. R., Aradottir, E. S., . . . Gunnlaugsson, E. (2016). Rapid carbon mineralization for permanent disposal of anthropogenic carbon dioxide emissions. *Science, 352*(6291), 1312-1314.

Matter, J. M., Takahashi, T., & Goldberg, D. (2007). Experimental evaluation of in situ CO2-water-rock reactions during CO2 injection in basaltic rocks:

Implications for geological CO2 sequestration. *Geochemistry, Geophysics, Geosystems, 8*(2).

Matthews, H. D., Gillett, N. P., Stott, P. A., & Zickfeld, K. (2009). The proportionality of global warming to cumulative carbon emissions. *Nature, 459*(7248), 829-832.

McCaffery, F., & Bennion, D. (1974). The effect OfWettability on two-phase relative penneabilities. *Journal of Canadian Petroleum Technology, 13*(04).

McGowan, C. W., Pearce, R. C., & Diehl, H. (1985). A comparison of the dissolution of model compounds and the kerogen of Green River oil shale by oxidation with perchloric acid—A model for the kerogen of Green River oil shale. *Fuel Processing Technology, 10*(2), 195-204.

Meinshausen, M., Meinshausen, N., Hare, W., Raper, S. C., Frieler, K., Knutti, R., . . . Allen, M. R. (2009). Greenhouse-gas emission targets for limiting global warming to 2 C. *Nature, 458*(7242), 1158-1162.

Memon, K. R., Mahesar, A. A., Ali, M., Tunio, A. H., Mohanty, U. S., Akhondzadeh, H., . . . Keshavarz, A. (2020). Influence of Cryogenic Liquid Nitrogen on Petro-Physical Characteristics of Mancos Shale: An Experimental Investigation. *Energy & Fuels, 34*(2), 2160-2168.

Meredith, W., Kelland, S.-J., & Jones, D. (2000). Influence of biodegradation on crude oil acidity and carboxylic acid composition. *Organic Geochemistry, 31*(11), 1059-1073.

Metz, B., Davidson, O., & De Coninck, H. (2005). *Carbon dioxide capture and storage: special report of the intergovernmental panel on climate change*: Cambridge University Press.

Mihajlović, S. R., Vučinić, D. R., Sekulić, Ž. T., Milićević, S. Z., & Kolonja, B. M. (2013). Mechanism of stearic acid adsorption to calcite. *Powder technology, 245*, 208-216.

Mills, J., Riazi, M., & Sohrabi, M. (2011). *Wettability of common rock-forming minerals in a CO2-brine system at reservoir conditions.* Paper presented at the International symposium of the society of core analysts.

Morrow, N. R. (1970). Physics and thermodynamics of capillary action in porous media. *Industrial & Engineering Chemistry, 62*(6), 32-56.

Morrow, N. R. (1976). Capillary pressure correlations for uniformly wetted porous media. *Journal of Canadian Petroleum Technology, 15*(04).

Morrow, N. R. (1990). Wettability and its effect on oil recovery. *Journal of Petroleum Technology, 42*(12), 1,476-471,484.

Naik, S., Malgaresi, G., You, Z., & Bedrikovetsky, P. (2018). Well productivity enhancement by applying nanofluids for wettability alteration. *The APPEA Journal, 58*(1), 121-129.

Naik, S., You, Z., & Bedrikovetsky, P. (2015). Rate enhancement in unconventional gas reservoirs by wettability alteration. *Journal of Natural Gas Science and Engineering, 26*, 1573-1584.

Naik, S., You, Z., & Bedrikovetsky, P. (2018). Productivity index enhancement by wettability alteration in two-phase compressible flows. *Journal of Natural Gas Science and Engineering, 50*, 101-114.

NASA, & NOAA. (2016). Warmest year on record globally.

Naylor, M., Wilkinson, M., & Haszeldine, R. (2011). Calculation of CO2 column heights in depleted gas fields from known pre-production gas column heights. *Marine and Petroleum Geology, 28*(5), 1083-1093.

Nazarahari, M. J., Manshad, A. K., Ali, M., Ali, J. A., Shafiei, A., Sajadi, S. M., . . . Keshavarz, A. (2021). Impact of a novel biosynthesized nanocomposite (SiO2@ Montmorilant@ Xanthan) on wettability shift and interfacial tension: Applications for enhanced oil recovery. *Fuel, 298*, 120773.

Nelson, P. H. (2009). Pore-throat sizes in sandstones, tight sandstones, and shales. *AAPG Bulletin, 93*(3), 329-340.

Neumann, A., & Good, R. (1972). Thermodynamics of contact angles. I. Heterogeneous solid surfaces. *Journal of colloid and interface science, 38*(2), 341-358.

Newell, R., Raimi, D., & Aldana, G. (2019). Global Energy Outlook 2019: The Next Generation of Energy. *Resources for the Future*, 8-19.

Nordbotten, J. M., Celia, M. A., & Bachu, S. (2005). Injection and storage of CO 2 in deep saline aquifers: analytical solution for CO 2 plume evolution during injection. *Transport in porous media, 58*(3), 339-360.

Nordhaus, W. (2014). *A question of balance: Weighing the options on global warming policies*: Yale University Press.

Nowrouzi, I., Manshad, A. K., & Mohammadi, A. H. (2020). Effects of TiO2, MgO and γ-Al2O3 nano-particles on wettability alteration and oil production under carbonated nano-fluid imbibition in carbonate oil reservoirs. *Fuel, 259*, 116110.

Nunes, L. J., Meireles, C. I., Pinto Gomes, C. J., & Almeida Ribeiro, N. (2020). Forest Contribution to Climate Change Mitigation: Management Oriented to Carbon Capture and Storage. *Climate, 8*(2), 21.

Nwidee, L., Al-Anssari, S., Barifcani, A., Sarmadivaleh, M., & Iglauer, S. (2016). *Nanofluids for enhanced oil recovery processes: wettability alteration using zirconium oxide.* Paper presented at the Offshore Technology Conference Asia.

Ochs, M., Ćosović, B., & Stumm, W. (1994). Coordinative and hydrophobic interaction of humic substances with hydrophilic Al2O3 and hydrophobic mercury surfaces. *Geochimica et Cosmochimica Acta, 58*(2), 639-650.

Orr, F. M. (2009). Onshore geologic storage of CO2. *Science, 325*(5948), 1656-1658.

Paterson, L., Boreham, C., Bunch, M., Ennis-King, J., Freifeld, B., Haese, R., . . . Stalker, L. (2011). The CO2CRC Otway stage 2b residual saturation and dissolution test: test concept, implementation and data collected. *Milestone Report to ANLEC*.

Pearce, J., Underschultz, J., & La Croix, A. (2019). Mineralogy, geochemical CO2-water-rock reactions and associated characterisation.

Pearce, J. K., Kirste, D. M., Dawson, G. K., Farquhar, S. M., Biddle, D., Golding, S. D., & Rudolph, V. (2015). SO2 impurity impacts on experimental and simulated CO2–water–reservoir rock reactions at carbon storage conditions. *Chemical Geology, 399*, 65-86.

Pentland, C., El-Maghraby, R., Georgiadis, A., Iglauer, S., & Blunt, M. (2011). Immiscible displacements and capillary trapping in CO2 storage. *Energy Procedia, 4*, 4969-4976.

Pentland, C. H., El-Maghraby, R., Iglauer, S., & Blunt, M. J. (2011). Measurements of the capillary trapping of super-critical carbon dioxide in Berea sandstone. *Geophysical Research Letters, 38*(6).

Pentland, C. H., Iglauer, S., Gharbi, O., Okada, K., & Suekane, T. (2012). *The influence of pore space geometry on the entrapment of carbon dioxide by*

capillary forces. Paper presented at the SPE Asia Pacific Oil and Gas Conference and Exhibition.

Plaisant, A., Maiu, A., Maggio, E., & Pettinau, A. (2017). Pilot-scale CO2 sequestration test site in the Sulcis Basin (SW Sardinia): preliminary site characterization and research program. *Energy Procedia, 114*, 4508-4517.

Ponmani, S., Nagarajan, R., & Sangwai, J. S. (2016). Effect of nanofluids of CuO and ZnO in polyethylene glycol and polyvinylpyrrolidone on the thermal, electrical, and filtration-loss properties of water-based drilling fluids. *SPE Journal, 21*(02), 405-415.

Porrostami, R., Zahedi Amiri, G., & Etemad, V. (2020). Spatial variability of carbon storage and sequestration in leaf litter and layers of soil in the forest area of Jahannama Park. *Iranian Journal of Forest, 12*(3), 317-330.

Purcell, W. (1950). Interpretation of capillary pressure data. *Journal of Petroleum Technology, 2*(08), 11-12.

Qin, C., Jiang, Y., Luo, Y., Zhou, J., Liu, H., Song, X., . . . Xie, Y. (2020). Effect of supercritical CO2 saturation pressures and temperatures on the methane adsorption behaviours of Longmaxi shale. *Energy, 206*, 118150.

Rackley, S. A. (2017). 14 - Geochemical and biogeochemical features, events, and processes. In S. A. Rackley (Ed.), *Carbon Capture and Storage (Second Edition)* (pp. 365-386). Boston: Butterworth-Heinemann.

Rackley, S. A. (2017). *Carbon capture and storage*: Butterworth-Heinemann.

Rahman, T., Lebedev, M., Barifcani, A., & Iglauer, S. (2016). Residual trapping of supercritical CO2 in oil-wet sandstone. *Journal of colloid and interface science, 469*, 63-68.

Ramandi, H. L., Pirzada, M. A., Saydam, S., Arns, C., & Roshan, H. (2019). Digital and experimental rock analysis of proppant injection into naturally fractured coal. *Fuel, 286*, 119368.

Rao, Z., Bao, S., Liu, X., Taylor, R. A., & Liao, S. (2020). Estimating allowable energy flux density for the supercritical carbon dioxide solar receiver: A service life approach. *Applied Thermal Engineering*, 116054.

Reddy, K. R., Gopakumar, A., & Chetri, J. K. (2019). Critical review of applications of iron and steel slags for carbon sequestration and environmental remediation. *Reviews in Environmental Science and Bio/Technology, 18*(1), 127-152.

Ren, M., Sevilla, M., Fuertes, A. B., Mokaya, R., Tour, J. M., & Jalilov, A. S. (2019). Pore Characteristics for Efficient CO2 Storage in Hydrated Carbons. *ACS Applied Materials & Interfaces, 11*(47), 44390-44398.

Rezk, M. G., Foroozesh, J., Zivar, D., & Mumtaz, M. (2019). CO2 storage potential during CO2 enhanced oil recovery in sandstone reservoirs. *Journal of Natural Gas Science and Engineering, 66*, 233-243.

Riaz, A., & Cinar, Y. (2014). Carbon dioxide sequestration in saline formations: Part I—Review of the modeling of solubility trapping. *Journal of Petroleum Science and Engineering, 124*, 367-380.

Rochelle, C. A., Czernichowski-Lauriol, I., & Milodowski, A. (2004). The impact of chemical reactions on CO2 storage in geological formations: a brief review. *Geological Society, London, Special Publications, 233*(1), 87-106.

Rosenberg, N. J. (1981). The increasing CO 2 concentration in the atmosphere and its implication on agricultural productivity. *Climatic Change, 3*(3), 265-279.

Roustaei, A., & Bagherzadeh, H. (2015). Experimental investigation of SiO 2 nanoparticles on enhanced oil recovery of carbonate reservoirs. *Journal of Petroleum Exploration and Production Technology, 5*(1), 27-33.

Ruprecht, C., Pini, R., Falta, R., Benson, S., & Murdoch, L. (2014). Hysteretic trapping and relative permeability of CO2 in sandstone at reservoir conditions. *International Journal of Greenhouse Gas Control, 27*, 15-27.

Rushton, J. C., Wagner, D., Pearce, J. M., Rochelle, C. A., & Purser, G. (2020). Red-bed bleaching in a CO2 storage analogue: Insights from Entrada Sandstone fracture-hosted mineralization. *Journal of Sedimentary Research, 90*(1), 48-66.

Sahle, M., Saito, O., Fürst, C., & Yeshitela, K. (2018). Quantification and mapping of the supply of and demand for carbon storage and sequestration service in woody biomass and soil to mitigate climate change in the socio-ecological environment. *Science of the total environment, 624*, 342-354.

Salama, A., Negara, A., El Amin, M., & Sun, S. (2015). Numerical investigation of nanoparticles transport in anisotropic porous media. *Journal of contaminant hydrology, 181*, 114-130.

Saraji, S., Piri, M., & Goual, L. (2014). The effects of SO2 contamination, brine salinity, pressure, and temperature on dynamic contact angles and interfacial tension of supercritical CO2/brine/quartz systems. *International Journal of Greenhouse Gas Control, 28*, 147-155.

Sarmadivaleh, M., Al-Yaseri, A. Z., & Iglauer, S. (2015). Influence of temperature and pressure on quartz–water–CO2 contact angle and CO2–water interfacial tension. *Journal of colloid and interface science, 441*, 59-64.

Schiermeier, Q., Tollefson, J., Scully, T., Witze, A., & Morton, O. (2008). Energy alternatives: Electricity without carbon. *Nature News, 454*(7206), 816-823.

Scott, J., & Barker, R. (2005). Characterization of sandstone by electrical spectroscopy for stratigraphical and hydrogeological investigations. *Quarterly Journal of Engineering Geology and Hydrogeology, 38*(2), 143-154.

Sevilla, M., Al-Jumialy, A. S. M., Fuertes, A. B., & Mokaya, R. (2018). Optimization of the pore structure of biomass-based carbons in relation to their use for CO2 capture under low-and high-pressure regimes. *ACS Applied Materials & Interfaces, 10*(2), 1623-1633.

Shafrin, E., & Zisman, W. (1962). Effect of progressive fluorination of a fatty acid on the wettability of its adsorbed monolayer. *The Journal of Physical Chemistry, 66*(4), 740-748.

ShamsiJazeyi, H., Miller, C. A., Wong, M. S., Tour, J. M., & Verduzco, R. (2014). Polymer-coated nanoparticles for enhanced oil recovery. *Journal of Applied Polymer Science, 131*(15).

Sharma, T., Kumar, G. S., & Sangwai, J. S. (2015). Comparative effectiveness of production performance of Pickering emulsion stabilized by nanoparticle–surfactant–polymerover surfactant–polymer (SP) flooding for enhanced oil recoveryfor Brownfield reservoir. *Journal of Petroleum Science and Engineering, 129*, 221-232.

Shi, X., Rosa, R., & Lazzeri, A. (2010). On the coating of precipitated calcium carbonate with stearic acid in aqueous medium. *Langmuir, 26*(11), 8474-8482.

Singh, K., Bijeljic, B., & Blunt, M. J. (2016). Imaging of oil layers, curvature and contact angle in a mixed-wet and a water-wet carbonate rock. *Water Resources Research, 52*(3), 1716-1728.

Snippe, J., Berg, S., Ganga, K., Brussee, N., & Gdanski, R. (2020). Experimental and numerical investigation of wormholing during CO2 storage and water alternating gas injection. *International Journal of Greenhouse Gas Control, 94*, 102901.

Solomon, S., Plattner, G.-K., Knutti, R., & Friedlingstein, P. (2009). Irreversible climate change due to carbon dioxide emissions. *Proceedings of the National Academy of Sciences, 106*(6), 1704-1709.

Song, J., & Zhang, D. (2013). Comprehensive review of caprock-sealing mechanisms for geologic carbon sequestration. *Environmental science & technology, 47*(1), 9-22.

Stalker, L., Varma, S., Van Gent, D., Haworth, J., & Sharma, S. (2013). South West Hub: a carbon capture and storage project. *Australian Journal of Earth Sciences, 60*(1), 45-58.

Standnes, D. C., & Austad, T. (2003). Wettability alteration in carbonates: Interaction between cationic surfactant and carboxylates as a key factor in wettability alteration from oil-wet to water-wet conditions. *Colloids and Surfaces A: Physicochemical and Engineering Aspects, 216*(1-3), 243-259.

Su, E., Liang, Y., Zou, Q., Niu, F., & Li, L. (2019). Analysis of effects of CO2 injection on coalbed permeability: Implications for coal seam CO2 sequestration. *Energy & Fuels, 33*(7), 6606-6615.

Sun, Q., Ampomah, W., Kutsienyo, E. J., Appold, M., Adu-Gyamfi, B., Dai, Z., & Soltanian, M. R. (2020). Assessment of CO2 trapping mechanisms in partially depleted oil-bearing sands. *Fuel, 278*, 118356.

Swapna, K., Mahamuda, S., Rao, A. S., Shakya, S., Sasikala, T., Haranath, D., & Prakash, G. V. (2014). Optical studies of Sm3+ ions doped zinc alumino bismuth borate glasses. *Spectrochimica Acta Part A: Molecular and Biomolecular Spectroscopy, 125*, 53-60.

Tabrizy, V. A., Denoyel, R., & Hamouda, A. (2011). Characterization of wettability alteration of calcite, quartz and kaolinite: Surface energy analysis. *Colloids and Surfaces A: Physicochemical and Engineering Aspects, 384*(1-3), 98-108.

Tang, Y., Hu, S., He, Y., Wang, Y., Wan, X., Cui, S., & Long, K. (2020). Experiment on CO2-brine-rock interaction during CO2 injection and storage in gas reservoirs with aquifer. *Chemical Engineering Journal*, 127567.

Thurman, E. M. (2012). *Organic geochemistry of natural waters* (Vol. 2): Springer Science & Business Media.

Tokunaga, T. K., & Wan, J. (2013). Capillary pressure and mineral wettability influences on reservoir CO2 capacity. *Reviews in Mineralogy and Geochemistry, 77*(1), 481-503.

Tong, R., Hemmati, H. D., Langer, R., & Kohane, D. S. (2012). Photoswitchable nanoparticles for triggered tissue penetration and drug delivery. *Journal of the American Chemical Society, 134*(21), 8848-8855.

Toquero, C. M. (2020). Challenges and Opportunities for Higher Education Amid the COVID-19 Pandemic: The Philippine Context. *Pedagogical Research, 5*(4).

Tosun, Y. İ. (2020). Microwave Caustic Slurry Carbonation of Flue Gas of Coal Power Plants in Double Hot Tube Bed for CO2 Sequestration *Carbon Capture*: IntechOpen.

Townsend, G. T., Prince, R. C., & Suflita, J. M. (2003). Anaerobic oxidation of crude oil hydrocarbons by the resident microorganisms of a contaminated anoxic aquifer. *Environmental science & technology, 37*(22), 5213-5218.

Tudek, J., Crandall, D., Fuchs, S., Werth, C. J., Valocchi, A. J., Chen, Y., & Goodman, A. (2017). In situ contact angle measurements of liquid CO2, brine, and Mount Simon sandstone core using micro X-ray CT imaging, sessile drop, and Lattice Boltzmann modeling. *Journal of Petroleum Science and Engineering, 155*, 3-10.

Ulrich, H. J., Stumm, W., & Cosovic, B. (1988). Adsorption of aliphatic fatty acids on aquatic interfaces. Comparison between two model surfaces: the mercury electrode and δ-Al2O3 colloids. *Environmental science & technology, 22*(1), 37-41.

Vaculikova, L., & Plevova, E. (2005). Identification of clay minerals and micas in sedimentary rocks. *Acta Geodynamica et geomaterialia, 2*(2), 167-175.

Vanithakumari, S., George, R., & Mudali, U. K. (2014). Influence of silanes on the wettability of anodized titanium. *Applied Surface Science, 292*, 650-657.

Venkatraman, A., Lake, L. W., & Johns, R. T. (2014). Gibbs free energy minimization for prediction of solubility of acid gases in water. *Industrial & Engineering Chemistry Research, 53*(14), 6157-6168.

Viete, D. R., & Ranjith, P. G. (2006). The effect of CO2 on the geomechanical and permeability behaviour of brown coal: implications for coal seam CO2 sequestration. *International Journal of Coal Geology, 66*(3), 204-216.

Walspurger, S., Cobden, P. D., Safonova, O. V., Wu, Y., & Anthony, E. J. (2010). High CO2 Storage Capacity in Alkali-Promoted Hydrotalcite-Based Material: In Situ Detection of Reversible Formation of Magnesium Carbonate. *Chemistry–A European Journal, 16*(42), 12694-12700.

Wan, J., Tokunaga, T. K., Ashby, P. D., Kim, Y., Voltolini, M., Gilbert, B., & DePaolo, D. J. (2018). Supercritical CO2 uptake by nonswelling phyllosilicates. *Proceedings of the National Academy of Sciences, 115*(5), 873-878.

Wang, C., Sheng, Y., Zhao, X., Pan, Y., & Wang, Z. (2006). Synthesis of hydrophobic CaCO3 nanoparticles. *Materials Letters, 60*(6), 854-857.

Wang, H., Yan, N., Li, Y., Zhou, X., Chen, J., Yu, B., . . . Chen, Q. (2012). Fe nanoparticle-functionalized multi-walled carbon nanotubes: one-pot synthesis and their applications in magnetic removal of heavy metal ions. *Journal of Materials Chemistry, 22*(18), 9230-9236.

Wang, L., & Mohanty, K. (2015). Enhanced oil recovery in gasflooded carbonate reservoirs by wettability-altering surfactants. *SPE Journal, 20*(01), 60-69.

Wang, N., Feng, Y., Liu, L., & Guo, X. (2018). Effects of preparation methods on the structure and property of Al-stabilized CaO-based sorbents for CO2 capture. *Fuel Processing Technology, 173*, 276-284.

Wang, S., & Tokunaga, T. K. (2015). Capillary pressure–saturation relations for supercritical CO2 and brine in limestone/dolomite sands: Implications for geologic carbon sequestration in carbonate reservoirs. *Environmental science & technology, 49*(12), 7208-7217.

Wang, Y., Yuan, L., Yao, C., Ding, L., Li, C., Fang, J., . . . Wu, M. (2014). A combined toxicity study of zinc oxide nanoparticles and vitamin C in food additives. *Nanoscale, 6*(24), 15333-15342.

Waples, D. W. (1981). *Organic geochemistry for exploration geologists*: Burgess Pub. Co.

Watson, J., Jones, D., Swannell, R., & Van Duin, A. (2002). Formation of carboxylic acids during aerobic biodegradation of crude oil and evidence of microbial oxidation of hopanes. *Organic Geochemistry, 33*(10), 1153-1169.

Wenzel, R. N. (1936). Resistance of solid surfaces to wetting by water. *Industrial & Engineering Chemistry, 28*(8), 988-994.

White, C. M., Strazisar, B. R., Granite, E. J., Hoffman, J. S., & Pennline, H. W. (2003). Separation and capture of CO2 from large stationary sources and sequestration

in geological formations—coalbeds and deep saline aquifers. *Journal of the Air & Waste Management Association, 53*(6), 645-715.

Wilcox, J. (2012). Introduction to carbon capture *Carbon Capture* (pp. 1-34): Springer.

Worden, R., & Morad, S. (2000). Quartz cementation in oil field sandstones: a review of the key controversies. *Special Publication-International Association of Sedimentologists, 29*, 1-20.

Xu, L., Yu, G., He, N., Wang, Q., Gao, Y., Wen, D., . . . Ge, J. (2018). Carbon storage in China's terrestrial ecosystems: A synthesis. *Scientific reports, 8*(1), 1-13.

Yang, D., Gu, Y., & Tontiwachwuthikul, P. (2008). Wettability determination of the reservoir brine− reservoir rock system with dissolution of CO2 at high pressures and elevated temperatures. *Energy & Fuels, 22*(1), 504-509.

Yang, L., Xu, T., Wei, M., Feng, G., Wang, F., & Wang, K. (2015). Dissolution of arkose in dilute acetic acid solution under conditions relevant to burial diagenesis. *Applied Geochemistry, 54*, 65-73.

Yang, Y., Cheng, T., Wu, H., You, Z., Shang, D., & Hou, J. (2020). Enhanced Oil Recovery Using Oleic Acid-Modified Titania Nanofluids: Underlying Mechanisms and Oil-Displacement Performance. *Energy & Fuels, 34*(5), 5813-5822.

Yu, H., Rezaee, R., Wang, Z., Han, T., Zhang, Y., Arif, M., & Johnson, L. (2017). A new method for TOC estimation in tight shale gas reservoirs. *International Journal of Coal Geology, 179*, 269-277.

Zargartalebi, M., Kharrat, R., & Barati, N. (2015). Enhancement of surfactant flooding performance by the use of silica nanoparticles. *Fuel, 143*, 21-27.

Zasadzinski, J., Viswanathan, R., Madsen, L., Garnaes, J., & Schwartz, D. (1994). Langmuir-blodgett films. *Science, 263*(5154), 1726-1733.

Zhang, D., & Song, J. (2014). Mechanisms for geological carbon sequestration. *Procedia IUTAm, 10*, 319-327.

Zhang, H., Ramakrishnan, T., Nikolov, A., & Wasan, D. (2016). Enhanced oil recovery driven by nanofilm structural disjoining pressure: flooding experiments and microvisualization. *Energy & Fuels, 30*(4), 2771-2779.

Zhang, W., Li, Y., Xu, T., Cheng, H., Zheng, Y., & Xiong, P. (2009). Long-term variations of CO2 trapped in different mechanisms in deep saline formations: A case study of the Songliao Basin, China. *International Journal of Greenhouse Gas Control, 3*(2), 161-180.

Zhang, X., Xiao, S., Zhou, J., & Tang, J. (2014). Experimental analysis of the feasibility of CF 3 I/CO 2 substituting SF 6 as insulation medium using needle-plate electrodes. *IEEE Transactions on Dielectrics and Electrical Insulation, 21*(4), 1895-1900.

Zhang, Y., Kogure, T., Nishizawa, O., & Xue, Z. (2017). Different flow behavior between 1-to-1 displacement and co-injection of CO2 and brine in Berea sandstone: Insights from laboratory experiments with X-ray CT imaging. *International Journal of Greenhouse Gas Control, 66*, 76-84.

Zheng, H., Zhong, Y., Mao, Z., & Zheng, L. (2018). CO2 utilization for the waterless dyeing: Characterization and properties of Disperse Red 167 in supercritical fluid. *Journal of CO2 Utilization, 24*, 266-273.

Zheng, J., Chong, Z. R., Qureshi, M. F., & Linga, P. (2020). Carbon dioxide sequestration via gas hydrates: a potential pathway toward decarbonization. *Energy & Fuels, 34*(9), 10529-10546.

Zhou, N., He, G., Romankiewicz, J., & Fridley, D. (2015). *A Review of Commercially Available Technologies in Developing Low Carbon Eco-cities*. Retrieved from

Zullig, J. J., & Morse, J. W. (1988). Interaction of organic acids with carbonate mineral surfaces in seawater and related solutions: I. Fatty acid adsorption. *Geochimica et Cosmochimica Acta, 52*(6), 1667-1678.

Copyright Declaration

Appendix

Attribution Statements

Organic acid concentration thresholds for ageing of carbonate minerals: implications for CO_2 trapping/storage						
	conception and design	acquisition of data & method	data conditioning & manipulation	analysis & statistical method	interpretation & discussion	Final Approval
Muhammad Ali	x	x	x	x	x	
I acknowledge that these represent my contribution to the above research output. Signed. [redacted]						
Sarmad Al-Anssari			x			
I acknowledge that these represent my contribution to the above research output. Signed. [redacted]						
Muhammad Arif			x	x		
I acknowledge that these represent my contribution to the above research output. Signed. [redacted]						
Ahmed Barifcani					x	x
I acknowledge that these represent my contribution to the above research output. Signed. [redacted]						
Mohammad Sarmadivaleh	x				x	x
I acknowledge that these represent my contribution to the above research output. Signed. [redacted]						
Linda Stalker					x	x
I acknowledge that these represent my contribution to the above research output. Signed. [redacted]						
Maxim Lebedev					x	x
I acknowledge that these represent my contribution to the above research output. Signed. [redacted]						
Stefan Iglauer					x	x
I acknowledge that these represent my contribution to the above research output. Signed. [redacted]						

CO_2-wettability of sandstones exposed to traces of organic acids: Implications for CO_2 geo-storage						
	conception and design	**acquisition of data & method**	**data conditioning & manipulation**	**analysis & statistical method**	**interpretation & discussion**	**Final Approval**
Muhammad Ali	x	x	x	x	x	
I acknowledge that these represent my contribution to the above research output. Signed. [redacted]						
Muhammad Arif			x			
I acknowledge that these represent my contribution to the above research output. Signed. [redacted]						
Muhammad Faraz Sahito				x		
I acknowledge that these represent my contribution to the above research output. Signed. [redacted]						
Sarmad Al-Anssari					x	
I acknowledge that these represent my contribution to the above research output. Signed. [redacted]						
Alireza Keshavarz					x	
I acknowledge that these represent my contribution to the above research output. Signed. [redacted]						
Ahmed Barifcani					x	x
I acknowledge that these represent my contribution to the above research output. Signed. [redacted]						
Linda Stalker					x	x
I acknowledge that these represent my contribution to the above research output. Signed. [redacted]						
Mohammad Sarmadivaleh	x				x	x
I acknowledge that these represent my contribution to the above research output. Signed. [redacted]						
Stefan Iglauer					x	x
I acknowledge that these represent my contribution to the above research output. Signed. [redacted]						

Influence of Organic Acids Concentration on Wettability Alteration of Cap-rock: Implications for CO_2 Trapping/Storage						
	conception and design	**acquisition of data & method**	**data conditioning & manipulation**	**analysis & statistical method**	**interpretation & discussion**	**Final Approval**
Muhammad Ali	x	x	x	x	x	
I acknowledge that these represent my contribution to the above research output. Signed. [redacted]						
Adnan Aftab			x	x		
I acknowledge that these represent my contribution to the above research output. Signed. [redacted]						
Zain-Ul-Abedin Arain			x			
I acknowledge that these represent my contribution to the above research output. Signed. [redacted]						
Ahmed Al-Yaseri					x	
I acknowledge that these represent my contribution to the above research output. Signed. [redacted]						
Hamid Roshan					x	x
I acknowledge that these represent my contribution to the above research output. Signed. [redacted]						
Ali Saeedi					x	x
I acknowledge that these represent my contribution to the above research output. Signed. [redacted]						
Stefan Iglauer					x	x
I acknowledge that these represent my contribution to the above research output. Signed. [redacted]						
Mohammad Sarmadivaleh	x				x	x
I acknowledge that these represent my contribution to the above research output. Signed. [redacted]						

Effect of nanofluid on CO_2-wettability reversal of sandstone formation; implications for CO_2 geo-storage						
	conception and design	**acquisition of data & method**	**data conditioning & manipulation**	**analysis & statistical method**	**interpretation & discussion**	**Final Approval**
Muhammad Ali	x	x	x	x	x	
I acknowledge that these represent my contribution to the above research output. Signed. [redacted]						
Muhammad Faraz Sahito			x			
I acknowledge that these represent my contribution to the above research output. Signed. [redacted]						
Nilesh Kumar Jha			x	x		
I acknowledge that these represent my contribution to the above research output. Signed. [redacted]						
Zain-Ul-Abedin Arain					x	
I acknowledge that these represent my contribution to the above research output. Signed. [redacted]						
Shoaib Memon				x		
I acknowledge that these represent my contribution to the above research output. Signed. [redacted]						
Alireza Keshavarz					x	
I acknowledge that these represent my contribution to the above research output. Signed. [redacted]						
Stefan Iglauer					x	x
I acknowledge that these represent my contribution to the above research output. Signed. [redacted]						
Ali Saeedi					x	x
I acknowledge that these represent my contribution to the above research output. Signed. [redacted]						
Mohammad Sarmadivaleh	x				x	x
I acknowledge that these represent my contribution to the above research output. Signed. [redacted]						

CO_2-wettability reversal of cap-rock by alumina nanofluid: Implications for CO_2 geo-storage						
	conception and design	**acquisition of data & method**	**data conditioning & manipulation**	**analysis & statistical method**	**interpretation & discussion**	**Final Approval**
Muhammad Ali	x	x	x	x	x	
I acknowledge that these represent my contribution to the above research output. Signed. [redacted]						
Adnan Aftab			x			
I acknowledge that these represent my contribution to the above research output. Signed. [redacted]						
Faisal Ur Rahman Awan				x		
I acknowledge that these represent my contribution to the above research output. Signed. [redacted]						
Hamed Akhondzadeh					x	
I acknowledge that these represent my contribution to the above research output. Signed. [redacted]						
Alireza Keshavarz					x	
I acknowledge that these represent my contribution to the above research output. Signed. [redacted]						
Ali Saeedi					x	x
I acknowledge that these represent my contribution to the above research output. Signed. [redacted]						
Stefan Iglauer					x	x
I acknowledge that these represent my contribution to the above research output. Signed. [redacted]						
Mohammad Sarmadivaleh	x				x	x
I acknowledge that these represent my contribution to the above research output. Signed. [redacted]						

Copyrights

ACS Publications
Most Trusted. Most Cited. Most Read.

Influence of Organic Acid Concentration on Wettability Alteration of Cap-Rock: Implications for CO2 Trapping/Storage

Author: Muhammad Ali, Adnan Aftab, Zain-Ul-Abedin Arain, et al
Publication: Applied Materials
Publisher: American Chemical Society
Date: Sep 1, 2020

PERMISSION/LICENSE IS GRANTED FOR YOUR ORDER AT NO CHARGE

This type of permission/license, instead of the standard Terms & Conditions, is sent to you because no fee is being charged for your order. Please note the following:

- Permission is granted for your request in both print and electronic formats, and translations.
- If figures and/or tables were requested, they may be adapted or used in part.
- Please print this page for your records and send a copy of it to your publisher/graduate school.
- Appropriate credit for the requested material should be given as follows: "Reprinted (adapted) with permission from (COMPLETE REFERENCE CITATION). Copyright (YEAR) American Chemical Society." Insert appropriate information in place of the capitalized words.
- One-time permission is granted only for the use specified in your request. No additional uses are granted (such as derivative works or other editions). For any other uses, please submit a new request.

BACK CLOSE WINDOW

Effect of nanofluid on CO2-wettability reversal of sandstone formation; implications for CO2 geo-storage

Author:
Muhammad Ali,Muhammad Faraz Sahito,Nilesh Kumar Jha,Zain-Ul-Abedin Arain,Shoaib Memon,Alireza Keshavarz,Stefan Iglauer,Ali Saeedi,Mohammad Sarmadivaleh
Publication: Journal of Colloid and Interface Science
Publisher: Elsevier
Date: 1 February 2020

Journal Author Rights

Please note that, as the author of this Elsevier article, you retain the right to include it in a thesis or dissertation, provided it is not published commercially. Permission is not required, but please ensure that you reference the journal as the original source. For more information on this and on your other retained rights, please visit: https://www.elsevier.com/about/our-business/policies/copyright#Author-rights

BACK CLOSE WINDOW

CO2-wettability reversal of cap-rock by alumina nanofluid: Implications for CO2 geo-storage

Author:
Muhammad Ali,Adnan Aftab,Faisal Ur Rahman Awan,Hamed Akhondzadeh,Alireza Keshavarz,Ali Saeedi,Stefan Iglauer,Mohammad Sarmadivaleh

Publication: Fuel Processing Technology

Publisher: Elsevier

Date: April 2021